Phase Equilibria and Thermodynamic Evaluation of the Fe-Ti-V-O System in Air

Willem Dutoit Malan

University of Pretoria

2018

PHASE EQUILIBRIA AND THERMODYNAMIC EVALUATION OF THE FE-TI-V-O SYSTEM IN AIR

by

Willem Dutoit Malan

submitted in partial fulfilment of the requirements for the degree

Doctor of Philosophy in Metallurgical Engineering

supervised by

Dr Johan Zietsman, Prof. Guven Akdogan (Stellenbosch University) and Prof. Pekka Taskinen (Aalto University, Finland)

in the

Department of Material Sciences and Metallurgical Engineering

of the

University of Pretoria

on

December 2018

Abstract

In this study, the iron-titanium-vanadium-oxygen (Fe-Ti-V-O) system in equilibrium with air was studied experimentally by high-temperature equilibration, quenching, scanning electron microscope and microprobe analysis coupled with critical assessment and thermodynamic evaluation. The thermodynamic evaluation was performed with FactSage 7.0. The purpose of the study was to develop a set of Gibbs equations for all compounds and solutions of the Fe-Ti-V-O system in equilibrium with air, using the well-known calculation of phase diagram (CALPHAD) technique. The study was categorically divided into three separate investigations. The lower order Fe-V-O and Ti-V-O systems in equilibrium with air were fist experimentally investigated and thermodynamically assessed. This was then followed by an experimental investigation and thermodynamic assessment of the Fe-Ti-V-O system in equilibrium with air.

The Fe-V-O and Ti-V-O systems in equilibrium with air were studied experimentally in temperatures ranging from 700 °C to 1500 °C. The measured concentration of Fe in the V-O slag is 35 weight % at 1400 °C, and the measured V concentration in the hematite phase reached a maximum of 4.4 weight % at 1350 °C. A significant amount of precipitation was observed for Fe-V-O samples quenched at 1400 °C, causing calculated standard deviations of Fe and V to be more than 1 weight %. The measured concentration of Ti in the V-O slag is less than 6 weight % at 1500 °C, and the measured V concentration in the rutile phase reached a maximum of 15 weight % at 1400 °C.

The solubility of V_2O_5(s) in the hematite and rutile phases was described with the compound energy formalism. The properties of the liquid phase were described with both the modified quasichemical model and the associate species model. A set of self-consistent thermodynamic parameters was estimated within acceptable error limits. The calculated phase diagrams of Fe-V-O and Ti-V-O in equilibrium with air are presented and compared to experimental observations and other literature data.

Before experiments in the Fe-Ti-V-O system in equilibrium with air were conducted, the Fe-Ti-O system in equilibrium with air was critically assessed and thermodynamically evaluated. This was due to the slag phase and solid solutions of the Fe-Ti-O system that were previously thermodynamically evaluated only under reducing conditions. However, limited data were available in literature, hence assumptions were required for the evaluation. Nevertheless, an improved phase diagram of the Fe-Ti-O system in equilibrium with air was calculated.

Thereafter, isothermal planes were calculated from optimized binary parameters to estimate a range of plausible starting compositions for experiments of the Fe-Ti-V-O system in equilibrium with air. The Gibbs phase rule was carefully applied to avoid redundant experiments. The Fe-Ti-V-O system in equilibrium with air was studied experimentally, ranging from 1000 °C to 1400 °C.

The properties of the liquid phase were successfully described with the quasichemical model by optimizing parameters only related to the Fe-Ti-O system. The model for the rutile solid solution was extended to describe the solubility of Fe_2O_3(s) and V_2O_5(s) simultaneously. The model for the hematite solid solution was similarly extended to describe the solubility of TiO_2(s) and V_2O_5(s) simultaneously. The ferropseudobrookite solid solution was modelled with a simple polynomial model to include a small solubility region of V_2O_5(s). A final set of self-consistent thermodynamic parameters was estimated within acceptable error limits. Calculated isothermal projections at 1000 °C, 1100 °C, 1200 °C, 1300 °C, and 1400 °C are presented and compared to experimental observations.

Keywords: Fe-Ti-V-O system, Thermodynamics, Static experiments, Phase diagram

List of Publications

The following articles have been published as partial fulfilment of the requirements for the degree Doctor of Philosophy in Metallurgical Engineering. The summaries of the publications are also given.

Publication i: W.D. Malan, G. Akdogan, P. Taskinen, J. Hamuyuni, J. Zietsman, Phase equilibria and thermodynamic evaluation of Fe-V-O system in air, CALPHAD: Computer Coupling of Phase Diagrams and Thermochemistry 63 (2018) 12-23

The Fe-V-O system in air was studied experimentally ranging from 700 °C to 1450 °C by high-temperature equilibration, quenching, scanning electron microscope and microprobe analysis. The thermodynamic evaluation was performed with FactSage 7.0. The solubility of V_2O_5(s) in Fe_2O_3(s) was described with the compound energy formalism. The properties of the liquid phase were described with both the quasichemical model and the associate species model. A set of self-consistent thermodynamic parameters were estimated within acceptable error limits. The calculated phase diagram of Fe-V-O in air is presented and compared to experimental observations and other literature data.

Publication ii: W.D. Malan, G. Akdogan, P. Taskinen, J. Hamuyuni, J. Zietsman, Phase equilibria and thermodynamic evaluation of Ti-V-O system in air, CALPHAD: Computer Coupling of Phase Diagrams and Thermochemistry 63 (2018) 220-228

The Ti-V-O system was studied experimentally from 700 °C to 1500 °C by high-temperature equilibration, quenching, scanning electron microscope and Energy-Dispersive X-Ray spectroscopy. The solubility of titanium in the slag is less than 3 mole % at 1500 °C and the vanadium solubility in the rutile phase reached a maximum of 7.8 mole % at 1400 °C. The thermodynamic evaluation was performed with FactSage 7.0. The solubility of vanadium in the rutile phase was developed within the framework of the compound energy formalism. The properties of the liquid phase were described with the quasichemical model. A set of self-consistent thermodynamic parameters was estimated well within acceptable limits. The calculated phase diagram of the Ti-V-O system in air is presented and compared to experimental observations and other phase diagram data from literature.

Publication iii: W.D. Malan, G. Akdogan, P. Taskinen, J. Zietsman, Phase equilibria and thermodynamic evaluation of Fe-Ti-V-O system in air, CALPHAD: Computer Coupling of Phase Diagrams and Thermochemistry, 65 (2019) 141-154

In this study, the iron-titanium-vanadium-oxygen (Fe-Ti-V-O) system in equilibrium with air was studied experimentally by high-temperature equilibration, quenching, scanning electron microscope and microprobe analysis coupled with critical assessment and thermodynamic evaluation. The properties of the liquid phase were successfully described with the quasichemical model by optimizing parameters only related to the Fe-Ti-O system; remaining parameters for the Fe-V-O and Ti-V-O sub-systems were adopted from recent optimisations. The model for the rutile and hematite solid solutions were described with the compound energy formalism. The ferropseudobrookite solid solution was modelled with a simple polynomial model to include a small solubility V_2O_5. A final set of self-consistent thermodynamic parameters was estimated within acceptable error limits. Calculated isothermal projections at 1000 °C, 1100 °C, 1200 °C, 1300 °C, and 1400 °C of the Fe-Ti-V-O system in equilibrium with air are presented and compared to experimental observations.

Dedication

This dissertation is dedicated to the everlasting memory of Reghardt Appel, a best friend never forgotten. 1988/04/20 - 2006/06/23

Acknowledgements

As the author of this dissertation, I would like to thank my chief supervisor, Dr Johan Zietsman for guiding me with his knowledge and infectious enthusiasm throughout the course of the project. Without him the project would not have been possible, because it was he who had identified the shortage of data on vanadium oxide systems in the FactSage database, which encouraged me to investigate these systems. I am greatly impressed by his wide range of knowledge and exceptional wisdom, which became extremely helpful in the event of problem-solving. He always seemed to have the answer or at least guided me in the right direction. He deserves the utmost credit for supporting this project and allowing me to create my own free atmosphere of independent thinking. My communication skills improved significantly under his supervision and this will undoubtedly assist me to become a more successful researcher.. It was an unbelievable honour to have him as my supervisor for my doctoral study and I look forward to continuing and expanding our relationship.

I would also like to thank Prof. Guven Akdogan from Stellenbosch University for his relentless effort and continuous support for the project from the beginning. He believed in my abilities, starting from undergraduate studies, and supervised me through my master's project. I am jubilant and overwhelmed that he was part of my doctoral studies. His expertise and experience in pyrometallurgy were invaluable, and became the backbone for understanding, delivering and interpretation during the experimental part of this project. Moreover, if it had not been for him, I would not have had the opportunity to travel to Finland and carry out my experimental work.

Next, I would like to express gratitude to Prof. Pekka Taskinen at Aalto University, School of Chemical Engineering for making their facilities available to me to carry out experimental work. During my time at Aalto Unviversity he was always willing to assist me when I had questions about my experimental work. He deserves plenty of respect for his professionalism and the manner in which he organised and galvanised everyone under his supervision in the TMS group. It was rewarding to observe how much can be achieved with his structures in place in a relatively small department. My discussions with Dr Rui Zhang from the TMS group regarding thermodynamic modelling were very fruitful.

I would like to thank Dr Joseph Hamuyuni and Dr Dmitry Sukhomlinov, my most influential colleagues at Aalto University. Without their help it would have been impossible to set up an experimental procedure. Moreover, Dr Joseph Hamuyuni's efforts and assistance at the beginning of my experimental work have to be acknowledged. And who can forget our sauna sessions every Tuesday and our ice-fishing excursions on weekends. Those were the best of times during the long and icy Finnish winters, and I will cherish those moments forever.

Next I would like to thank Dr Christian Reinke at the University of Johannesburg for his assistance and cooperation with EPMA work. For SEM-EDS analysis, I would like to thank Lassi Klemettinen for the SEM tutorial lecture and allocating his time to assist me analysing my samples. His notes explaining the correct procedure for SEM-EDS analysis were very useful.

Finland is such a magnificent country and I will forever be grateful to everyone that I met, and befriended there. The exultant times with friends from around the world (Spain, Mexico, Canada, Russia, Portugal etc.) are unforgettable; the bicycle tours to Helsinki, tours to Estonia and Latvia, "braai's"/grills in the cold and the late-night tennis matches in summer.

Last, but not least, I have to acknowledge and thank my parents, who have morally and financially supported me unconditionally. It made it so much easier to complete my doctoral studies successfully.

Contents

List of Figures

List of Tables

Part I

Introduction

Chapter 1

Background

1.1 Project Background

During the extraction and refining of vanadium from titaniferous magnetite concentrates (see Section 1.2), impurities such as iron, silicon, titanium, calcium and aluminium etc. require removal. The separation of vanadium via pyrometallurgical and hydrometallurgical routes takes place through the formation of solid solutions, molten slags (e.g. furnace and shaking ladle slags), molten alloys (pig iron) and aqueous solutions (leaching) predominantly containing iron, silicon, and titanium oxides with appreciable amounts of other impurities, such as CaO, Na_2O, MgO and Al_2O_3 (Steinberg and Geyser 2011). The distribution of vanadium among these phases is dependent on process conditions such as temperature, overall elemental composition and oxygen partial pressure. A smelting process is generally isobaric and carried out under atmospheric pressure, hence the effect of system pressure on equilibrium is negligible compared to other system properties such as temperature, overall elemental composition and oxygen partial pressure (Lee 1999).

Recent trends and developments in experimental and modelling techniques have made it possible to obtain accurate data of many multi-component oxide systems. These techniques include dynamic and static experimental investigations of lower-order systems, followed by employing the calculation of phase diagram (CALPHAD) approach to extrapolate the binary and ternary systems into higher-order systems (Lukas, Fries, and Sundman 2007). This approach has been proven to make accurate predictions of phase equilibria of higher-order systems and has been implemented in computer algorithms (ChemSage) to develop thermochemical software such as FactSage (Bale et al. 2002), MTdata (Davies et al. 2002) and Thermo-Calc (Anderson et al. 2002) capable of estimating phase diagram and thermodynamic properties of many multi-component oxide systems. However, FactSage thermochemical software contains no data of the multi-component oxide systems involving vanadium oxide largely because of the lack and contradiction of experimental data found in the literature. As a result, it was undertaken to critically assess and experimentally investigate the iron-titanium-vanadium-oxygen (Fe-Ti-V-O) system in equilibrium with air, given its significance in the extraction of vanadium from titaniferous magnitite ores

The materials containing any multi-component system are extremely difficult to investigate owing to high experimental temperature, long equilibration and diffusion time and corrosive impact. The result is a lack of empirical knowledge on the phase equilibrium, thermodynamic properties and micro-structure, which largely determine the properties of the final product species for industrial application (Zhang 2016).

Furthermore, the iron-vanadium-oxygen (Fe-V-O) system has raised interest in understanding the corrosion mechanism of the vanadium based resistant steels, the processes in the treatment of vanadium containing metallurgical slag and from thermal power plants. The low melting point of vanadium pentoxide oxide, which can form liquids down to 650 °C, contributes to the destruction of protective oxide layers. For these reasons, a number of studies have investigated phase equilibria

of the Fe-V-O system in air (Burdese 1957; Kerby and Wilson 1973; Fotiev, Cheshnitskii, and Surat 1983; Walczak et al. 1985). Some authors have also attempted to study the Fe-V-O system at intermediate oxygen partial pressures, given that iron, titanium and vanadium have multiple oxidation states (Fotiev, Surat, and Tretyakov 1980; Petric and Jacob 1982; Kumar and Jacob 1987; Volkov 1980; Batalin and Zinewich 1988; Raghavan 1989).

Fewer studies have investigated phase equilibria of titanium-vanadium-oxygen (Ti-V-O) in air and at lower oxygen partial pressures (Solacolu and Zaharescu 1972; Fotiev, Surat, and Tret'yakov 1981; Coetsee and Pretorius 2000; Habel et al. 2006; Habel et al. 2008; Hiroi et al. 2013). Nevertheless, applications of the Ti−V−O system under oxidizing conditions were reported by numerous studies (Vejux and Courtine 1978; Bond, Sarkany, and Parfitt 1979; Habel et al. 2006; Habel et al. 2008). One such application of the Ti-V-O system under oxidising conditions concerns its effect as supportive promoter for catalysis during the selective oxidation of butadiene, 1-butene, and benzene to maleic anhydride, and of naphtalene and o-oxylene to phthalic anhydride (Vejux and Courtine 1978). A better knowledge of phase relations assists in identifying appropriate processing conditions and to understand the ageing phenomena of catalysts (Habel et al. 2006).

1.2 Industry Background

1.2.1 Sources and Applications of Vanadium

The Republic of South Africa (RSA) is one of the leading suppliers of vanadium (V) and the strategic metal is mostly found in titaniferous magnetite ores, which are mostly contained in the Bushveld complex, one of the world' largest mafic intrusives. The ore has an average of 1.5 wt. % vanadium pentoxide (V_2O_5) and is contained within seams that can be traced for a strike approaching 325 km. The titanium (Ti) and vanadium in the ore are present mainly as a solid solution in the titanium-rich magnetite phase, otherwise known as ulvospinel (Fe_2TiO_5). In the magnetite-ulvospinel, the Fe^{3+} cations are replaced by V^{3+} cations (Rhohrmann 1985).

The reserves of the RSA are estimated to be 12.5 million tonnes of contained vanadium. At present this is known as the largest vanadium reserves in the world. The reserves in China and Russia follow closely. Vanadium is widely distributed among other minerals of which the most important are carnotite ($K_2(UO_2)_2(VO_4)_2.3H_2O$), roscoelite ($K(M)_2AlSi_3O_{10}(OH)_2$ where $M = V^{3+}$, Al, Mg), vanadinite ($Pb_5(VO_4)_3Cl$), mottramite ($PbCu(VO_4)(OH)$), and patronite (VS_4) (Moskalyk and Alfantazi 2003).

The majority of the world's vanadium is produced in the Republic of South Africa, Russia and China. Some major vanadium-producing companies in the RSA include, Highveld Steel and Vanadium Corporation Ltd, Rhombus Vanadium Ltd (Rhovan), Vametco Minerals Corp. and Vanadium Technologies (PTY) Ltd (Vantech). Vanadium's attributes of high tensile strength, rust resistance and hardness make it useful to form alloys such as nickel/vanadium, chrome/vanadium and ferrovanadium. About 85 % of vanadium consumption arises from the production of high-strength and low-alloy steels in conjunction with tool and die steels. About 10 % is employed in the aerospace industry, which requires titanium-aluminium alloys, while the remainder is used in the chemical industry. For example, vanadium pentoxide is used as catalyst for conversion of sulphur dioxide to trioxide when producing sulphuric acid and maleic anhydride (Moskalyk and Alfantazi 2003).

Vanadium is never found in its pure form and is extracted from primary sources such as ores, concentrates, metallurgical slags, and petroleum residues (Reese 2001). Vanadium is mostly recovered as pure vanadium, pure vanadium pentoxide or ferrovanadium from secondary production. This implies that vanadium is generated from iron and steel manufacture, or as co-product from uranium production and recycling. Pure vanadium is difficult to produce, since it is easily contaminated by many other elements. Processes to extract the pure metal include (Moskalyk and Alfantazi 2003):

- Calcium reduction
- Thermal decomposition
- Solvent extraction
- Electrolyte refining.

1.2.2 Vanadium Pentoxide Extraction via a Pyrometallurgical Route

In South Africa, vanadium pentoxide is extracted in viscous slag form from titaniferous ores via a pyrometallurgical route, followed by hydro-metallurgical extraction of vanadium pentoxide to its pure form. Figure 1.1 is a flow sheet for the production of vanadium pentoxide at Evraz Highveld Steel. The process is briefly explained. Typical compositions and block flow diagrams are given to identify and support the industrial significance of the research topic.

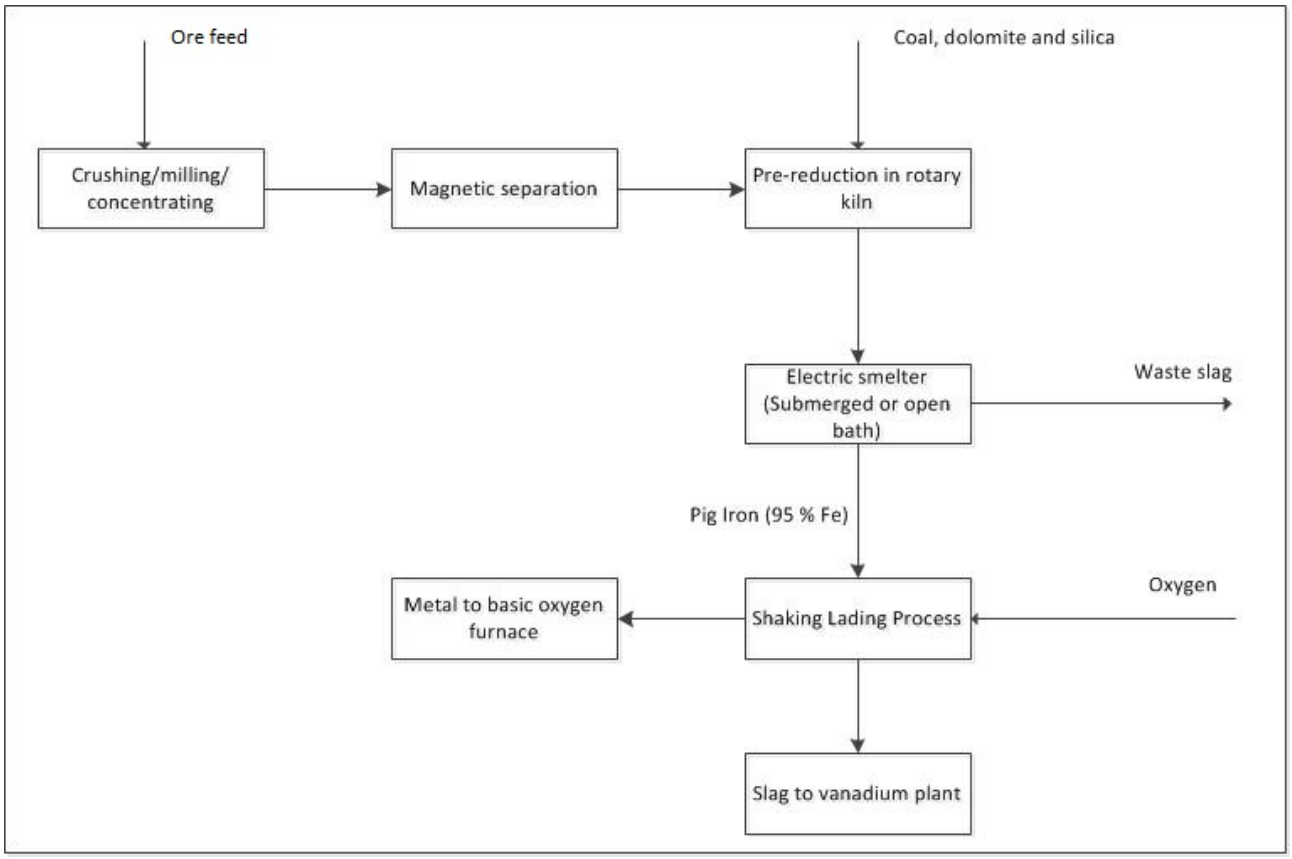

Figure 1.1: The Highveld Steel and Vanadium Process - Vanadium products flow - V_2O_5 extraction via a pyrometallurgical extraction route (Redrawn from (Perron 2001))

Referring to Figure 1.1, the Bushveld titnaniferous magnetite ore is concentrated in a series of crushing and magnetic separation steps. Thereafter, the magnetic particles are crushed and screened and sent to the pelletising plant. Because of the high titanium dioxide content of this concentrate, conventional blast furnace technology cannot be used, as it poses a risk of blocking the hearth and tuyeres with refractory titanium carbide (Steinberg and Geyser 2011; Taylor et al. 2005). Table 1.1 gives the typical composition of a magnetite concentrate used at Evraz Highveld Steel.

Table 1.1: Typical composition in weight % of the magnetite charge used at Evraz Highveld Steel (Steinberg and Geyser 2011).

Fe(t)	FeO	Fe_2O_3	SiO_2	Al_2O_3	MgO	CaO	MnO	V_2O_5	Cr_2O_3	TiO_2
54.80	16.50	60.00	2.00	4.80	1.60	0.10	0.30	1.65	0.40	12.70

Coal, dolomite, and quartz are added to the magnetite concentrate for charge to the pre-reduction rotary kiln. The purpose of the kilns is to pre-reduce the magnetite concentrate by using an inexpensive form of energy in the form of pulverised coal, injected through a continuous burner at the feed end. Solid-gas reduction occurs at a temperature of $+/-$ 1140 °C. The solid state pre-reduced charge is fed into a submerged arc furnace, where it is heated to a temperature of 1340 °C. Carbon is added to control fluidity and iron reduction. The denser alloy phase known as pig iron separates from the titanium-rich slag, which is drawn off at the start of tapping (Steinberg and Geyser 2011; Taylor et al. 2005). Table 1.2 and Table 1.3 give typical compositions of pig iron and slag produced at Evraz Highveld Steel.

Table 1.2: Typical composition of pig iron in weight % at Evraz Highveld Steel (Steinberg and Geyser 2011).

Ti	Fe	Si	Mn	V	Cr	C
0.20	94.50	0.20	0.20	1.29	0.34	3.20

Table 1.3: Typical composition of slag in weight % tapped at Evraz Highveld Steel (Steinberg and Geyser 2011).

TiO_2	FeO	SiO_2	Al_2O_3	MgO	CaO	MnO	V_2O_5	Cr_2O_3
35.60	1.00	16.20	18.00	14.10	14.10	0.40	0.90	0.20

The slag is crushed, and entrained metal prills are recovered by magnetic separation and recycled through the process again. The pig iron, which has a vanadium concentration of 1.20%, is transferred to the steel plant for further processing. The vanadium in the liquid metal needs to be transferred to a slag and this is done through a shaking ladle process. The shaking ladle follows a soft oxygen blowing practice where the following reactions take place at a temperature below 1400 °C (Steinberg and Geyser 2011; Rhohrmann 1985):

$$2\,\mathrm{V(l)} + \tfrac{3}{2}\,\mathrm{O_2(g)} \longrightarrow \mathrm{V_2O_3(l)} \tag{1.1}$$

$$\mathrm{Fe(l)} + \tfrac{1}{2}\,\mathrm{O_2(g)} \longrightarrow \mathrm{FeO(l)} \tag{1.2}$$

$$2\,\mathrm{V(l)} + 3\,\mathrm{FeO(l)} \longrightarrow 3\,\mathrm{Fe(l)} + \mathrm{V_2O_3(l)}. \tag{1.3}$$

Although vanadium, carbon (C), silicon (Si), titanium, manganese (Mn) and chrome (Cr) have a higher affinity for oxygen than iron, most of the oxygen blown will react with iron (Fe). This will be followed by the reaction of FeO with silicon, titanium, manganese, vanadium and chrome in the hot metal to form soluble oxides. Scrap and iron ore are used as coolant and also to increase FeO activity in the slag, which will promote the oxidation of vanadium from the metal. Anthracite is used to replace the carbon that is unintentionally oxidised to carbon monoxide and carbon dioxide. Since the temperature of the slag is below the liquidus temperature, the slag has the characteristics of a viscous paste. The liquidus phase is a vanadium-bearing spinel belonging to the $Fe_3O_4{-}FeV_2O_4$ solid-solution series. The vanadium recovery in such a blowing process is between 90 and 92 % (Steinberg and Geyser 2011; Rhohrmann 1985). A typical shaking ladle slag composition is given in Table 1.4.

Table 1.4: Typical shaking ladle slag composition in weight % at Evraz Highveld Steel (Steinberg and Geyser 2011).

FeO	V_2O_5	CaO	MgO	SiO_2	Al_2O_3	TiO_2	Cr_2O_3	MnO
29.00	24.00	5.00	4.00	15.00	5.00	9.00	5.00	3.00

1.2.3 Pure Vanadium Extraction via a Hydrometallurgical Route

The slag from the shaking ladle process is treated in a slag vanadium plant (see Figure 1.2, where it is blended with a magnetite concentrate and sodium carbonate flux, followed by roasting in a coal-fired kiln. The calcine product is conveyed to one of three leach dams that are used to recover the vanadium-bearing solution. Barren solid residue is mechanically scraped from the dams and conveyed to the calcine stockpile. To remove silica from the solution, aluminum sulphate is added, followed by filtration. Ammonium metavanadate is precipitated from the clean pregnant solution by adding ammonium sulphate, followed by filtration. The ammonia is removed in two electric kilns to form vanadium pentoxide powder, which in turn is melted in an electric furnace to form vanadium pentoxide flakes. Next, vanadium pentoxide is exothermically converted to ferrovanadium ingots and an alumina slag by adding aluminium, iron and lime (Moskalyk and Alfantazi 2003).

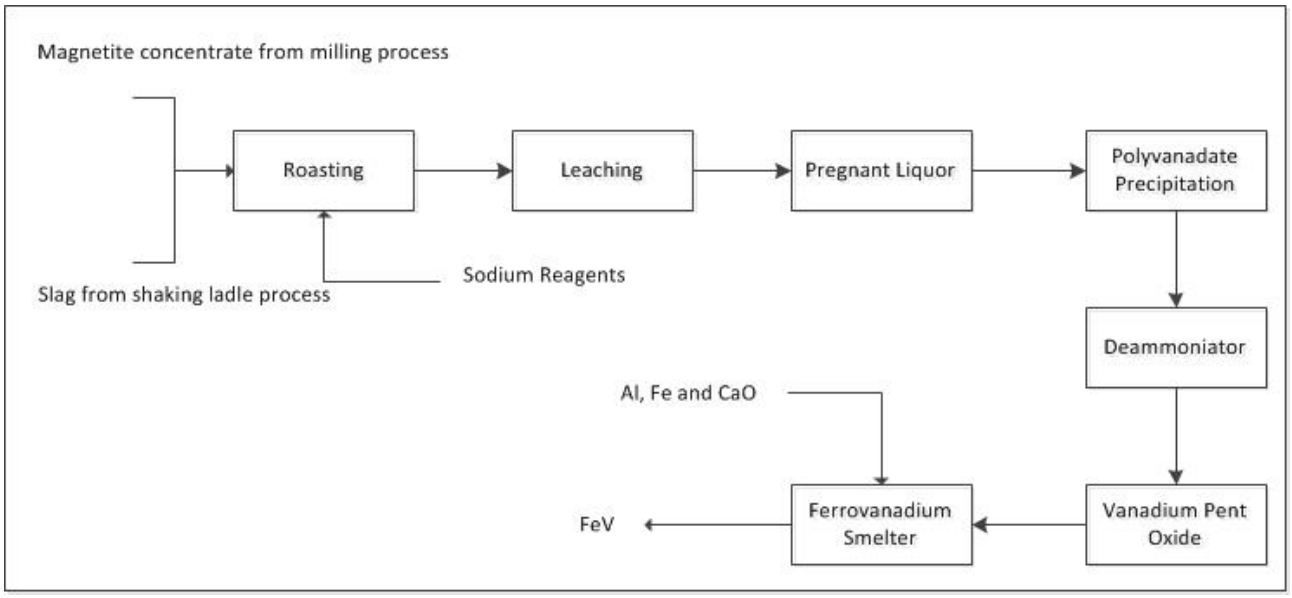

Figure 1.2: The Highveld Steel and Vanadium Process - Pure vanadium extraction via a hydrometallurgical extraction route (Redrawn from (Perron 2001))

1.3 Theoretical Background

1.3.1 Criteria for Chemical Equilibrium

The analysis of chemical reactions forms the central part of any chemical/metallurgical engineering environment. There is an infinite possibility of arrangements of chemical bonds between elements to form molecules. The main idea associated with applying equilibrium analysis to chemical reactions is to determine the extent to which products are favoured from a specified elemental composition, temperature and pressure. In other words, thermodynamics indicates if a given reaction will proceed and if so, how far it will proceed (Koretsky 2004).

During the extraction and reduction of any concentrate or ore at high temperatures where chemical reactions proceed fast and are not constrained by the reaction rate, the final product is a combination of product species with the lowest Gibbs energy from a reactant input. A combination of the first and second laws of thermodynamics attributes the following behaviour to a closed system (Lee 1999; Koretsky 2004).

$$0 \geq (dG_i)_{T,P}. \tag{1.4}$$

Thus, according to Equation 1.4, the Gibbs energy always decreases (or stays the same) in any isobaric and isothermal spontaneous process. In other words, at equilibrium the Gibbs energy is minimised and no property changes can occur any more. This approach is very useful for developing Gibbs minimisation algorithms such as FactSage to solve reactions for complex systems. Some fundamental equations for the solution of multiple reaction equilibria by minimisation of Gibbs energy are presented and described (Eriksson 1971; Eriksson and Hack 1990; Koretsky 2004; Lukas, Fries, and Sundman 2007):

$$\sum_{i=1}^{m} n_i \beta_{ij} = b_j. \tag{1.5}$$

In Equation 1.5, β_{ij} is known as the formula coefficient. The matrix relates the j elements, b_j, in a system to the species i. The molar Gibbs energy of the system is now given by Equation 1.6.

$$G_m = \sum_{i=1}^{m} \mu_i n_i. \tag{1.6}$$

A new function, Equation 1.7 is defined with the introduction of the Langrangian multipliers, λ_j.

$$G'_m = \sum_{i=1}^{m} \mu_i n_i + \sum_{j=1}^{l} \lambda_j (\sum_{i=1}^{m} n_i \beta_{ij} - b_j). \tag{1.7}$$

Inspection of Equation 1.5 reveals that the term that was added in Equation 1.7 must be zero. Therefore, the problem shifts back to minimisation of G'_m. To find the composition at which the function is a minimum, the derivative with respect to n_i, is set to zero:

$$\frac{\delta G'_m}{\delta n_i} = 0 = \mu_i + \sum_{j=1}^{l} \lambda_j \beta_{ij}. \tag{1.8}$$

Equation 1.8 is followed by replacing the chemical potential, μ_i, with the phase-appropriate expression:

$$G_i^{\circ} + RTlna_i + \sum_{j=1}^{l} \lambda_j \beta_{ij} = 0. \tag{1.9}$$

It is now possible to substitute the Gibbs energy of formation for the standard-state Gibbs energy of species i in Equation 1.9, followed by writing one equation for every species in the system. Thus, Equation 1.10 is obtained:

$$\Delta G_i^f + RTlna_i + \sum_{j=1}^{l} \lambda_j \beta_{ij} = 0. \tag{1.10}$$

Equation 1.5 and Equation 1.10 represent a set of $m + l$ equations that can be solved for the unknown mole fractions and λ_j. Such a set of equations can be solved simultaneously with

a computer algorithm, which typically employs a modified Newton-Raphson root finder. Solution models have been developed to describe the behaviour of constituents in non-ideal solutions (see Section 6.3) and can subsequently be used to develop expressions for a_i.

Furthermore, mathematical methods (see Bale et al. (2002), Bale et al. (2009), and Bale et al. (2016) are used to derive more information from the Gibbs energy (of phase(s) or whole systems) as depicted in Figure 1.3.

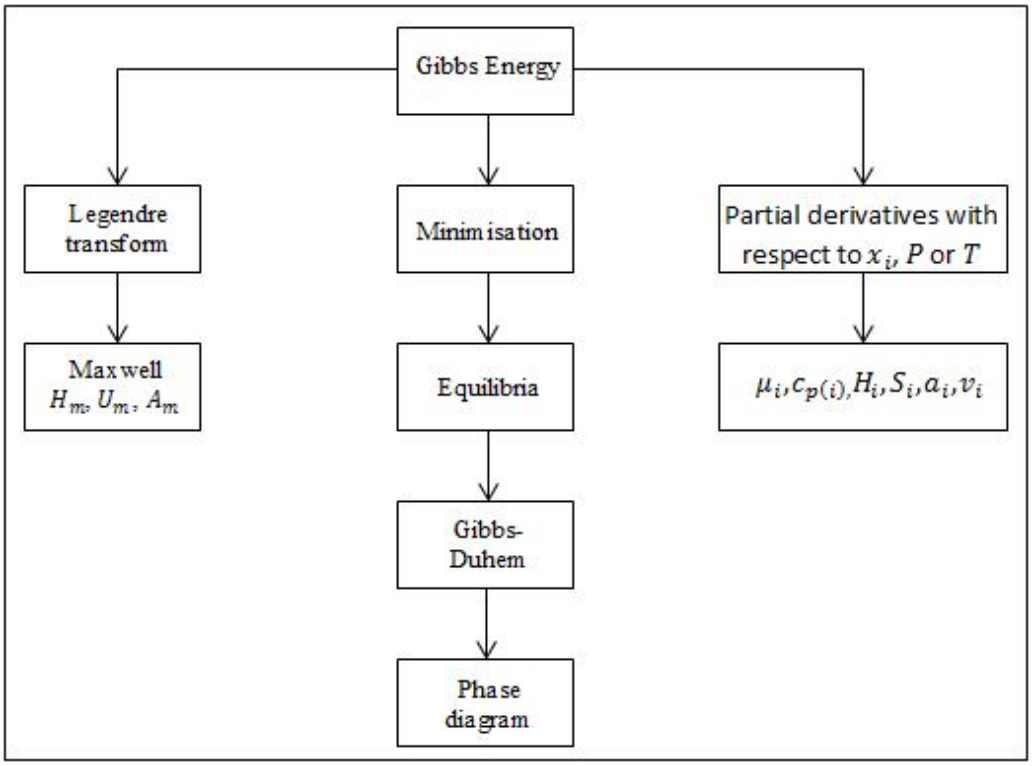

Figure 1.3: The Gibbs Energy tree - Redrawn from Bale et al. (2002).

1.3.2 Development and Application of Computer Algorithms

The ChemSage program, based on the SOLGASMIX Gibbs energy minimiser (Eriksson 1971; Eriksson and E.Rosen 1973; Eriksson and Rosen 1984), was developed to conduct three types of thermochemical calculations involving phases that have non-ideal mixing properties.

Figure 1.4 presents a network of steps for the calculation of thermodynamic functions, heterogeneous phase equilibria, and steady-state conditions for the simulation of simple multistage reactors. The thermodynamic functions module calculates specific heat, enthalpy, entropy, and Gibbs energy with respect to a chosen reference state for a given phase and, if this phase is a mixture, the partial properties of its components. Chemical equilibrium calculations can be made for a system that was specifically defined with respect to temperature, pressure (or volume), and composition. Furthermore, it is possible to replace one of these quantities with an extensive property or phase target, for the calculation of adiabatic, liquidus and solidus temperatures and compositions (Eriksson and Hack 1990).

With recent developments in these advanced computational modelling techniques, otherwise known as the CALPHAD technique, it is now possible to create a complete and accurate database capable of describing complex multi-component systems. Subsequently, FACT-Win (formerly F*A*C*T)) and ChemSage (formerly SOLGASMIX) were merged into one unified package in 2001 and became known as FactSage. The latter was developed by Bale et al. (2002) and employs the Gibbs energy minimisation algorithm for treating complex heterogeneous equilibrium using compound and solution

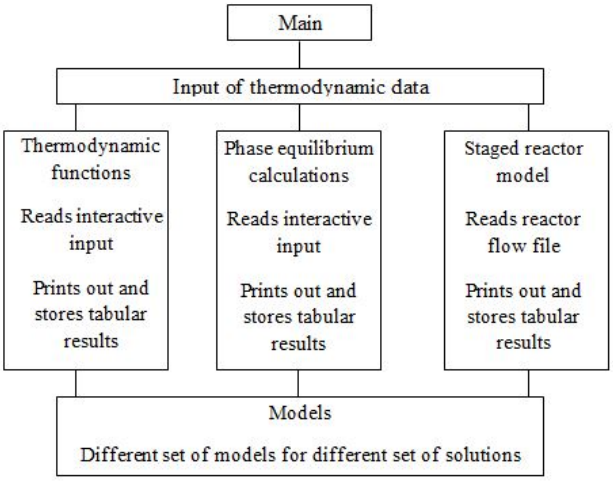

Figure 1.4: Structure sheet with major blocks of ChemSage (Redrawn from Eriksson and Hack (1990))

databases. These databases were created from experimental data and thermodynamic models using sophisticated optimization algorithms such as the PARROT module in the Thermo-Calc software package or OPTISAGE module in FactSage. Most of the experimental data used are quantitatively related to the thermodynamic functions, therefore availability and accuracy of the experimental measurements have a significant influence on the quality of thermodynamic parameters in the database (Zhang 2016).

Chapter 2

Research Definition

2.1 Problem Statement

Detailed information about phase equilibria (e.g. liquidus temperatures) of the V-Al-Ca-Fe-Na-Ti-Si-O system, especially in high temperature processes where reactions take place fast, is essential to understand how vanadium distributes among phases. Thermochemical software such as FactSage exists to estimate phase equilibria for various feed compositions and temperature ranges. However, FactSage contains no data of the multi-component oxide systems involving vanadium oxide owing to the lack and contradictions of experimental data from the literature pertaining to the vanadium-containing oxide systems.

Although previous studies have been conducted on the Fe-Ti-V-O system (see Chapter 5), most were done with dynamic equilibration techniques (e.g. differential scanning calorimetry (DSC), differential thermal analysis (DTA), thermogravimetric analysis (TGA)), of which the recording accuracy relies heavily on a system with fast phase change. Many oxide systems have sluggish transport kinetics and consequently, dynamic techniques can sometimes produce spurious results. This is due to the sample not being at equilibrium due to the dynamic nature of the techniques. The equilibration-quench analysis experimental technique that was used in this study is static by nature and emulates a system that is near or at equilibrium (see Chapter 7).

Knowing that the problem at question can be addressed by a static equilibrium approach where equilibrium is preserved, a large number of static experiments were carried out to characterise phase assemblages and study phase transformation on the Fe-Ti-V-O system in air.

2.2 Research Purpose

The purpose of this study was to develop a set of model equations for Gibbs energies of all phases and compounds of the Fe-Ti-V-O system in air as a function of temperature, composition and to some degree, $\mathrm{pO_2}$, using phase equilibria results obtained from the equilibration-quench analysis experimental technique. An additional purpose of this project is to inform fellow researchers from metallurgical departments across South Africa how to employ an equilibration/quench/analysis technique, and conduct a thermodynamic evaluation. Therefore, this document is purposely written with the intention to serve as a hierarchy for inexperienced assessors in order to avoid common mistakes and minimise research time.

2.3 Research Objectives

The main research objectives of this study are summarised as follows:

- Investigate high-temperature vanadium extraction processes and identify areas of uncertainty where thermodynamic data are required. An example is the shaking ladle process at Evraz Highveld Steel where a highly viscous vanadium-rich slag is produced under oxidising conditions (see Section 1.2).
- Establish a set of experimental procedures to study liquidus and solidus compositions of the Fe-Ti-V-O system in air at fixed temperatures.
- Measure the effect of major experimental parameters such as composition and temperature on the formation of compounds and solution phases at equilibrium.
- To characterise and quantify all phases produced from phase equilibria experiments using a scanning electron microscope (SEM) and the electron probe micron-analyser (EPMA).
- The experimental results of this study are compared with results from previous studies to resolve contradictions and uncertainties.
- Optimise thermodynamic excess Gibbs model parameters and other thermodynamic properties, followed by back-calculating phase diagrams using the CALPHAD method to validate solution models. In this way, all the data are rendered self-consistent and consistent with thermodynamic principles.

2.4 Research Scope

In this study, the Fe-Ti-V-O system was experimentally studied to quantify liquidus composition, identify intermediate species and possible solid solutions in equilibrium with air. However, it is known that the oxygen partial pressure has a significant effect on phase equilibrium owing to multiple oxidation states of Fe, Ti and V. For this reason, the $\mathrm{pO_2}$ was fixed to adhere to equilibrium conditions pertaining to the Fe-Ti-V-O system in air.

A thermodynamic evaluation was carried on the basis of experimental results. Moreover, many thermodynamic models for describing slags are available in the literature to determine thermodynamic properties such as activities, heat capacities, enthalpy of a mixture, phase transition temperatures etc. However, only the MQM and ASM were used to describe the slag phase of the Fe-Ti-V-O system in air.

2.5 Research Approach

The flowchart in Figure 2.1 graphically presents a broad, but simple research design.

Initially, a critical assessment of the literature had identified gaps, shortcomings and contradictions from previous experimental studies of the Fe-Ti-V-O system in air. The literature survey was coupled with model identification for a description of solution phases. A critical assessment of the literature was succeeded by static equilibration experiments. Samples were viewed with SEM, and analysed with EPMA and energy dispersive spectrometry (EDS). Phase homogeneity was used as the main criterion to confirm equilibrium.

Liquidus and solidus data from this study and other studies were used to optimise excess Gibbs model parameters and other thermodynamic properties. A set of model equations for all compounds and solutions was obtained for the Fe-Ti-V-O system in air, and stored in a FactSage customised database. From the database, thermodynamic properties and phase diagram data were calculated, and compared to experimental data from this study and from the literature (where available).

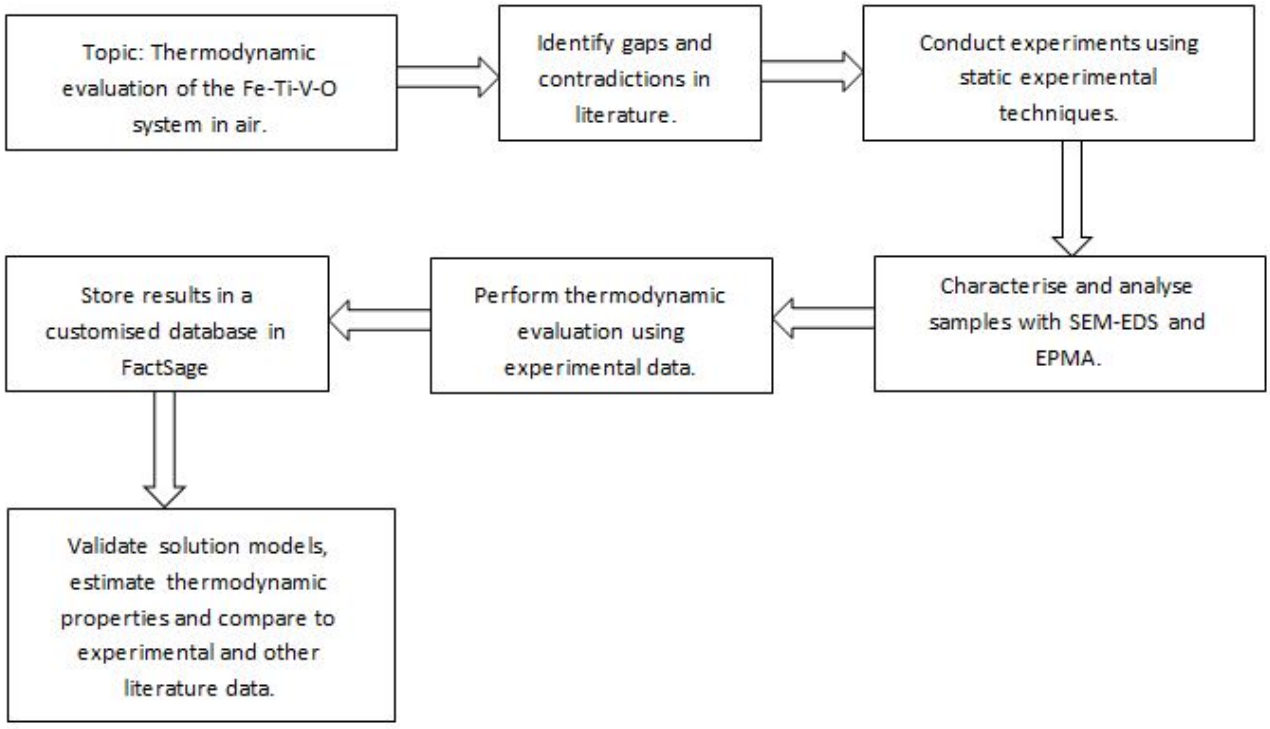

Figure 2.1: A simple project design schematic showing interaction among the most important steps followed to complete this study successfully. Each step was treated as an individual sub-project.

2.6 Thesis Layout

This dissertation is divided into five parts, a appendix and a list of references. A summary of each part follows briefly.

- Part I contains an introduction explaining the background of vanadium refining, the purpose and scope of this study, and approach to the project. Along with this, it also contains the primary objectives of the study, significance of the study and reasons why it will be relevant.
- Part II contains a the literature study into previous work of the Fe-Ti-V-O system in air and describes thermodynamic models to be used in the assessment. It also includes a description of the thermodynamic assessment methodology.
- Part III describes the experimental procedure and thermodynamic modelling methodology.
- Part IV discusses the experimental and thermodynamic assessment results.
- Part V contains a conclusion and a recommendation on future work.
- Part VII contains references used in the thesis.
- Appendix A contains additional graphs and tables from analytical results
- Appendix B contains additional thermodynamic data of all compounds in the Fe-Ti-V-O system under oxidising conditions.
- Appendix C contains a working example of SOLUTION and the OPTISAGE module in FactSage.

Part II

Literature Review

Overview

Purpose of the Review

The main purpose of the literature review was to gather as much information as possible on the system of interest, which included phase diagram and other thermodynamic data. An accumulation of a wide variety of data was necessary to execute a thermodynamic evaluation successfully with well-established modelling and optimisation techniques. The knowledge gained from the survey could also be used in the future to evaluate other systems containing vanadium oxide successfully.

Organisation of the Review

The survey is divided into the following chapters:

- Chapter 3 contains a brief introduction of predictive thermochemistry and how it relates to pyrometallurgical processes.
- Chapter 4 is an investigation of the well-known Fe-O, Ti-O and V-O systems. An inspection of pure metal oxide systems gave an initial indication of which compounds are stable under oxidising conditions.
- In Chapter 5 all previous studies of the Fe-Ti-V-O system that were found are scrutinized to identify gaps and shortcomings. This is followed by a summary of the main findings, which attempts to support the objectives of this study.
- In Chapter 6, the fundamental principles of the CALPHAD technique and some important Gibbs energy equations to describe compounds and solutions are delineated. An assessment methodology how to execute a thermodynamic evaluation successfully is chronologically summarised.
- Chapter 7 briefly looks at dynamic equilibration techniques, followed by a description on the application of static equilibration techniques to binary and ternary systems.

Chapter 3

Introduction to Literature Survey

When investigating reactions in a thermodynamically constrained system, there are three variables that serve as control parameters, namely, pressure, temperature and composition. The stability of phases in a system is thereby governed by these three variables. The relationship among these variables is best described graphically using phase diagrams; however acquiring information of materials and their respective phase diagrams have been challenging. The equilibrium paradigm (see next section) has led to the development of many methods to accurately acquire phase equilibrium information for many systems (Lee 1999; Hamuyuni 2016).

The evolution of these methods have made it possible to implement reliable equilibrium data into computer databases to study thermochemical behaviour of multicomponent systems as a function of temperature, pressure and composition (Zhang 2016). Moreover, it is discussed in this chapter that the thermochemical behaviour of multicomponent systems can be estimated successfully from interpolation and extrapolation of information from lower-order systems.

3.1 The Equilibrium Paradigm

There is an abundance of literature embracing binary, ternary, quaternary, quinary, senary and even higher-order oxide systems at atmospheric pressure and high temperatures. These systems have been investigated with profound emphasis on the effect of temperature, composition and $\mathrm{pO_2}$ on the formation of stoichiometric compounds, solid solutions, slags and a gas phase. Processes for pyrometallurgical extraction of metals from their ores inevitably involve several chemical constituents and solution phases. These separation processes take place in furnaces at elevated temperatures where mass and heat transfer are fast. These regimes where interaction between reactants takes place are known to be thermodynamically controlled; however transport kinetics can still have a significant influence, simply due to furnace geometry and other factors, such as slag-matte/alloy surface tension, slag viscosity and liquid density (Habashi 1997; Koretsky 2004).

On the contrary, processes at lower temperatures are said to be reaction-rate controlled, since reaction rates are generally characterised by an exponential dependence on temperature as given by the Arrhenius expression (Fogler 2006). Pyrometallurgical processes are very seldom reaction rate constrained/controlled in areas where good interaction between reactants occur, therefore valuable insight and understanding of a process are obtained if it is assumed to be at equilibrium or at the very least, in a state of quasi-equilibrium (Habashi 1997; Koretsky 2004).

A good example of a thermodynamically controlled process is the carbothermic reduction of iron oxide from a raw concentrate feed to pig iron form in an arc furnace. The reduction process includes a gas, two liquid phases (slag and alloy) as well as a selection of crystalline phases. Valuable process parameters such as slag and alloy liquidus temperatures, activities and distribution of chemical constituents in the phases, gas composition, energy requirements etc., are predominantly calculated on the basis of the assumption of equilibrium. For instance, it is therefore globally recognised

that the various aspects of slags - including its formation, chemistry, removal and separation of valuable (e.g. metal) and less valuable phases (e.g. slag) from one another - are critical process parameters. The mixing of chemical constituents in slags and other phases rarely behave ideally and as a result, thermochemical modelling of the partition of components between phases has hitherto been undertaken mainly for individual processes and limited ranges of temperature, composition and in some systems, depending on the valence stability of an element, $\mathrm{pO_2}$. However, this approach, although useful, has limitations because it prevents the development of a consistent database that can allow knowledge to be extended from one range of slag compositions to another (Barry, Dinsdale, and Gisby 1993; Gisby et al. 2002).

Nevertheless, many studies have attempted to understand and critically assess thermodynamic properties of oxide compounds and solutions that can be extended to multiple processes through database development. For example, the well-recognised Ellingham diagram has been developed to present the variation of standard Gibbs free energy as a function of temperature in graphical from. The nature of the diagram is such that standard Gibbs free energy has a linear relationship with temperature (A + BT) between discontinuity points. At that point on the diagram, phase change occurs of a specie involved in the formation reaction. The diagram describes the relative stability ranges of compounds as function of $\mathrm{pO_2}$ and $\mathrm{CO/CO_2}$ ratio. In addition, the most stable compound is found at the bottom of the diagram, while the least stable oxide compound is found at top of the diagram. That said, the relative stability ranges of oxide compounds are easy distinguishable. Moreover, the diagram gives an indication of which element has a greater affinity for oxygen, which is instrumental for reduction purposes. To put these into perspective, the Ellingham diagram has three main uses (Lee 1999):

1. Determine the relative ease of reducing a given metallic oxide to metal. Reactions closer to the top of the diagram are the most noble metal, and their oxides are unstable and easily reduced. The metals at the bottom part of the diagram are more reactive and their oxides become harder to reduce.

2. Determine the partial pressure of oxygen that is in equilibrium with a metal oxide at a given temperature. The significance of this is that if the oxygen partial pressure is higher than the equilibrium $\mathrm{pO_2}$, the metal will not be reduced, however if the $\mathrm{pO_2}$ is lower than the equilibrium $\mathrm{pO_2}$, the metal will be reduced. The $\mathrm{pO_2}$ is found on the right hand side of the diagram.

3. Determine $\mathrm{CO/CO_2}$ ratio that is required to reduce the oxide to metal at a given temperature. The harder the oxide is to reduce, the greater the proportion of CO needed in the gas.

Although the diagram is useful for making predictions of pure compounds, it does accurately account for solutions. The nature of oxide compounds is that they are rarely found in a pure state and more often in solid or liquid solutions. A few solutions that are present during vanadium extraction from titaniferous magnitite concentrates are given in Table 3.1. The treatment, processing and extraction of valuable metals from a cluster of oxide compounds in solution will normally involve conversion from one solution to another at different process stages. The treatment of titaniferous magnitite concentrates at the smelting stage essentially involves the extraction of vanadium from spinel solid solution to an alloy through carbothermic reduction, followed by the oxidation of vanadium, and deportation to a slag phase in the shaking ladle process. The formation and stability of oxide solutions are mainly dependent on composition, temperature and $\mathrm{pO_2}$ (Steinberg and Geyser 2011; Lukas, Fries, and Sundman 2007).

Thermochemical software such as FactSage has the ability to estimate equilibrium of many oxide systems as a function of composition, temperature and $\mathrm{pO_2}$ accurately (see Subsection 1.3.1), given that it has the largest set of evaluated and optimised thermodynamic databases for inorganic systems in the world. The solution databases (for solutions of oxides, salts, metals, etc.) have

Table 3.1: Examples of oxide solutions. Crystallographic and physical property data acquired from Smyth (1997).

Solution	Crystal Structure	Space Group	Stoichiometric chemical formula
Slag	N/A	N/A	AxOy−AxBy−BxOy
Spinel	fcc	$FD3m$	AB_2O_4
Monoxide	Rocksalt	$FD3m$	AO
Corundum	Corundum Structure	R3c	A_2O_3
Olivine	Orthorhombic	$Pbnm$	A_2SiO_4
Melilite	Tetragonal	$P42_1m$	$A_2BSi_2O_7$
Pyroxenes	ortho, proto, clino-, and low clino	$Pbca$ and $C2/c$	$ABSi_2O_6$

all been developed by evaluation and optimisation obtained from the literature. These FactSage thermodynamic databases such as FToxid, FTSalt, FTmisc etc. are developed as follows (Bale et al. 2002; Bale et al. 2009; Bale et al. 2016):

1. A mathematical model for $\mathrm{G_m}$ (T, P, composition) is identified and developed for each phase (see Chapter 6).
2. The model parameters are optimised simultaneously by using all available thermodynamic and phase equilibria data from the literature (see Section 6.8).
3. The models and database are used to estimate properties of multicomponent systems.
4. Through the minimisation of Gibbs energy, thermodynamic properties and phase equilibria are calculated (see for example Section 10.3).

As mentioned before, these databases in FactSage contains no data on vanadium oxide solutions, therefore equilibrium can not be estimated accurately for the pyrometallurgical extraction of vanadium oxide from titaniferous magnitite concentrates. However, the Ftoxid database can be expanded easily to include vanadium oxide knowing that similar experimental and modelling methods can be followed that were used to include data of other major oxide components in the Ftoxid database.

3.2 Structuring the Survey

One's understanding of the extraction and refining of vanadium from titaniferous magnitite concentrates depends greatly on equilibrium data obtained from experimental investigations, and thermodynamic assessments of lower order systems. It was mentioned in Section 2.4 that this study is limited to the Fe-Ti-V-O system under oxidising conditions, therefore the survey is limited to information related to this system.

Before the system was wholly investigated, knowledge of the Fe-O, Ti-O and V-O unary oxide systems was required, because Fe, Ti and V have multiple oxidation states. The unary oxide systems have been the subject of many previous investigations (see Chapter 4) and many compounds and solutions have been reported at various temperatures and oxygen partial pressures.

Thereafter, a survey on the Fe-V-O, Ti-V-O and Fe-Ti-O systems under oxidising conditions was conducted to acquire phase diagram data, and other thermodynamic properties (see Chapter 5). Finally, any reported data of the Fe-Ti-V-O system under oxidising conditions were taken into consideration before experiments in the Fe-Ti-V-O system in equilibrium with air were conducted. Discrepancies in results from past studies are carefully scrutinised and discussed. The order of the critical assessment of the Fe-Ti-V-O system under oxidising conditions is the accepted order from

Lukas, Fries, and Sundman (2007), who reported that any investigated multi-component system should always start from investigations of unary and binary systems.

Chapter 4

M-O Systems

In this chapter, the V-O, Ti-O and Fe-O systems are briefly discussed because it is well-known that Fe, Ti, V have two, three and four oxidation states, respectively. Because of the multiple oxidation states of Fe, Ti and V, a substantial number of stable compounds and solid solutions exist over a wide range of oxygen partial pressures. The thermodynamically assessed V-O, Ti-O and Fe-O systems give an early indication of stable and metastable compounds and solutions in the temperature range of this study. Moreover, it is likely that the same thermodynamic models can be used to describe solutions of the Fe-Ti-V-O system in air. The models that were used in the thermodynamic assessment of the respective systems are mentioned here, but are comprehensively discussed in Chapter 6.

4.1 The V-O System

4.1.1 Stable Compounds and Phases

It is well known, that V has four oxidation states, namely, V^{2+} V^{3+} V^{4+} and V^{5+}. The complexity of the V-O system due to its numerous phases has led to controversial findings. A literature review was carried out by Alcock and Ji (1990) and Wriedt (1989). The equilibrium solid phases in the V-O system, according to Wriedt (1989), are: α (body-centred cubic), β (body-centred tetragonal), γ (monoclinic), δ (face-centred cubic i.e. halite), δ' (body-centred tetragonal), i.e. $V_{52}O_{64}$, V_2O_3 (corrundum), V_3O_5 monoclinic, Magneli phases $\mathrm{V_nO_{2n-1}}$ where n = 4, 5, 6, 7 and 8 (triclinic), β - VO_2(tetragonal), α - VO_2(monoclinic), V_6O_{13} (monoclinic), V_3O_7 (monoclinic) and V_2O_5 (othorombic).

4.1.2 T-$\mathrm{pO_2}$ Phase Diagram

The critically assessed V-O system is the first step to thermodynamic modelling of multi-component oxide systems containing vanadium. For this reason, Kang (2012) and Yang, Mao, and Selleby (2015) went on to assess the VO-$\mathrm{VO_{2.5}}$ and V-O systems critically and thermodynamically using the CALPHAD method (see Chapter 6). The available experimental phase diagram data and other experimental thermochemical properties were critically examined, and a self-consistent set of equations for each phase was acquired. The liquid phase (slag) in Yang, Mao, and Selleby (2015) was modelled with the quasichemical model along with a symmetric Kohler ternary interpolation technique, which is the preferred model for describing slag phases in the FToxid database. The model was developed by considering all four valance states of vanadium, i.e. VO(l), V_2O_3(l), VO_2(l) and V_2O_5(l) are end-member species in the quasichemical model. Yang, Mao, and Selleby (2015) used an ionic two-sub-lattice model with the formula $(\mathrm{V^{2+}})_\mathrm{p}(\mathrm{O^{2-}}, \mathrm{Va^{-Q}}, \mathrm{VO_{1.5}}, \mathrm{VO_2}, \mathrm{VO_{2.5}})_\mathrm{Q}$ to describe the liquid phase.

Kang (2012) used pure substance data from the FACTPS database and adjusted the thermodynamic property data of some compounds slightly to reproduce experimental phase diagram data. Such is the complexity of the system, that 20 phases were included in the binary V-O system from Yang, Mao, and Selleby (2015). Five of the phases were treated as solid solutions within the framework of the compound energy formalism. The stability ranges and model parameters of pure compounds and solid solutions were obtained by the authors through careful consideration of the equilibrium oxygen partial pressure that was obtained from experimental data.

It was mentioned here that the system has only recently been the subject of studies, therefore only limited thermodynamic property and phase diagram data are available in commercial thermochemical software such as FactSage. Figure 4.1 shows the calculated V-O phase diagrams developed with the CALPHAD method from FactSage. Although the phase diagram calculated with FactSage does not delineate all solid phases and solutions in the $VO-V_2O_5$ system, it can still be used to estimate the valance stability of V in air. However, the recent thermodynamic assessments of Kang (2012) and Yang, Mao, and Selleby (2015) have made it possible to make reliable predictions of the behaviour of V as a function of temperature and $\mathrm{p_{O2}}$.

4.1.3 Stable Compounds Under Oxidising Conditions

Although the $VO_2-V_2O_5$ phase diagram from FactSage is incomplete, some useful conclusions can be drawn on the behaviour of V under oxidising and reducing conditions aided by thermodynamic evaluations of Kang (2012) Yang, Mao, and Selleby (2015). It is observed from Figure 4.1 that a $\mathrm{pO_2}$ higher than 10^{-2} atm be maintained to avoid falling in the VO_2 stable region and to remain within the investigated region of this study ($\mathrm{pO_2}$ = 0.21 atm). It is well observed that V_2O_5(s) remains stable in a low temperature range and at a $\mathrm{pO_2}$ = 0.21 atm. This conclusion is consistent with the findings of Kang (2012) Yang, Mao, and Selleby (2015). Moreover, the temperature needs to be increased and at the same time, $\mathrm{pO_2}$ needs to be lowered to reduce the oxidation state from V^{5+} to V^{4+}, therefore favouring compounds and solutions in the $VO_2-V_2O_5$ system thermodynamically. This behaviour is common for oxide systems where a metallic element has more than one oxidation state.

Another prediction is made on the oxidation state of V in the liquid phase under oxidising conditions. According to the quasichemical model from Kang (2012), the liquid phase of a vanadium-bearing slag in air is likely to consist of V^{5+} with dilute concentrations of V^{4+}.

4.2 The Fe-O System

4.2.1 Stable Compounds and Phases

The literature on the Fe-O system is voluminous and only a brief description is given here. The system is key to thermodynamic modelling of multicomponent spinel, slag, corundum and wüstite, which are imperative for metallurgy, ceramics and petrology. Thermodynamic assessment had been the subject of numerous studies (Goel, Kellogg, and Rrain 1980; Bjorkman 1985; Sundman 1991; Kowalski and Spencer 1995; Degterov et al. 2001; Hidayat et al. 2015). Again, all experimental data have been critically assessed to obtain one set of Gibbs model equations for all phases to produce a self-consistent set of thermodynamic properties and phase diagram data. The main difference between the thermodynamic assessment studies was the model used for describing the liquid phase. Goel, Kellogg, and Rrain (1980), Bjorkman (1985) and Kowalski and Spencer (1995) used the associate species model. Fe, FeO and $\mathrm{FeO_{1.5}}$ were modelled on one sub-lattice. Non-ideal behaviour between end-members was sufficiently described by the various associates. Some of these studies have included small interaction polynomial terms between the associates to reproduce the liquidus accurately. Sundman (1991) applied the ionic two-sub-lattice model for describing the

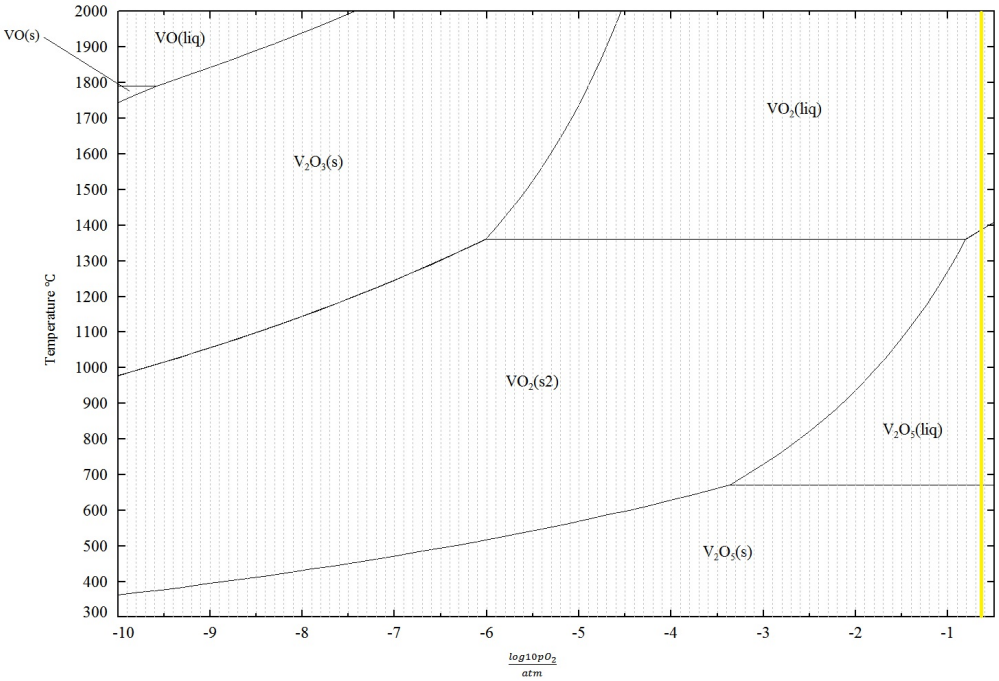

Figure 4.1: Calculated V-O phase diagrams from the FToxid database in FactSage 7.0. The yellow line indicates the pO_2 focus area of this study.

liquid. The model is characterised by mixing of cations on one sub-lattice and mixing of anions or neutral species on the other sub-lattice. The quasichemical model, which takes short-range ordering into account, was used by Wu et al. (1993), Degterov et al. (2001), and Hidayat et al. (2015).

4.2.2 T-$\mathrm{pO_2}$ Phase Diagram

The Fe-O system has been fully optimised and is available in FactSage 7.0 (see Figure 4.2). Given its availability in FactSage 7.0, it is assumed that thermodynamic properties and phase diagram data are reliable. Therefore, feasible conclusions can be made with regard to the stability regions of phases. Fe is mostly stable as Fe_2O_3 under oxidising conditions and transforms to spinel (magnetite) at elevated temperatures, but is dependent on $\mathrm{pO_2}$. The liquid phase under oxidising conditions consists of Fe^{3+} and dilute concentrations of Fe^{2+}. The thermodynamically favoured region of wüstite and pure Fe was avoided, given that it falls outside the investigated $\mathrm{pO_2}$ of this study. If hypothetically these experimental conditions were attained, V is not stable as V^{5+} or V^{4+}, but rather as V^{3+} and V^{2+}.

4.2.3 Stable Compounds Under Oxidising Conditions

The compound hematite has a trigonal structure based on the hcp oxygen packing scheme. The space group is $\mathrm{R\bar{3}C}$. Hematite is slightly non-stoichiometric (oxygen-deficient) at high temperatures when in equilibrium with magnetite (spinel); however contradictions on the percentage of non-stoichiometry are found among different studies. The latest thermodynamic re-evaluation of Hidayat et al. (2015) reported a deviation of 1 % from ideal stoichiometry. This was also reported by Wriedt (1991). In this study, it was assumed that hematite is stoichiometric.

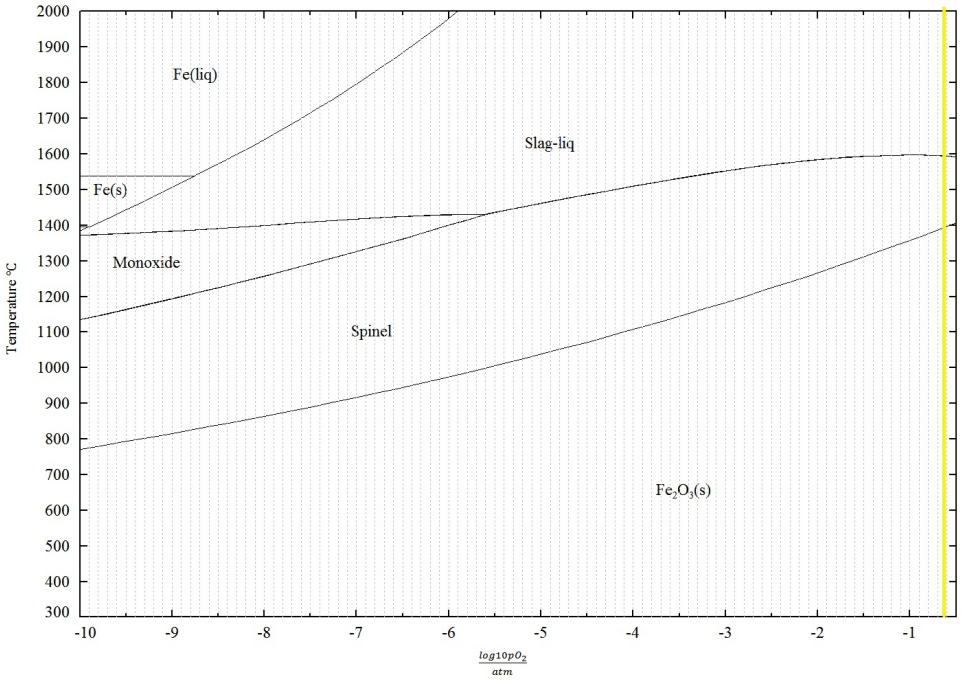

Figure 4.2: Calculated Fe-O phase diagram from the FTOxid database in FactSage 7.0. The yellow line indicates the pO_2 focus area of this study.

4.3 The Ti-O System

4.3.1 Stable Compounds and Phases

The Ti-O system has been critically assessed and thermodynamically evaluated by Chase et al. (1975) and, again by Murray and Wriedt (1987), Cancarevic, Zinkevich, and Aldinger (2007) and Hampl and Schmid-Fetzer (2015). The system consists of high and low temperature monoxide phases based on the NaCl structure. However, other crystal structures have also been reported. Ti_2O_3 undergoes a transition from semiconducting $\alpha - \mathrm{Ti_2O_3}$ at low temperatures to metallic $\beta - \mathrm{Ti_2O_3}$ somewhere near 180 °C. The compound has a negligible deviation from stoichiometry. Two other compounds, namely Ti_3O_5 and Ti_4O_7, are also stable in the Ti-O binary system. Ti_3O_5 is said to have one polymorph and Ti_5O_7 was found to have two equilibrium modifications.

It is reported that five polymorphs of TiO_2 exist, which are low-temperature, low-pressure forms. However, only anantase and rutile are found in the FToxid database. The transition of anatase to rutile is a nucleation and growth process and has been shown in most cases to transform between 600 and 700 °C. The transition temperature is dependent on particle size, particle shape, surface area, atmosphere, volume of the sample, nature of the sample container, heating rate, soaking rate, impurities and measurement technique (Hanaor and Sorrel 2009). Moreover, it has been reported that rutile has a deviation from stoichiometry corresponding to oxygen deficiency (see Subsubsection 6.3.3).

Several Magneli phases have been reported, $\mathrm{Ti_nO_{2n-1}}$, where $\mathrm{n} \geq 4$ and ranges to values above $\mathrm{n} = 20$. Phases ranging within $4 \leq \mathrm{n} \leq 10$ have crystal structures derived from the rutile structure by crystallographic shear. When n is above 10, structures are based on other shear operations (Murray and Wriedt 1987). Eriksson and Pelton (1993) described the liquidus within the TiO_2 and Ti_2O_3 region with the quasichemical model. The model parameters were determined by optimisation

from the liquidus points of Brauer and Litttke (1960).

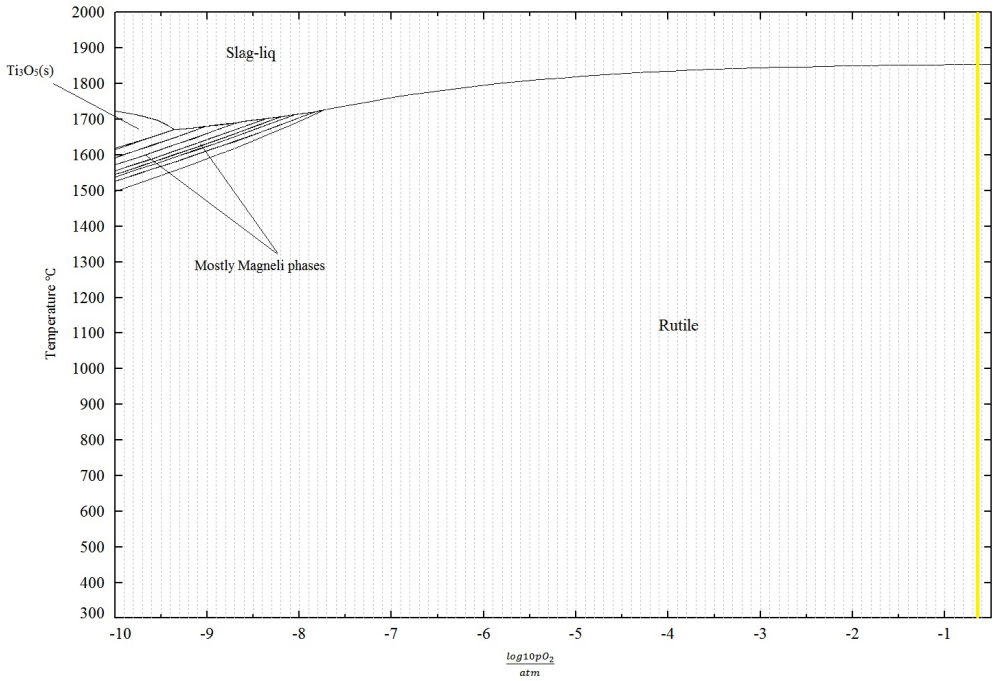

Figure 4.3: Calculated Ti-O phase diagram from the FToxid database in FactSage 7.0. The yellow line indicates the pO_2 focus area of this study.

4.3.2 T-pO_2 Phase Diagram

The Ti-O system has been fully optimised and is available in FactSage 7.0 (Bale et al. 2009). See Figure 4.3. The thermodynamic properties and phase diagram data are considered accurate, hence feasible conclusions can be made with regard to the stability regions of phases.

4.3.3 Stable Compounds Under Oxidising Conditions

It is observed from Figure 4.3 that rutile is stable at room temperature and ambient pressure under oxidising conditions. Rutile does not spontaneously transform to anatase; however it was mentioned that anatase transforms irreversibly to rutile at temperatures between 900 and 1000 °C. Moreover, this process is time-dependent, because it is reconstructive (Habel et al. 2006). A slag-liquid under oxidising conditions predominantly contains Ti^{4+} cations, with dilute concentrations of Ti^{3+} cations (Eriksson and Pelton 1993).

4.4 Notable Findings

Notable and valuable findings from the literature survey of V-O, Fe-O and Ti-O systems are:

- The V-O, Fe-O and Ti-O systems have been thermodynamically evaluated from a large set of experimental data by numerous authors; subsequently thermodynamic properties such as, $\Delta H^{\circ}_{f,298K}$, S°_{298K} and heat capacities of pure compounds were used for modelling efforts.

- Fe, V and Ti have two, four and three oxidation states. Fe_2O_3(s1), V_2O_5(s) and TiO_2(s)-anatase are stable in atmospheric conditions, in other words, under oxidising conditions and at room temperature.

- The dissolution of V_2O_5 in Fe_2O_3(s), and V_2O_5 in TiO_2(s) and vice versa in the sub-solidus regions will possibly be limited, given the difference of oxidation states of metals. However, this assumption does not take into account ionic radii of Fe^{3+}, Ti^{4+} and V^{5+}, and it has been shown that a solute will dissolve in a solvent when the difference in atomic radii between atom types is less than $\pm$15 % (Callister 2007).

- When the Fe-Ti-V-O system in air is saturated in Fe_2O_3(s), the latter is likely to transform to spinel (magnetite) at elevated temperatures and then to slag, provided that the temperature is further increased.

- The Fe$-$Ti$-$V$-$O liquid phase (slag) will comprise Fe, Ti and V in their various oxidation states even under oxidising conditions. This is because of the equilibrium reactions $\mathrm{V_2O_5(l) = 2VO_2(l) + 1/2O_2(g)}$ (Suito and Gaskell 1971), $\mathrm{2TiO_2(l) = Ti_2O_3(l) + 1/2O_2(g)}$ (Cancarevic, Zinkevich, and Aldinger 2007; Hampl and Schmid-Fetzer 2015) and the decomposition of Fe_3O_4(l) to form FeO(l) and Fe_2O_3(l) (Bale et al. 2009).

- The quasichemical parameters of the Fe_2O_3-FeO, $V_2O_5-VO_2$ and $TiO_2-Ti_2O_3$ liquids were optimised by Degterov et al. (2001), Eriksson and Pelton (1993), and Kang (2012). The modelled slag phases of the V-O, Fe-O and Ti-O systems were successfully reproduced under oxidising conditions by including Fe^{3+}, Fe^{2+}, V^{5+}, V^{4+}, Ti^{4+} and Ti^{3+} cations.

Chapter 5

Previous Studies on M-V-O systems

This chapter addresses previous studies of the Fe-Ti-V-O system in air. A short description of experimental techniques and results from previous studies is given, followed by a concise summary of the most important findings including shortcomings and contradictions. The survey considers the Fe-V-O, Ti-V-O and Fe-V-O systems under oxidizing conditions independently, and all past studies are advocated by phase diagrams. A critical assessment of the Fe-Ti-O system in conjunction with an evaluation of the thermodynamic properties and phase diagram data was already conducted by Eriksson and Pelton (1993) and later again by Eriksson et al. (1996). Consequently, this system is largely excluded from the survey, given that it is available in the FToxid database of FactSage 7.0 (Bale et al. 2009).

5.1 Fe-V-O System in Air

It was found that this system was investigated by Burdese (1957), Kerby and Wilson (1973), Fotiev, Cheshnitskii, and Surat (1983) and Walczak et al. (1985).

Burdese (1957) did not report oxide purities, experimental techniques, and details about construction of their phase diagram (Figure 5.1a). Therefore, the results were deemed unreliable and no feasible conclusion was made from the study.

The V_2O_5–Fe_2O_3 pseudo-binary system (Figure 5.1b) was studied by DTA and powder X-ray diffraction, using 15 compositions, which were prepared from reagent grades of V_2O_5(s) and Fe_2O_3(s). The phase diagram is similar to one given by Burdese (1957), except that it shows melting of $FeVO_4$(s) to form two immiscible liquids, a phenomenon also apparently encountered in another unreferenced study. The study does not state how the shape of the miscibility gap was determined or if any thermodynamic models were used for construction of the diagram. $Fe_2V_4O_{13}$(s), was not detected. A major concern with the study is that oxygen partial pressure was not given for the V_2O_5–Fe_2O_3 pseudo-binary system; however the $\mathrm{pO_2}$ of the Na_2O–V_2O_5 pseudo-binary system, another investigated system of this study, was fixed at 0.2 atm and 1 atm. For this reason, it has to be assumed that experiments pertaining to the V_2O_5–Fe_2O_3 pseudo-binary system were carried out in air ($\mathrm{pO_2} = 0.21$ atm) and in pure oxygen ($\mathrm{pO_2} = 1$ atm). The authors then mentioned "no effect of oxygen partial pressure on the melting temperature was found." Although it is not entirely clear what the authors meant by this, some valuable conclusions were made from this study. For example, the accuracy of the liquidus and eutectic on the V_2O_5 appears realistic; however the miscibility gap and the way in which it was practically verified, appear to be improbable.

The study of Fotiev, Cheshnitskii, and Surat (1983) pointed out discrepancies in previous studies regarding determination of phase composition and the peritectic decomposition temperatures of $FeVO_4$(s) and $Fe_2V_4O_{13}$(s). The compounds $FeVO_4$(s) and $Fe_2V_4O_{13}$(s) were synthesised in air from special-purity grade materials (Fe_2O_3 and V_2O_5) at 800 °C and 650 °C, with repeated remixing. No mention was made of contamination. The single-phase nature of the specimens was checked by the

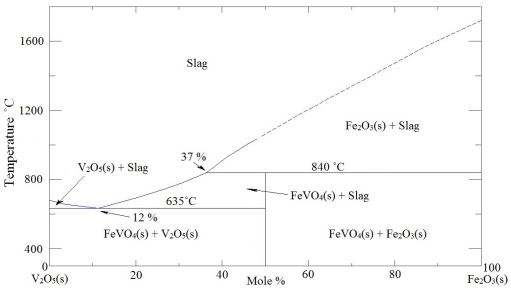

(a) The original pseudo-binary phase diagram of the Fe-V-O system in air from the study of Burdese (1957).

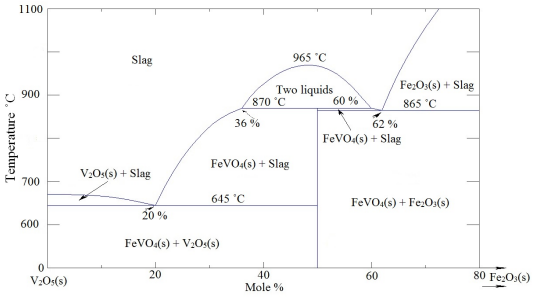

(b) The original pseudo-binary phase diagram of the Fe-V-O system in air from the study of Kerby and Wilson (1973).

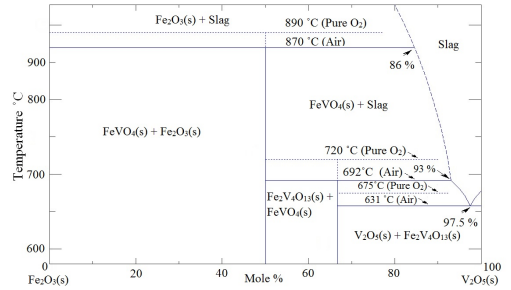

(c) The original pseudo-binary phase diagram of the Fe-V-O system in air from the study of Fotiev, Cheshnitskii, and Surat (1983).

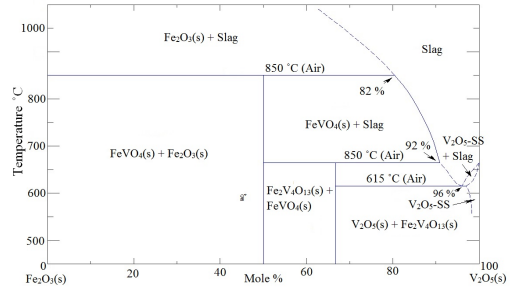

(d) The original pseudo-binary phase diagram of the Fe-V-O system in air from the study of Walczak et al. (1985).

Figure 5.1: The available Fe-V-O phase diagrams in air, acquired from the ACerS-NIST Phase Equilibria Diagrams software (Society 2003).

visual-optical method. X-ray diffraction examination of these iron vanadates with Cu K(α) radiation, and infrared spectroscopy confirmed their identity as per the published data. The following mixtures were made for DTA: up to 33.3 mole % Fe_2O_3, from V_2O_5 and $Fe_2V_4O_{13}$; from 33.3 to 50 mole % Fe_2O_3, from $Fe_2V_4O_{13}$ and $FeVO_4$; above 50 mole % Fe_2O_3, from $FeVO_4$ and Fe_2O_3. These mixtures were thoroughly reground and heated further in air at 630 °C, 650 °C, and 800 °C, respectively. A range of specimens was heated in an oxygen atmosphere. The specimens between 1 and 10 mole % Fe_2O_3 were synthesised in 1 mole % intervals.

DTA heating curves were recorded at a heating rate of 10 °C/min, with DTA heating curves-Al_2O_3 as standard. The equilibrium diagram of a mixture was constructed (see Figure 5.1c) from the peaks recorded on the heating curves with an accuracy of $\pm$ 4 °C. For a series of compositions, the recording was repeated after cooling. The formation of $Fe_2V_4O_{13}$(s) and $FeVO_4$(s) was verified. The peritectic melting points of $Fe_2V_4O_{13}$(s) and $FeVO_4$(s) and the eutectic between $Fe_2V_4O_{13}$(s) and V_2O_5(s) were found to depend on $\mathrm{pO_2}$ during synthesis of the specimens and are shown as dotted lines on the figure.

In the study of Walczak et al. (1985), starting materials were analytically pure grade V_2O_5(s) and Fe_2O_3(s). Fe_2O_3(s) was obtained by precipitating $Fe(OH)_3$ from solution, drying, and decomposing thermally at 450 °C in air. 28 mixtures were ground, pelletised, heated in air from 500 - 750 °C, and slowly cooled down to room temperature. Some samples were ground and heated at 725 °C and then quenched down to room temperature. Phases were identified by X-ray powder diffraction (XRD) using a diffractometer with CoK_α radiation. DTA was carried out in air with fused-silica crucibles. Temperatures were measured with an accuracy of 5 °C. An unindexed X-ray pattern for $Fe_2V_4O_{13}$(s) was given. A working phase diagram (Figure 5.1d) was constructed from the results of DTA experiments.

5.2 Ti-V-O System in Air

It was mentioned in Chapter 1 that this system has not been the subject of many studies. However, some studies have investigated sub-solidus regions of the Ti-V-M-O system (where M refers to metallic elements such as Na, K, Ca, Mg, Ti, Cr, Mn, Fe, Al, and Si) under oxidising conditions. Applications of the Ti−V−O system under oxidizing conditions were reported by numerous studies (Vejux and Courtine 1978; Bond, Sarkany, and Parfitt 1979; Habel et al. 2006; Habel et al. 2008). These applications are typically for selective oxidation and the effect of V_2O_5 and TiO_2 on selectivity and activity of catalysts.

Fotiev, Surat, and Tret'yakov (1981) studied compatibility relations among crystalline phases of the oxide components Fe_2O_3, TiO_2, and V_2O_5 in air employing a quenching technique. Reagent grade oxides (purity not stated) were weighed and mixed thoroughly in the desired ternary proportions. Thereafter, the mixtures were pressed into tablets under a pressure of 1000 $\mathrm{kg/cm^2}$. The pellets were heated at selected temperatures below the solidus for 20 hours, followed by grinding and powder XRD analysis of the reaction products. The cycle was then repeated for additional 20 h intervals of heating and subsequent grinding and X-ray analysis until two successive X-ray analyses yielded identical results. Figure 5.2a presents solid-phase compatibility triangles applicable to restricted temperature ranges at 700 °C for the $Fe_2O_3-TiO_2-V_2O_5$ pseudo-ternary system.

It was deducted from their study that no intermediate compounds or solid solutions existed in the $TiO_2-V_2O_5$ system. In addition, no ternary compounds were reported. The same authors proceeded to study compatibility relations among crystalline phases of the $Al_2O_3-TiO_2-V_2O_5$ and $Cr_2O_3-TiO_2-V_2O_5$ pseudo-ternary systems. An identical experimental method was employed as for the $Fe_2O_3-TiO_2-V_2O_5$ ternary system. No binary compounds were reported in the $V_2O_5-TiO_2$ phase region.

Another study, Golovkin, Volkov, and Skobeleva (1989) investigated sub-solidus regions in the $CaO-TiO_2-V_2O_5$ pseudo-ternary system. Chemically pure grade V_2O_5, TiO_2, and $CaCO_3$ were used as starting materials. The ternary mixtures were thoroughly mixed and pellitised. Thereafter, samples were treated at 700 °C with repeated re-grinding and pellitising cycles. Phases were identified with XRD and the Ca content in the products was quantified with atomic absorption spectroscopy. The detected phases at 700 °C are presented on Figure 5.2b.

The observations from the study were identical to those of Fotiev, Surat, and Tret'yakov (1981). In other words, no intermediate compounds or solid solutions were found to exist in the $TiO_2-V_2O_5$ system. Compositions not connected by tie-lines in other phase regions do not exist at 700 °C.

Solacolu, Dinescu, and Zaharescu (1970) and Millet, Roth, and Parker (1986)(see Figure 5.2c) went on to study phase relations in the $BaO-TiO_2-V_2O_5$ pseudo-ternary system. Both these groups reported intermediate binary compounds in the $BaO-V_2O_5$ region and one ternary compound. No intermediate compounds or solid solutions were reported in the $TiO_2-V_2O_5$ system.

Habel et al. (2006) and Habel et al. (2008) reported a wide solubility range of V_2O_5 in the rutile phase. The main aim of their work was phase development during catalyst processing under oxidising conditions. A phase field for a rutile solid solution with up to 12.5 mole % V_2O_5 at 675 °C was identified and an eutectic reaction was also found at 631 °C by means of DTA. A working phase diagram displaying a large solubility area of V_2O_5 in rutile was deduced from a set of XRD results (see Figure 2 in Habel et al. (2006)).

It was reported that the unit cell of the rutile solid solution is smaller than that of pure rutile, because V^{5+} and V^{4+} ions are smaller than Ti ions. This type of behaviour indicates a substitutional replacement. Three defect models were proposed, describing V_2O_5(s) solubility in the rutile phase (Habel et al. 2006).

- Vanadium remains completely in a 5+ valance state, which indicates that no oxygen was lost

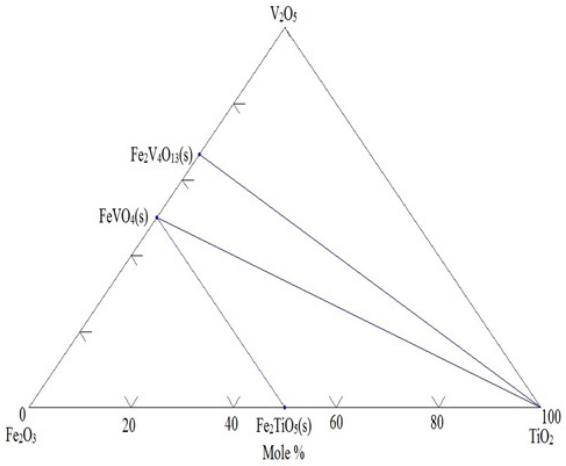

(a) The $Fe_2O_3-TiO_2-V_2O_5$ ternary phase diagram from the study of Fotiev, Surat, and Tret'yakov (1981) at 700 °C.

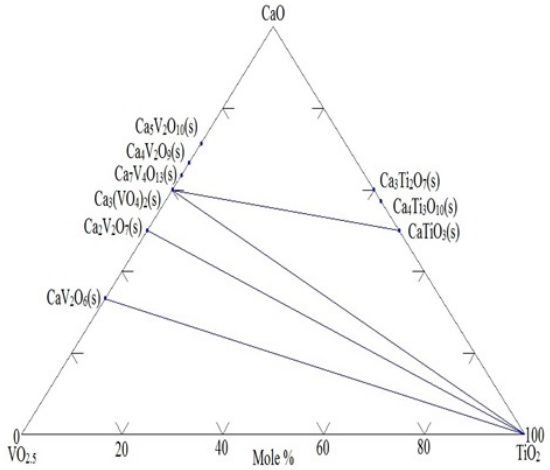

(b) The $CaO-TiO_2-V_2O_5$ ternary phase diagram from the study of Golovkin, Volkov, and Skobeleva (1989) at 700 °C.

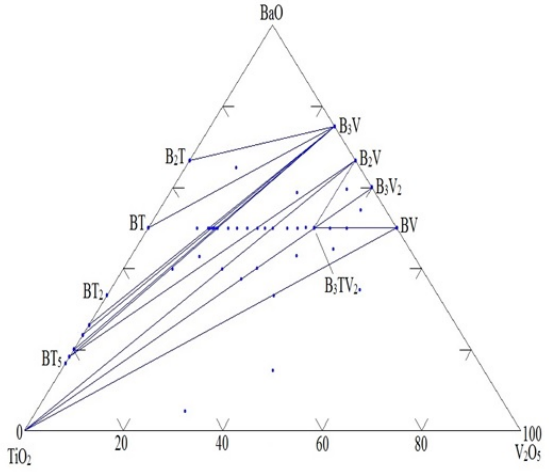

(c) The $BaO-TiO_2-V_2O_5$ ternary phase diagram from the study of Millet, Roth, and Parker (1986) at 700 °C. Compounds presented are abbreviations of BaO = B, $T = TiO_2$ and $V = V_2O_5$. For example, $B_2V = Ba_2V_2O_7$.

Figure 5.2: The available Ti-Me-V-O phase diagrams in air, acquired from the ACerS-NIST Phase Equilibria Diagrams software (Society 2003).

and charge compensation on the crystal lattice of rutile is preserved by interstitial oxygen ions:

$$V_2O_5 \Rightarrow 2V_{Ti} + O_i + 4O_{o^x}. \tag{5.1}$$

- Vanadium remains entirely in a 5+ valance state, which indicates that no oxygen was lost and charge compensation on the crystal lattice of rutile is preserved by vacancies on the vanadium site:

$$2V_2O_5 \Rightarrow 4V_{Ti} + Va_{Ti} + 10O_{o^x}. \tag{5.2}$$

- Vanadium is reduced to a 4+ valance state with a loss of $1/2O_2$

$$2V_2O_5 \Rightarrow 2V_{Ti^x} + 4O_{o^x} + 1/2O_2(v) \uparrow. \tag{5.3}$$

To date it is not clear which defect model applies for this rutile solid solution. X-ray photoelectron spectroscopy (XPS) studies by Habel et al. (2006) revealed an oxidation state of 4.75 for V in the rutile phase at 675 °C. They went on to report that V in the rutile solid solution is a mixture of V in the 5+ and 3+ oxidation state owing to differences in the binding energies. However, it is likely that V^{3+} is present in low concentrations, given the measured oxidation state of 4.75. As a result, the first and second defect models were used to derive a thermodynamic model for describing the dissolution of V_2O_5 in the rutile phase (see Subsubsection 6.3.3).

The Ti-V-O system was thermodynamically evaluated by Enomoto (1996) and later again by Yang et al. (2017) in response to new experimental phase diagram data obtained under relatively reducing conditions (Habel et al. 2006; Habel et al. 2008; Hiroi et al. 2013). The crystallographic data on all the solid phases are reported in these publications. The assessment of Yang et al. (2017) was based on recent assessments of the V-O and Ti-O binary systems (Yang, Mao, and Selleby 2015; Hampl and Schmid-Fetzer 2015).

Yang et al. (2017) used the ionic liquid model to describe the liquid phase and all solid phases were developed within the framework of the compound energy formula. All available experimental data pertaining to the Ti-V-O system were critically evaluated and a set of self-consistent thermodynamic model parameters was obtained. However, limited data on the TiO_2–V_2O_5 phase region were obtained and the phase diagram presented by Yang et al. (2017) was exclusively based on data from Habel et al. (2006) (see Figure 5.3).

As a result, the higher temperature areas of the TiO_2–V_2O_5 phase diagram were extrapolated with thermodynamic calculations using the parameters obtained from Yang et al. (2017). Because of the lack of experimental data, it was stated by Yang et al. (2017) that "it is important to note that more reliable experimental investigations are necessary to further improve the description of this system".

5.3 Fe-Ti-O System in Air

The Fe-Ti-O system has been the subject of many previous investigations and have been included in the FTOxid database of FactSage. References are also listed as part of the documentation provided by FactSage commercial software (Bale et al. 2009). However, the focus of this study is narrowed down to oxidising conditions, hence the Fe-Ti-O phase diagram presented on Figure 5.4 was calculated at a fixed pO_2 of 0.21 atm.

Figure 5.4 shows two solid compounds, rutile and hematite, and one slag phase. There is also an area where a transition of hematite to pure spinel/magnetite takes place. However, this calculated phase diagram is incomplete and does not delineate all solid solution phases in detail. Wittke (1967) showed experimentally that there is an area of Fe_2O_3(s) dissolution in the rutile phase. The dissolution of TiO_2 in the hematite phase is therefore also possible; however this has not

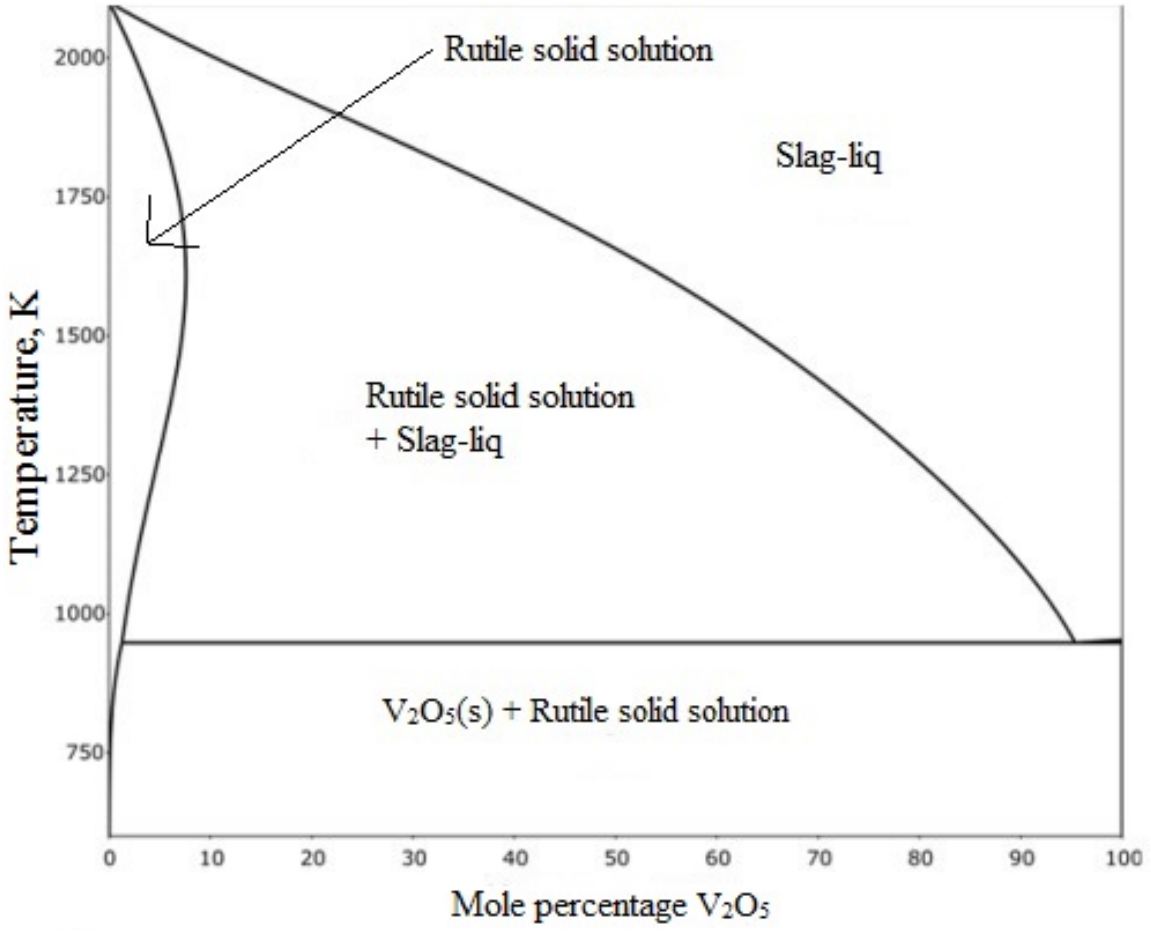

Figure 5.3: The calculated TiO_2–V_2O_5 phase diagram from the thermodynamic assessment of Yang et al. (2017). Reprinted from Yang et al. (2017) with permission from Elsevier©.

been investigated experimentally. It is reported in the description of the FToxid database that slags containing Fe_2O_3 and TiO_2 have not been evaluated. As a result, calculations can only be made with the FToxid database under reducing conditions where Fe is mainly present as Fe^{2+}, although reasonable calculations of the Fe^{3+} content can be obtained as long as the Fe^{3+} content is low (Bale et al. 2009). However, the calculations in this study were performed in air and Fe^{3+} is known to be the dominant valance of iron under these conditions.

Furthermore, ferropseudobrookite solid solution or solid compound, Fe_2TiO_5(s), is known to exist at an Fe_2O_3 and TiO_2 mole ratio of 1:1 (Haggerty and Lindsley 1970; Navrotsky 1975). In these studies, the ternary compound was shown to decompose into its respective binary oxides, Fe_2O_3 and TiO_2 at 565±15 °C. The free energy of formation of $FeTi_2O_5$(s) from Fe_2O_3(s) and TiO_2 between 700 and 1200 K, was measured and calculated by Navrotsky (1975) as $\Delta G^{\circ}(T) = 1990 - 2.4T$ Cal (T in Kelvin). Guo et al. (1999) had investigated the crystal structure by means of x-ray diffraction (XRD), Mössbauer spectroscopy and neutron diffraction. The results confirmed that the $Fe_{1+x}Ti_{2-x}O_5$ ferropseudobrookite solid solution has an orthorhombic structure with D_{2h}^{17}(Cmcm) spacegroup. In their work they also showed that site occupancies obtained from both Mössbauer spectra and neutron diffraction data indicated that the cation (Fe^{2+}, Fe^{3+} and Ti^{4+}) distributions in the available sites, 4c and 8f, are neither random nor perfectly ordered. The compound, Fe_2TiO_5(s), melts congruently at 1388 °C. However, this congruent melting point is estimated with FactSage and has not been determined experimentally.

A further investigation into a description of solutions from FactSage databases revealed that Fe^{3+} is not a component of the ferropseudobrookite solid solution series (FToxid-PSEU). Therefore, the ferropseudobrookite solid solution series from the FToxid database can only be used under reducing

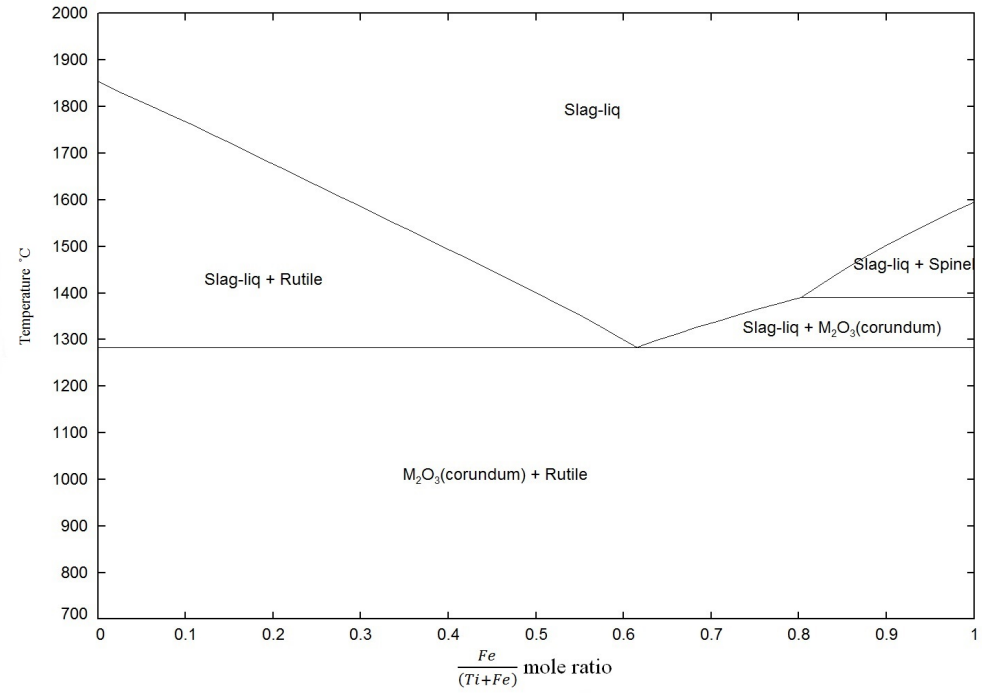

Figure 5.4: Fe-Ti-O phase diagram in air estimated with FactSage Bale et al. 2016.

conditions.

Hitherto little work has been done on Fe-Ti-O system in air, but a critical assessment of the literature and a thermodynamic evaluation were nonetheless conducted. This is because the phase diagram and thermodynamic data from the Fe-Ti-O system in air have a significant effect on calculations of the Fe-Ti-V-O system in air.

5.4 Notable Findings from Literature

Previous studies of the Fe-Ti-V-O system in air have at times been grossly contradictory and the need for new phase diagram data is critical. Based on the review, a summary of the major findings that formed part of and assisted with the thermodynamic evaluation of the Fe-Ti-V-O system in air is given.

- All previous studies have conducted phase equilibria experiments using dynamic techniques, such as DTA, TGA or DSC. Any system with sluggish transport kinetics will not reach chemical equilibrium and achieve only partial equilibrium.

- The studies of Burdese (1957) and Kerby and Wilson (1973) have not been able to detect the intermediate compound, $Fe_2V_4O_{13}$, in contrast to those of Walczak et al. (1985) and Fotiev, Cheshnitskii, and Surat (1983) that had identified the compound. Other authors, Weddle and Preece (1955), even suggested the existence of several iron vanadates, which include $Fe_2O_3 \cdot 2\,V_2O_5$, $Fe_2O_3 \cdot V_2O_5$(s) and $2\,Fe_2O_3 \cdot V_2O_5$(s).

- No intermediate compounds were detected in the sub-solidus region of the TiO_2—V_2O_5. These were the findings of (Fotiev, Surat, and Tret'yakov 1981; Golovkin, Volkov, and Skobeleva 1989; Solacolu, Dinescu, and Zaharescu 1970; Millet, Roth, and Parker 1986).

- Discrepancies in the composition and temperature of eutectic and peretectic points are noted in the Fe-V-O system in air. This was deduced from the more reliable studies of Fotiev, Cheshnitskii, and Surat (1983) and Walczak et al. (1985) . For example, an incongruent melting range of $FeVO_4$ ranging from 840 - 870 °C, has been postulated. Liquidus and solidus temperature lines have also not corresponded. Kerby and Wilson (1973) had postulated that the compounds, Fe_2O_3(s) and $FeVO_4$(s) melted within a liquid miscibility gap. However, this melting behaviour is highly unlikely and was possibly misconstrued.

- To the best of the researcher's knowledge, no study has attempted to estimate the liquidus and solidus regions in the Ti-V-O system under oxidizing conditions above 700 °C.

- Several studies (Burzo. and Stanescu 1976; Burzo. and Stanescu 1978; Palanna, Mohanand, and Biswas 1978) have reported a small solubility range of Fe^{3+} in the V_2O_5 matrix up to a ratio of $\mathrm{Fe}/(\mathrm{Fe}+\mathrm{V}) = 0.05$. The Fe^{3+} ions dissolved in the V_2O_5 matrix appear to occupy interstitial and substitutional positions.

- No studies have experimentally investigated the Fe-V-O system under oxidising conditions above 900 °C.

- The Fe-Ti-O system has been partially assessed and optimised, and is available in the FToxid database of FactSage. An inspection of the FToxid database indicated that the Fe-Ti-O system can only be accurately reproduced under reducing conditions. A small solubility range of Fe_2O_3 in the rutile phase was detected by Wittke (1967). Ferropseudobrookite solid solution was another component known to be present, but is not included in FactSage calculations under oxidising conditions.

- The Ti-V-O system has been partially assessed and optimised by Yang et al. (2017), but is not available in the FToxid database of FactSage.

- Although phase diagrams, in particular that of the Fe-V-O system in air, have been obtained from previous studies, none mentioned the use of thermodynamic models and the CALPHAD technique. It is likely that diagrams have been manually drawn by simply fitting the results from phase transitions. Therefore, other thermodynamic properties cannot be calculated computationally. Phase diagram data from previous studies were used in the thermodynamic evaluation of this study. This methodology for thermodynamic evaluation is further explained in Chapter 6 and Chapter 9.

Chapter 6

Thermodynamic Modelling

In this chapter, the principle of thermochemical equilibrium calculation is explained with focus on the CALPHAD method. Mathematical models that are used to describe compounds and solutions in oxide systems are discussed. In the last section, the assessment methodology outlining the correct procedure for the thermodynamic evaluation is discussed.

6.1 The CALPHAD Method

High-temperature processes are complex in nature, involving many types of compounds and solution phases. As a result, it is at times difficult to investigate a specific problem experimentally or even clearly understand the problem in question without output from reliable and robust thermodynamic models. Therefore, it is important that a thermodynamic model has the ability to calculate accurate thermodynamic properties from a mixture of compounds (for example oxides and sulphide minerals) as a function of temperature, composition and pressure (Barry, Dinsdale, and Gisby 1993).

The total Gibbs free energy is minimised to determine a state of chemical equilibrium (see Subsection 1.3.1). Minimisation algorithms such as ChemSage and FactSage have been developed and explained in previous studies (see Subsection 1.3.2). The CALPHAD method (Saunders and Miodownik 1998; Lukas, Fries, and Sundman 2007) has been defined as an algorithm utilising models developed for the Gibbs energy, G, of phases in smaller systems as a function of temperature, pressure and composition, starting from pure compounds and binaries. These models describe the Gibbs energy of each phase in a system, including stable and metastable temperature and composition ranges. By fitting a set of critically evaluated and selected experimental data (for example phase diagram information, thermodynamic measurements and the results of first principle calculations), it is possible to calculate optimum model parameters, followed by storage in a database.

Although the CALPHAD method is convenient and efficient for predicting and estimating thermodynamic properties and phase equilibrium data, it is unable to predict the existence of a phase unless it was experimentally confirmed and included in the thermodynamic assessment. The latter highlights the need for accurate experiments, because optimised parameters in a thermodynamic assessment is dependent on experimental data.

It has been shown that accurate behaviour of higher-order systems can be predicted by interpolating and extrapolating thermodynamic data from lower-order systems (Bale et al. 2002; Davies et al. 2002). This encourages practical usage, provided that thermodynamic properties and phase equilibria of lower-order systems were determined experimentally. In addition, it is possible to calculate thermodynamic properties and simulate transformations of multicomponent systems utilising modelled Gibbs energies and their respective derivatives. Figure 6.1 presents a flowchart of the CALPHAD method. The steps shown in Figure 6.1 were followed meticulously to execute the thermodynamic assessment of the Fe-V-O, Ti-V-O and Fe-Ti-V-O systems successfully.

Thermochemistry modelling software, such as MTdata (Davies et al. 2002), FactSage (Bale

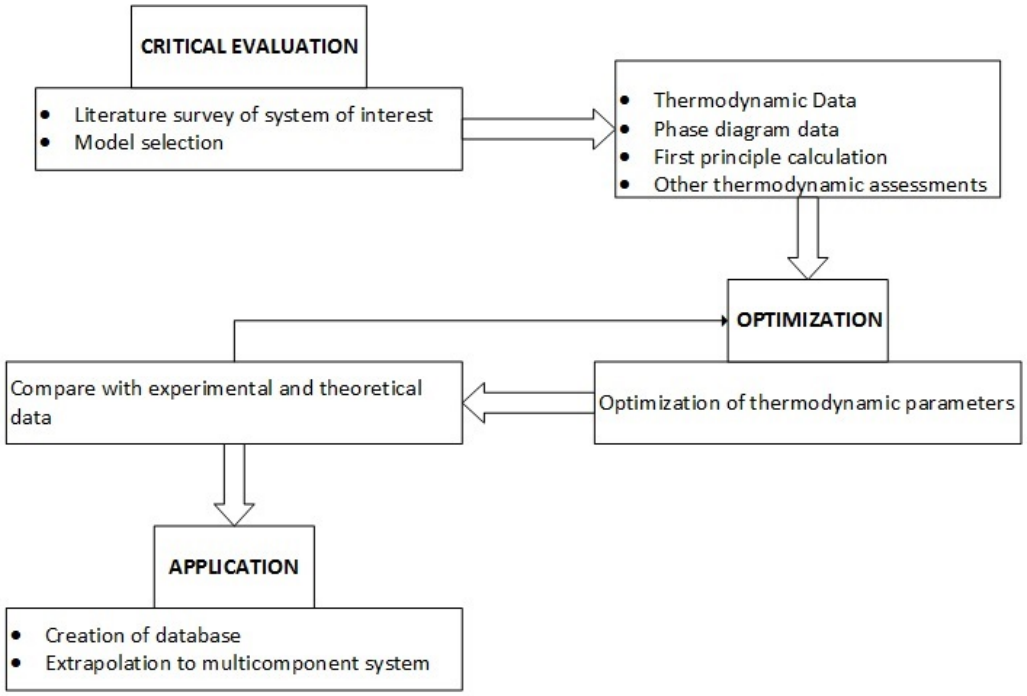

Figure 6.1: A flowchart of the CALPHAD method summing up the necessary steps to carry out a thermodynamic evaluation. (Lukas, Fries, and Sundman 2007).

et al. 2002), Thermo-Calc (Anderson et al. 2002) and Pandat (Chen et al. 2003) permits one to determine chemical equilibrium from a diverse set of chemical constituents. For example, the pseudo-binary phase diagram of the Fe-V-O system in air has been calculated with the MTdata thermochemistry software using the MTOX database (see Figure 6.2). The phase diagram and other thermodynamic properties were obtained through thermodynamic optimisation, by evaluating all available experimental phase-equilibrium data (Burdese 1957; Kerby and Wilson 1973; Fotiev, Cheshnitskii, and Surat 1983; Walczak et al. 1985). The Fe-V-O phase diagram in air has been back-calculated from a set of model equations for Gibbs energies of all phases as functions of temperature and composition. Discrepancies in the available data were partially resolved, and interpolations and extrapolations were made in a thermodynamically correct manner. However, it should be reiterated that FactSage thermochemistry software has no thermochemical data of the Fe-Ti-V-O system. As a result, all thermochemical database development was done with FactSage 7.0.

6.2 Pure Compounds

The Gibbs energies of stoichiometric compounds and of the components of solution phases are expressed in the form of $\mathrm{G_m} - \sum \mathrm{H_{SER}}$ and are also a function of temperature. The $\sum \mathrm{H_{SER}}$ (standard element reference - SER) is the sum of enthalpies of the elements at 298 K and 1 bar pressure. This term is required because there is no absolute value of the enthalpy of a system and it is important to select some reference state, which usually is zero if one proceeds working with formation energies. This reference state is normally omitted from the solution models because it has been set to zero. The molar Gibbs energy of unary oxides are expressed by polynomials and is a function of temperature (Barry, Dinsdale, and Gisby 1993; Lukas, Fries, and Sundman 2007):

$$G_m^\circ - \sum H_{SER} = a + bT + cTlnT + dT^2 + eT^{-1} + fT^3 + gT^7 + hT^{-9} \tag{6.1}$$

The coefficients of Equation 6.1 are obtained from critical analysis and computer optimisation of experimental spectroscopic, heat capacity, enthalpy, entropy, and Gibbs energy data, as well as

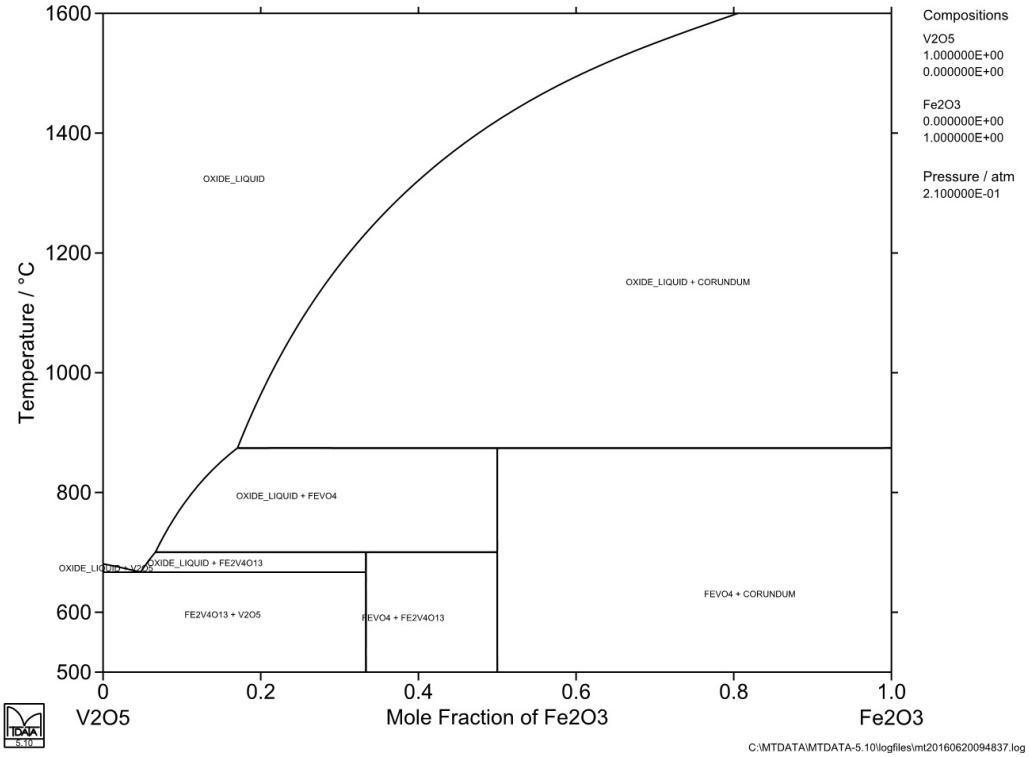

Figure 6.2: The pseudo-binary phase diagram of the Fe-V-O system in air, generated by MTdata thermochemistry software (Davies et al. 2002).

from studies of phase equilibria. The molar Gibbs energy of intermediate/stoichiometric compounds, A_mB_n in the A-B system can be expressed through Equation 6.1 identically if the heat capacity data are available (Lukas, Fries, and Sundman 2007):

$$G^{\circ}_{A_mB_n} - mH^{SER}_A - nH^{SER}_B - (m+n)H^{SER}_O = a + bT + cTlnT + dT^2 + eT^{-1} \tag{6.2}$$

If insufficient heat capacity data are available, the empirical Neuman-Kopp rule has to be applied to predict the heat capacity of mixed or higher-order oxides. It is assumed that the heat capacity of a compound is equal to the stoichiometric average of the heat capacities of the pure elements in the SER. From numerous applications of the Neuman-Kopp rule, it has been shown to give reasonable approximations for most mixed oxides around room temperature. The accuracy of the prediction decreases significantly at both low and high temperatures. The application of the Neuman-Kopp rule can also be extended to estimations for heat capacities of solution end-members (Lukas, Fries, and Sundman 2007).

$$G^{\circ}_M - \sum_t b_i G^{SER}_t = a + bT \tag{6.3}$$

The Neuman-Kopp rule, which is expressed by Equation 6.3, requires the determination of only two coefficients in comparison to Equation 6.2. This is because the heat capacity is taken from the descriptions of the pure elements. The rule was recently modified to increase the reliability of the estimation (Qiu and White 2001; Leitner et al. 2002). In mathematical terms, a ternary solid compound $\mathrm{A_aB_bC_c}$ (where C is a symbol for the element, O) is formed by a reaction of the binary compounds $\mathrm{AC_1}$ and $\mathrm{BC_2}$ as shown in Equation 6.4:

$$mAC_o(s) + nBC_o(s) = A_mB_nC_o(s) \tag{6.4}$$

followed by the assumption:

$$C_p(A_mB_nC_o(s)) = mC_p(AC_o, s) + nC_p(BC_o, s). \tag{6.5}$$

The coefficients of Equation 6.1, Equation 6.2 and Equation 6.5 are optimised based on heat capacity data. For thermodynamic assessment purposes, the standard molar Gibbs energy of stoichiometric compounds is reported by the combination of standard enthalpy of formation, standard entropy and heat capacity terms:

$$\Delta G^{\circ}_{f,298K}(T) = \left(\Delta H^{\circ}_{f,298K} + \int_{298K}^{T} C_p(T)dT\right) - T\left(S^{\circ}_{298K} + \int_{298K}^{T}(C_p(T)/T)dT\right) \tag{6.6}$$

6.3 Solution Phases

The Gibbs energy of any phase can be due to two main factors, the bonding between the constituents and their atom configuration. The configuration of atoms enhances the bonding of dissimilar atoms. When the bond energy between two dissimilar atoms is more negative than the bond energy between similar atoms, it creates a tendency for compound formation or ordering. However, when bond energy between dissimilar atoms is more positive than the bond energy between equal atoms it creates a tendency for miscibility gaps. Hence, the selection of a model for a phase must be based on chemical and physical property knowledge. Some factors to consider include, crystallography, type of bonding, order-disorder transitions and magnetic properties. Most of the models described here for crystalline phases take into account the crystal structure by dividing it into sub-lattices characterised by different crystallographic symmetries and numbers of the nearest neighbours (Lukas, Fries, and Sundman 2007).

In any system, the total molar Gibbs free energy is minimised to determine a state of chemical equilibrium (see Subsection 1.3.1). The following equation holds for any solution, for any number of chemical constituents:

$$G_m = G^{\circ}_m - T.S_{config} + G_{phys} + G_e \tag{6.7}$$

Equation 6.7 presents a general form for $\mathrm{G_m(T, x, P)}$ and consists of four contributions: the **reference term** (constituents in their pure state), the **configurational entropy**, **physical contribution** largely due to magnetic transitions and an **excess term**. The contribution owing to pressure difference is negligible in most systems (see Section 6.6). The excess term, which accounts for the non-ideal behaviour of constituents in a solution, can have many forms. Many models have already been developed to describe non-ideal behaviour in a slag and solid solutions. For example, the ionic liquid model, modified quasichemicel model (MQM) and the associate species model (ASM) have all been demonstrated to describe the behaviour of slags successfully, while a simple single lattice model with random mixing of cations on a single lattice has been used to predict the behaviour of monoxide and corundum solid solutions. A simple single lattice model can be used in such a case, since the anion lattice contains only $\mathrm{O^{2-}}$ ions (Saunders and Miodownik 1998; Lukas, Fries, and Sundman 2007).

Furthermore, a set of parameters is used to describe a particular model, e.g. excess parameter. In some cases, these parameters can be a function of temperature, pressure or composition and therefore they may be broken down into several other parameters. Each parameter can have multiple coefficients, with each coefficient assigned a single numerical value that was optimised to fit a set of experimental data.

Thus, the molar Gibbs energy function for a stable compound in any phase, θ, with respect to temperature is usually described by a polynomial and is valid within a limited temperature region only (Saunders and Miodownik 1998; Lukas, Fries, and Sundman 2007):

$$G_m^\theta - \sum_i b_i H_i^{SER} = a_0 + a_1 T + a_2 T Ln(T) + a_3 T^2 + a_4 T^{-1} + a_5 T^3 + ... \quad (6.8)$$

After mathematical manipulation, these coefficients are related to thermodynamic quantities that can be measured and calculated.

$$H_m^\theta - \sum_i b_i H_i^{SER} = a_0 - a_2 T - a_3 T^2 + 2a_4 T^{-1} - 2a_5 T^3 + ... \quad (6.9)$$

$$S_m^\theta = -a_1 - a_2[1 + ln(T)] - 2a_3 T + a_4 T^{-2} - 3a_5 T^2 + ... \quad (6.10)$$

$$C_p^\theta = -a_2 - 2a_3 T - 2a_4 T^{-2} - 6a_5 T^2 + ... \quad (6.11)$$

Equation 6.8 is used from 298 K upwards, as portrayed by the Gibbs energies found in SGTE. For most cases, the lower temperature limit of 298 K is adequate to allow the calculations of equilibrium in heterogeneous systems where diffusion is required to reach a state of equilibrium. However, diffusion is slow at lower temperatures, making an extension of the thermodynamic model impractical. In other words, there is little practical interest in extending the model to lower temperatures.

The coefficients $\mathrm{a_0, a_1, a_2, a_3}$..., which are similar as in Equation 6.1, are temperature-dependent and are set to be optimised by fitting the critical set of experimental and theoretical data employing a least-square method. The minimisation of the global Gibbs energy of the whole system is based on a least-square method (see Subsection 6.8.1) (Lukas, Fries, and Sundman 2007). Section 6.8 addresses the fundamental principles of data fitting and optimisation.

6.3.1 Gas Phase

In most metallurgical systems, where calculations are based on thermochemical equilibrium, the total pressure is low, hence a gas phase exhibits ideal behaviour. Such an assumption is validated by the following limiting condition (Koretsky 2004):

$$\lim_{\mathrm{P}\to 0} \frac{f_i}{P_i} \equiv 1. \quad (6.12)$$

Equation 6.12 defines that as meaning that when pressure goes to zero, all gases behave ideally. As a result, the assumption of ideal behaviour at 1 atm (absolute) holds, and the molar Gibbs energy of the gas phase is given by Equation 6.13 (Koretsky 2004):

$$G_m = \sum_i y_i G_i^\circ + RT \sum_i y_i ln y_i + RT ln(P_i/P_\circ) \quad (6.13)$$

where, $\mathrm{y_i}$ is the molar fraction of a gaseous constituent i, $\mathrm{P_\circ}$ is the standard pressure of 1 atm and $\mathrm{P_i}$ is the partial pressure of a gaseous constituent, i.

6.3.2 Liquid Models

Slags and molten salts, can be some of the most complex liquids in binary and ternary systems to model. These systems have been observed to show contradictory behaviour. For example, SiO_2 has been shown to form liquid immiscibility regions with other oxides as well as stable compounds. Immiscibility is usually associated with positive deviations from ideality and arises from a complex Gibbs energy change with composition. Although Gibbs energy of mixing can be negative over the whole composition range, inflections in the mixing curve give rise to spinodal points, where decomposition into two liquids occurs. The use of simple mixture models for ionic liquids have

not been successful, given that a large number of coefficients are needed to mimic sharp changes in enthalpy around critical compositions. Moreover, these modelled lower order systems tend to predict the behaviour of multi-component systems with gross inaccuracy (Saunders and Miodownik 1998).

Many models have been proposed and developed to account for thermodynamic behaviour in ionic liquids and some of them are listed:

- Cellular models
- Modified quasichemical models (MQM)
- Sub-lattice models
- Associate species models (ASM).

Only the MQM and ASM are discussed further with regard to their application to ionic liquids and the system of interest. These two models are used to describe the slag and salt phases in FactSage (Bale et al. 2009) and MTData thermochemistry (Davies et al. 2002) software, respectively.

Associate Species Model

The ASM was developed in the 1980s to describe the thermochemical behaviour of liquid oxide solutions. The model was originally developed by Hastie, Bonnell and co-workers and is substantially easier for non-specialists to understand, unlike the modified quasichemical model (Hastie and Bonnell 1985; Hastie 1984; Hastie, Plante, and Bonnell 1983; Bonnell and Hastie 1989). Nevertheless, both models were used in the investigation to make some useful and interesting comparisons.

The bonding or interaction energies are included in the associate model by adding "associate species" from end-member interaction, with their respective energies, to the solution. Therefore, the complex interaction terms are simply embodied in additional species in the solution. The associate model has several advantages (Besman and Spear 2002; Besman, Spear, and Beahm 2002):

- It accurately represents the thermodynamic behaviour of very complex systems over a wide range of temperature and composition.
- It accurately predicts the activities of stable and metastable equilibrium phases.
- It allows for logical and accurate estimation of unknown thermodynamic properties within a required composition and temperature range that is more than adequate for predicting useful engineering limits on thermodynamic activities in solutions.
- It is relatively easy to understand and to apply.

In this approach, it is assumed that the liquid mixture behaves ideally and that any non-ideal behaviour is represented by the intermediate associate species. Therefore, Equation 6.7 is reduced to the first two terms. The ideal mixing contribution to the partial free energy is $\mathrm{RTLny_i}$, where $\mathrm{y_i}$ is the mole fraction of the liquid species i in the solution. In this case, because the solution is considered ideal, the activity of a specie is simply equal to the mole fraction of a specie in the solution. The value of $\mathrm{y_i}$ can vary, depending on the assumed stoichiometry of the species, even though the metal:non-metal ratio remains constant. Therefore, to give equal weight to all liquid species in the solution with regard to the entropy of mixing, each associate specie is specified to have formulas that contain two non-oxygen atoms per mole. For example, in a binary system, each specie in the liquid phase is written as follows:

$$mM + nM^{'} = 2/formula\ unit\ of\ M_mM_n^{'}O_o(l) \tag{6.14}$$

where $\mathrm{M_m}$ and $\mathrm{M'_n}$ are dissimilar metals. It was found in previous work (Besman and Spear 2002; Besman, Spear, and Beahm 2002; Besman, Kulkarni, and Spear 2006), that for all systems (aluminates, borates, silicates, aluminosilicates, etc) thermodynamic data can be more easily optimised when liquid species contain two non-oxygen atom species instead of one. The fundamental reason for the better phase diagram fits that have been obtained in the literature is not understood.

In some systems, non-ideal behaviour between associates arises. The interaction between associates - or the excess Gibbs energy $\mathrm{G_e}$, is described by Redlich-Kister equation and is also used to model miscibility gaps.:

$$G_e = \sum\sum\sum y_i y_j (y_i - y_j)^p L_{ijp} + \sum\sum\sum\sum y_i y_j y_k (y_m - \frac{1}{3}(1 - y_i - y_j - y_k)) L_{ijkm} \quad (6.15)$$

where m takes the value i, j and k in turn and p takes integer values from zero up to a usual maximum of two. The respective summations represent contributions from binary and ternary interactions between species i, j and k.

The model coefficients, L, are functions of temperature, for example $\mathrm{L_{ijp} = L_0 + L_1 T}$. When the model coefficients are zero, the solution is considered ideal. That said, non-ideal behaviour between compounds is described successfully by their associates, signifying that the interaction between various associates is ideal.

Quasichemical Model

The quasichemical model was developed by Pelton and Blander in the 1980s (Pelton and Blander 1986; Pelton and Blander 1987). It involves determining the interactions, or bonding between second-nearest-neighbour metals (SNN). The change in energy due to these bonds or interactions is represented by a mathematical equation, which expands in composition and has temperature-independent and temperature-dependent terms. By fitting thermodynamic properties and phase equilibria in the binary, ternary and quaternary systems for each constituent, the authors were able to expand compositions to multi-component systems. The result however has been a multiplication of terms that makes the systems quite complex. This technique has been used intensively through the years and has been successful in representing phase equilibria and chemical thermodynamics (ativities) of liquid alloys (Kang et al. 2007; Kang et al. 2008; Kang et al. 2009), molten salts (Chartrand and Pelton 2001a; Chartrand and Pelton 2001b), molten sulphides (Waldner and Pelton 2004b; Waldner and Pelton 2004a; Waldner and Pelton 2005), and an abundance of molten oxide systems (Hidayat et al. 2015; Wu et al. 1993; Kang 2012; Xie et al. 2016; Eriksson et al. 2000; Wu, Eriksson, and Pelton 1993; Degterov et al. 2001). The thermochemistry software, FactSage, has adapted the modified quasichemical model to describe multi-component slag systems (Bale et al. 2002). A short description of the model follows.

The atoms of Equation 6.16 are distributed over the sites of the quasi-lattice. In the binary AxOy−BxOy solution, for example, short-range ordering is taken into account by considering the SNN pair exchange reaction:

$$(A - O - A) + (B - O - B) = 2(A - O - B), \;\; \Delta g_{AB} \quad (6.16)$$

where $\mathrm{\Delta g_{AB}}$ in chemical reaction 6.16 is the non-configurational Gibbs energy change for the formation of two moles of pairs, (A-O-B). The total Gibbs energy of the solution is given by Equation 6.17:

$$G = n_{A_xO_y} g^{\circ}_{A_xO_y} + n_{B_xO_y} g^{\circ}_{B_xO_y} - T\Delta S^{config} + n_{AB} \;\; (\Delta g_{AB}/2) \quad (6.17)$$

where $\mathrm{n_{AB}}$ is the number of moles of (A-B) bonds at equilibrium. No expression is known for the entropy of mixing in three dimensions. Therefore, an approximation equation is used. The configurational entropy ($\mathrm{\Delta S^{config}}$) of mixing expression for the random mixing of the bonds over

bond sites in one dimension (Ising approximation) is given by Equation 6.18 and is a function of $\mathrm{n_{AB}}$ (Eriksson et al. 2000). The expression for configurational entropy is expressed in pair fractions and coordination equivalent fractions.

$$\Delta S^{config} = -R(n_A ln x_A + n_B ln x_B) - R[n_{AA} ln(\frac{X_{AA}}{{Y^2}_A}) + n_{BB} ln(\frac{X_{BB}}{{Y^2}_B}) + n_{AB} ln(\frac{X_{AB}}{2Y_A Y_B})]. \quad (6.18)$$

The pair fraction is defined by Equation 6.19:

$$X_{ij} = \frac{n_{ij}}{n_{AA} + n_{BB} + n_{AB}} \quad (6.19)$$

$\mathrm{Y_A}$ and $\mathrm{Y_B}$ are coordination equivalent site fractions and are expressed as follows:

$$Y_A = \frac{Z_A n_A}{Z_A n_A + Z_B n_B} = \frac{Z_A X_A}{Z_A X_A + Z_B X_B} = 1 - Y_B. \quad (6.20)$$

Each cation specie has a corresponding coordination number, Z in Equation 6.20. According to the existing FactSage FTOxid database, the divalent Z is always set at 1.3774. Therefore, the following Z's are defined in Equation 6.21 for cation species with different valances:

$$\frac{Z_{A^{5+}}}{5} = \frac{Z_{A^{4+}}}{4} = \frac{Z_{A^{3+}}}{3} = \frac{Z_{A^{+}}}{1} = \frac{1.3774}{2}. \quad (6.21)$$

To obtain an equilibrium amount of $\mathrm{n_{AB}}$, the partial differential $\frac{\partial \mathrm{G}}{\partial \mathrm{n_{AB}}}$ is set to zero. This results effectively in a quasichemical equilibrium constant for chemical reaction 6.16.

$$\frac{X_{AB}^2}{X_{AA} X_{BB}} = 4exp(\frac{-\Delta g_{AB}}{RT}) \quad (6.22)$$

$\Delta \mathrm{g_{AB}}$ in Equation 6.22 can be expanded as an empirical polynomial function in the mole fractions of pairs. This function is given by Equation 6.23.

$$\Delta g_{AB} = \Delta g^{\circ}_{AB} + \sum_{i \geq 1} g^{i0}_{AB} X^i_{AA} + \sum_{j \geq 1} g^{0j}_{AB} X^j_{BB} \quad (6.23)$$

Equation 6.23 can also be expressed in terms of "coordination-equivalent" fractions. In addition to the binary terms, the model can have ternary terms, $\Delta \mathrm{g_{AB(C)}}$, which account for the effect of the component C upon the energy $\Delta \mathrm{g_{AB}}$ of pair exchange reaction. The term is typically expressed as a function of mole fraction of pairs or in terms of the "coordination-equivalent" fractions. See Eriksson et al. (2000) for a further explanation of the quasichemical model.

6.3.3 Solid Solutions

It is known that there are two types of solid solutions: substitutional and interstitial. For the substitutional type, solute atoms substitute for the host atoms. It is stated in Callister (2007) that there are several features of the solute and solvent atoms that determine the degree of solubility, and these are as follows:

- **Atomic size**: An appreciable amount of solute will dissolve in the solvent when the difference in atomic radii between the atom types is less than about $\pm$15 %.

  It is seen in Table 6.1 that the ionic radii of Fe, Ti and V corresponding to the highest positive charges are within 15 % of each other. Therefore, complete or partial solubility between V_2O_5(s), TiO_2(s) and Fe_2O_3(s) will occur on the basis of atomic size factor.

- **Crystal structure**: For appreciable solubility, crystal structures of both atom types must be the same.
- **Electronegativity**: The higher the positive valence one element and the lower the negative valance of another other element, the greater the likelihood that they will form an intermetallic compound instead of a substitutional solid solution.
- **Valence**: A metal will have more of a tendency to dissolve another metal of higher valency than one of a lower valency, provided that all aforementioned factors are equal.

Table 6.1: Ionic radii of elements V, Ti and Fe (Shannon 1976).

Species	Ionic radius (pm)	Species	Ionic radius (pm)	Species	Ionic radius (pm)
V^{2+}	93	Ti^{2+}	100	Fe^{2+} (High spin)	92
V^{3+}	78	Ti^{3+}	81	Fe^{3+} (High spin)	78.5
V^{4+}	72	Ti^{4+}	74.5		
V^{5+}	68				

For interstitial solid solutions, impurity atoms fill the voids or interstices among the host atoms. This type of solid solution normally forms when the atomic diameter of an interstitial impurity is significantly smaller than that of the host atoms. Normally, the maximum allowable concentration of interstitial impurity atoms is below 10 molar % (Callister 2007).

Solid solutions in the Fe-Ti-V-O system in air are assumed to be substitutional and were developed within the framework of the compound energy formalism (CEF) (Hillert and Staffansson 1970; Sundman and Agren 1981; Hillert 2001). This means that a mathematical expression such as the CEF is more general than the actual physical model and can be applied to various constituents with different behaviour in a phase. When such a generalised expression is obtained, it is referred to as a formalism. It has been shown that the CEF is well suited to model solid solutions with two or more distinct sub-lattices. Furthermore, it allows for cations and anions of different valances to mix in different sub-lattices, corresponding to the structure of a solid solution (Lukas, Fries, and Sundman 2007).

$$G_m = \sum_i \sum_j X_i X_j G^{\circ}_{ij} - TS_{config} + G_e \tag{6.24}$$

$\mathrm{X_i}$ and $\mathrm{X_j}$ in Equation 6.24 represent the site fractions of constituents i and j on the first and second sublattices, respectively. $\mathrm{S_{config}}$ is the configurational entropy and is given by Equation 6.25:

$$S_{config} = -R(n \sum_i X_i ln X_i + m \sum_j X_j ln X_j) \tag{6.25}$$

with n and m being the stoichiometric constants of each lattice and R the ideal gas constant.

Spinel Phase

Spinels are some of the most complicated phases to model and require a number of assumptions to reproduce experimental data. Spinels have the chemical formula $A_1B_2O_4$where A is a divalent and B a trivalent cation. The A and B atoms occupy tetrahedral (T) and octahedral (O) sites in the elemental cell. When T-sites are fully occupied by B atoms, while O-sites are occupied by A and B in equal amount, the spinel is called an inverse spinel. The spinel can be described by the general chemical formula $(\mathrm{A_{1-i}B_i})^{\mathrm{T}}[\mathrm{A_iB_{2-i}}]^{\mathrm{O}}\mathrm{O_4}$ with degree of inversion i. The inversion parameter

is defined as the fraction of B cations occupying tetrahedral sites. Typically, some oxygen non-stoichiometry occurs at higher oxygen pressures, which can be modelled by neutral vacancies (Va) on a cation sub-lattice. The vacancies are assumed to be on the octahedral sub-lattice, although no experimental evidence can support this assumption. One mole of solution can then be typically written as $(\mathrm{A},\mathrm{B})(\mathrm{A},\mathrm{B},\mathrm{Va})_2\mathrm{O}_4$. For this type of spinel, six end-members are derived accordingly and each has its own respective Gibbs energy, $\mathrm{G_{ij}}$ (Sundman 1991; Degterov et al. 2001; Barry et al. 1992).

The models for spinel solid solutions are developed within the framework of the CEF. It is well suited to model solid solutions with two or more distinct sub-lattices. The Gibbs free energy expression per formula unit is given by Equation 6.24. $\mathrm{S_{config}}$ is the configurational entropy and is derived from Equation 6.25:

$$S_{config} = -R(\sum_i X_i lnX_i + 2\sum_j X_j lnX_j) \tag{6.26}$$

with n in Equation 6.25, the stoichiometric constant of the octahedral lattice equalling = 2. The application of CEF for spinels has been discussed by Sundman (1991), Barry et al. (1992), and Degterov et al. (2001) and their approach was used in this study. The treatment of spinels essentially assumes that the excess Gibbs energy in Equation 6.24 equals zero and that the end-members/pseudocomponents are sufficient to describe the solution. A set of linear combinations that are related to the energies of classical site exchange reactions is developed. These linear combinations, which have physical sense, are optimised in a sequence of optimisation. The optimisation sequence and parameters are carefully chosen to minimise the number of combinations required. The rest of the parameters are then set to zero. This approach has been followed in several other studies (Degterov et al. 2001; Jung, Deceterov, and Pelton 2004; Zhang and Chen 2013) and has successfully described spinel solid solutions.

In this study, only model parameters that were previously optimised by other authors are used. For example, magnetite is modelled as a two-sub-lattice developed within the framework of the CEF. It has the chemical formula $(\mathrm{Fe^{2+}},\mathrm{Fe^{3+}})^{\mathrm{T}}[\mathrm{Fe^{2+}},\mathrm{Fe^{3+}},\mathrm{Va}]_2^{\mathrm{O}}\mathrm{O}_2^{4-}$. The solution is treated as ideal, hence six end-members are required to describe the phase. They have the following chemical formulas: $\mathrm{Fe^{2+}Fe_2^{2+}O_4}$, $\mathrm{Fe^{3+}Fe_2^{3+}O_4}$, $\mathrm{Fe^{3+}Fe_2^{2+}O_4}$, $\mathrm{Fe^{2+}Fe_2^{3+}O_4}$ and $\mathrm{Fe^{3+}Va_2O_4}$ and $\mathrm{Fe^{2+}Va_2O_4}$. However, all but one end-member component, $\mathrm{Fe^{2+}Fe_2^{3+}O_4}$, are electrically charged, and the remainder can therefore not exist physically. The only possible equilibrium combination that is neutral falls in the composition plane presented on Figure 6.3:

Figure 6.3 presents a schematic/prism of the pseudocomponents and the composition range of a spinel on a neutral plane. A complete inverse spinel has Fe^{3+} cations occupying tetrahedral sites and equal molar amounts Fe^{3+}, Fe^{2+} occupying octahedral sites. There is one more neutral apex that lies on the line $\mathrm{Fe^{3+}},\mathrm{Fe^{3+}}$-$\mathrm{Fe^{3+}},\mathrm{Va}$ and is marked $\gamma - \mathrm{Fe_2O_3}$. It has a composition, $\mathrm{Fe^{3+}[Fe_{5/6}^{3+}Va_{1/6}]_2}$ and corresponds to 4/3 moles of the γ modification of the oxide Fe_2O_3(s), which in turn has a spinel-related structure. The end-member compounds of the model are $(\mathrm{Fe^{3+}})_{\mathrm{T}}[\mathrm{Fe_2^{3+}}]_{\mathrm{O}}\mathrm{O}_4^{2-}$ and $(\mathrm{Fe^{3+}})^{\mathrm{T}}[\mathrm{Va_2}]^{\mathrm{O}}\mathrm{O}_4^{2-}$. Eight moles of $\gamma - \mathrm{Fe_2O_3}$ are given by Equation 6.27:

$$8\gamma - Fe_2O_3 = 6G_m = 5G^{\circ}_{Fe^{3+}Fe^{3+}} + G^{\circ}_{Fe^{3+}Va} - 2RT[5ln5 + 6ln6] \tag{6.27}$$

The line between a normal and inverse spinel corresponds to all possible situations for stoichiometric composition. For the case of higher Fe^{3+} concentration, a set of parallel lines is presented on the plane in which the Gibbs energy is minimised to find the state of equilibrium.

It is not possible to determine standard Gibbs energies of formation of end-members experimentally with non-neutral composition. Therefore, the degree of inverse, otherwise known as the inverse parameter, and exchange reaction parameters need to be defined to subsequently derive Gibbs energy expressions for end-member components. In addition, excess oxygen on the octahedral lattice is described by two parameters, $\mathrm{V_{Fe^{2+}}}$ and $\Delta_{\mathrm{Fe^{2+}Fe^{3+}Va}}$. These mathematical notations were

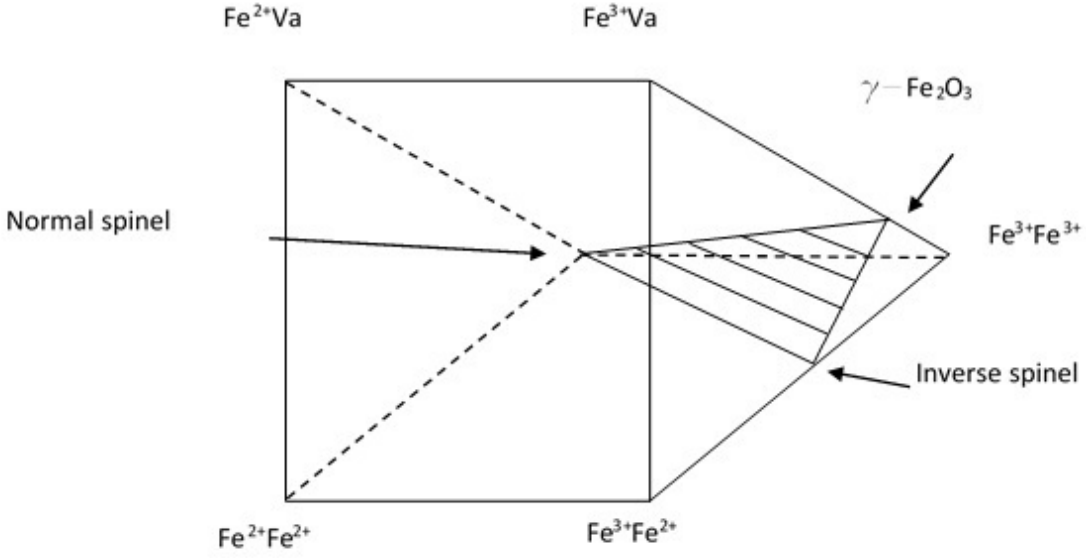

Figure 6.3: The neutral plane in the FeO–Fe_2O_3 spinel with excess Fe_2O_3. Each corner represents an end-member of the solution (Barry et al. 1992).

derived in the studies of Degterov et al. (2001) and Barry et al. (1992), and only the final reciprocal expressions for end-member components are shown here in Equation 6.28-Equation 6.36:

$$\mathrm{I_{Fe^{2+}Fe^{3+}}} = \mathrm{G^{\circ}_{Fe^{2+}Fe^{2+}}} + \mathrm{G^{\circ}_{Fe^{3+}Fe^{2+}}} - 2\mathrm{G^{\circ}_{Fe^{2+}Fe^{3+}}} \tag{6.28}$$

$$\Delta_{\mathrm{Fe^{2+}Fe^{3+}}} = \mathrm{G^{\circ}_{Fe^{2+}Fe^{2+}}} + \mathrm{G^{\circ}_{Fe^{3+}Fe^{3+}}} - \mathrm{G^{\circ}_{Fe^{2+}Fe^{3+}}} - \mathrm{G^{\circ}_{Fe^{3+}{+}Fe^{2+}}} \tag{6.29}$$

$$V_{Fe^{3}+} = G^{\circ}_{Fe^{3+}Va} - 5/7G^{\circ}_{Fe^{3+}{+}Fe^{2+}} \tag{6.30}$$

$$V_{Fe^{3}+} = 8G^{\circ}_{\gamma-Fe_2O_3} - 2RT(5ln5 - 6ln6) - 5G^{\circ}_{Fe^{2+}Fe^{2+}} - 5/7G^{\circ}_{Fe^{3+}{+}Fe^{2+}} \tag{6.31}$$

$$\Delta_{Fe^{3+}Fe^{2+}Va} = G^{\circ}_{Fe^{2+}Fe^{2+}} + G^{\circ}_{Fe^{3+}Va} - G^{\circ}_{Fe^{3+}Fe^{2}+} - G^{\circ}_{Fe^{2+}Va} = 0 \tag{6.32}$$

In addition, the condition, $\mathrm{G_{Fe^{3+}{+}Fe^{2+}}} = \mathrm{G_{Fe^{2+}Fe^{3+}}}$ was proposed by Sundman (1991) and adopted by Degterov et al. (2001). Subsequently, the expressions for the end-members are derived from this condition and from rearrangement of Equation 6.28, Equation 6.29, Equation 6.31 and Equation 6.32.

$$G^{\circ}_{Fe^{2+}Fe^{2+}} = G^{\circ}_{Fe^{2+}Fe^{3+}} - I_{Fe^{2+}Fe^{3+}} + \Delta_{Fe^{2+}Fe^{3+}} \tag{6.33}$$

$$G^{\circ}_{Fe^{3+}Fe^{3+}} = G^{\circ}_{Fe^{3+}{+}Fe^{2+}} + I_{Fe^{2+}Fe^{3+}} \tag{6.34}$$

$$G^{\circ}_{Fe^{3+}Va} = \frac{5}{7}G^{\circ}_{Fe^{3+}{+}Fe^{2+}} + V_{Fe^{3}+} \tag{6.35}$$

$$G^{\circ}_{Fe^{2+}Va} = \frac{5}{7}G^{\circ}_{Fe^{3+}{+}Fe^{2+}} + V_{Fe^{3}+} - I_{Fe^{2+}Fe^{3+}} + \Delta_{Fe^{2+}Fe^{3+}} - \Delta_{Fe^{3+}Fe^{2+}Va} \tag{6.36}$$

All of the parameters and end-members for magnetite/spinel have previously been optimised in the study of Degterov et al. (2001) and are subsequently used in this study without any adjustments. Moreover, the spinel solid solution Fe-O system exhibits magnetic ordering. The contribution to the Gibbs energy of the solution due to magnetic ordering is further discussed in Section 6.5.

Non-stoichiometry of Rutile

It is postulated from the thermodynamic assessment of Eriksson and Pelton (1993), Kang, Jung, and Lee (2006), and Cancarevic, Zinkevich, and Aldinger (2007) that rutile or titanium dioxide might exhibit a degree of non-stoichiometry. In this case, the degree of non-stoichiometry is characterised by the ratio of oxygen to titanium, which is less than two. The nature of the defect has a structure $\mathrm{TiO_{2-x}}$. Cancarevic, Zinkevich, and Aldinger (2007) discovered some controversy in the literature, meaning that experimental data suggested either the existence of double oxygen vacancies and free electrons or their combination with interstitially dissolved Ti^{3+} ions. In their work, the oxygen vacancy model was preferred, the reason being that the lack of negative charge in the anion sub-lattice due to oxygen vacancies, is effectively compensated for by an inclusion of Ti^{3+} cations on the cation sub-lattice. The non-stoichiometry of rutile is described and developed in the framework of the CEF. Rutile has the chemical formula $(\mathrm{Ti^{4+}, Ti^{3+}})(\mathrm{O, Va})_2$, followed by the molar Gibbs energy being expressed as:

$$\begin{aligned} G_{TiO_{2-x}} = X_{Ti^{4+}}X_{O^{2-}}G^{\circ}_{Ti^{4+}:O^{2-}} + X_{Ti^{3+}}X_{O^{2-}}G^{\circ}_{Ti^{3+}:O^{2-}} + X_{Ti^{4+}}X_{Va}G^{\circ}_{Ti^{4+}:Va} + \\ X_{Ti^{3+}}X_{Va}G^{\circ}_{Ti^{3+}:Va} + RT(X_{Ti^{4+}}lnX_{Ti^{4+}} + X_{Ti^{3+}}lnX_{Ti^{3+}}) \\ +2RT(X_{O^{2-}}lnX_{O^{2-}} + X_{Va}lnX_{Va}) + G_e. \end{aligned} \tag{6.37}$$

The non-stoichiometry of rutile is treated similar to spinel. The excess term in Equation 6.37 is set to zero and charged end-member species are used as model representatives. In this case, a two-dimensional square plane (see Figure 6.4), with a neutral line is used to explain the non-stoichiometry model of rutile.

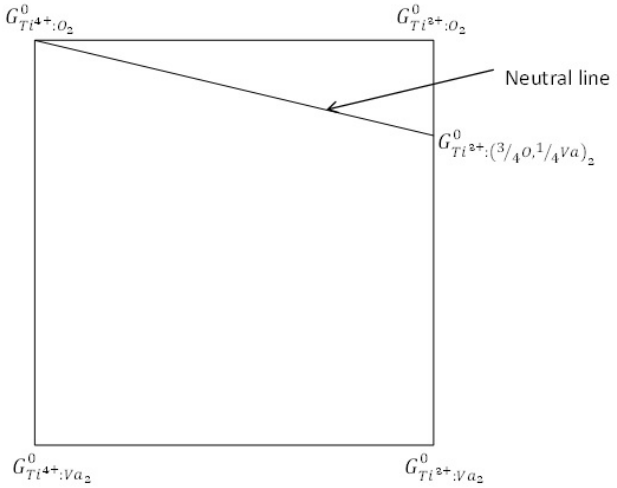

Figure 6.4: Schematic representation of end-member components and possible composition ranges on a neutral line of non-stoichiometric rutile (Cancarevic, Zinkevich, and Aldinger 2007).

The four end-member species are presented on the corners of the square. The neutral end-member, $\mathrm{G^{\circ}_{Ti^{4+}:O^{2-}}}$ corresponds to stoichiometric rutile, while the other three compounds have a net charge of more or less than zero and cannot physically exist. The neutral compound Ti_2O_3 has a rutile-related structure and is a combination of $(\mathrm{Ti^{3+}})(\mathrm{O^{2-}})$ and $(\mathrm{Ti^{3+}})(\mathrm{Va})$. The thermodynamic properties of $\mathrm{TiO_{1.5}}$ are derived in a similar way to the γ modification of the oxide Fe_2O_3(s) and are expressed as follows (Cancarevic, Zinkevich, and Aldinger 2007):

$$G^{\circ}_{TiO_{1.5}} = 1/2G^{\circ}_{R-Ti_2O_3} = \frac{3}{4}G^{\circ}_{Ti^{3+}:O^{2-}} + \frac{1}{4}G^{\circ}_{Ti^{3+}:Va} + 2RT(\frac{3}{4}ln\frac{3}{4} + \frac{1}{4}ln\frac{1}{4}). \tag{6.38}$$

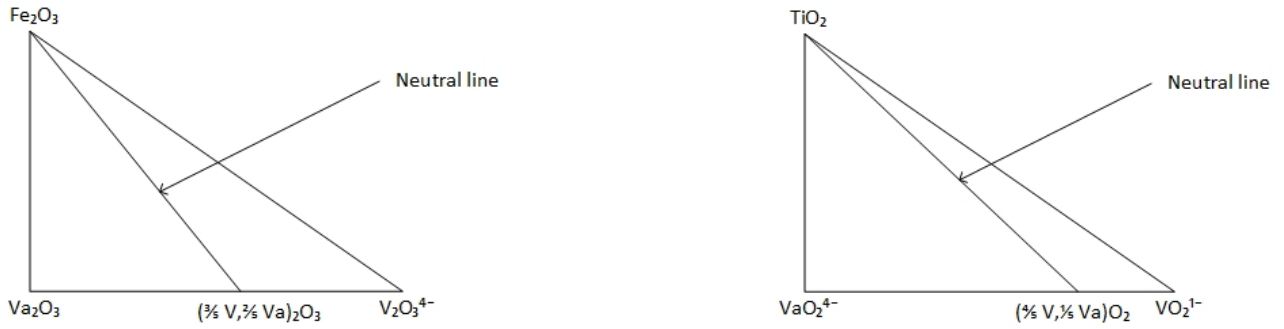

(a) Hematite solid solution triangle.

(b) Rutile solid solution triangle.

Figure 6.5: Schematic representation of end-member components and possible composition ranges on a neutral line of a rutile and hematite solid solution.

The third term in Equation 6.38 is an entropy of mixing attribution on the anion lattice. Furthermore, the additional end-members are derived and are given by Equation 6.39 and Equation 6.40:

$$G^{\circ}_{Ti^{4+}:Va} = G^{\circ}_{TiO_2} - G^{\circ}_{O_2(g)} \tag{6.39}$$

$$G^{\circ}_{Ti^{4+}:O^{2-}} - G^{\circ}_{Ti^{3+}:Va} = G^{\circ}_{Ti^{4+}:Va} - G^{\circ}_{Ti^{3+}:O^{2-}} \tag{6.40}$$

The values of end-members are functions of temperature and were derived from the thermodynamic assessment of the Ti-O system by Cancarevic, Zinkevich, and Aldinger (2007). The model parameters could have been used in this evaluation without any alteration when the ASM was used to describe the slag phase. Cancarevic, Zinkevich, and Aldinger (2007) had used the ASM to describe the liquid phase of the Ti-O system. Therefore, it was not necessary to develop another set of model equations for describing the behaviour between Ti_3O_2(l) and TiO_2(l) in the slag phase of the Ti-V-O system when some model parameters were already optimised. In other words, interaction parameters to describe non-ideal behaviour between Ti_3O_2(l) and TiO_2(l) in the slag are taken from Cancarevic, Zinkevich, and Aldinger (2007).

However, when the MQM was used to describe the liquid phase, a simple Henrian solution of $\mathrm{TiO_{1.5}}$ in TiO_2 had to be used to describe the non-stoichiometry of rutile. This approach was adopted by Eriksson and Pelton (1993) and Kang, Jung, and Lee (2006). Again, the aim is to remain consistent with the literature and to reduce the number of parameters that were optimised in this study.

$\mathrm{V_2O_5}$ Dissolution in Hematite and Rutile Phases

The dissolution of V_2O_5(s) in the hematite and rutile phases was shown experimentally to occur. As a result, an identical approach to that of spinel and rutile non-stoichiometry is followed, because metals with different oxidation states mix. The Gibbs free energy of the solutions are developed within the framework of the CEF (Equation 6.24). In the model, it is assumed that all cations mix in one lattice and all anions mix in a second lattice. Some vacancies are introduced into the cation sub-lattice for charge neutrality.

Hematite is represented as a mixture of V^{5+}, Fe^{3+} ions and vacancies on cation sites and oxygen, being the only anion, in the second sub-lattice. It has the chemical formula $(\mathrm{V^{5+}, Fe^{3+}, Va})_2(\mathrm{O})_3$, and charged end-member species are used as model representatives. A triangular plane with a neutral line is presented in Figure 6.5a and explain the dissolution of V_2O_5(s) in the hematite phase.

The apexes of the triangle in Figure 6.5a each represents an end-member, and they have the following chemical formulas: $\mathrm{Fe_2^{3+}O_3^{2-}}$, $\mathrm{V_2^{5+}O_3^{2-}}$ and $\mathrm{Va_2O_3^{2-}}$.

The rutile solid solution (see Figure 6.5b) is also represented by three end-members, namely, $\mathrm{Ti}^{4+}\mathrm{O}_2^{2-}$, $\mathrm{V}^{5+}\mathrm{O}_2^{2-}$ and VaO_2^{2-}. Habel et al. (2006) showed experimentally a substitutional replacement of Ti^{4+} for V^{5+} in the rutile phase. To remain consistent with this finding, it was assumed that V dissolves substitutionally in the cation lattice. The model for the rutile solid solution is based on the second defect model proposed by Habel et al. (2006)(see Section 5.2). The model is represented by a mixture of V^{5+}, Ti^{4+} ions and vacancies on cation sites and oxygen being the only anion, in the second sub-lattice.

The molar Gibbs energies of both solid solutions are given by Equation 6.41a and Equation 6.41b:

$$G_{hem} = X_{Fe^{3+}}X_{O^{2-}}G^{\circ}_{Fe^{3+}:O^{2-}} + X_{V^{5+}}X_{O^{2-}}G^{\circ}_{V^{5+}:O^{2-}} + X_{Va}X_{O^{2-}}G^{\circ}_{Va:O^{2-}} + \\ +2RT(X_{Fe^{3+}}lnX_{Fe^{3+}} + X_{V^{5+}}lnX_{V^{5+}} + X_{Va}lnX_{Va}) + 3RT(X_{O^{2-}}lnX_{O^{2-}}) + G_e \tag{6.41a}$$

$$G_{Rut} = X_{Ti^{4+}}X_{O^{2-}}G^{\circ}_{Ti^{4+}:O^{2-}} + X_{V^{5+}}X_{O^{2-}}G^{\circ}_{V^{5+}:O^{2-}} + X_{Va}X_{O^{2-}}G^{\circ}_{Va:O^{2-}} + \\ +RT(X_{Ti^{4+}}lnX_{Ti^{4+}} + X_{V^{5+}}lnX_{V^{5+}} + X_{Va}lnX_{Va}) + 2RT(X_{O^{2-}}lnX_{O^{2-}}) + G_e. \tag{6.41b}$$

However, the last two components mentioned in both solid solutions are electrically charged and cannot physically exist. The compound, $(\frac{3}{5}\mathrm{V}, \frac{2}{5}\mathrm{Va})_2\mathrm{O}_3$ on the neutral line in Figure 6.5a corresponds to 3/5 mole of V_2O_5(s), which in turn has a hematite-related structure.

An identical compound exist on the rutile solid solution neutral line and has the chemical formula $(\frac{4}{5}\mathrm{V}, \frac{1}{5}\mathrm{Va})\mathrm{O}_2$. It corresponds to 2/5 mole of V_2O_5(s), which has a rutile-related structure. Therefore, the neutral species, $(\frac{3}{5}\mathrm{V}, \frac{2}{5}\mathrm{Va})_2\mathrm{O}_3$ and $(\frac{4}{5}\mathrm{V}, \frac{1}{5}\mathrm{Va})\mathrm{O}_2$, which are a combination of the two electrically charged end-members, are written as follows:

$$3/5G^{\circ}_{V_2O_5(s)-Hem} = \frac{3}{5}G^{\circ}_{V^{5+}:O^{2-}} + \frac{2}{5}G^{\circ}_{Va:O^{2-}} + 2RT(\frac{3}{5}ln\frac{3}{5} + \frac{2}{5}ln\frac{2}{5}) \tag{6.42a}$$

$$2/5G^{\circ}_{V_2O_5(s)-Rut} = \frac{4}{5}G^{\circ}_{V^{5+}:O^{2-}} + \frac{1}{5}G^{\circ}_{Va:O^{2-}} + RT(\frac{4}{5}ln\frac{4}{5} + \frac{1}{5}ln\frac{1}{5}). \tag{6.42b}$$

The third term in Equation 6.42a and Equation 6.42b is an entropy of mixing attribution on the cation lattices. In addition, the end-members are derived, rearranged and expressed as follows:

$$G^{\circ}_{Va:O^{2-}Hem} = 0 \tag{6.43a}$$

$$G^{\circ}_{Va:O^{2-}Rut} = 0 \tag{6.43b}$$

$$G^{\circ}_{V^{5+}:O^{2-}Hem} = G^{\circ}_{Hem-V_2O_5} - \frac{2}{3}G^{\circ}_{Va:O^{2-}} - \frac{10}{3}RT(\frac{3}{5}ln\frac{3}{5} + \frac{2}{5}ln\frac{2}{5}) \tag{6.44a}$$

$$G^{\circ}_{V^{5+}:O^{2-}Rut} = \frac{1}{2}G^{\circ}_{Rut-V_2O_5} - \frac{1}{4}G^{\circ}_{Va:O^{2-}} - \frac{5}{2}RT(\frac{4}{5}ln\frac{1}{5} + \frac{1}{5}ln\frac{1}{5}) \tag{6.44b}$$

$$G^{\circ}_{Fe^{3+}:O^{2-}} = G^{\circ}_{Fe2O3(s)} \tag{6.45a}$$

$$G^{\circ}_{Ti^{4+}:O^{2-}} = G^{\circ}_{TiO2(s)}. \tag{6.45b}$$

The terms, $\mathrm{G}^{\circ}_{\mathrm{Va:O^{2-}Hem}}$ and $\mathrm{G}^{\circ}_{\mathrm{Va:O^{2-}Rut}}$ are reference terms for other systems and have been set to zero (Zieniert and Fabrischnaya 2015). The other two terms, $\mathrm{G}^{\circ}_{\mathrm{V^{5+}:O^{2-}Hem}}$ and $\mathrm{G}^{\circ}_{\mathrm{V^{5+}:O^{2-}Rut}}$, were optimised with respect to their enthalpy of formation and standard entropy.

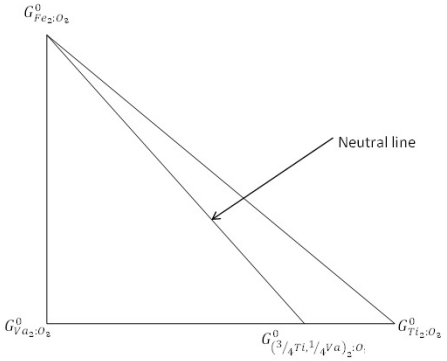

(a) Hematite solid solution triangle

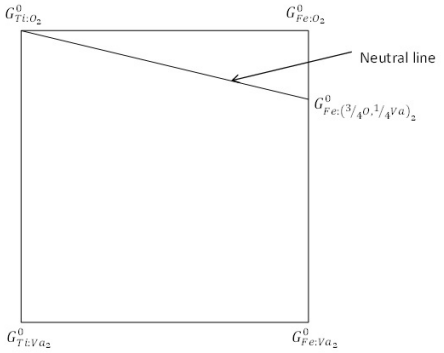

(b) Rutile solid solution square plane

Figure 6.6: Schematic representation of end-member components and possible composition ranges on a neutral line of a rutile and hematite solid solution in the Fe-Ti-O system.

Fe_2O_3 and TiO_2 Dissolution in Rutile and Hematite Phases

In Section 5.3 a solubility range of Fe_2O_3 in the rutile phase was first proposed and then investigated by Wittke (1967). The experimental data from Wittke (1967) indicated a solubility region of Fe_2O_3 in rutile. However, no experimental data were found in the literature describing TiO_2(s) dissolution in the hematite phase. Nevertheless, dissolution of Fe_2O_3(s) in the rutile phase and TiO_2(s) in the hematite phase is developed within the framework of the CEF. The rutile solid solution and hematite solid solution of the Fe-Ti-O system in air have the chemical formulas $(\mathrm{Ti}^{4+},\mathrm{Fe}^{3+})(\mathrm{O},\mathrm{Va})_2$ and $(\mathrm{Fe}^{3+},\mathrm{Ti}^{4+},\mathrm{Va})_2(\mathrm{O})_3$. The molar Gibbs energies of rutile solid solution and hematite solid solution of the Fe-Ti-O system in air are expressed as follows:

$$\begin{aligned} G_{Rut} = {} & X_{Ti^{4+}}X_{O^{2-}}G^{\circ}_{Ti^{4+}:O^{2-}} + X_{Fe^{3+}}X_{O^{2-}}G^{\circ}_{Fe^{3+}:O^{2-}} + X_{Ti^{4+}}X_{Va}G^{\circ}_{Ti^{4+}:Va} + \\ & X_{Fe^{3+}}X_{Va}G^{\circ}_{Fe^{3+}:Va} + RT(X_{Ti^{4+}}lnX_{Ti^{4+}} + X_{Fe^{3+}}lnX_{Fe^{3+}}) \\ & + 2RT(X_{O^{2-}}lnX_{O^{2-}} + X_{Va}lnX_{Va}) + G_e \end{aligned} \tag{6.46a}$$

$$\begin{aligned} G_{hem} = {} & X_{Fe^{3+}}X_{O^{2-}}G^{\circ}_{Fe^{3+}:O^{2-}} + X_{Ti^{4+}}X_{O^{2-}}G^{\circ}_{Ti^{4+}:O^{2-}} + X_{Va}X_{O^{2-}}G^{\circ}_{Va:O^{2-}} + \\ & 2RT(X_{Fe^{3+}}lnX_{Fe^{3+}} + X_{Ti^{4+}}lnX_{Ti^{4+}} + X_{Va}lnX_{Va}) + 3RT(X_{O^{2-}}lnX_{O^{2-}}) + G_e. \end{aligned} \tag{6.46b}$$

Where the CEF was used to develop and describe any solution, the excess terms are set to zero. The last term in Equation 6.46 and Equation 6.46b is again set to zero and end-member species serve as model representatives. A two-dimensional square plane (see Figure 6.4) and triangle, with neutral lines are used to explain the rutile solid solution and hematite solid solution of the Fe-Ti-O system in air.

For the rutile solid solution, four end-member species are presented on the corners of the square. The neutral end-member, $\mathrm{G}^{\circ}_{\mathrm{Ti}^{4+}:\mathrm{O}^{2-}}$ corresponds to stoichiometric rutile, while the other three compounds have a net charge of higher or lower than zero and cannot physically exist. The neutral compound, $\mathrm{G}^{\circ}_{(\mathrm{Fe})(3/4\mathrm{O},1/4\mathrm{Va})_2}$ has a rutile-related structure and is a combination of $(\mathrm{Fe}^{3+})(\mathrm{O}^{2-})$ and $(\mathrm{Fe}^{3+})(\mathrm{Va})$. The thermodynamic properties of $\mathrm{FeO}_{1.5}$ are derived in a similar way to the γ modification of the oxide $\mathrm{TiO}_{1.5}$ in Subsubsection 6.3.3.

For the hematite solid solution, three end-member species are presented on the corners of the triangle, of which two compounds have a net charge of higher or lower than zero. The neutral compound, $\mathrm{G}^{\circ}_{(3/4\mathrm{Ti},1/4\mathrm{Va})_2:\mathrm{O}_3}$ has a hematite-related structure and is a combination of $\mathrm{G}^{\circ}_{\mathrm{Va}_2:\mathrm{O}_3}$ and

$\mathrm{G_{Ti_2:O_3}}$. This model was derived in a similar way compared to the hematite solid solution of the Fe-V-O system in air (see Subsubsection 6.3.3).

$$G^{\circ}_{FeO_{1.5}} = 1/2G^{\circ}_{Fe_2O_3-Rut} = \frac{3}{4}G^{\circ}_{Fe^{3+}:O^{2-}} + \frac{1}{4}G^{\circ}_{Fe^{3+}:Va} + 2RT(\frac{3}{4}ln\frac{3}{4} + \frac{1}{4}ln\frac{1}{4}) \tag{6.47a}$$

$$6/4G^{\circ}_{TiO2(s)-Hem} = \frac{3}{4}G^{\circ}_{Ti^{4+}:O^{2-}} + \frac{1}{4}G^{\circ}_{Va:O^{2-}} + 2RT(\frac{3}{4}ln\frac{3}{4} + \frac{1}{4}ln\frac{1}{4}) \tag{6.47b}$$

The third term in Equation 6.47a and Equation 6.47b is an entropy of mixing attribution on the anion and cation lattices. Furthermore, the additional end-members from the rutile solid solution are derived and expressed as follows:

$$G^{\circ}_{Ti^{4+}:Va} = G^{\circ}_{TiO_2} - G^{\circ}_{O_2(g)} \tag{6.48}$$

$$G^{\circ}_{Ti^{4+}:O^{2-}} - G^{\circ}_{Fe^{3+}:Va} = G^{\circ}_{Ti^{4+}:Va} - G^{\circ}_{Fe^{3+}:O^{2-}}. \tag{6.49}$$

Equation 6.47a, Equation 6.48 and Equation 6.49 are combined and rearranged to obtain expressions for $\mathrm{G^{\circ}_{Fe^{3+}:Va}}$ and $\mathrm{G^{\circ}_{Fe^{3+}:O^{2-}}}$:

$$G^{\circ}_{Fe^{3+}:Va} = -\frac{3}{4}G^{\circ}_{O_{2(g)}} + \frac{1}{2}G^{\circ}_{Fe_2O_3-Rut} + 2RT(\frac{3}{4}ln\frac{3}{4} + \frac{1}{4}ln\frac{1}{4}) \tag{6.50}$$

$$G^{\circ}_{Fe^{3+}:O^{2-}} = \frac{1}{4}G^{\circ}_{O_{2(g)}} + \frac{1}{2}G^{\circ}_{Fe_2O_3-Rut} + 2RT(\frac{3}{4}ln\frac{3}{4} + \frac{1}{4}ln\frac{1}{4}). \tag{6.51}$$

A thermodynamic evaluation of the Fe-Ti-O system in air was conducted by optimising enthalpies of formation and standard entropies of compounds $\mathrm{Fe_2O_3 - Rut}$ and $\mathrm{TiO_4 - Hem}$. Experimental data were reproduced well within acceptable error limits (see Section 12.1).

6.4 Ternary Interpolation

The slag solution in the Fe-Ti-V-O system in air was successfully described from binary $\mathrm{G_e}$ terms without the use of ternary $\mathrm{G_e}$ terms. However, small ternary terms can be introduced to fit experimental data, if required. Considering the system, 1, 2 and 3, the estimated binary excess Gibbs energy, can successfully be applied to estimate the excess Gibbs energy at point "p" in a ternary system from points a,b and c in Figure 6.7 using Equation 6.52.

$$g^e = x_1x_2\alpha_{12(a)} + x_2x_3\alpha_{23(b)} + x_1x_3\alpha_{13(c)} + (ternaryterms) \tag{6.52}$$

Several methods have been proposed in the literature. These geometric models can be either symmetric or asymmetric. The Kohler (Kohler 1960) and Muggianu (Muggianu, Gambino, and Bros 1975) models are symmetric models and are normally applied when all three constituents are chemically similar. The Kohler/Toop (Toop 1965) and Muggianu/Toop models are asymmetric in nature; therefore, one component is singled out. In these two asymmetric models, the $\mathrm{G_e}$ terms , α_{12} and α_{31}, are assumed to remain constant along the lines where $\mathrm{x_1}$ is constant. For example, in the quasichemical model, substituting component 2 with component 3 is assumed to have no effect on the energy, α_{12} in the formation of (1-2) nearest neighbour pairs, and similarly for (3-1) pairs. Examples of such systems are SiO_2−CaO−MgO, S-Fe-Cu, Na-Au-Ag and $AlCl_3$−NaCl−KCl. The asymmetric component in these respective systems has been written first (Pelton 2001; Bale et al. 2002; Saunders and Miodownik 1998).

It has been demonstrated that not all systems can be described with a symmetric model. This is particularly true for systems where $\mathrm{G_e}$ is large and α_{12} and α_{13} depend strongly on composition.

When the chemical components 2 and 3 are similar ($\alpha_{23} = 0$), the $\mathrm{G_e}$ will remain nearly constant at $\mathrm{x_1}$ and this is predicted by the asymmetric models. However, the symmetric model will calculate an incorrect region of immiscibility (Pelton 2001; Bale et al. 2002).

After the MQM parameters of Equation 6.23 for the Fe-V-O, Fe-V-O and Fe-Ti-O systems in air were optimised, $\mathrm{G_e}$ of the ternary solution was estimated using a symmetric or asymmetric approximation. If, for example, the Kohler-type approximation is chosen for α_{12}, the ratio $\frac{\mathrm{x_2}}{\mathrm{x_1 + x_2}}$ along the line "ap" in Figure 6.7 remains constant. In addition, this ratio is equal to $\mathrm{x_2}$ at point "a" where $x_1 + x_2 = 1$. The function α_{12} is consequently written as follows (Pelton 2001; Bale et al. 2002; Saunders and Miodownik 1998):

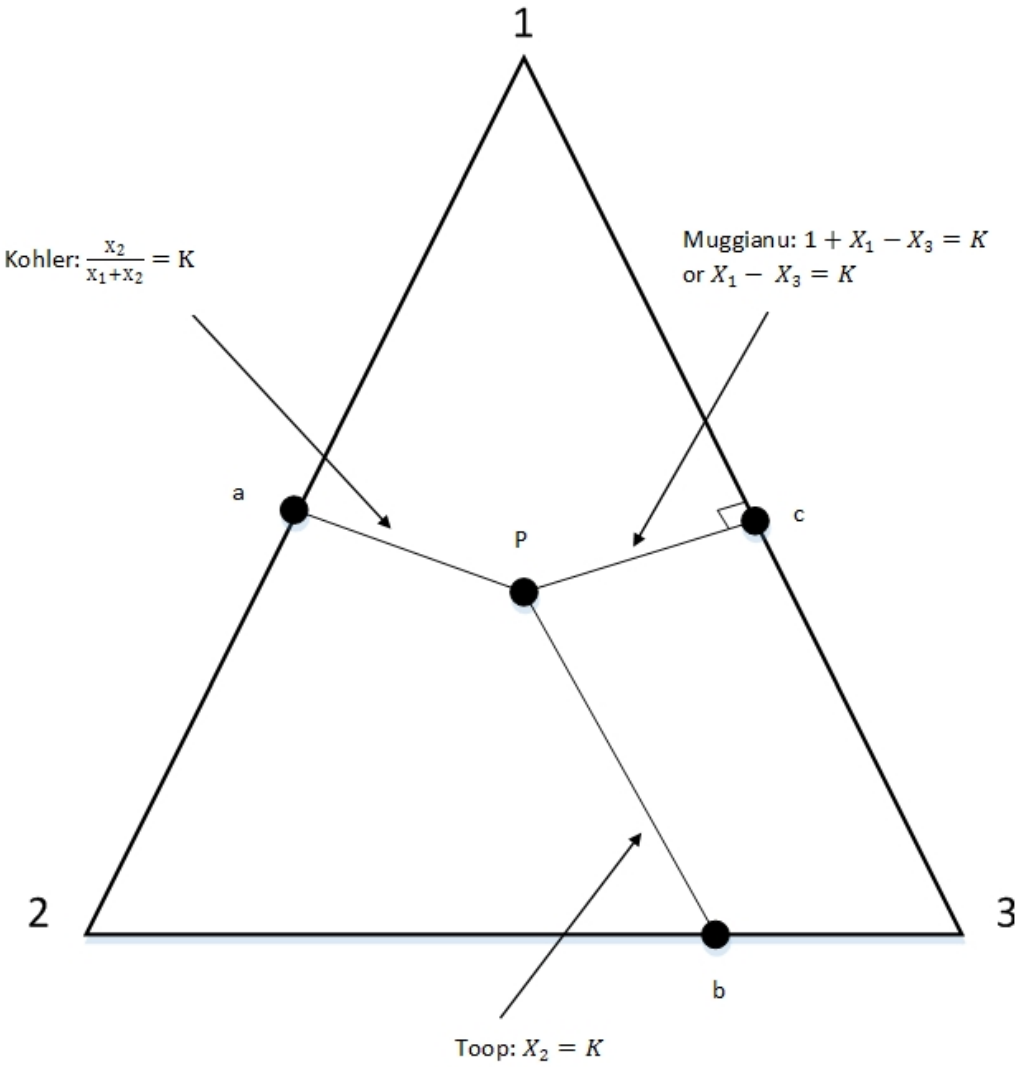

Figure 6.7: A geometric model for estimating ternary thermodynamic properties from optimized binary data - Redrawn from Bale et al. (2002) and Pelton (2001).

$$\alpha_{12(a)} = \sum_{p\geq 0}\sum_{q\geq 0} g_{12}^{pq}\left(\frac{x_2}{x_1+x_2}\right)^p\left(\frac{x_2}{x_1+x_2}\right)^q \tag{6.53}$$

where $\mathrm{g_{12}^{pq}}$ in Equation 6.53 are the binary coefficients of Equation 6.23. However, if the 1-2 binary system has been optimised with a Redlich-Kister expansion, α_{12} in Equation 6.52 is written as:

$$\alpha_{12(a)} = \sum_{p\geq 0} L_{12p}(\frac{x_1 - x_2}{x_1 + x_2})^p \tag{6.54}$$

where the $\mathrm{L_{12p}}$ are the binary coefficients from Equation 6.15. The approximations for α_{13} and α_{23} are written in terms of ratios $\frac{\mathrm{x_3}}{\mathrm{x_3 + x_1}}$ and $\frac{\mathrm{x_2}}{\mathrm{x_3 + x_2}}$ respectively.

A Toop interpolation method was used to approximate α_{23} along lines of constant $\mathrm{x_3}$ as in Figure 6.7. Subsequently, α_{23} is set along these lines of constant $\mathrm{x_3}$ by means of substitution (Pelton 2001; Bale et al. 2002):

$$\alpha_{23(b)} = \sum_{p\geq 0}\sum_{q\geq 0} g_{23}^{pq} x_3^p (1 - x_3)^q \tag{6.55}$$

or with Redlich-Kister expansion,

$$\alpha_{23(b)} = \sum_{p\geq 0} L_{23p}(x_3 - (1 - x_3)^p), \tag{6.56}$$

and finally, if a Muggianu-type method is used to approximate α_{13}, it is noted that $(\mathrm{x_1 - x_3})$ is constant along line "cp". If $\mathrm{g_{13}}$ of the binary system 1-3 was expressed with the Redlich-Kister polynomial, Equation 6.15 can be directly substituted into Equation 6.52. This model is sometimes referred to as the "Muggianu-Redlich-Kister model" (Pelton 2001; Bale et al. 2002).

However, if α_{13} is expressed as general polynomial as in Equation 6.23, then it is noted that the functions $(1 + \mathrm{x_1 - x_3})/2$ and $(1 - \mathrm{x_1 + x_3})/2$ are both constant along line "cp" in Figure 6.7. Moreover, these functions are equal to $\mathrm{x_1}$ and $\mathrm{x_3}$ in the 1-3 binary system. Therefore, $\alpha_{13(c)}$ is expressed along the line "cp" as follows (Pelton 2001; Bale et al. 2002):

$$\alpha_{13(c)} = \sum_{p\geq 0}\sum_{q\geq 0} g_{13}^{pq}(\frac{1 + x_1 - x_3}{2})(\frac{1 - x_1 + x_3}{2}). \tag{6.57}$$

From these three models, many sets of approximations for each of the three binary α_{pq} functions can be made. In total, there are sixty-four possible geometric ternary models. Of these, the four models that have been used frequently for thermodynamic assessments are the Kohler, Kohler/Toop, Muggianu and Muggianu/Toop models. These models can then be used further for the extension to multicomponent systems (four or more components). However, such developments are outside the scope of the study and are not discussed.

6.5 Magnetic Ordering

In Section 6.3, the excess Gibbs energy of some solutions is defined. This resulted in expressions to describe deviations from ideal-solution behaviour. However, not all physical effects can be integrated into these mathematical expressions, hence some effects are modelled separately.

One such effect is the magnetic ordering in ferromagnetic materials such as Fe, Ni or Co. Where "Ferro" refers to the element, Fe. These elements and their ores are classified as ferromagnetic, and will exhibit permanent magnetism attributed to unpaired electrons in atomic orbitals. In other words, an unpaired electron is free to align its magnetic moment in any direction, in contrast to paired electrons that have their magnetic moments paired in opposite directions, consequently causing their magnetic fields to cancel out. In addition, the magnetic moments in ferromagnetic materials will line up parallel to one another, in order to maintain a lower energy state and retain magnetic characteristics in the absence of an applied field. Other forms of magnetism include paramagnetic (attraction to magnetic field), diamagnetic (repulsed by a magnetic field) (Saunders and Miodownik 1998; Lukas, Fries, and Sundman 2007; Janssens et al. 2007).

All materials exhibiting ferromagnetism behaviour have their own unique "offset temperature", better known as the Curie temperature. The Curie temperature is the Curie point where a material loses its ferromagnetic properties. The thermal tendency to disorder firmly overwhelms the energy-lowering caused by ferromagnetic ordering. A hematite and spinel solid solution (magnetite) exhibits magnetic ordering. The contribution of magnetic ordering of ferromagnetic materials to the molar Gibbs energy can be described by the model developed by Inden (1976). The equation describes the transition from the disordered state to the magnetic ordered state through a series based on the normalised $\tau = \mathrm{T}/\mathrm{T_c}$ and the magnetic moment β_m, where $\mathrm{T_c}$ is the Curie temperature and is defined by the inflection point of the magnetic entropy. In essence, the Gibbs energy contribution from magnetic ordering above the Curie temperature (>1) is described by the following expression:

$$G_m^{mo} = -RTln(\beta_m + 1)\Big(\frac{\tau^{-5}}{10} + \frac{\tau^{-15}}{315} + \frac{\tau^{-25}}{1500}\Big)/\Big(\frac{518}{1125} + \frac{11692}{15975}\Big(\frac{1}{p} - 1\Big)\Big) \tag{6.58}$$

and described by the next expression when below the Curie temperature (<1):

$$\begin{aligned} G_m^{mo} = &- RTln(\beta_m + 1)\Big(1 - \Big[\frac{79\tau^{-1}}{140p} + \frac{474}{497}\Big(\frac{1}{p} - 1\Big)\Big(\frac{\tau^3}{6} + \frac{\tau^9}{135} + \frac{\tau^15}{600}\Big)\Big] \\ &/\Big(\frac{518}{1125} + \frac{11692}{15975}\Big(\frac{1}{p} - 1\Big)\Big)\Big), \end{aligned} \tag{6.59}$$

where $\mathrm{T_c}$, parameter p and magnetic moment (β_m) for hematite are 955.67 °C, 0.28 and 8.3667, respectively (Bale et al. 2002). The CEF was used to describe spinel solid solution, therefore β_m and $\mathrm{T_c}$ need to be expressed as a function of composition. However, with limited experimental information available, some assumptions are required to make reasonable approximations for the values of β_m and $\mathrm{T_c}$. Degterov et al. (2001) proposed using the values of the three apexes of the neutral volume in Figure 6.3 and assumed that β_m changes linearly along the edges of the neutral volume. However, because of the severe lack of experimental data, it was assumed that the β_m and $\mathrm{T_c}$ remain constant along the neutral line representing simple spinel, $(\mathrm{Fe^{2+}, Fe^{3+}})^\mathrm{T}[\mathrm{Fe^{2+}, Fe^{3+}}]_2^\mathrm{O}\mathrm{O}_4^{2-}$. In other words, $\beta_{\mathrm{Fe^{2+}Fe^{3+}}} = \beta_{\mathrm{Fe^{3+}Fe^{2+}}}$ and the same is true for $\mathrm{T_c}$ (Degterov et al. 2001).

6.6 Pressure Dependence of Gibbs Energy

Often, the pressure contribution to the Gibbs energy of a compound or solution is ignored because of the low system pressures. The pressure-dependent properties of condensed phases such as volume and thermal expansivity do become more significant at very high pressures and can therefore not be ignored. Several models for condensed phases have been suggested and some of them are listed (Lukas, Fries, and Sundman 2007):

- The Murnaghan pressure model (Murnaghan 1944) - In the Murnaghan model it is assumed that the bulk modulus can be expressed by a linear pressure dependence. Moreover, the pressure-dependent terms are integrated into the Gibbs energy expression (see Equation 5.8 in Lukas, Fries, and Sundman (2007)).
- A new pressure model was proposed by Lu, Selleby, and Sundman (2005), which made it possible to have meaningful calculations of the partial Gibbs energies. Furthermore, the model can account for composition dependence of the parameters and is better equipped for modelling solution phases. Another advantage is that the model can be extended to higher pressure ranges compared to the Murnaghan model. It has a very simple form when integrated into the Gibbs energy expression (see Equation 5.10 in Lukas, Fries, and Sundman (2007)).

For the gas phase, except close to the critical point or the boiling point, the term $\mathrm{RTln}\frac{\mathrm{P_i}}{\mathrm{P_0}}$ is sufficient to describe pressure dependence. Although the pressure of a system needs to be considered, most metallurgical open and closed systems operate at relatively low pressures. As a result, the effect of pressure on the condensed phases of the Fe-V-Ti-O system in air is assumed to be negligible.

6.7 Gibbs Phase Rule

In any system at equilibrium, homogeneous of heterogeneous, the number of fixed experimental variables is limited by the "Gibbs phase rule", or simply the "phase rule". This rule was derived from the works of J. Williard Gibbs dating back to 1870s and published in Transactions of Connecticut Academy of Sciences (Gibbs 1875-1876; Gibbs 1877-1878). For example, if temperature and pressure are fixed in a one-component gaseous system, the volume is uniquely determined by the equation of state. That said, the system is fully defined (univariant) by specifying two variables, or in other words, the number of degrees of freedom is equal to two. The "phase rule" is a combination of phases and components, and is given by Equation 6.60.

$$f = c - p + 2 \tag{6.60}$$

where c is the number of components and p is the number of phases. Some key remarks of the phase rule are (Lee 1999):

- The phase rule offers an effective way to determine the minimum number of intensive variables that have to be specified to determine the thermodynamic state of a system unambiguously.
- When applying the phase rule, one does not require knowledge of the actual constituents of a phase.
- The phase rule is only applicable to a system that is at equilibrium.

The significance and value of the phase rule becomes more evident in Section 7.2 and Subsection 8.1.7.

6.8 Assessment Methodology

In Section 6.3 a selection of models was discussed to understand how they can be used to fit experimental data. In the upcoming section, the basics of the assessment methodology are outlined. These include a critical assessment of the literature and the type of data that can be considered. The reliability of data is validated through a list of guidelines. Furthermore, these data are combined with thermodynamic models to develop an analytical description. The estimation of adjustable model parameters is often done using the least squares method to obtain a description that can reproduce experimental data well within acceptable error limits (Lukas, Fries, and Sundman 2007).

6.8.1 The Basic Principle of Data Fitting

The principle of data fitting and parameter optimisation is based on a least-squares method, that is, an objective function is written in terms of the difference between the calculated value of a given property and an experimental value of the same property. This difference is known as the residual. It is possible to acquire a set of optimised model parameters by minimising the sum of the square

of the residual over all measured points. For example, one can create an objective function based on liquidus temperature (Koretsky 2004):

$$OF_{TLiquidus} = \sum (T_{exp} - T_{calc}). \tag{6.61}$$

In Equation 6.61, $\mathrm{T_{exp}}$ is the experimental temperature and $\mathrm{T_{calc}}$ is the calculated value using thermodynamic models. The OPTISAGE module in FactSage 7.0 uses a **Bayesian optimisation technique** (Bale et al. 2002). The module has the ability to fit the thermodynamic parameters to the experimental data at stable and metastable state. Bayesian optimisation employs a technique of setting a prior over the objective function and combining it with evidence to get a posterior function. It is called Bayesian because it uses the well-known "Bayes theorem", which states simply that the posterior probability of a model (or theory, or hypothesis), M, given evidence (or data, or observations) E, is proportional to the likelihood of E, given M, multiplied by the prior probability of M. This relationship is expressed as follows (Brochu, Cora, and Freitas 2010):

$$P(M \mid E) \propto P(E \mid M)P(M). \tag{6.62}$$

Relationship 6.62 is instrumental for optimising the objective function. In Bayesian optimisation, the prior represents one's "belief" about the space of possible objective functions. Consider an objective function $\mathrm{f(x_i)}$ as the observation at the ith sample. During the accumulation of observations, $\mathrm{D_{1:t}} = \{\mathrm{x_{1:t}}, \mathrm{f(x_{1+t})}\}$, the prior distribution is combined with the likelihood function, $\mathrm{P(D_{1+t} \mid f)}$. Basically, this is what one think one knows about the prior, from data that have been observed. For example, if it is believed that the objective function is very smooth and noise-free, data with high variance or oscillations should be considered less likely than data that deviate slightly from the mean. These are then combined to acquire a posterior distribution (Brochu, Cora, and Freitas 2010):

$$P(f \mid D_{1+t}) \propto P(D_{1+t} \mid f)P(f) \tag{6.63}$$

In relationship 6.63, the posterior captures the beliefs of the unknown objective function. This step of Bayesian optimization is also interpreted as estimation of an objective function with a "surrogate" function (also called a response surface), which is formally described with a posterior mean function of a Gaussian process. Data from Bayesian optimisation is efficiently sampled with an acquisition function to determine the next location $\mathrm{x_{t+1}} \varepsilon \mathrm{A}$ to sample. Moreover, this takes into account both exploration (sampling from areas where the objective function has high uncertainty) and exploitation (sampling areas likely to offer improvement over the current best observation). In a nutshell, the optimisation technique is useful in that it aims to minimise the number of objective function evaluations. Furthermore, it will perform well in settings where the objective function has more than one local maxima. The Bayesian optimisation approach is very complex, hence is not discussed further here. A detailed mathematical description and practical applications are found in Brochu, Cora, and Freitas (2010) and Königsberger and Gämsjager (1990).

6.8.2 Setting Up a Thermodynamic Optimisation File in FactSage

A collection of files is required to optimise model parameters in the OPTISAGE module. In the first step, compounds that had been included in the FACTPS database needed to be defined. For example, the orthovanadates, $FeVO_4$(s) and $Fe_2V_4O_{13}$(s), were created in a customised compound database. The thermodynamic properties and basic molecular data of the respective otrhovanadate compounds were stored in a CDB file. The next step involved defining models and known parameters, using the SOLUTION module. All solution phases were created and stored as an SLN file. Upon completion of the first two steps, the EQUILIB module was used to finally create a ChemSage DAT file. The DAT file is a final assembly of pure compounds and solution phases. Finally, the DAT file was compiled in the OPTISAGE module, followed by importing a collection of experimental data from a EXL

file. A working example, with figures and step-by-step instructions of a thermodynamic evaluation using SOLUTION and OPTISAGE, is given in Appendix C. Figure 6.8 presents a schematic of steps involved for thermodynamic evaluation in FactSage.

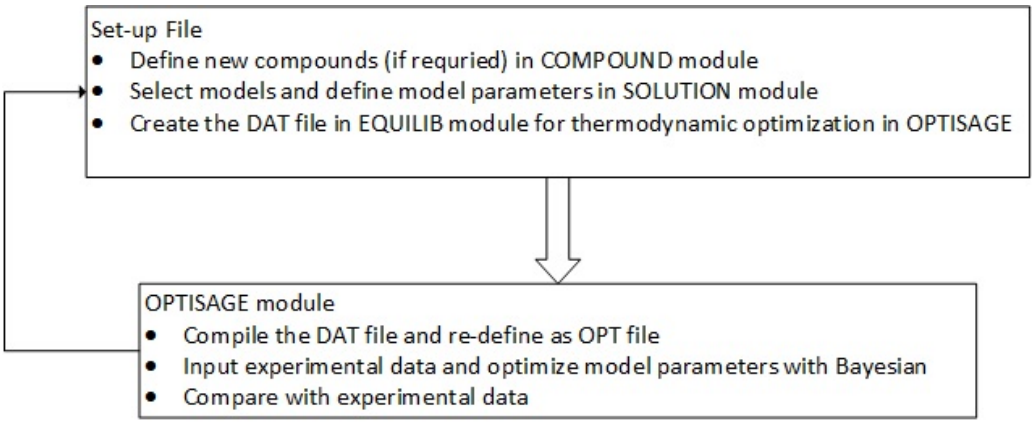

Figure 6.8: A flowchart of optimization in FACTSAGE.

6.8.3 General Sequence of Optimisation

At first, all model parameters were optimised individually by suppressing other model parameters. In this way, a reasonable fit of experimental data were obtained. These values are then used as initial values to reduce optimisation steps required for the simultaneous optimization of all model parameters. The optimised parameters were stored collectively in a previously created solution file, given that the OPTISAGE module has no calculation abilities. EQUILIB and phase diagram modules can extract data for intermittent phase and property diagram calculations. These back-calculated diagrams are then easily compared to experimental data, so that the validity and reliability of the thermodynamic parameters can be evaluated.

6.8.4 Selection of Experimental Data

The first step of the assessment normally involves a the literature survey. It is important to consider all available data, old and new, for the optimisation one wants to carry out. It is useful to categorise the literature data according to types of measured quantities. Lukas, Fries, and Sundman (2007) categorised the following set of data available in the literature:

- Experimental thermodynamic data such as enthalpies and their variation with temperature and composition
- Phase diagram data. This type of data can be obtained through a variety of methods, of which some of the most common are, thermal analysis, metallography, X-ray diffraction, solidification-path experiments and equilibration-quench analysis.
- Other experimental data, which are quantitatively related to thermodynamic properties through derivatives of the Gibbs energy. These include: bulk moduli, thermal expansions, elastic constants, etc.
- The type of data that can assist in selection of details of models for solution phases. These include, crystal-structure data, point defects, densities (vacancies), ordering, resistivity, vibrations, etc.

- Theoretical papers for calculations of total energies at zero and/or at finite temperature, estimates, trends, thermodynamic properties, and phase diagrams of similar systems.
- Papers of previous thermodynamic assessments. This implies that the system under scrutiny has already been optimised; however improvements might be required. If improvements are made, arguments should be listed to motivate them.
- Miscellaneous data: Any information that is indirectly connected to Gibbs energies. This may include information on kinetics, micro-structure and solidification, which may aid in practical plausibility of the phase diagram.

On the basis of these listed and categorised data and information, a well-organised and concise collection of data was obtained and stored for assessment purposes. Where possible, each batch of data that was used, as superimposed onto phase diagrams and other thermodynamic property diagrams.

6.8.5 Reliability of Experimental Data

It must be mentioned that no precise method exists to predict how reliable and accurate experimental data are. The selection and usage of experimental data are purely subjective. As a result, personal judgement and experience play an instrumental role in the weight distribution of each piece of experimental data. Ultimately, a list of factors/questions were presented and played a decisive role in the selection of experimental data that were included in the thermodynamic evaluation of this study (Lukas, Fries, and Sundman 2007; Zhang 2016).

- When was the first date of publication?
- In which journal have the experimental data been published?
- What was the grade of the materials?
- Did the author give a detailed description of the experimental set-up and procedure used?
- Has an author mentioned anything about the repeatability of experiments?
- What analytical techniques and standards were used for chemical and phase characterisation?
- How well do data correspond to data obtained from different experimental techniques?
- How do experimental results from a specific study compare to those of other studies?
- What was the estimated accuracy of the experiment?

It is important that these questions are answered with a high degree of certainty and precision. For instance, were the latest and most innovative experimental techniques used and well described? Was the article published in a peer-reviewed journal? Moreover, is the journal well-known and respected in the community, and does it have a relatively high impact factor. This enables one to weigh the experimental data that were found sensibly and is called the 'critical set'.

6.8.6 Determining the Effect of Adjustable Model Parameters

To reproduce experimental data from the adjustable model parameters it is important to have a clear understanding of the effect of each coefficient on the many diverse measurements. Moreover, each measured value contributes to many of the coefficients and therefore the strategy would be to select the best possible agreement of all the coefficients for all experimental values. Although the least-squares method allows non-quantitative knowledge of the final value of a coefficient, it is important to judge qualitatively whether a certain coefficient is well-defined by an available set of measured values. That said, the effect of each coefficient on the shapes of a calculated curve should be known to some extent. Knowing the effect will avoid the selection of coefficients, which will not necessarily improve the fit between calculated results and the experimental dataset. However, if too many coefficients are selected, a calculation will follow with just a scatter of the experimental values, creating maxima and minima where a smooth line is physically more plausible. Furthermore, it is likely that a calculation will not converge, which can lead to a solution with many possibilities (Lukas, Fries, and Sundman 2007; Saunders and Miodownik 1998).

An investigation into a experimental dataset will usually not indicate whether a certain parameter corresponds to the 'fit' of the dataset. Nevertheless, it is important to guess a set of parameters that can be used to calculate a phase diagram with reasonable agreement with the critical set of data. However, this selection process is extremely challenging if one is not an experienced assessor. Lukas, Fries, and Sundman (2007) suggested the following recommendations when starting with an assessment:

- Start the assessment with as few coefficients as possible and include additional coefficients as necessary.
- Through the application of the least-square method, with and without a coefficient, it is possible to observe whether a certain parameter is related to the critical set of experimental data.
- Systematically calculating a curve from a set of coefficients and comparing the curve to a series of experimental points will usually assist to clarify which coefficients should be added.
- If the effect of a coefficient is not well-defined, it usually does not show up in the comparison of measured values and calculated curves. Moreover, there is the further likelihood that it may have a bad influence on the behaviour of the extrapolation of the calculation into parts not experimentally determined.

6.8.7 Verifying the Results of an Optimisation

Knowing when the best possible set of parameters has been obtained is difficult. The answer depends on the use for which one wants the description obtained. That said, a well-optimised set of parameters for the Gibbs energies of phases should be able to reproduce the experimental phase diagram and other thermodynamic property diagrams in the best possible manner. The strategy outlined by Lukas, Fries, and Sundman (2007) was followed to check the results of the optimisation of this study.

- Visually comparing calculated phase diagrams to experimental observations. This is a useful strategy to identify any curves of the diagram not reproduced by the calculation.
- Looking at the sum of squares of errors from the least-squares fit. This another indication of a good or bad fit. However, it should only be used as part of a set of criteria for checking optimisation results.

- Using binary model parameters to extrapolate to higher-order systems. This is to check if the description reproduces experimental data in a ternary system. If a good fit is not obtained, the binary set of parameters needs to be re-evaluated.

- Analysing the plausibility of the values of parameters found by the optimisation technique. The signs and values of parameters should be checked to determine whether they are plausible to do this. For example, a negative $\mathrm{a_0}$ value of the $\mathrm{c_p}$ term or negative standard entropy value is not physically possible. Moreover, the entropy of mixing in solutions also need to be positive at all times. If not, the set of parameters needs to be re-evaluated to produce values that are plausible.

- Removing non-significant digits. Parameters with many significant numbers may give the impression that they have been very well determined; however in many cases, only the first few numbers are significant. There is nevertheless a danger of unsatisfactory agreement between calculated and experimental data when values of parameters are rounded off to an arbitrary number. To avoid such a risk, it is suggested that the parameter with the highest relative standard deviation be set to a rounded value, followed by re-optimizing of the other parameters. This method can be repeated until all parameters have been rounded to an appropriate number of significant numbers.

- Confirming that $\mathrm{S^\circ_{298}}$ and $\mathrm{C_p}$ of all phases are within reasonable and acceptable limits.

Chapter 7

Experimental Techniques and Application

Many experimental techniques have been employed to estimate thermodynamic properties and phase relationships in oxide systems. These techniques can be divided into two groups; dynamic and static methods. Table 7.1 presents a list of dynamic and static techniques that have been demonstrated to determine phase equilibria successfully in oxide systems (Jak and Hayes 2008).

Table 7.1: Typical static and dynamic techniques employed to estimate phase equilibria in oxide systems.

Method	Technique	Application for oxide systems
Static	Electrochemical	Thermodynamic properties e.g. a_i, ΔG and ΔS
	Vapour pressure	Knudsen: low metal vapour pressure, non-aggressive slag Reactive gas equilibriation: low metal vapour pressure (pO_2 control) Isopeistic equilibria: high metal vapour pressure
	X-ray powder diffraction	Phase detection/identification; extensive solid solutions: lattice parameters at temperatures
	Hot stage microscopy	Liquidus of low vapour pressure systems, transparent liquids
	Calorimetry	Enthalpies of formation, of solution and of phase transition
	Equilibration/quench/analysis techniques	Liquidus of high viscosity liquids
Dynamic	TGA	Gas/solid and gas/liquid reactions
	DTA	Rapid phase transitions (melting point of congruently melting compounds); liquidus of low viscosity liquids
	DSC	Latent heats of of low viscosity liquids

7.1 Dynamic Techniques

The most common dynamic techniques used are thermal analysis, DTA, DSC and TGA. These techniques measure property changes due to phase transformation. The drawback of a dynamic techniques is that the system is by definition not in equilibrium. This phenomenon is particularly common for systems with sluggish phase transformations, brought about by kinetic and metastable effects. As a result, dynamic methods cannot be accurately used in silica-containing systems or any

system in which nucleation and growth reactions are known to be slow, and for most reconstructive solid state phase transformations that entail solid state diffusional processes. (Jak and Hayes 2008).

Consider a case application of approaching equilibrium from cooling. In other words, the temperature is set above the desired equilibration temperature and then allowed to cool down to the desired temperature. During solidification of a melt, the equilibrium solid phase composition remains homogeneous and in equilibrium with the melt, and systematically changes with the system temperature. However, if a melt is cooled more rapidly, the solid phase will be non-homogeneous in composition owing to insufficient time for mass transport. In other words, the core of the solid will have the composition of the first solid formed and the surface of the solid will have the composition of the precipitate in equilibrium with the last liquid to solidify. Consequently, the mean composition of the solid is not the same equilibrium condition, and the estimated solidus is not a reflection of the true equilibrium solidus for a given bulk composition (Jak and Hayes 2008).

This scenario is profound for systems in which primary precipitate exhibits solid solution. Dynamic techniques can be applied to systems that approach their state of equilibrium during cooling or heating, i.e. reactions that do not occur through diffusion mechanisms. Such systems are investigated by making measurements at a range of heating and cooling rates and if required, corrections are applied to take kinetic effects into account (Flynn 1988).

7.2 Static Techniques

In contrast, static equilibria techniques will allow a sample to approach equilibrium at a constant temperature and pressure. This approach enables accurate control of temperature and $\mathrm{pO_2}$. Furthermore, oxides at equilibrium can then be studied by, for example, high-temperature XRD, hot stage microscopy, EMF measurements and quenching techniques.

7.2.1 Limitations of the Equilibration-quench Analysis Technique

The quench technique involves equilibration in a controlled atmosphere, followed by rapid cooling to preserve high-temperature phases. The ability of a sample to preserve its high-temperature phase assembly during quenching, depends on a number of factors (Jak and Hayes 2008):

- Viscosity: Materials such as silica slags with high viscosity tend to preserve their glass phase more easily.
- Sample size: A sample size less than 1 g is recommended to induce a cooling rate in the range of $10^3 - 10^6 \mathrm{K.s}^1$.
- Containment material: A sample contained in a crucible or envelope will decrease heat transfer from a material to a quenching medium. Direct contact between the slag and the quenching medium provides the fastest cooling.
- Quenching medium: Ice water or brine. Quenching into liquid nitrogen will result in a protective nitrogen gas film, which will slow down the cooling rate.

Aside from the quenching ability of a sample, the following assumptions are required when employing the quenching technique to estimate liquidus and solidus composition:

- A large number of experiments need to be conducted to estimate the liquidus temperature.
- The materials in a sample will not react with the gas phase or containment material, or vaporize to avoid a change in the bulk composition of the sample.

- The sample has achieved equilibrium at a set temperature.
- No or little precipitate forms during quenching. If some crystallisation has occurred, then it should be identified to exclude during analysis.
- Solid phases in equilibrium with the liquid can be detected.

7.2.2 Application of the Equilibration-quench Analysis Technique

Envisage that a series of tests have to be carried out to determine the liquidus composition as a function of temperature in an oxide system with slow phase change. For example, the thermodynamically assessed phase diagram of the Fe-Ti-O system in air demonstrates how the equilibration-quench analysis technique can be applied (see Figure 7.1a). The phase diagram was developed with FactSage 7.0 utilising the FToxid database. The phase diagram presents a series of "imaginary" experimental points at which various phases appear or disappear from the quenched samples. The starting composition is chosen accordingly so that a solid phase is in equilibrium with the liquid, under the assumption that the sample has indeed reached equilibrium.

To calculate the bulk fraction of a phase, the Lever rule can be applied. For example, the relative amount of liquid phase at 1400 °C is calculated by Equation 7.1.

$$X_{Liquid} = \frac{ED}{ED + DF}. \tag{7.1}$$

This technique can easily be expanded to ternary systems. Another example of estimating the relative bulk composition of a phase in a scalene triangle, which typically appears in a ternary system, is graphically demonstrated in Figure 7.1b. In this case, point P, a mixture of X, Y and Z, is inside the subsystem XYZ, and the proportion of each is then calculated by Equation 7.2 (Lee 1999).

$$X_{Proportion} = \frac{bZ}{XZ} \tag{7.2a}$$

$$Y_{Proportion} = \frac{ab}{XZ} \tag{7.2b}$$

$$Z_{Proportion} = \frac{Xa}{XZ}. \tag{7.2c}$$

The liquidus composition can be estimated with one or two solid phases in equilibrium with liquid. However, the number of experiments required to estimate the bulk composition of liquid to solid increases significantly. For example, a sample with a bulk starting composition of 50 % specie X, 30 % specie Y and 20 % specie Z has five other possible composition arrangements of identical composition values. However, this does not mean a sample that had five different initial compositions will necessarily have five different equilibrium states.

This phenomenon is well explained by the Gibbs phase rule (see Section 6.7). For example, consider sub-sections marked 1 and 2 in an isothermal section of the Fe-P-Ti-O system in air at 1200 °C, and 1 atm absolute shown in Figure 7.2. In the sub-section marked 1, there is one solid phase in equilibrium with the slag. The gas phase is suppressed in this particular case and according to Equation 6.60, there are four degrees of freedom. c = Fe, P, Ti and O, respectively. However, temperature, pressure and oxygen partial pressure have all been fixed, reducing the number of degrees of freedom to one. The composition of one specie in the slag phase need to be fixed to reduce F to zero. As a result, the composition of the liquid is free to vary within sub-section 1.

On the contrary, the liquid composition remains uniform and independent of the initial composition, if p is equal to 3. Such is the case in sub-section 2. Any initial composition that is within the boundaries of sub-section 2 will have an identical equilibrium phase assemblage and composition.

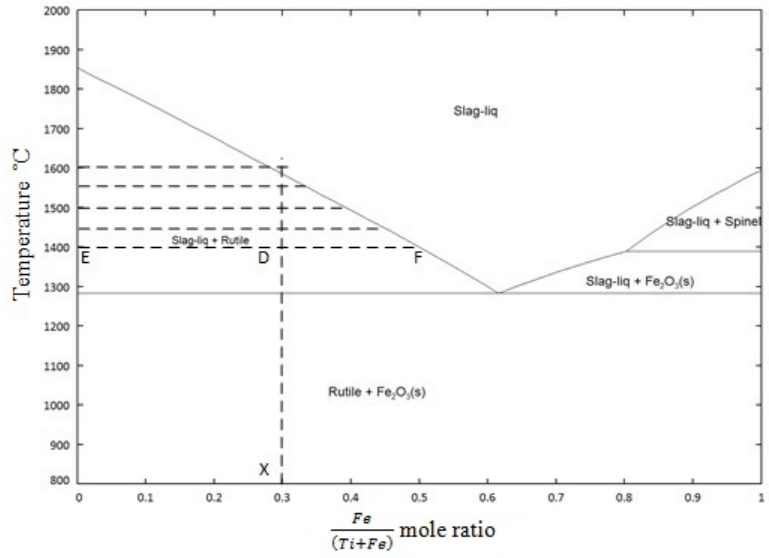

(a) Estimating relative bulk amount of a phase in a binary sub-system using the equilibration quench technique.

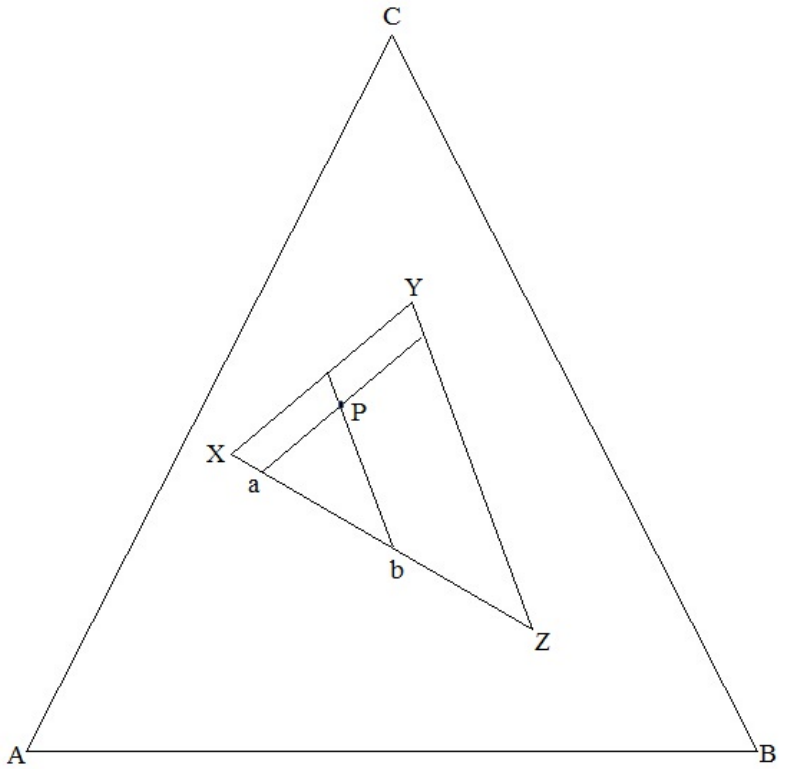

(b) Estimating relative bulk amount of a phase in an isothermal ternary sub-system using the equilibration quench technique.

Figure 7.1: A application of the lever rule in binary and ternary systems.

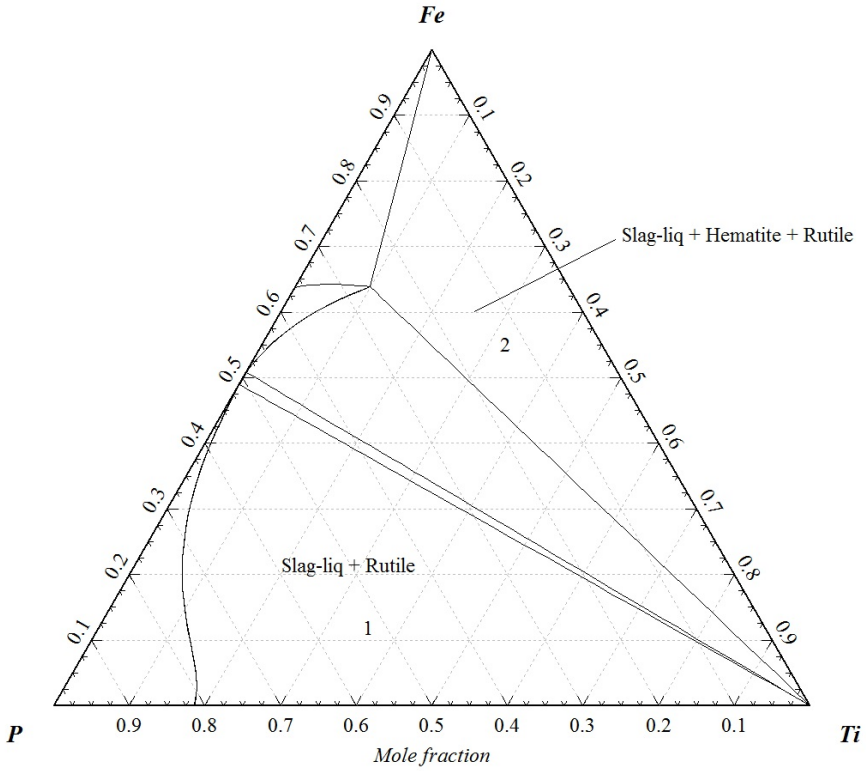

Figure 7.2: Estimating liquidus composition in a Fe-P-Ti-O system in air at 1200 °C using quench techniques.

In this way, redundant experiments are avoided in multi-component systems, because irrespective of the number of components and phases, the Gibbs phase rule will always apply to any system that is in equilibrium.

Part III

Materials and Methods

Overview

Purpose of Part on Materials and Methods

The main purpose of the part on materials and methods is to elaborate on all experimental, analytical and mathematical modelling techniques that were used to obtain and assess phase diagram data on the Fe-Ti-V-O system in air.

Organization of Materials and Methods

The part is divided into two chapters:

- Chapter 8 presents the principle, methodology and materials employed in the experimental equilibration of Fe-Ti-V-O in air. All experimental work was done in the pyro-metallurgical laboratory of the Material Science and Engineering building, Aalto University. Sample preparation, experimental procedures and analysis of specimens are chronologically outlined.
- In Chapter 9 structure and phase transformation data, liquidus and solidus data, and thermodynamic data of the Fe-Ti-V-O system in air are given. The models for all solutions in the Fe-Ti-V-O system in air are also described.

Chapter 8

Experimental Methods

8.1 Experimental Methodology

8.1.1 Sample Preparation

The starting materials used for the experiments were V_2O_5(s), TiO_2(s) and Fe_2O_3(s). The material, source and purity are presented in Table 8.1. Mixtures of selected bulk compositions were prepared by weighing the oxide powders, followed by mixing them thoroughly using an agate mortar and pestle. The samples were pellitised to 20 Mpa. The mass of all samples were below 0.5 g.

Table 8.1: Purity of initial materials and sources from which they were acquired.

Material	Source	Purity
Divanadium Pentaoxide	SIGMA ALDRICH, RSA	99.60%
Ferric Oxide	SIGMA ALDRICH, RSA	>99 %
Anatase	SIGMA ALDRICH, RSA	99.90%

8.1.2 General Experimental Set-up and Procedure

All equilibration experiments were conducted in a vertical electrical resistance tube furnace (Lenton, UK) with a 35 mm inner diameter alumina work tube. The maximum operating temperature is 1600 °C. Figure 8.1 is an image of the furnace at Aalto University during the time an experiment was conducted. Figure 8.2 is a schematic of the furnace with auxiliaries.

Determining the Hot Zone

The first step involved determining the thermal profile of the furnace worktube to identify the hot "spot/zone" in the tube furnace. The S-type thermocouples were calibrated according to the melting point of copper. A calibrated S-type thermocouple connected to a Keithley 2010 DMM multimeter (Cleveland, OH, USA) and a cold junction compensation was connected to a Keithley 2000 multimeter (Cleveland, OH, USA) to measure the ambient temperature with a PT100 sensor (Platinum Resistance thermometer, SKS Group, Finland). The temperature was captured and logged every 2 seconds with a NI labVIEW temperature logging program. A small hot zone of 4 - 5 cm in length was established. The deviation of temperature measurements in the hot zone was less then 2 °C. The hot zone is indicated in Figure 8.2a as an area within the two dashed lines.

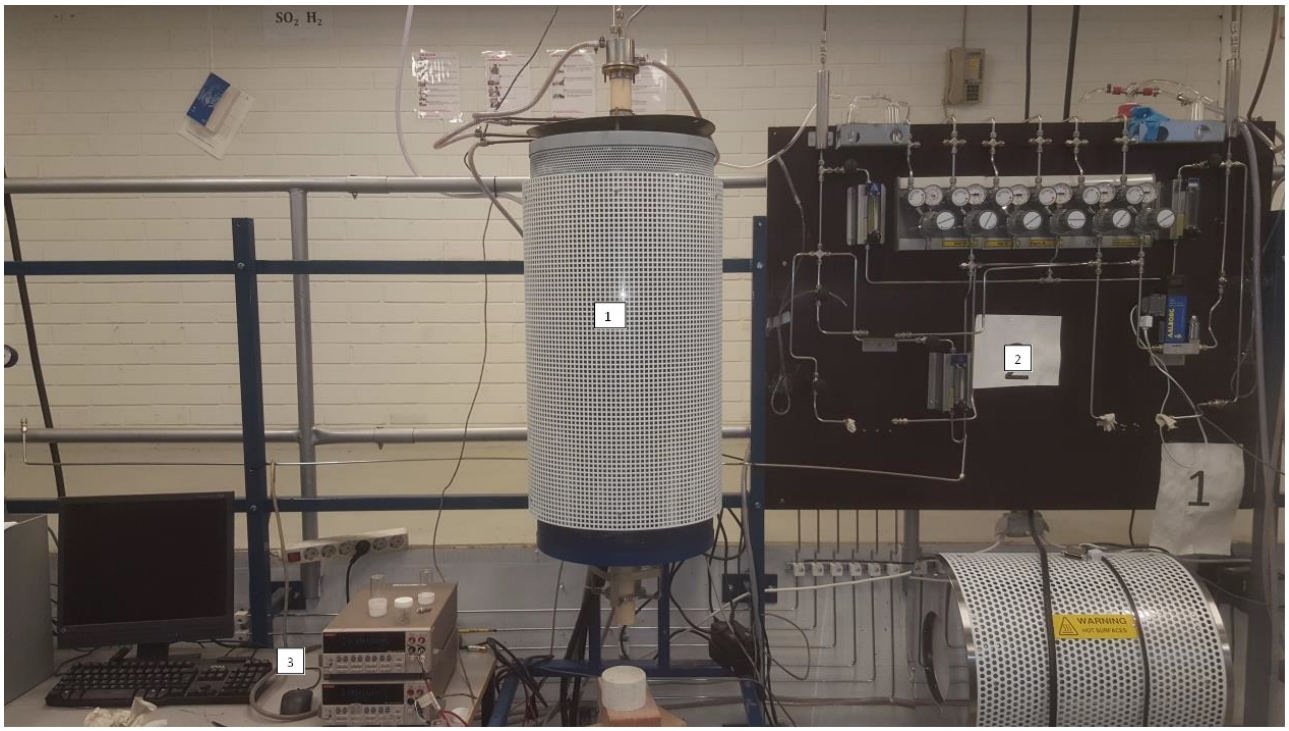

Figure 8.1: Vertical electrical tube furnace at Aalto University, Espoo, Finland. 1 - Lenton vertical electrical resistance tube furnace (Type; LTF- 16/450), 2 - Gas flow control set-up, 3 - Temperature measurement devices.

Establishing Equilibrium

The required equilibration time was determined by comparing samples with identical starting composition at fixed time intervals to one another at constant temperature, and assessing compositional homogeneity of the phases with SEM-EDS and EPMA. In addition, equilibrium can be confirmed by approaching equilibrium from different temperature directions, i.e. from heating and cooling. However, the former method was sufficient to confirm equilibrium and the latter was not used. Time interval experiments were done prior to experiments at different temperatures. All specimens were lowered into the furnace with platinum (Pt) wire in a Pt envelope (see Figure 8.2b). Three advantages of using Pt as containing material are:

- The Pt wire and envelope will not react with oxygen to then dissolve in the oxide phases of a specimen.
- Pt melts at 1770 °C, which is well above the desired temperature range of this study.
- A manually assembled envelope with small voids was chosen over Pt foil to allow the specimen to come into direct contact with the quenching medium.

Some added advantages of this technique is that the sample mass is low (<0.5 g), which increased homogeneity in the sample once quenched, and the specimen will come into direct contact with the quenching medium once equilibrium has been attained. Quenching of the sample was achieved by releasing the specimen rapidly into a beaker of ice water or brine, situated no more than 10 mm from the exterior of the alumina working tube. The specimen was rapidly removed from the beaker and dried with compressed air. This minimised the possibility of the quenched specimen dissolving in water.

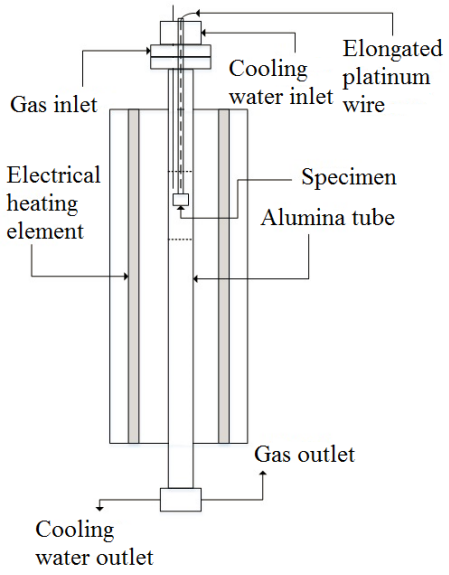

(a) Schematic of the vertical front view section of the furnace and auxiliaries.

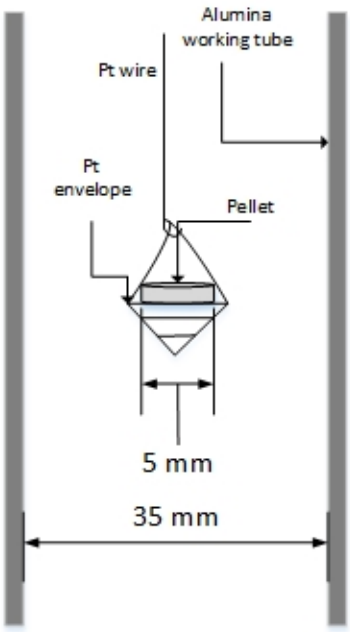

(b) Envelope design and suspension of the pellet in the furnace.

Figure 8.2: Furnace and suspension design.

Conducting Experiments in Air

Experiments in air were undertaken with the bottom of the tube furnace open and exposed to the atmosphere. The sample was introduced into the furnace from the bottom by slowly pulling on the wire from the top of the furnace. The slag behaved extremely aggressively, which made slag containment in the Pt envelope difficult. This was attributed to experimental temperatures being well above the melting temperature of V_2O_5 (669.85 °C). The melting point was determined with FactSage 7.0 (Bale et al. 2009). This in turn caused a superheated V-O slag to form. A systematic increase in temperature was required to contain the aggressive slag. The specimen was allowed to melt slowly by keeping the sample in a lower temperature area of the furnace for 30 to 45 s before finally raising it into the hot zone.

However, below 700 °C, temperature recordings were fluctuating, resulting in a less accurate estimated temperature range. The uncertainty of temperature measurements below 700 °C increased to within a range of 5 - 10 °C. Consequently, it was impossible to estimate eutectic reactions of Fe-V-O and T-V-O systems within 2 - 3 °C because of design limitations of the furnace temperature controller. The Fe-V-O and Ti-V-O systems in air had reported eutectic temperatures below 700 °C.

Thereafter, small pieces of the specimen were mounted in epoxy resin. Mounted specimens had a ratio of 7.5 ml of Epofix resin to 1 ml of EpoFix hardener. Both liquids were acquired from Struers, Denmark. The specimen in liquid epoxy was placed in a dry storage room for 24 hours to expedite solidification. The solidified mounted specimen was dry-polished on sandpaper; the grid sizes were 240, 400, 800, 1200 and 2000 P, respectively. Finally, the sample was polished on 3 and 1 micron diamond-coated surfaces. Overall, a well-polished cross-section of the sample was prepared using conventional dry metallographic grinding and polishing techniques. A dry technique was employed as a precaution because V_2O_5 has a solubility of 0.8 g/l in water (Robert 1981). For this reason, propylene glycol (Sigma Aldrich, Germany) and DP Lubricant Brown (Struers, Munich, Denmark) were used.

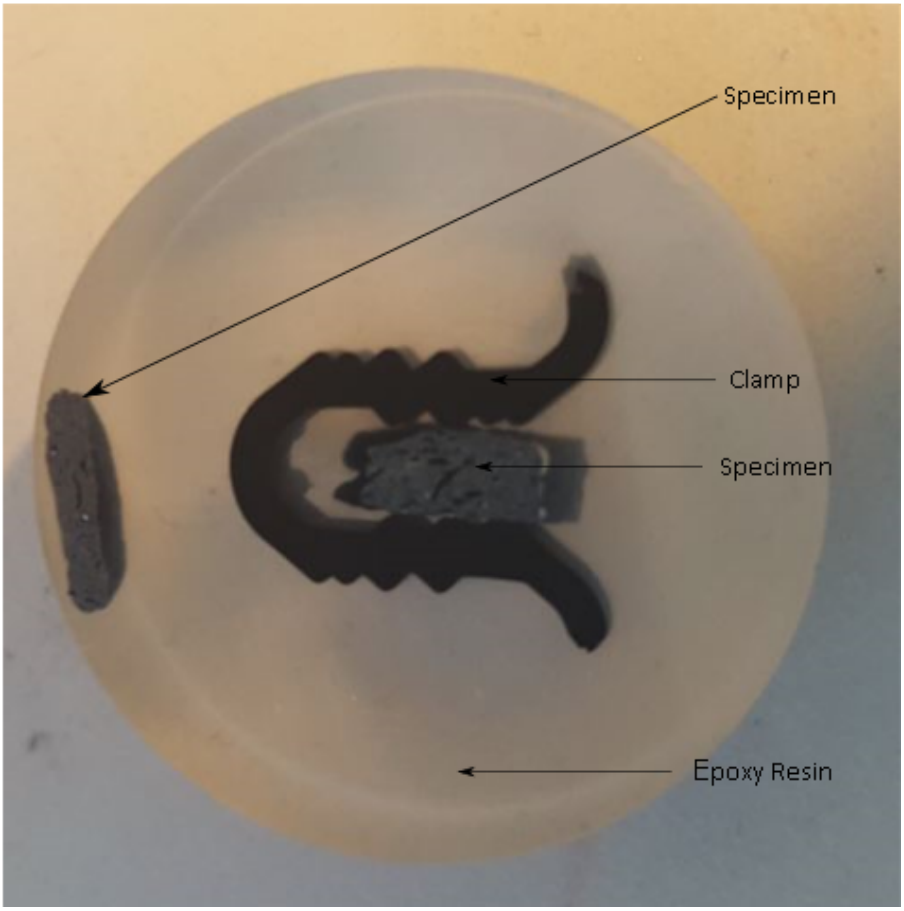

Figure 8.3: A mounted specimen after conventional dry metallographic grinding and polishing technique.

8.1.3 Synthesis of $Fe_2V_4O_{13}$

The compound, $Fe_2V_4O_{13}$(s), was largely not detected in previous studies of the Fe-V-O system under oxidising conditions, supposedly because of its slow formation. Another contributing factor that has been postulated by Walczak et al. (1985) is the undefined X-ray pattern of $Fe_2V_4O_{13}$(s), which had been difficult to distinguish from X-ray patterns of V_2O_5(s), Fe_2O_3(s) and $FeVO_4$(s). The latest studies of Fotiev, Cheshnitskii, and Surat (1983) and Walczak et al. (1985) did however identify the X-ray pattern of the compound, which was brought about by synthesising a mixture of Fe_2O_3(s) and V_2O_5(s) with a molar ratio of 1:2 at temperatures ranging between 600 and 620 °C. This approach was also followed in this study. The compound was calcinated for 72 hours in a muffle furnace at 600 °C, then slowly cooled, re-ground and pelletised again. After three such cycles, the sample was mounted on epoxy and prepared for SEM-EDS analysis and EPMA using standard metallographic techniques. Furthermore, an attempt to understand the sluggish reaction mechanism of $Fe_2V_4O_{13}$(s) was made by varying the synthesis time and starting composition of V_2O_5(s) and Fe_2O_3(s) from 80 mole % V_2O_5(s) down to 55 mole % V_2O_5(s).

8.1.4 Fe-V-O Liquidus and Solidus Experiments in Air

Experiments on the Fe_2O_3 saturated side of the Fe-V-O system in air had a starting composition, which allowed for two condensed phases in equilibrium at a desired temperature. The initial compositions presented in Table 8.3 were estimated from a preliminary critical assessment and thermodynamic evaluation of the Fe-V-O system in air. In this case, only the MQM was used to describe the slag phase. The liquidus data from Fotiev, Cheshnitskii, and Surat (1983) and Walczak et al.

Figure 8.4: Muffle furance with temperature controller for synthesis of $Fe_2V_4O_{13}$(s).

(1985) were used to optimise MQM parameters. Figure 8.5 presents the optimised phase diagram from a critical assessment of the literature. The optimised model parameters of the MQM are presented in Table 8.2. All other thermodynamic data used in the evaluation are found in Appendix A.

All selected initial compositions are within a two-phase region (slag + solid). The initial composition was carefully selected so that the relative amount of each phase was sufficient for SEM-EDS analysis and EPMA. For this estimation, Equation 7.1 was used. See Chapter 9 for a thorough description of executing a thermodynamic assessment.

Equilibration times are also presented in Table 8.3. To affirm equilibrium, two sets of time interval experiments were conducted at 800 and 1200 °C. At 800 °C, time intervals were chosen as 4, 8, 16, 24 and 48 hours. The homogeneity of samples was confirmed with SEM-EDS analysis and also EPMA. Once equilibration time had been minimised, a series of time intervals was determined at 1200 °C. The optimum equilibration time is predominantly dependent on temperature. Equilibration is dependent on temperature because transport and reaction kinetics are faster at higher temperatures. Other factors, better known as physic-chemical properties, such as solid-liquid surface tension, liquid viscosity and density, have a less significant effect on equilibration time.

When experiments were conducted below 1100 °C, the specimen was suspended in the furnace

Table 8.2: The optimized parameters of solutions in the Fe-V-O system in air before experiments.

Liquid: FeO-Fe_2O_3-FeO-V_2O_5
Quasichemical Model
FeO-Fe_2O_3 binary parameters
Taken from the study of Degterov et al. (2001)
V_2O_5-Fe_2O_3 binary parameters
$Z_{Fe^{2+}} = 1.37, Z_{Fe^{3+}} = 2.0661,\ Z_{V_2O_3^{4+}} = 2.7548$
$g^{10}_{Fe^{3+}-V_2O_3} = -137429.1 + 82.5531T^1$
$g^{01}_{Fe^{3+}-V_2O_3} = -18.9919T$

Table 8.3: Experiments on the system Fe-V-O in equilibrium with air.

Experiment	Temperature °C	V_2O_5 mass fraction	Fe_2O_3 mass fraction	Equilibration time (hr)
1	700	0.750	0.125	72
2	750	0.675	0.325	72
3	750	0.650	0.350	72
4	800	0.625	0.375	72
5	850	0.600	0.400	48
6	900	0.575	0.425	32
7	950	0.550	0.450	32
8	1000	0.525	0.475	16
9	1050	0.500	0.500	8
10	1100	0.475	0.525	8
11	1150	0.450	0.550	8
12	1200	0.425	0.575	4
13	1250	0.400	0.600	4
14	1300	0.35	0.650	4
15	1350	0.300	0.700	4
16	1400	0.250	0.750	4
17	1450	0.200	0.800	4

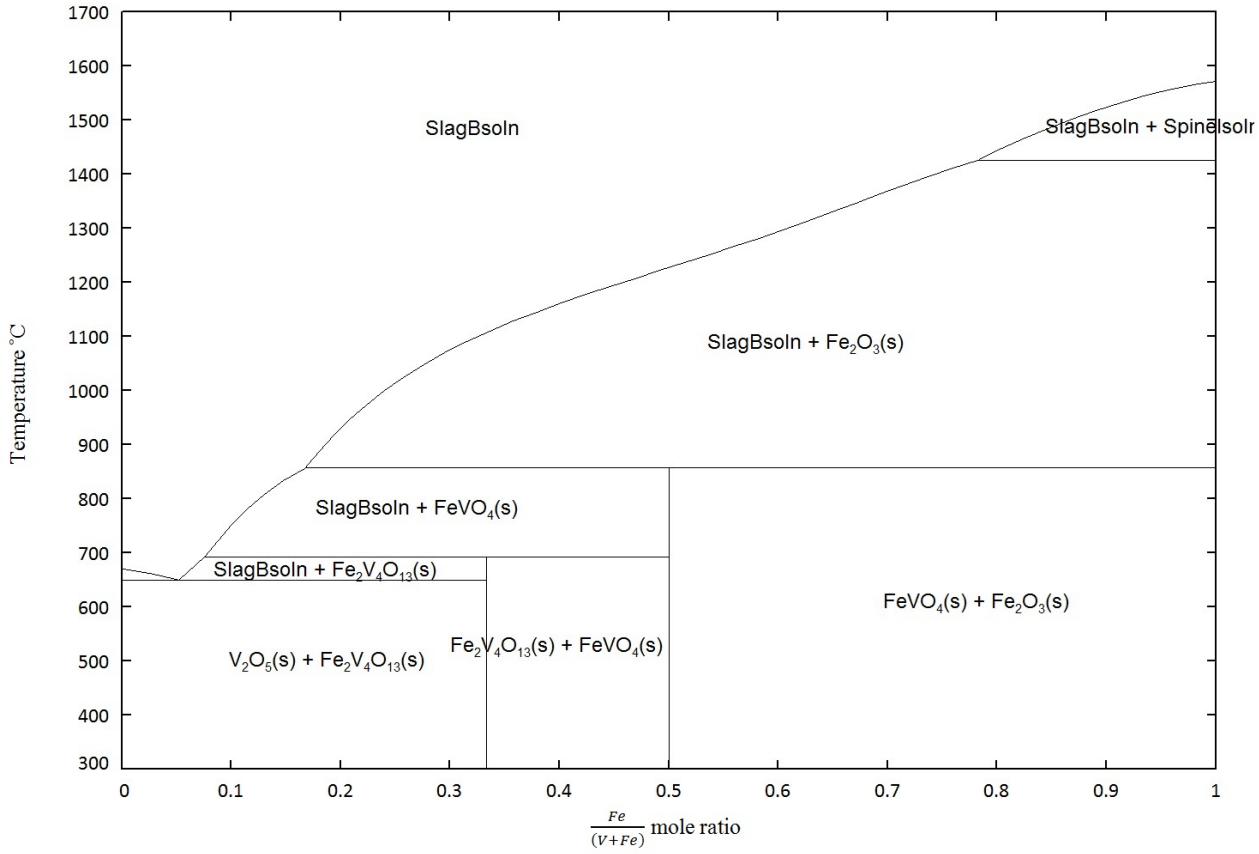

Figure 8.5: A preliminary Fe-V-O phase diagram in air optimised from a critical assessment of literature.

with kanthal wire in a Pt manually assembled envelope. This preserved the expensive Pt wire for experiments at and above 1100 °C. For experiments up to 1000 °C, melting of the sample was facilitated by a pre-melting stage, which involved raising the temperature to 50 °C above equilibration temperature, and keeping it there for 30 minutes before bringing it back to the desired equilibration temperature. As a result, the specimen was brought into equilibrium at a faster rate.

Peritectic and Eutectic Reactions

The Fe-V-O system in air undergoes two peritectic reactions and one eutectic reaction (see Figure 8.5). These transformation reactions and their proposed temperature ranges are as follows:

$$\mathrm{Fe_2V_4O_{13}(s) + FeVO_4(s) \longleftrightarrow Liquid(610 - 655^{\circ}}C) \tag{8.1}$$

$$\mathrm{Fe_2V_4O_{13}(s) \longleftrightarrow FeVO_4(s) + Liquid(660 - 700^{\circ}}C) \tag{8.2}$$

$$\mathrm{FeVO_4(s) \longleftrightarrow Fe_2O_3(s) + Liquid(840 - 875^{\circ}}C). \tag{8.3}$$

The proposed temperature ranges were selected from the studies of Fotiev, Cheshnitskii, and Surat (1983) and Walczak et al. (1985). Furthermore, an uncertainty of 5 °C has been reported by both authors. In other words, the boundary values are increased by 5 °C to account for experimental error. Another objective of this study was to narrow down the proposed ranges within experimental error range. The measured temperature in the vertical electrical resistance tube furnace is accurate within 2-3 °C.

8.1.5 Ti-V-O Liquidus and Solidus Experiments in Air

An identical experimental approach was followed compared to experiments on the Fe-V-O system in air. However, it was concluded from the literature that no intermediate species exist in the Ti-V-O system in air. All specimens were saturated in TiO_2, after which, starting compositions were selected to have a solid and liquid in equilibrium at the desired temperature. Again, to affirm equilibrium, two sets of time interval experiments were conducted at 800 and 1200 °C. At 800 °C, time intervals were chosen as 4, 8, 16, 24 and 48 hours. Afterwards, the minimum time required to attain equilibrium was estimated and a series of time intervals was determined for experiments at 1200 °C.

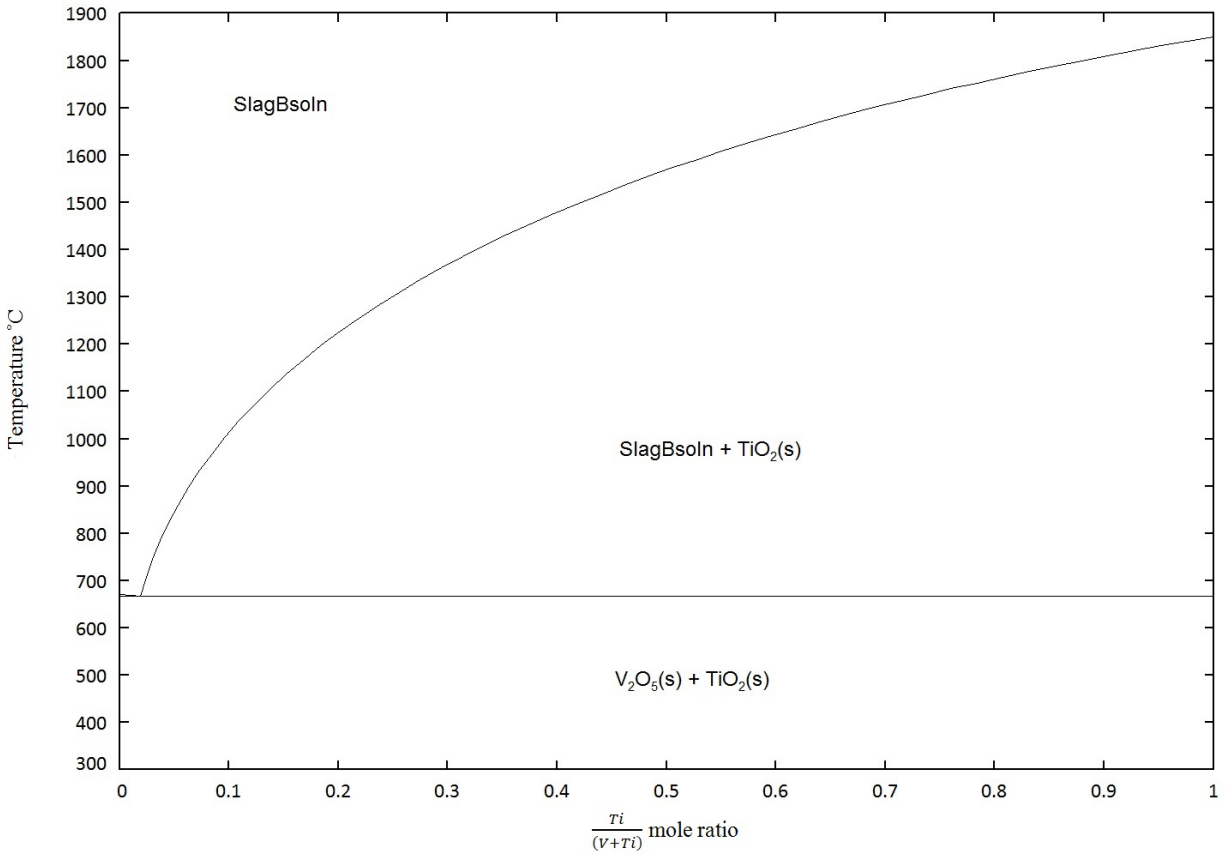

Figure 8.6: The estimated phase diagram in air based on the assumption that the slag phase behaves ideally.

The initial compositions presented in Table 8.4 were deduced by assuming that the Ti-V-O slag behaves ideally, no solid solution exists between V_2O_5(s) and TiO_2(s), and one eutectic reaction exists (see Figure 8.6). Moreover, the eutectic composition contains a relatively high amount of V_2O_5 owing to a large difference between the empirical melting points of V_2O_5 and TiO_2. Chapter 9 chronologically explains the logic and methodology behind thermodynamic assessment and thermodynamic property determinations. Minor adjustments of initial compositions were sometimes required to have sufficient liquid phase for EPMA.

Table 8.4: Experiments on the system Ti-V-O in equilibrium with air.

Experiment	Temperature °C	V_2O_5 mass fraction	TiO_2 mass fraction	Equilibration time (hr)
1	675	0.800	0.200	48
2	700	0.750	0.125	48
3	750	0.675	0.325	48
4	750	0.650	0.350	48
5	800	0.625	0.375	24
6	850	0.600	0.400	24
7	900	0.575	0.425	24
8	950	0.550	0.450	24
9	1000	0.525	0.475	24
10	1050	0.500	0.500	24
11	1100	0.475	0.525	24
12	1150	0.450	0.550	24
13	1200	0.425	0.575	4
14	1250	0.400	0.600	4
15	1300	0.350	0.650	4
16	1350	0.300	0.700	4
17	1400	0.250	0.750	4
18	1450	0.200	0.800	4
19	1500	0.150	0.850	4
20	1550	0.100	0.900	4

8.1.6 Fe-Ti-V-O Experiments in Air

After equilibration experiments on the Fe-V-O and Ti-V-O systems in air had been successfully completed, excess Gibbs model parameters and some other thermodynamic properties were optimised to reproduce experimental phase diagram data. With the optimised binary parameters, phase diagram data and other thermodynamic properties of the Fe-Ti-V-O system in air were estimated using ternary interpolation techniques (see Section 9.2). A set of plausible starting compositions and equilibration temperatures for the Fe-Ti-V-O system were then derived. All further discussions with regard to experiments on the Fe-Ti-V-O system in air are done in Chapter 12.

8.1.7 Applying the Gibbs Phase Rule

The Fe-V-O and Ti-V-O systems in air are considered first. The pressure is fixed at 1 atm (isobaric), hence Equation 6.60 reduces to:

$$f = c - p + 1. \tag{8.4}$$

In this case, $\mathrm{c} = 4$ (V, Fe or Ti, O and N), and $\mathrm{p} = 3$ (solid oxide, liquid slag, and gas). Although the gas phase contains small quantities of other gaseous species, such as, CO(g), CO_2(g), H_2O(g) and Ar(g), their partial pressures are very low compared to O_2(g) and N_2(g). These can therefore be assumed to have a negligible effect on the total pressure of the system. According to Equation 8.4, $\mathrm{f} = 2$. Experiments for the Fe-V-O and Ti-V-O system in air were undertaken with the bottom and top of the working tube left open to the atmosphere. The air composition fixed the partial pressure of O_2, an intensive property, at 0.21 atm, which reduced f by one. Temperature, another intensive variable, was fixed at the furnace set-point during experiments, which reduced f by one again. This left the system fully defined and invariant. As a result, the equilibrium liquid and solid compositions could be determined unambiguously, knowing that the system state had been defined completely.

Next, the Fe-Ti-V-O system in air is considered. In this case $\mathrm{c} = 5$ (Fe, Ti, V O_2 and N_2) and

p = 3 or 4 (gas, slag and one or two solid solutions). If two solid phases are in equilibrium with the slag phase, $\mathrm{f} = 2$. Therefore, two variables are at the researcher's discretion, and the remainder are fixed. Such a system is bivariant. The temperature is fixed at the desired temperature and oxygen partial pressure, an intensive property, is fixed at 0.21 atm, hence fully defining the system. However, if only one solid phase is in equilibrium with the slag phase, $\mathrm{f} = 3$ (trivariant). With three variables at the researcher's discretion, the composition, another intensive property, of one specie in the slag or solid solution is fixed together with the temperature, which was fixed at the furnace set-point and oxygen partial pressure again fixed at 0.21 atm. However, fixing the composition of the slag or solid solution was not possible, given that the aim was to determine the compositions of both solutions experimentally. Knowing that the initial composition is at the researcher's discretion, it was possible to directly chose a set of initial compositions that was confined to an area where the slag was in equilibrium with one solid phase. This allowed one to vary the equilibrium slag and solid composition indirectly. In such a case, more than one experiment was done at the same temperature. The application of the Gibbs phase rule to the Fe-Ti-V-O system in air is again discussed in Chapter 12.

8.2 Analysis of the Specimen

In this section, the analytical techniques that were used are described. All samples were carbon-coated with a Leica EM SCD050 Coater (supplied by Leica Mikrosysteme GmbH, Vienna), before SEM analysis and EPMA. A SEM-EDS was used to do preliminary analysis of specimens owing to its relative ease of usage and fast analytical capabilities. However, the limitations of SEM-EDS have given it a reputation as only achieving "semi-quantitative"results (Newbury and Ritchie 2015). EPMA has been widely accepted as an analytical tool for high accuracy and precision quantification of liquid oxide phases. There have been some recent developments and improvements in SEM-EDS that may restore its reputation as fully quantitative. The advantages and disadvantages of SEM-EDS are briefly discussed and are set to support quantitative analysis with SEM-EDS. SEM-EDS analysis and EPMA were chosen as quantitative analytical techniques in this study and measured results from both analytical techniques are shown, and compared in Part IV.

8.2.1 Recent Trends in SEM-EDS Development

A SEM focuses a beam of electrons on a specimen to acquire information as to its structure and composition. The major advantages of SEM-EDS over WDS have been well reported (Newbury and Ritchie 2015):

- All elements of a unknown sample are measured simultaneously, which minimises the dose to the specimen.
- A larger solid angle of the EDS compared to WDS further improves the efficiency of detection, which again lowers the required dose compared to WDS.
- The spectra of standards could be stored and recalled owing to the stability of EDS.

Unfortunately, some major disadvantages associated with SEM-EDS have arisen because of the introduction of the "standardless" quantitative analysis. For this analytical technique, only the EDS spectrum of the unknown is required, and as a consequence, the need to measure standards locally or by specification of electron dose is eliminated. Standardless analysis is designed to provide the required standard intensity for each element in an unknown sample by theoretical calculation of X-ray generation and propagation in a pure element target. Another approach requires the use of a library of actual standards measured on a well-characterised EDS detector for a wide range of beam

energies under well-defined conditions. The beam energies under these conditions can be related to the efficiency as a function of photon energy of the local EDS. However, the reliability of true first principle implementation of standardardless analysis requires an extensive database of X-ray parameters, many of which are poorly known. These include (Newbury and Ritchie 2015):

- Ionization are
- X-ray fluorenscence yield
- X-ray mass absorption coefficient.

Another drawback of standardless analysis is the normalisation to unity of concentrations of species in an unknown sample. Although this may be seen as convenient, it can lead to significant relative errors. The relative error being defined by Equation 8.5:

$$Relative\,error = [Measured\,concentration - reference]/reference. \tag{8.5}$$

Newbury and Ritchie (2015) evaluated and compared relative error ranges of standardless EDS analysis to EPMA of well-known minerals and deduced that standardless EDS analysis can often contribute to poor accuracy, and an unacceptably wide relative error range. However, recent developments of a modified structure for SDD-EDS have once again made it possible to analyse samples quantitatively within a small relative error range, if a careful measurement science regime is thoroughly followed. This was again exemplified by Newbury and Ritchie (2015):

- A well-polished surface is created to overcome typography and geometry defects.
- The sample is coated with a conducting material that has a typical thickness of 8 - 10 nm.
- Spectra of unknowns and standards should thus be estimated under known and reproducibility conditions of beam energy, dose and EDS operating conditions.
- The K-ratio protocol needs to be rigorously followed.

Under these conditions SEM-EDS (SDD) can accurately determine phase composition within a very narrow relative error range. Moreover, having two reliable, high-precision analytical techniques can collectively assist in successful characterisation and quantification of phases.

8.2.2 Analytical Procedure

SEM-EDS Operating Conditions

Before SEM-EDS and EPMA analysis, a sample was carbon-coated in order to create a conductive surface. This avoids charge build-up of a specimen, which reduces thermal damaging of samples and improves the secondary electron signal, thereby improving imaging. For SEM analysis, a Model:LEO 1450 (Carl Zeiss Microscopy GmbH, Jena, Germany) SEM coupled to an Inca E-sight 7366 EDS analyser (Oxford Instruments plc, Abingdon, Oxfordshire, Uk) at the Material Science and Engineering departments of Aalto University was used and operated at acceleration voltages ranging between 15 and 20 kV. The accelerating voltage of the SEM was 15 KV and the standard intensities for O, Fe, V and Ti were hematite, pure Fe, V and Ti, respectively. The SEM is equipped with the following detectors:

1. Secondary electron detector (SED)
2. Variable pressure secondary electro detector

3. Backscattered electron detector (BSD)
4. Energy dispersive X-ray spectrometer with silicon drift detector (EDS or EDX: GENESIS XM2)
5. Cathodoluminescence detector.

Figure 8.7: SEM-EDS that was used for quantification of phases in samples, at the Department of Material Science and Engineering, Aalto University.

Although the SEM is not equipped with an SDD, a fully quantitative analysis of samples was done with SEM-EDS by complying with the measurement science regime outlined by Newbury and Ritchie (2015).

EPMA Operating Conditions

EPMA (Cameca SX 100, University of Johannesburg) is a combined qualitative and quantitative analytical tool used for phase characterisation and composition estimation. EMPA employs WDS for analysing samples and has a higher peak resolution, meaning that elements in trace amounts can be detected more accurately than in SEM-EDS. As a result, EPMA is superior in quantifying the composition of a liquid. On top of this, EPMA can accurately determine concentrations of elements up to 1 wt.% accuracy and has a detection limit of 100 ppm (Goldstein et al. 1981).

The samples for EPMA were analysed at 15 kV accelerating voltage and 40 nA beam current. All elements were measured on their Kα lines, using wavelength-dispersive spectrometers. Fe was calibrated on Fe_2O_3, Ti on TiO_2 and V on pure V, but the measured V mass fractions were adjusted as if V had been calibrated on vanadinite ($Pb_5(VO_4)_3Cl$). This was done to match the matrix of the calibration standard better with the (oxidic) matrix of the samples. The matrix correction in the probe software was based on the "X-PHI" model (Merlet 1994).

Chapter 9

Thermodynamic Modelling Methodology

The thermodynamic assessment (modelling or description) of Fe-Ti-V-O in air has not been available, despite its necessity. One objective of the project is to perform a critical assessment of the experimental data (including experimental results from this study), followed by a thermodynamic evaluation of the system. It was however difficult to determine all phase diagram and thermodynamic data required for the thermodynamic assessment experimentally. Therefore, some phase diagram data from the literature were used in the assessment. The low temperatures at which eutectic reactions take place cannot be accurately estimated owing to experimental constraints. The literature summary in Chapter 5 has identified controversy in previous studies and consequently, some data of previous studies were omitted from the thermodynamic evaluation.

The scope of this study is also limited to oxidizing conditions and as result, V_2O_5 is the dominant oxide from the available V-O compounds. All calculations of phase diagram and thermodynamic properties were done using FactSage 7.0 software (Bale et al. 2009). The subsequent sections summarise all necessary information and data required for a thermodynamic evaluation of the Fe-V-Ti-O system in air.

9.1 M-V-O Systems in Air

9.1.1 Structure and Phase Transformation Data

Fe-V-O System in Air

Two vanadate compounds have been reported between Fe_2O_3 and V_2O_5, namely $FeVO_4$ (orthovanadate) and $Fe_2V_4O_{13}$. The 1:1 Fe:V mole ratio othovanadate belongs to the space group $P1$ and The been detected by numerous authors with X-ray diffraction (Burdese 1957; Kerby and Wilson 1973; Slobodin, Fotiev, and Miller 1976; Burzo et al. 1978; Fotiev, Cheshnitskii, and Surat 1983; Walczak et al. 1985). The compound presents four high-pressure phases, labelled i, ii, iii and iv (Muller and Joubert 1975). Phase i is less dense and stable under atmospheric conditions. The other three $FeVO_4$ phases are classified by increasing density. The transition of i - ii, ii - iii and iii - iv has been observed by Hotta et al. (1984) at 800 °C and 5.5 GPa. This finding suggests that $FeVO_4$-i is stable under the thermodynamically favourable conditions used in this study, given that all experiments and assessments were conducted at 1 atm. Furthermore, it is known that the compound melts incongruently and that the melting behaviour of $FeVO_4$ depends greatly on the synthesis conditions, but primarily on the partial pressure of oxygen. That said, the amount of disorder in the crystal lattice affects the incongruent melting point. This phenomenon was confirmed by Fotiev, Cheshnitskii, and Surat (1983), who noted that changing the oxygen partial pressure from

1 atm to 0.211 atm depressed the melting range by 20 K. Moreover, $FeVO_4$ is stable under oxidising conditions, and decomposes according to Equation 9.1 when the partial oxygen pressure is lowered (Lebrun and Perrot 2010):

$$2\,\mathrm{FeVO_4(s)} \longrightarrow \mathrm{Fe_2O_3(s)} + 2\,\mathrm{VO_2(s)} + 0.5\,\mathrm{O_2(g)} \tag{9.1}$$

The second vanadate, $Fe_2V_4O_{13}$, has a single paramagnetic phase that belongs to the space group $\mathrm{P2_1/c}$, and was detected by Pletnev, Fotiev, and Lisson (1975) and Permer and Laligant (1997) using NMR. Wang et al. (1998) used a flux method from a starting mixture of 95% V_2O_5 and 5% Fe_2O_3 to prepare the compound, while Si et al. (2012) used a liquid precipitation method to synthesize it. The starting materials, $Fe(NO_3)\cdot H_2O$ and NH_4VO_3, were dissolved in distilled water at molar ratios of Fe:V = 1:2 and stirred for 3 hours in an ultrasonic instrument. The precipitate was separated by centrifugation, followed by washing and drying for an extended period. A final calcining step was employed at 300 and 400 °C to obtain $Fe_2V_4O_{13}$. The compound was analytically identified with XRD and SEM-EDS. It has a monoclinic structure, and melts incongruently (Walczak et al. 1985; Fotiev, Cheshnitskii, and Surat 1983). Furthermore, the liquidus temperature of the compound decreased by roughly 28 K when oxygen partial pressure was changed from 1 atm to 0.21 atm.

Ti-V-O System in Air

To date, no intermediate compounds have been reported in the T-V-O system under oxidising conditions.

Habel et al. (2006) investigated the transformation from anatase to rutile in the presence of V_2O_5 and reported a transformation temperature ranging between 525 °C and 550 °C. This finding suggested that V_2O_5 encouraged the transformation of rutile to anatase. This experimental observation supports the experimental assumption that anatase in the presence V_2O_5 was transformed to rutile, given that all experiments of this study were conducted at and above 700 °C with relatively long equilibration times.

The structures and spacegroups of TiO_2(s)(rutile), Fe_2O_3(s) V_2O_5(s) and Fe_2TiO_5(s) were given in Chapter 4. The compounds have been well described in numerous studies.

9.1.2 Liquidus and Solidus data

Fe-V-O System in Air

Some liquidus and solidus data of the Fe-V-O system in air are available in the literature. The method of investigation and invariant points from the respective studies are summarised in Table 9.1. Limited information from the study of Burdese (1957) was ascertained, therefore the results from the study were not used in the evaluation. The invariant points of Kerby and Wilson (1973) are unusual and controversial, attributed to their observation that the compounds Fe_2O_3(s) and $FeVO_4$(s) melted within a liquid miscibility gap. An inspection of the instability of a single liquid phase revealed that for a liquid-liquid miscibility gap to appear, like interactions (i-i, j-j) need to be significantly stronger than unlike interactions (i-j) (Lukas, Fries, and Sundman 2007). This is normally the case with silica systems, where an SiO_2 component is chemically very different compared to many other metal oxides. In these systems, attraction between like molecules (i-i, j-j) is stronger than between unlike molecules (i-j). Although no experimental evidence exists to determine the interaction strength in a Fe-V-O slag, it is unlikely that such melting behaviour would occur, because in principle, Fe and V ions based on their ionic radii are chemically similar (Shannon 1976). On the basis of chemical similarity, it is assumed that attraction between unlike molecules (Fe-V) is stronger than the attraction between like molecules (Fe-Fe, V-V). Furthermore, no liquid-liquid miscibility gap was observed in the results of this study or any of the other reported studies of Fe-V-O system in air (Fotiev, Cheshnitskii, and

Surat 1983; Walczak et al. 1985). Therefore, it was decided to exclude the liquidus and solidus data of Kerby and Wilson (1973) from the thermodynamic assessment.

Table 9.1: Invariant reactions and phase transitions in the Fe−V−O system in air from literature.

Method	Composition (V_2O_5 mole %)	Temperature °C	Type of invariant	Equilibrium solid phases	Reference
DTA and X-Ray	89	634	Eutectic	V_2O_5, $FeVO_4$	Burdese 1957
Diffraction	37	843	Peritectic	Fe_2O_3, $FeVO_4$	Burdese 1957
DTA and X-Ray	80	645	Eutectic	V_2O_5, $FeVO_4$	Kerby and Wilson 1973
Diffraction	64	843	Peritectic	$FeVO_4$	Kerby and Wilson 1973
	40	843	Peritectic	$FeVO_4$	Kerby and Wilson 1973
	38	645	Eutectic	Fe_2O_3, $FeVO_4$	Kerby and Wilson 1973
DTA and X-Ray	97	658	Eutectic	V_2O_5, $Fe_2V_4O_{13}$	Fotiev, Cheshnitskii, and Surat 1983
Diffraction	93	692	Peritectic	$FeVO_4$, $Fe_2V_4O_{13}$	Fotiev, Cheshnitskii, and Surat 1983
	85	870	Peritectic	$FeVO_4$, Fe_2O_3	Fotiev, Cheshnitskii, and Surat 1983
DTA and X-Ray	96	615	Eutectic	V_2O_5, $Fe_2V_4O_{13}$	Walczak et al. 1985
Diffraction	91	665	Peritectic	$FeVO_4$, $Fe_2V_4O_{13}$	Walczak et al. 1985
	80	850	Peritectic	$FeVO_4$, Fe_2O_3	Walczak et al. 1985

The reported invariant point data from the studies of Fotiev, Cheshnitskii, and Surat (1983) and Walczak et al. (1985) were given an identical weight contribution in the assessment. Both studies identified and included the compound, $Fe_2V_4O_{13}$ and reported good agreement with the accepted melting point (669.85 °C) of V_2O_5 (Bale et al. 2016). Some differences of invariant points were however noted. For example, a transition temperature of the invariant reaction, $FeVO_4 \rightarrow$ Liquid + Fe_2O_3, ranging from 840 °C to 870 °C, has been postulated. Liquidus and solidus temperature lines have also not corresponded, with Walczak et al. (1985) reporting a higher solubility of Fe_2O_3 in the slag at corresponding temperatures. Walczak et al. (1985) even included a solubility range of Fe_2O_3 in V_2O_5, which was first suggested by Burzo. and Stanescu (1976) and later detected by Burzo. and Stanescu (1978) and Palanna, Mohanand, and Biswas (1978). The liquidus data above the $FeVO_4$ peritectic point have been extrapolated in all previous studies and were not considered in the assessment.

Ti-V-O System in Air

Little liquidus and solidus data have been reported for the Ti-V-O system in air. Nevertheless, solubility of V_2O_5(s) in the rutile phase has been reported by Habel et al. (2006) and Habel et al. (2008). It is also known that one eutectic transformation reaction exists close to pure V_2O_5 owing to a large difference in melting points of TiO_2(s) and V_2O_5(s). Some invariant points have been reported and are presented in Table 9.2. The V_2O_5-TiO_2 phase diagram data obtained from the thermodynamic assessment of Yang et al. (2017) were mostly extrapolated from model parameters and were not considered in the assessment of this study.

Table 9.2: Invariant reactions and phase transitions in the Ti−V−O system in air from literature.

Method	Composition (V_2O_5 mole %)	Temperature °C	Type of invariant	Equilibrium solid phases	Reference
DTA	95	670	Eutectic	V_2O_5, TiO_2	Habel et al. 2006
Thermodynamic assessment	95	675	Eutectic	V_2O_5, TiO_2	Yang et al. 2017

9.1.3 Thermodynamic data

Fe-V-O System in Air

The enthalpies of formation and standard entropies of $FeVO_4$(s) and $Fe_2V_4O_{13}$(s) were obtained from EMF measurements (Otsubu and Utsumi 1971; Volkov 1979). The heat capacities of $FeVO_4$ and $Fe_2V_4O_{13}$(s) were calorimetrically determined by Cheshnitski, Kozhevnikov, and Fotiev (1985) in temperatures ranging from, 298 K to 973 K. Moreover, the heat capacity of $FeVO_4$ was also calorimetrically determined in a low temperature range from 60 K to 300 K by Borukhovich et al.

(1975), who used X-ray diffraction and spectroscopic analysis to study the single phase nature of the sample.

An inspection of Equation 9.14 revealed that thermodynamic data of Fe_2O_3(l) were required for a description of the slag phase by the MQM and ASM. However, in reality, the Fe_2O_3(l) compound does not exist because of hematite's solid state transition to magnetite at 1388.73 °C in air (see Equation 9.2). The value was determined with FactSage 7.0.

$$3\,\mathrm{Fe_2O_3(s)} \longrightarrow 2\,\mathrm{Fe_3O_4(s)} + 0.5\,\mathrm{O_2(g)} \tag{9.2}$$

At oxidizing conditions, the slag in any Fe-M-O (M = metal) system predominantly contains Fe^{3+} cations surrounded by O^{2-} anions. Although it was mentioned that Fe_2O_3(l) does not exist, theoretically it needs be part of the calculation to model Fe^{3+} solubility in a V-O slag. The theoretical Fe_2O_3(l) thermodynamic data were not available in the FACTPS database and were taken from the study of Kowalski and Spencer (1995), but were adjusted slightly in this study to reproduce experimental data within acceptable limits. Moreover, thermodynamic data of all other stable compounds of the Fe-V-O system in air were taken from the FactPS database (Bale et al. 2016). The thermodynamic data of all stable compounds that were used are summarised in Table B. These data were used in the optimisation, with minor adjustments made to $\Delta H^{\circ}_{f,298}$ and S°_{298} values of compounds $FeVO_4$(s), $Fe_2V_4O_{13}$(s) and Fe_2O_3(l) to reproduce experimental data. See Section 10.3.

Ti-V-O System in Air

All thermodynamic data of V_2O_5(s,l) and TiO_2(s,l) were taken from the FactPS database (Bale et al. 2016), unless otherwise stated. No other thermodynamic data of the T-V-O system in air were found in the literature, which highlights the need for experimental data.

9.1.4 Modelling of Stoichiometric Compounds

The standard Gibbs energy of stoichiometric compounds is described by Equation 6.6. All thermodynamic data of stoichiometric compounds before the assessment are presented in Table B.

9.1.5 Modelling of the Liquid phase

The ASM and the MQM were used to describe the liquid phases in the Fe-V-O and Ti-V-O systems. These models are discussed in Section 6.3. However, only the MQM was used to describe the liquid phase in the higher-order Fe-Ti-V-O system owing to lack of data on ASM parameters related to the Fe-Ti-O system (see Section 12.1). A short description of how the models were applied is given:

Quasichemical Model

The quasichemical model, which takes into account short-range ordering of SNN, was recently used by Xie et al. (2016) to describe the liquid phase in the $PbO-V_2O_5$ system. It was assumed that liquid V_2O_5 is made up of the building unit VO_4^{3-}, which in turn corresponds to VO^{3+} cation specie. It was however stated by Xie et al. (2016), that $V_2O_7^{4-}$ can also be used as a building unit. A description of the V_2O_5 melt with these building units was found in the study of Kawakita et al. (1999), which investigated the local structures of liquid and vitreous V_2O_5 and P_2O_5 melt. A similar finding was made by Hawakawa and Yoko (1995), who in turn investigated structure of lead vanadate glasses. Moreover, it was found from the study of Kawakita et al. (1999) that the characteristics of liquid P_2O_5 are similar to those of V_2O_5. Similarly, Hudon and Jung (2014) and Rahman, Hudon, and Jung (2013) successfully adopted $P_2O_7^{4-}$ as building unit of P_2O_5 in the $CaO-P_2O_5$ and $SiO_2-P_2O_5$ systems, respectively. This approach has also been adopted by FactSage for describing slag phases consisting of P_2O_5 (Bale et al. 2016).

To remain consistent with the modelling methods of the FToxid database in FactSage, V_2O_5 will have the building unit $V_2O_7^{4-}$, which can be surrounded by four broken oxygen atoms. This constitutes $V_2O_3^{4+}$ as corresponding cation specie. The quasichemical reaction between cations in liquid Fe-Ti-V-O in air can be expressed as follows:

$$(Fe^{3+} - Fe^{3+}) + (V_2O_3^{4+} - V_2O_3^{4+}) = 2(Fe^{3+} - V_2O_3^{4+}) \qquad \Delta g_{Fe^{3+}-V_2O_3^{4+}} \tag{9.3}$$

$$(Fe^{2+} - Fe^{2+}) + (V_2O_3^{4+} - V_2O_3^{4+}) = 2(Fe^{2+} - V_2O_3^{4+}) \qquad \Delta g_{Fe^{2+}-V_2O_3^{4+}} \tag{9.4}$$

$$(Ti^{4+} - Ti^{4+}) + (V_2O_3^{4+} - V_2O_3^{4+}) = 2(Ti^{4+} - V_2O_3^{4+}) \qquad \Delta g_{Ti^{4+}-V_2O_3^{4+}} \tag{9.5}$$

$$(Ti^{3+} - Ti^{3+}) + (V_2O_3^{4+} - V_2O_3^{4+}) = 2(Ti^{3+} - V_2O_3^{4+}) \qquad \Delta g_{Ti^{3+}-V_2O_3^{4+}} \tag{9.6}$$

$$(Ti^{4+} - Ti^{4+}) + (Fe^{3+} - Fe^{3+}) = 2(Ti^{4+} - Fe^{3+}) \qquad \Delta g_{Ti^{4+}-Fe^{3+}} \tag{9.7}$$

$$(Ti^{4+} - Ti^{4+}) + (Fe^{2+} - Fe^{2+}) = 2(Ti^{4+} - Fe^{2+}) \qquad \Delta g_{Ti^{4+}-Fe^{2+}} \tag{9.8}$$

$$(Ti^{3+} - Ti^{3+}) + (Fe^{2+} - Fe^{2+}) = 2(Ti^{3+} - Fe^{2+}) \qquad \Delta g_{Ti^{3+}-Fe^{2+}} \tag{9.9}$$

$$(Fe^{3+} - Fe^{3+}) + (Ti^{3+} - Ti^{3+}) = 2(Fe^{3+} - Ti^{3+}) \qquad \Delta g_{Fe^{3+}-Ti^{3+}} \tag{9.10}$$

$$(Fe^{3+} - Fe^{3+}) + (Fe^{2+} - Fe^{2+}) = 2(Fe^{3+} - Fe^{2+}) \qquad \Delta g_{Fe^{3+}-Fe^{2+}} \tag{9.11}$$

$$(Ti^{4+} - Ti^{4+}) + (Ti^{3+} - Ti^{3+}) = 2(Ti^{4+} - Ti^{3+}) \qquad \Delta g_{Ti^{4+}-Ti^{3+}} \tag{9.12}$$

where $\Delta g_{Fe^{3+}-V_2O_3^{4+}}$, $\Delta g_{Fe^{2+}-V_2O_3^{4+}}$, $\Delta g_{Ti^{4+}-V_2O_3^{4+}}$, $\Delta g_{Ti^{3+}-V_2O_3^{4+}}$, $\Delta g_{Ti^{4+}-Fe^{3+}}$,$\Delta g_{Ti^{4+}-Fe^{2+}}$, $\Delta g_{Ti^{3+}-Fe^{3+}}$, $\Delta g_{Fe^{3+}-Fe^{2+}}$ and $\Delta g_{Ti^{4+}-Ti^{3+}}$ are non-configurational Gibbs energy changes for the formation of 2 moles of SNN pairs.

Optimized parameters for the binary FeO-Fe_2O_3 slag solution are taken from Degterov et al. (2001). The qausichemical model parameters of the $TiO_2-Ti_2O_3$ system were first optimised by Eriksson and Pelton (1993) and later again by Kang, Jung, and Lee (2006) in response to the publication of more recent experimental data. Hence, the parameters of Kang, Jung, and Lee (2006) are used in this study. Furthermore, the Fe-Ti-O system was thermodynamically assessed by Eriksson and Pelton (1993) and later again by Eriksson et al. (1996). The optimised quasichemical parameters from their studies are used in the thermodynamic assessment of this study. However, all the assessments of the Fe-Ti-O system were performed under reducing conditions. Therefore, it was undertaken to optimise the Fe-Ti-O system under oxidizing conditions from experimental data of the Fe-Ti-V-O system in air. This required optimizing parameters related to the $Fe_2O_3-TiO_2$ solution and back-calculating the Fe-Ti-O phase diagram in air.

The molar Gibbs energy of the respective FeO$-V_2O_5$, $Fe_2O_3-V_2O_5$, $TiO_2-V_2O_5$, $Ti_2O_3-V_2O_5$ and $Fe_2O_3-TiO_2$ solutions that were optimised in this study, are expanded according to Equation 6.17 as follows:

$$G_m = n_{FeO}G^{\circ}_{FeO} + n_{V_2O_5}G^{\circ}_{V_2O_5} - T\Delta S^{config} + n_{Fe^{2+}-V_2O_3^{4+}}(\Delta g_{Fe^{2+}-V_2O_3^{4+}}/2) \tag{9.13}$$

$$G_m = n_{Fe_2O_3}G^{\circ}_{Fe_2O_3} + n_{V_2O_5}G^{\circ}_{V_2O_5} - T\Delta S^{config} + n_{Fe-V_2O_3^{4+}}(\Delta g_{Fe^{3+}-V_2O_3^{4+}}/2) \tag{9.14}$$

$$G_m = n_{TiO_2} G^{\circ}_{TiO_2} + n_{V_2O_5} G^{\circ}_{V_2O_5} - T\Delta S^{config} + n_{Ti^{4+}-V_2O_3^{4+}} (\Delta g_{Ti^{4+}-V_2O_3^{4+}}/2) \quad (9.15)$$

$$G_m = n_{Ti_2O_3} G^{\circ}_{Ti_2O_3} + n_{V_2O_5} G^{\circ}_{V_2O_5} - T\Delta S^{config} + n_{Ti^{3+}-V_2O_3^{4+}} (\Delta g_{Ti^{3+}-V_2O_3^{4+}}/2) \quad (9.16)$$

$$G_m = n_{TiO_2} G^{\circ}_{TiO_2} + n_{Fe_2O_3} G^{\circ}_{Fe_2O_3} - T\Delta S^{config} + n_{Ti^{4+}-Fe^{3+}} (\Delta g_{Ti^{4+}-Fe^{3+}}/2). \quad (9.17)$$

The terms $\Delta g_{Fe^{3+}-V_2O_3^{4+}}$, $\Delta g_{Fe^{2+}-V_2O_3^{4+}}$, $\Delta g_{Ti^{4+}-V_2O_3^{4+}}$, $\Delta g_{Ti^{3+}-V_2O_3^{4+}}$ and $\Delta g_{Fe^{3+}-Ti^{4+}}$ are expanded according to Equation 6.23 as follows:

$$\Delta g_{Fe^{3+}-V_2O_3^{4+}} = \Delta g^{\circ}_{Fe^{3+}-V_2O_3^{4+}} + \sum_{i\geq 1} g^{i0}_{Fe^{3+}-V_2O_3^{4+}} X^i_{Fe^{3+}-Fe^{3+}} + \sum_{j\geq 1} g^{0j}_{Fe^{3+}-V_2O_3^{4+}} X^j_{V_2O_3^{4+}-V_2O_3^{4+}} \quad (9.18)$$

$$\Delta g_{Fe^{2+}-V_2O_3^{4+}} = \Delta g^{\circ}_{Fe^{2+}-V_2O_3^{4+}} + \sum_{i\geq 1} g^{i0}_{Fe^{2+}-V_2O_3^{4+}} X^i_{Fe^{2+}-Fe^{2+}} + \sum_{j\geq 1} g^{0j}_{Fe^{2+}-V_2O_3^{4+}} X^j_{V_2O_3^{4+}-V_2O_3^{4+}} \quad (9.19)$$

$$\Delta g_{Ti^{4+}-V_2O_3^{4+}} = \Delta g^{\circ}_{Ti^{4+}-V_2O_3^{4+}} + \sum_{i\geq 1} g^{i0}_{Ti^{4+}-V_2O_3^{4+}} X^i_{Ti^{4+}-Ti^{4+}} + \sum_{j\geq 1} g^{0j}_{Ti^{4+}-V_2O_3^{4+}} X^j_{V_2O_3^{4+}-V_2O_3^{4+}} \quad (9.20)$$

$$\Delta g_{Ti^{3+}-V_2O_3^{4+}} = \Delta g^{\circ}_{Ti^{3+}-V_2O_3^{4+}} + \sum_{i\geq 1} g^{i0}_{Ti^{3+}-V_2O_3^{4+}} X^i_{Ti^{3+}-Ti^{3+}} + \sum_{j\geq 1} g^{0j}_{Ti^{3+}-V_2O_3^{4+}} X^j_{V_2O_3^{4+}-V_2O_3^{4+}} \quad (9.21)$$

$$\Delta g_{Fe^{3+}-Ti^{4+}} = \Delta g^{\circ}_{Fe^{3+}-Ti^{4+}} + \sum_{i\geq 1} g^{i0}_{Fe^{3+}-Ti^{4+}} X^i_{Fe^{3+}-Fe^{3+}} + \sum_{j\geq 1} g^{0j}_{Fe^{3+}-Ti^{4+}} X^j_{Ti^{4+}-Ti^{4+}} \quad (9.22)$$

$\Delta g^{\circ}_{Fe^{3+}-V_2O_3^{4+}}$, $\Delta g^{\circ}_{Ti^{4+}-V_2O_3^{4+}}$, $\Delta g^{\circ}_{Fe^{3+}-Ti^{4+}}$, $g^{0j}_{Fe^{3+}-V_2O_3^{4+}}$, $g^{0j}_{Ti^{4+}-V_2O_3^{4+}}$, $g^{0j}_{Ti^{4+}-Fe^{3+}}$, $g^{i0}_{Fe^{3+}-V_2O_3^{4+}}$, $g^{i0}_{Ti^{4+}-V_2O_3^{4+}}$ and $g^{i0}_{Fe^{3+}-Ti^{4+}}$ are all temperature-dependent adjustable model parameters, and were optimised to reproduce the liquidus within the limits of experimental error.

$Fe^{2+} - V_2O_3^{4+}$ and $Ti^{3+} - V_2O_3^{4+}$ binary pairs were assumed to have ideal mixing behaviour, hence the terms in Equation 9.19 and Equation 9.21 were set to zero. Under oxidizing conditions, Ti^{3+} and Fe^{2+} concentrations were assumed to be low in the studied temperature range (700 °C to 1500 °C) compared to $V_2O_3^{4+}$ concentration. Under oxidizing conditions, the $Fe^{2+} - V_2O_3^{4+}$ and $Ti^{3+} - V_2O_3^{4+}$ binary pairs might only start contributing to the Gibbs energy of the liquid phase significantly in regions near the melting points of spinel/Fe_3O_4(s) and TiO_2(s). This is because of the melting of spinel/Fe_3O_4(s) to from FeO(l) and Fe_2O_3(l) and the decomposition of TiO_2(l) to Ti_2O_3(l) and O_2(g) above 1500 °C (Bale et al. 2009).

The $\Delta g^{\circ}_{Fe^{3+}-V_2O_3^{4+}}$ and $\Delta g^{\circ}_{Ti^{4+}-V_2O_3^{4+}}$ terms have a major influence at compositions of maximum short-range ordering. It is known that maximum short-range ordering usually occurs at the intermediate compound with the highest melting point (congruent melting) and the minimum mixing enthalpy. This was the finding from the recent studies of Xie et al. (2016), Hudon and Jung (2014),

Cao et al. (2017), and Protstakova et al. (2015). However, it is supported experimentally that no intermediate compounds in the Fe-V-O and Ti-V-O systems in air melt congruently. Therefore, the $\Delta g^{\circ}_{Fe^{3+}-V_2O_3^{4+}}$ and $\Delta g^{\circ}_{Ti^{4+}-V_2O_3^{4+}}$ terms have a less significant impact on the Gibbs energy of the liquid phase. The terms, $g^{i0}_{Fe^{3+}-V_2O_3^{4+}}$, $g^{0j}_{Fe^{3+}-V_2O_3^{4+}}$, $g^{i0}_{Ti^{4+}-V_2O_3^{4+}}$ and $g^{0j}_{Ti^{4+}-V_2O_3^{4+}}$ have a significant influence on the Gibbs energy of the liquid. It was estimated with FactSage that Fe_2TiO_5 (if selected from the list of pure compounds) melts congruently in the Fe-Ti-O system in air (see Figure 12.1). Therefore, the term $\Delta g^{\circ}_{Fe^{3+}-Ti^{4+}}$ has a significant effect on the Gibbs energy of the Fe-Ti-O liquid.

Moreover, when $Y_{V_2O_3^{4+}}$ is $< 1/2$, $X_{V_2O_3^{4+}-V_2O_3^{4+}}$ is small and $g^{0j}_{Fe^{3+}-V_2O_3^{4+}} X_{V_2O_3^{4+}-V_2O_3^{4+}}$ have a small effect on the Gibbs energy of the liquid. In this region, only the parameters $g^{i0}_{Fe-V_2O_3^{4+}}$ and $g^{i0}_{Ti^{4+}-V_2O_3^{4+}}$ largely contribute to the Gibbs energy. The opposite is true when $Y_{V_2O_3}$ is $> 1/2$. It is also possible to add cross-terms to Equation 9.18. For example, $\sum g^{ij}_{Fe^{3+}-V_2O_3^{4+}} X_{Fe^{3+}-Fe^{3+}} X_{V_2O_3^{4+}-V_2O_3^{4+}}$ with $i \geq 1$ and $j \geq 1$ (Eriksson et al. 2000).

Associates Species Model

The ASM, which accounts for non-ideal behaviour of a liquid phase by including intermediate/associate species in Equation 6.7 is used by MTdata thermochemistry software to describe the liquid phase.

For the Fe-V-O system in air, it has been mentioned here that neither $FeVO_4$ nor $Fe_2V_4O_{13}$ melts congruently. Consequently, these two compounds are not used as associates. The model effectively reduces to a substitutional model, with V_2O_5(l), FeO(l) and Fe_2O_3(l) the liquid components, respectively.

$$\begin{aligned} G_m =& y_{V_2O_5} G^{\circ}_{V_2O_5} + y_{Fe_2O_3} G^{\circ}_{Fe_2O_3} + y_{FeO} G^{\circ}_{FeO} \\ &+ RT(y_{V_2O_5} Lny_{V_2O_5} + y_{Fe_2O_3} Lny_{Fe_2O_3} + y_{FeO} Lny_{FeO}) + G^e_m \end{aligned} \tag{9.23}$$

Parameters representing interactions between Fe_2O_3 and V_2O_5 are introduced by adopting Equation 6.15 and possibly FeO and V_2O_5 to model the liquidus curve close to V_2O_5, $Fe_2V_4O_{13}$ and $FeVO_4$. Therefore, the excess Gibbs energy is described by the following expression:

$$\begin{aligned} G^e_m = y_{V_2O_5} y_{Fe_2O_3} {}^0L_{V_2O_5-Fe_2O_3} + y_{V_2O_5} y_{FeO} {}^0L_{V_2O_5-FeO} + y_{FeO} y_{Fe_2O_3} {}^0L_{FeO-Fe_2O_3} + \\ y_{V_2O_5} y_{Fe_2O_3} {}^1L_{V_2O_5-Fe_2O_3} (y_{V_2O_5} - y_{Fe_2O_3}). \end{aligned} \tag{9.24}$$

The same approach is followed for the Ti-V-O system in air. In this case, the liquidus curve is described by species TiO_2, Ti_2O_3 and V_2O_5. The molar Gibbs energy of the liquid is as follows:

$$\begin{aligned} G_m =& y_{V_2O_5} G^{\circ}_{V_2O_5} + y_{Ti_2O_3} G^{\circ}_{Ti_2O_3} + y_{TiO_2} G^{\circ}_{TiO_2} \\ &+ RT(y_{V_2O_5} Lny_{V_2O_5} + y_{Ti_2O_3} Lny_{Ti_2O_3} + y_{TiO_2} Lny_{TiO_2}) + G^e_m \end{aligned} \tag{9.25}$$

and the excess molar Gibbs energy is given by Equation 9.26 through application of Equation 6.15:

$$\begin{aligned} G^e_m = y_{V_2O_5} y_{TiO_2} {}^0L_{V_2O_5-TiO_2} + y_{V_2O_5} y_{Ti_2O_3} {}^0L_{V_2O_5-Ti_2O_3} + y_{TiO_2} y_{Ti_2O_3} {}^0L_{TiO_2-Ti_2O_3} \\ + y_{TiO_2} y_{Ti_2O_3} {}^1L_{TiO_2-Ti_2O_3} (y_{TiO_2} - y_{Ti_2O_3}) + y_{V_2O_5} y_{TiO_2} {}^1L_{V_2O_5-TiO_2} (y_{V_2O_5} - y_{TiO2}). \end{aligned} \tag{9.26}$$

The parameter L is a linear function of temperature, equated as $L = a + bT$ and $i = 1, 2, 3..n$. Kowalski and Spencer (1995) successfully described the liquid phase of a Fe-O system with Fe,

FeO and Fe_2O_3 as associates. Similarly, Cancarevic, Zinkevich, and Aldinger (2007) successfully reproduced the liquidus curve of the Ti-O system. Ti, O, TiO, Ti_2O_3 and TiO_2 were used for description of the liquid. A Redlich-Kister function was introduced to describe non-ideal behaviour between components.

Furthermore, the interaction terms from the study of Kowalski and Spencer (1995) were initially used and then optimised to reproduce the liquidus curve in the FeO–Fe_2O_3-rich region. In other words, the transition of Fe_2O_3(s) to spinel/Fe_3O_4(s) and the reported melting temperature of pure spinel/Fe_3O_4, were reproduced as accurately as possible. The interaction parameters from the study of Cancarevic, Zinkevich, and Aldinger (2007) were used for description of non-ideal mixing behaviour between Ti_2O_3(l) and TiO_2(l).

9.1.6 Spinel Phase

Magnetite, also known as spinel, has a cubic spinel structure, space group $Fd3m$, prototype $MgAl_2O_4$. The thermodynamic model is explained in Section 6.3. The model and its parameters were chronologically described and optimised elsewhere (Degterov et al. 2001). The model for magnetite is used without any modification to remain consistent with previous thermodynamic assessments linked to the FToxid database in FactSage 7.0.

9.1.7 Rutile Solid Solution

A solid solution between V_2O_5 and TiO_2 has been shown to exist (rutile solid solution). The Gibbs free energy of the rutile solid solution is developed within the framework of the CEF. Therefore, to account for V solubility in rutile structure, V can be introduced substitutionally with interstitially dissolved oxygen. If it is assumed that O dissolves interstitially, the rutile structure is extended and expressed as $(\mathrm{Ti}^{4+}, \mathrm{Ti}^{3+}, \mathrm{V}^{5+})(\mathrm{O}, \mathrm{Va})(\mathrm{O}, \mathrm{Va})_2$. Vacancies are introduced into the O sub-lattice for charge neutrality. The extended rutile structure has twelve end-member species, compared to four end-member species when non-stoichiometry is not considered with the introduction of Ti^{3+} ions.

Therefore, for the sake of simplicity, non-stoichiometry was not compensated for the thermodynamic evaluation of the Ti-V-O system in air. In the model, it is assumed that V dissolves substitutionally in the cation lattice. As a result, vacancies are introduced on the cation sub-lattice for charge neutrality instead of interstitially dissolved oxygen. The model with representative end-members is explained in Subsubsection 6.3.3.

9.1.8 Hematite Solid Solution

A solid solution between V_2O_5 and Fe_2O_3 has been shown to exist (hematite solid solution). The Gibbs free energy of the hematite solid solution is developed within the framework of the CEF (Equation 6.24). In the model, it is assumed that all cations mix in one lattice and all anions in a second lattice. The model with representative end-members are explained in Subsubsection 6.3.3. .

9.2 Fe-Ti-V-O System in Air

Sub-solidus experimental data of the system exist up to 700 °C. Fotiev, Surat, and Tret'yakov (1981) investigated compatibility relations among crystalline phases for ternary combinations of Fe_2O_3, TiO_2 and V_2O_5 in air. No ternary compounds were observed and no intermediate compounds were detected in the V_2O_5 and TiO_2 region. All samples were heat-treated below the liquidus temperature. No liquidus data of the Fe-T-V-O system under oxidizing conditions were found in the literature.

Nevertheless, ternary interpolation techniques (see Section 6.4) were used and applied to quasi-chemical parameters of the Fe-V-O and Ti-V-O systems in air, to estimate thermodynamic properties of the liquid phase.

The solid solution models of the hematite and rutile phases are expanded to account for the solubility of Ti^{4+} and Fe^{3+} ions in cation sub-lattices of the hematite and rutile phases, respectively. It is then possible to estimate equilibrium at various temperatures and compositions of the Fe-Ti-V-O system in air from binary data, followed by estimating a set of plausible initial compositions for experiments related to this system.

Some added advantages that support the need for experimentally determined liqiudus and solidus compositions of the Fe-T-V-O system in air include:

- Better indication of which ternary interpolation technique should be used.
- Confirmation of no intermediate ternary compounds.
- Confirmation whether any ternary terms (see Equation 6.52) are necessary to reproduce experimental phase diagram data within acceptable error limits.

9.2.1 Expansion of the MQM

The number of ternary interpolation relations are dependent on the number of quasichemical interaction pairs. It is estimated that the Fe-Ti-V-O liquid phase requires a total of 10 ternary interpolation relations when extended from the Fe-V-O and Ti-V-O systems. These are as follows:

1. $Fe_2O_3-FeO-V_2O_5$
2. $Fe_2O_3-FeO-TiO_2$
3. $Fe_2O_3-FeO-Ti_2O_3$
4. $Fe_2O_3-FeO-V_2O_5$
5. $Fe_2O_3-TiO_2-V_2O_5$
6. $Fe_2O_3-Ti_2O_3-V_2O_5$
7. $Fe_2O_3-TiO_2-Ti_2O_3$
8. $FeO-TiO_2-V_2O_5$
9. $FeO-TiO_2-Ti_2O_3$
10. $TiO_2-Ti_2O_3-V_2O_5$.

A Kohler-like interpolation method, which is symmetric in nature, is used as an initial approach for estimating thermodynamic properties and phase diagram data from binary model parameters. This interpolation method is based on the assumption that all components are chemically similar and has been successful in describing the slag phases of higher order systems (Bale et al. 2016; Jung, Deceterov, and Pelton 2004; Zhang and Chen 2013; Prostakova et al. 2015). However, $\mathrm{G_e}$ is calculated to validate the assumption of chemically similar constituents. In other words, if $\mathrm{G_e}$ of one binary pair is two or three orders of magnitude larger than that of another binary pair, an asymmetric approach should be used to avoid spurious estimations from Kohler-like symmetrical interpolation.

9.2.2 Expansion of Solid Solution Models

The dissolution of Fe_2O_3(s) in the rutile phase was experimentally observed by Wittke (1967) (see Section 5.3). On the contrary, no experimental evidence from any previous study had reported on TiO_2 dissolution in the hematite phase. From the assessed Fe-V-O and Ti-V-O systems in air, a solubility range of V_2O_5(s) in the rutile and hematite phases was shown to exist. The models were described in Subsubsection 6.3.3. The models from Subsubsection 6.3.3 are now expanded to include Fe ions in the rutile phase and Ti ions in the hematite phase.

Furthermore, no experimental evidence exists on structural and atomic configurations to substantiate the assumption of substitutional dissolved V, Fe and Ti. However, these atomic arrangements were chosen to minimise the number of end-member components. For instance, the number of end-member components in the expanded rutile solid solution increase from eight to twelve, if it is assumed that O dissolves interstitially. The model for the expanded rutile solid solution is further explained in Subsubsection 9.2.2.

Rutile Solid Solution

The Gibbs free energy of the solution is developed within the framework of the CEF (Equation 6.24). Similar, to modelling of V_2O_5 dissolution in the rutile phase, it is assumed in the expanded rutile solid solution model that all cations mix in one lattice and all anions in a second lattice. That said, V and Fe dissolve substitutionally in the rutile phase and vacancies are formed on both cation and anion sub-lattices to account for charge neutrality. The model is then simply expanded from Fe-V-O and Fe-Ti-O systems, and has the chemical formula, $(\mathrm{Ti}^{4+},\mathrm{Fe}^{3+},\mathrm{V}^{5+},\mathrm{Va})(\mathrm{O}^{2-},\mathrm{Va})_2$. Moreover, the rutile solid solution models from Subsubsection 6.3.3 and Subsubsection 6.3.3 are combined and eight end-member species are formed (see Figure 9.1) from which expressions were already derived for six end-members from rutile solid solutions models of the Fe-Ti-O and Fe-V-O systems in air. Two new end-members, marked, $\mathrm{G}^{\circ}_{\mathrm{Va:Va_2}}$ and $\mathrm{G}^{\circ}_{\mathrm{V^{5+}:Va_2}}$ and one neural apex on the line $\mathrm{G}^{\circ}_{\mathrm{V^{5+}:O_2^{2-}}}$, $\mathrm{G}^{\circ}_{\mathrm{Fe^{3+}:O_2^{2-}}}$ marked $\mathrm{G}^{\circ}_{(\frac{1}{2}\mathrm{V^{5+}},\frac{1}{2}\mathrm{Fe^{3+}}):\mathrm{O_2^{2-}}}$ are observed in Figure 9.1, and Gibbs energy expressions can be derived from reciprocal relations:

$$G^{\circ}_{V^{5+}:O_2^{2-}} + G^{\circ}_{Fe^{3+}:Va_2} = G^{\circ}_{V^{5+}:Va_2} + G^{\circ}_{Fe^{3+}:O_2^{2-}} \tag{9.27}$$

$$G^{\circ}_{Ti^{4+}:O_2^{2-}} + G^{\circ}_{Va:Va_2} = G^{\circ}_{Ti^{4+}:Va_2} + G^{\circ}_{Va:O_2^{2-}}. \tag{9.28}$$

The two new end-members from exchange reactions 9.27 and 9.28 are derived by substituting for known expressions from Equation 6.38-Equation 6.40 and Equation 6.42b-Equation 6.44b, followed by rearrangement:

$$G^{\circ}_{Va:Va_2} = -G^{\circ}_{O_2(g)} \tag{9.29}$$

$$G^{\circ}_{V^{5+}:Va_2} = \frac{1}{2}G^{\circ}_{V_2O_5(s)-Rut} - G^{\circ}_{O_2(g)} - \frac{5}{2}RT\left(\frac{4}{5}ln\frac{4}{5} + \frac{1}{5}ln\frac{1}{5}\right). \tag{9.30}$$

Hematite Solid Solution

The hematite solid solution is expanded by combining models from Subsubsection 6.3.3 and Subsubsection 6.3.3. The models were developed to account for V_2O_5 and TiO_2 dissolution in the hematite phase for Fe-V-O and Fe-Ti-O systems in air. The expanded hematite solid solution has the chemical formula, $(\mathrm{Fe}^{3+},\mathrm{Ti}^{4+},\mathrm{V}^{5+},\mathrm{Va})_2(\mathrm{O}^{2-})_3$. Contrary to the expanded rutile solid solution where two new end-members were formed, no additional end-members are formed from the expansion. Expressions for end-member components were derived in Subsubsection 6.3.3 and Subsubsection 6.3.3.

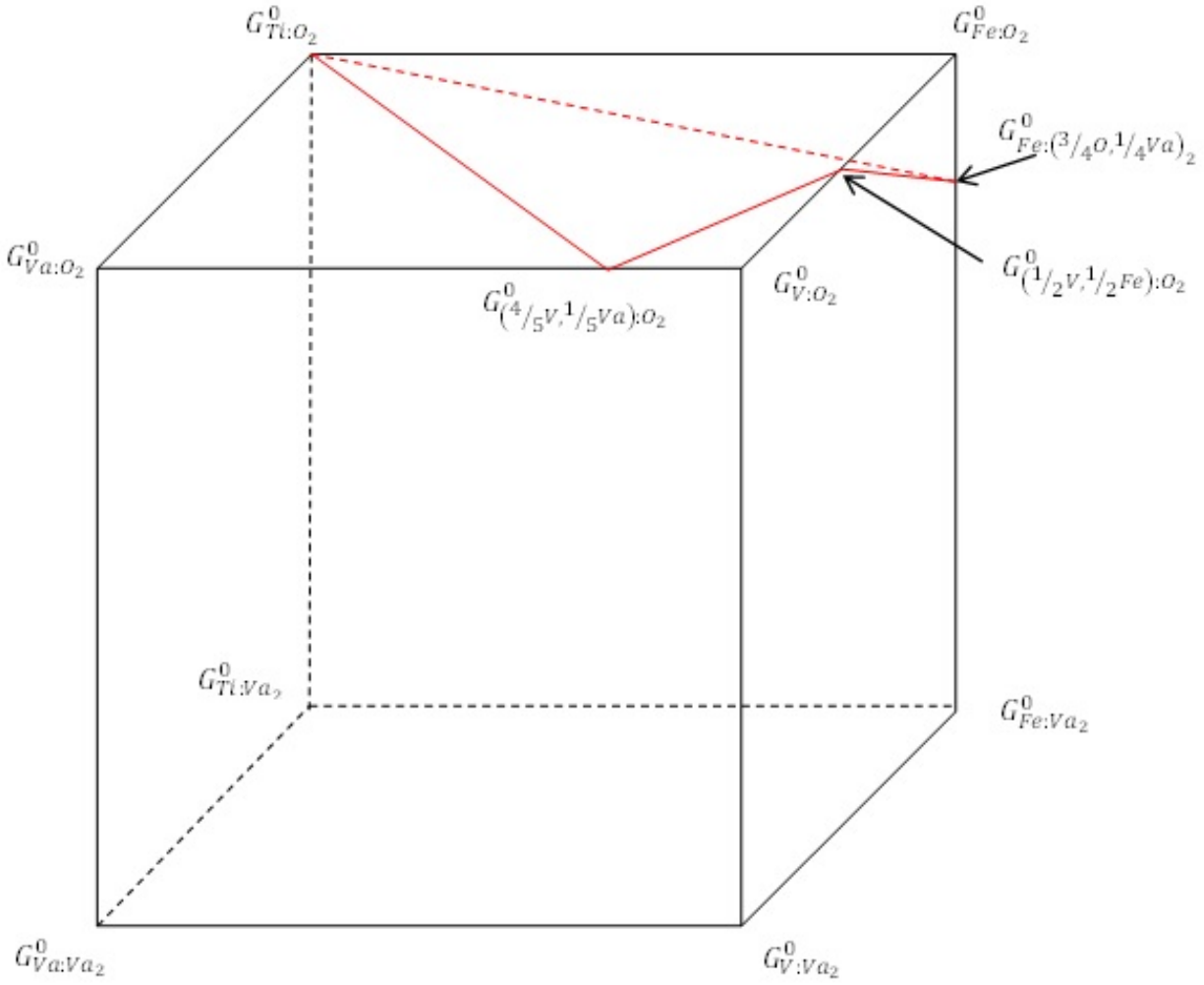

Figure 9.1: The neutral plane (in red) in the expanded rutile solid solution. Each corner represents an end-member of the solution.

Nevertheless, a schematic of the hematite solid solution with a neutral triangle and end-member components is shown in Figure 9.2.

Ferropseudobrookite Solid Solution

A solid solution, ferropseudobrookite, is known to exist in the Fe-Ti-O system under oxidizing and reducing conditions. However, it is reported in the FTOxid database that the model for ferropseudobrookite solid solution may only be used under relatively reducing conditions. Fe_2O_3 is not a component of the ferropseudobrookite solid solution in the model. Therefore, any calculations of Fe-Ti-O system under oxidizing conditions excludes Fe_2O_3. The model was developed within the framework of the CEF by Eriksson et al. (1996), in which the solution of $FeTi_2O_5$ and Ti_3O_5 was represented as $(\mathrm{Fe}^{2+}_{1-x}, \mathrm{Ti}^{3+}_{x})(\mathrm{Ti}^{4+}_{2-x}, \mathrm{Ti}^{3+}_{x})$, with the ions mixing randomly on each site. The model successfully reproduced experimental results under reducing conditions.

No experimental or theoretical data of the ferropseudobrookite solid solution under oxidizing conditions have been reported. Therefore, the dissolution of TiO_2(s) and Fe_2O_3(s) in ferropseudobrookite solid solution under oxidizing conditions cannot be reproduced with the available model and data in FactSage. However, a small solubility V_2O_5 in the Fe_2TiO_5(s) phase was observed from the experimental results of the Fe-Ti-V-O system in air (see Chapter 12).

To include solubility of V_2O_5 in the existing model of ferropseudobrookite solid solution would require expanding the solution to include Fe^{3+}, Ti^{4+} and V^{5+} ions. The number of end-members

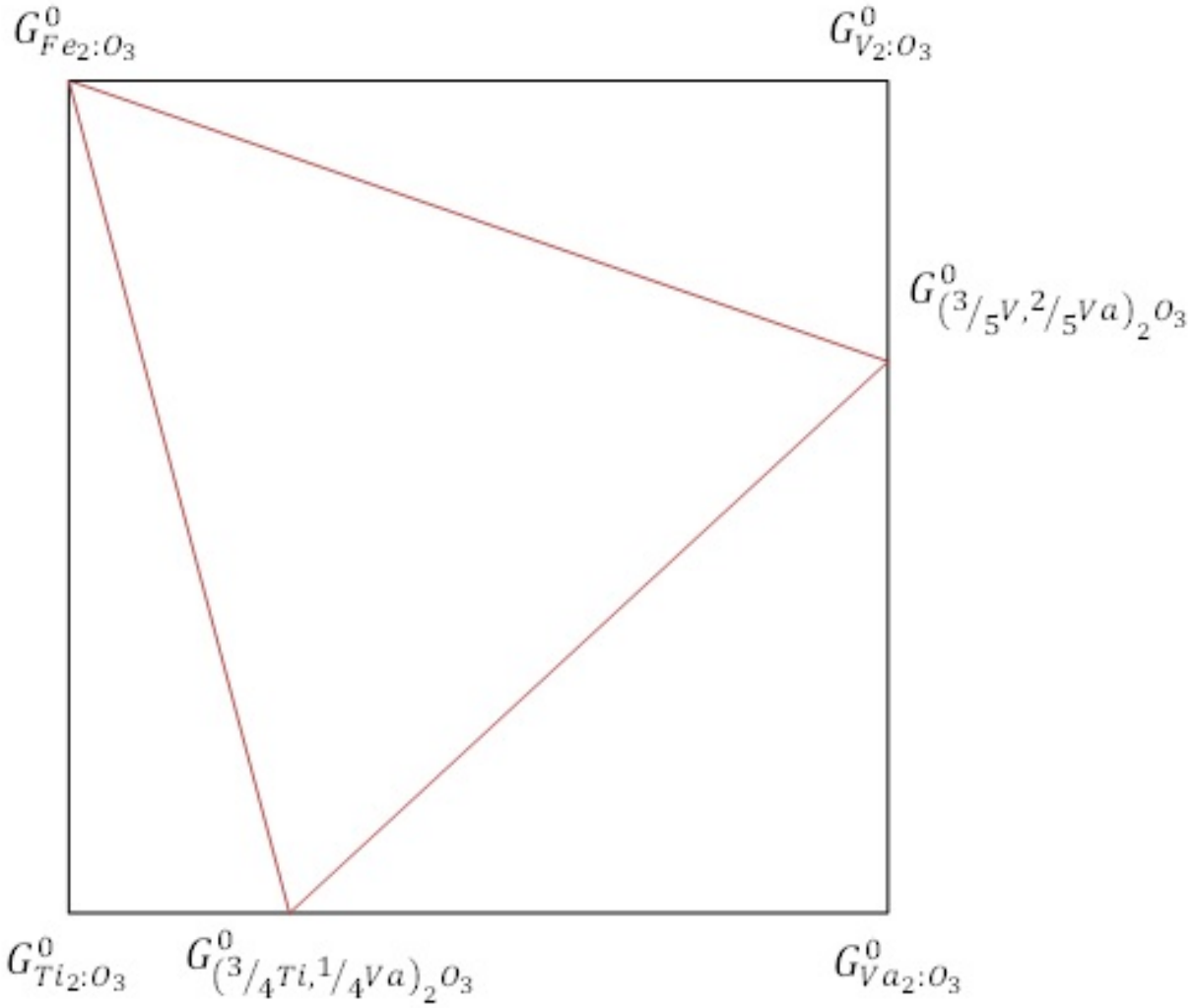

Figure 9.2: The neutral triangle (in red) in the expanded hematite solid solution. Each corner represents an end-member of the solution.

will increase significantly, provided Fe^{3+}, Ti^{4+} and V^{5+} ions are included in both sub-lattices. However, there is no experimental evidence to support this ion distribution configuration. Moreover, the new end-members need to be mathematically derived, from which end-members consisting of Fe^{3+}, Ti^{4+} and V^{5+} ions require optimization from experimental data. The only solubility data of ferropseudobrookite solid solution under oxidizing conditions are available from this study, ranging from 1000 °C to 1400 °C.

It was not possible to model ferropseudobrookite solid solution under oxidizing conditions with the CEF owing to the shortage of occupancy data. In other words, the distribution of Fe^{3+}, Ti^{4+} and V^{5+} ions between the sub-lattices are not known. Nevertheless, the Gibbs energy of ferropseudobrookite solid solution is represented by a simple polynomial model. The components of the solution are Fe_2TiO_5(s) and V_2O_5(s).

$$G_m = y_{V_2O_5}G^{\circ}_{V_2O_5} + y_{Fe_2TiO_5}G^{\circ}_{Fe_2TiO_5} + RT(y_{V_2O_5}Lny_{V_2O_5} + y_{Fe_2TiO_5}Lny_{Fe_2TiO_5}) + G^e_m \quad (9.31)$$

and the excess molar Gibbs energy of Equation 9.31 is given by Equation 9.32:

$$G^e_m = \sum_i \sum_j y_i y_j L^{qp}_{ij}, \quad (9.32)$$

L_{ij}^{qp} are interaction parameters that may be temperature-dependent. The powers of q and p are ≥ 0 and < 2. The interaction parameters are optimised from experimental data to reproduce ferropseudobrookite solid solution accurately.

Although this model is a simplification and does not accurately represent the bonding between constituents of the ferropseudobrookite solid solution and their configuration, it still has the ability to reproduce the measured composition of ferropseudobrookite solid solution. Furthermore, with the inclusion of the ferropseudobrookite solid solution, slag, rutile and hematite solid solutions compositions were more accurately reproduced. If the ferropseudobrookite solid solution had been modelled only as Fe_2TiO_5(s), the composition of Fe, Ti and V in the slag phase would have been more inaccurate.

9.3 Sequence of Optimisation

The principle of data fitting, assessment methodology and parameter optimisation is based on a least-squares method. That is, an objective function is expressed as the difference between the calculated value of a given property and a experimental value of the same property (see Subsection 6.8.1). This difference is known as the residual. It is possible to acquire a set of optimised model parameters by minimising the sum of the square of residuals over all measured points. The optimisation was performed using the OPTISAGE tool in FactSage 7.0 which has the ability to consider all types of data simultaneously. The assessment methodology guidelines explained in Section 6.8 were closely followed.

9.3.1 Fe-V-O System in Air

In the first step of optimisation, the quasichemical temperature dependent parameters in Equation 9.18 were optimised to obtain a reasonable fit of the liquidus curve. The initial values of these parameters were set to zero, assuming ideal behaviour of the binary pairs, $FeO-V_2O_3$ and $Fe_2O_3-V_2O_3$. At this step of optimisation, the solid solution, hematite, was modelled as pure Fe_2O_3(s). Thereafter, thermodynamic properties of the two vanadates, $Fe_2V_4O_{13}$(s) and $FeVO_4$(s) were slightly adjusted to reproduce peritectic transition temperatures.

Prior to the final step of optimisation, the enthalpy of formation and standard entropy of $G^{\circ}_{V_2O_5(s)-Hem}$ from solid solution, hematite, were optimised. In the final step of optimisation all thermodynamic parameters were simultaneously optimised by considering all liquidus and solidus data. An identical approach was followed when using the associate species model to describe the liquid phase.

9.3.2 Ti-V-O System in Air

In the first step of optimisation, the quasichemical temperature dependent parameters in Equation 9.20 were optimised to obtain a reasonable fit of the liquidus curve. The initial values of these parameters were set to zero, assuming ideal behaviour of the binary pairs, $Ti^{4+} - V_2O_3^{4+}$ and $Ti^{3+} - V_2O_3^{4+}$. Moreover, at this step of optimisation, the solid solution, rutile, was modelled as pure TiO_2(s). Thereafter, the enthalpy of formation and standard entropy of $G^{\circ}_{V_2O_5(s)-Rut}$ from the rutile solid solution were optimised. $\Delta g_{Ti^{4+}-V_2O_3^{4+}}$ and $G^{\circ}_{V_2O_5(s)-Rut}$ were optimised simultaneously in the final step of optimisation by considering experimental measurements from this study and the eutectic measurements from Habel et al. (2006). The eutectic temperature of Solacolu and Zaharescu (1972) was not considered, because in their work only a melt projection is presented, which in turn indicated a eutectic reaction in the V_2O_5-rich regime.

9.3.3 Fe-Ti-V-O System in Air

In the first step of the optimisation, $G_{V_2O_5(s)-Rut}$ from the Ti-V-O system in air was re-optimised by considering the experimental data from Chapter 11. This is because of two additional end-members, ($G^{\circ}_{V^{5+}:Va_2}$ and $G^{\circ}_{Va:Va_2}$) that were derived in Subsubsection 9.2.2. Thereafter, the quasichemical model parameters related only to the Fe-Ti-O system, and enthalpy of formations and standard entropies of $G^{\circ}_{TiO_2(s)-hem}$ and $G^{\circ}_{Fe_2O_3-Rut}$ from solid solutions, hematite and rutile, were optimised.

At the same time, parameters of the ferropseudobrookite solid solution were optimised. It is further known that $FeTi_2O_5$(s) is not included in the FToxid database, but inside the FactPS database of FactSage signifying that its thermodynamic properties were never properly assessed. Therefore, it would not have been prudent to simply copy the properties and put the reference to FactSage. Properties such as enthalpy of formation and standard entropy were optimised to reproduce present experimental data within acceptable error limits.

In these steps, parameters from different solutions were optimised independently. All thermodynamic parameters were simultaneously optimised in the final step of optimisation by considering all experimental information from this study.

Part IV

Results and Discussion

Overview

Purpose

The main purpose of Part IV is to present all experimental and thermodynamic modelling results of the Fe-Ti-V-O system in air. A final self-consistent set of thermodynamic models consisting of Gibbs energy descriptions for all phases of the Fe-Ti-V-O system in air is given as a function of temperature, composition and to some limited extent, oxygen partial pressure.

Organization

The results and discussion is divided into three chapters:

- Chapter 10 presents experimental and thermodynamic modelling results of the Fe-V-O system in air.
- Chapter 11 presents experimental and thermodynamic modelling results of the Ti-V-O system in air.
- Chapter 12 presents experimental and thermodynamic modelling results of the Fe-Ti-V-O system in air.

Chapter 10

Fe-V-O System in Air

The results of the study on Fe-V-O system in air are summarised in this sub-section. Some data are also presented in appendix A of this dissertation.

10.1 Synthesis of $Fe_2V_4O_{13}$

Some discrepancies in the literature have been found regarding the existence and stability of the vanadate, $Fe_2V_4O_{13}$(s). It was therefore undertaken to synthesize the compound thermally at 600 °C to resolve some contradictions from previous studies. The synthesis was carried out in a muffle furnace and the temperature in the furnace did not deviate more than 5 °C. Another advantage of having the synthesized vanadate compound was that it made it easier to determine the incongruent melting point in the Fe-V-O system in air owing to the narrow temperature stability range of the compound when in equilibrium with the slag.

The method proposed and used by Walczak et al. (1985) was followed, i.e. three cycles of 72 hours with repeated re-grinding, followed by SEM-EDS analysis. Different starting compositions were selected in an attempt to gain better understanding of the reaction mechanism and kinetics of the vanadate, $Fe_2V_4O_{13}$(s). The synthesis time and starting compositions of V_2O_5(s) to Fe_2O_3(s) are listed in Table 10.1.

Table 10.1: Experiments for the synthesis of $Fe_2V_4O_{13}$.

Experiment	Temperature °C	V_2O_5 mole%	Fe_2O_3 mole %	Equilibration time (hr)
1	600	0.750	0.250	24
2	600	0.550	0.450	24
3	600	0.750	0.250	48
4	600	0.550	0.450	48
5	600	0.750	0.250	96
6	600	0.550	0.450	96
7	600	0.750	0.250	216
8	600	0.550	0.450	216
9	600	0.750	0.250	504
10	600	0.550	0.450	504

Figure 10.1 presents polished sections of the synthesized samples at 24, 48, 96 and 216 hours. Two or three crystalline phases are always present and are identified with SEM-EDS as either V_2O_5(s) and $Fe_2V_4O_{13}$(s) or $FeVO_4$(s) and $Fe_2V_4O_{13}$(s), respectively. It is observed that three phases are present after, 24, 48 and 96 hours, but according to Equation 8.4, only two phases are allowed for

a fully defined system. This implies that the system has not yet reached equilibrium and one phase has to be metastable.

The $FeVO_4$(s) phase appears to be less at 96 hours, when compared to a similar micro-image at 24 hours. After 216 hours of equilibration time, only small traces of the $FeVO_4$(s) phase were observed, suggesting that equilibrium had not been reached owing to mass transfer and other rate phenomena effects. This finding is further supported by a sample synthesized for 21 days, which revealed no traces of $FeVO_4$(s). It is therefore likely that slow kinetics was the reason why some authors did not detect, $Fe_2V_4O_{13}$(s) after very short equilibration times. This is especially relevant when dynamic experimental techniques that rely on fast phase transformations, are used to estimate liquidus and solidus temperatures.

In the present investigation, $FeVO_4$(s) formed in the early stages of equilibration. This means that the first part of the mechanism ($\mathrm{V_2O_5 + Fe_2O_3 \rightarrow 2FeVO_4}$) was fairly fast. However, the bulk composition and temperature placed the system in the V_2O_5–$Fe_2V_4O_{13}$ two-phase region. $Fe_2V_4O_{13}$ was then formed in the second step of the mechanism ($\mathrm{2FeVO_4 + V_2O_5 \rightarrow Fe_2V_4O_{13}}$) and this step was significantly slower than the first step of the mechanism. An identical mechanism was followed for a sample with an initial bulk composition of 55 mole % V_2O_5. However, in this case the bulk composition and temperature placed the system in the $FeVO_4$–$Fe_2V_4O_{13}$ two-phase region. Therefore, after 21 days, the products were $FeVO_4$(s) and $Fe_2V_4O_{13}$(s), and very little V_2O_5(s) was still present.

Another important conclusion can be drawn. The solubility of Fe_2O_3(s) in V_2O_5(s) was lower then 1 mole %. This discovery contradicts the analytical observations of Walczak et al. (1985), who suggested a solubility of 3 mole % at the eutectic temperature and between 2 and 3 mole % at 600 °C. However, all synthesized samples were air-quenched and this could subsequently allow for Fe diffusion from the V_2O_5(s) lattice to form $Fe_2V_4O_{13}$(s). Nevertheless, this result is enough to substantiate the decision to neglect the small solubility range of Fe_2O_3(s) in the V_2O_5(s) crystal lattice during the assessment. This decision is further supported by Fotiev, Cheshnitskii, and Surat (1983) who ruled out a solubility of 3 mole % owing to the presence of an eutectic composition of 2.5 mole % between V_2O_5(s) and $Fe_2V_4O_{13}$(s).

10.2 Phase Characterisation and Quantification

All samples analysed had two phases, a solid and liquid oxide. No immiscibility field in the liquid phase was observed in any analysed samples. Micrographs of phase assemblages are shown in Figure 10.2. Some scratches are seen on the images because of a dry polishing method employed to avoid water reacting with a sample containing V_2O_5. The raw EPMA data are found in Table 10.2. The standard deviation of each element is also calculated and given. It is noted that the raw data from SEM-EDS (see Table 10.2) compared well to the raw data of EPMA and complete homogeneity of the molten phase was achieved in the equilibration and quenching. The raw data from EPMA were converted from V to V_2O_5 and Fe to Fe_2O_3, and then normalised. This was also the case for the Ti-V-O system in air and for the higher-order Fe-Ti-V-O system in air. Furthermore, each experiment on the Fe-V-O, Ti-V-O and Fe-Ti-V-O systems was repeated at least once. Section A.3 addresses repeatability of experiments.

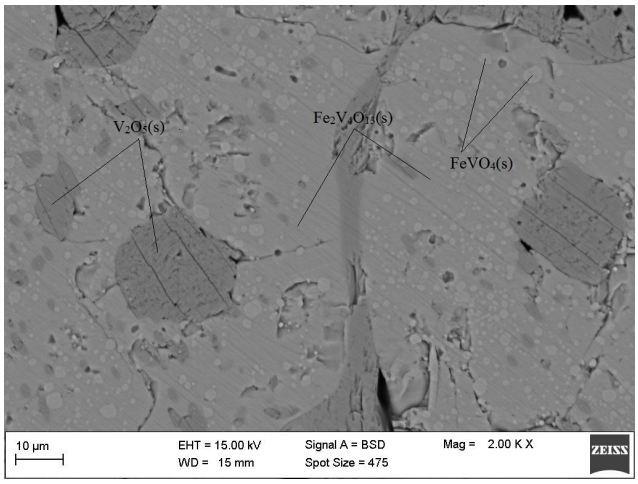

(a) 24 hours

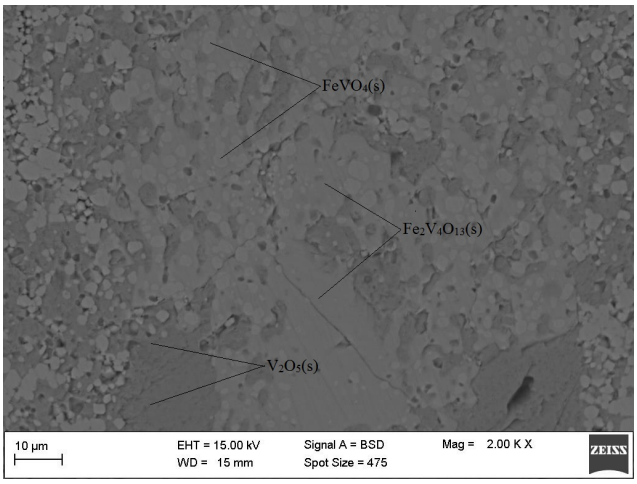

(b) 48 hours

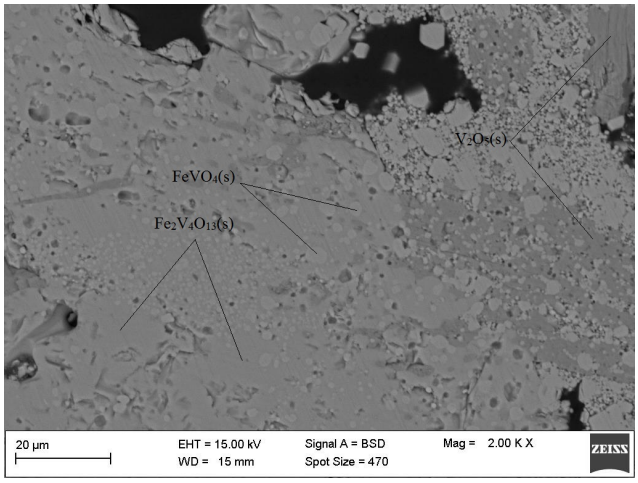

(c) 96 hours

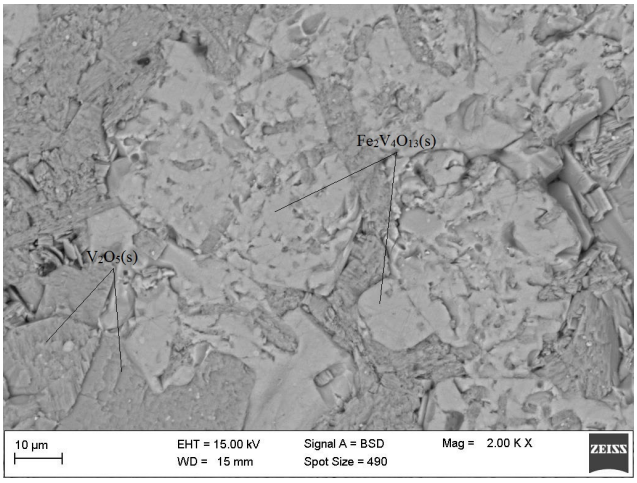

(d) 216 hours

Figure 10.1: BSE micrographs of $Fe_2V_4O_{13}$ synthesis samples prepared at 600 °C and an initial concentration of 75 mole % V_2O_5(s). Light crystals in (a), (b) and (c) are $FeVO_4$(s) and darker crystal phases wrapped around $FeVO_4$(s) are $Fe_2V_4O_{13}$(s). The darkest phase is V_2O_5(s).

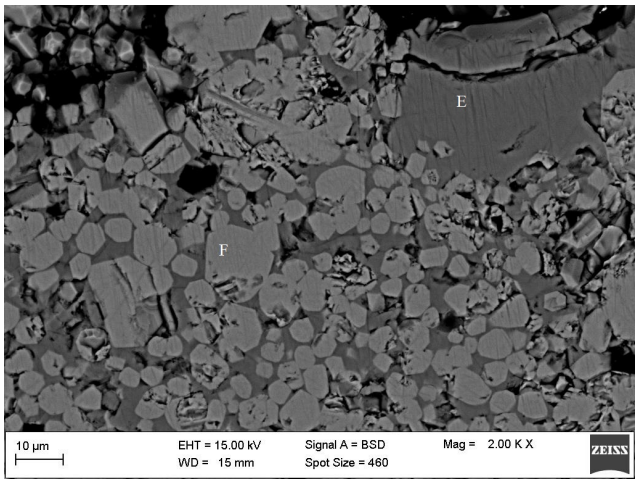

(a) 800 °C

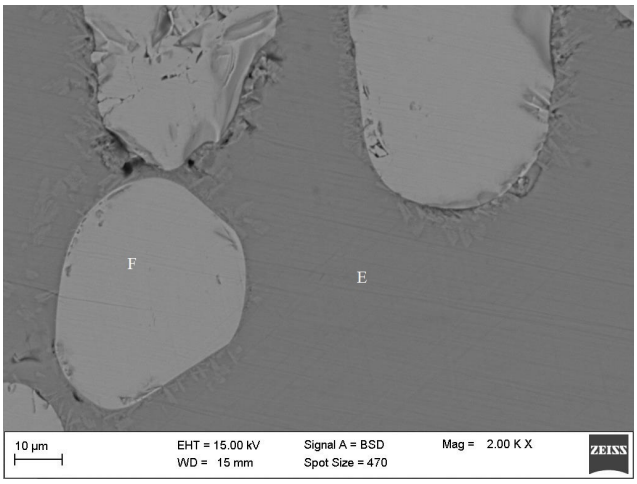

(b) 1000 °C

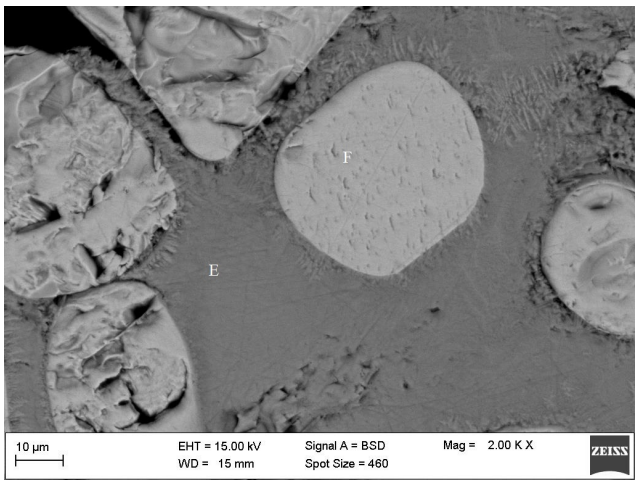

(c) 1200 °C

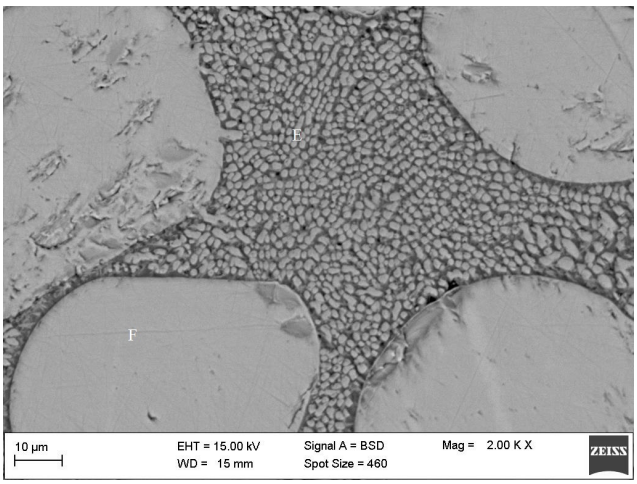

(d) 1400 °C

Figure 10.2: BSE micrographs of quenched samples: light crystals in (a) are $FeVO_4$(s) (F) and non-crystalline dark glassy phase is molten slag (E). For, (b),(c) and (d) light crystals are hematite solid solution and lighter crystalline phases embedded in the molten slag are precipitate from quenching.

Table 10.2: Summary of raw data from the Fe-V-O system in air analysed using EPMA.

	Molten Phase						FeVO4(s)						Hematite-SS					
Temperature °C	Fe	Fe (σ)	V	V (σ)	O (Stoi.)	Total	Fe	Fe (σ)	V	V (σ)	O (Stoi.)	Total	Fe	Fe (σ)	V	V (σ)	O (Stoi.)	Total
700	3.64	0.09	54.13	0.22	44.07	101.84	31.22	0.40	31.78	0.46	34.54	98.41						
750	5.88	0.28	52.73	1.19	43.94	102.55	31.86	0.31	32.38	0.42	35.56	100.54						
800 (SS)							31.84	0.30	31.99	0.67	34.55	99.35	68.72	0.49	1.05	0.67	30.36	101.29
800	8.44	0.49	50.51	0.31	43.29	102.24	31.52	0.14	31.99	0.11	35.15	98.90						
850	11.09	0.12	48.00	0.08	42.46	101.56	31.71	0.26	31.93	0.07	35.18	99.14						
860	12.49	0.16	47.06	0.22	42.32	101.87							68.36	0.19	2.06	0.13	31.00	101.42
900	13.67	0.61	46.61	0.39	42.48	102.76							68.91	0.21	1.50	0.22	30.79	101.20
950	15.66	0.17	44.65	0.12	41.79	102.10							67.29	0.64	1.54	0.07	30.13	98.96
1000	16.81	0.78	43.50	0.59	41.38	101.68							67.04	0.17	1.68	0.03	30.13	98.84
1050	17.87	1.50	42.33	1.05	40.92	101.11							66.90	0.28	2.07	0.21	30.37	99.34
1100	20.32	1.59	40.94	1.03	40.88	102.13							66.14	0.20	2.38	0.10	30.29	98.80
1150	21.53	1.68	40.05	1.02	40.70	102.28							66.42	0.09	2.64	0.17	30.62	99.68
1200	22.98	1.60	38.93	1.31	40.45	102.36							65.46	0.30	2.96	0.05	30.46	98.88
1250	26.42	2.02	36.12	1.90	39.72	102.26							66.17	0.28	3.77	0.14	31.40	101.34
1300	28.10	2.14	34.39	1.57	39.08	101.57							65.90	0.25	3.97	0.13	31.44	101.31
1350	31.20	2.09	33.19	1.14	38.82	103.21							63.32	0.36	4.35	0.19	30.63	98.30
1400	36.13	5.85	27.47	4.92	37.10	100.70							64.86	0.56	3.47	0.35	30.60	98.93
1450	N/A	N/A	N/A	N/A	N/A	N/A							67.16	0.42	2.50	0.07	30.82	100.48

Table 10.3: Summary of raw data from the Fe-V-O system in air analysed using SEM-EDS.

	Molten Phase						FeVO4(s)						Hematite-SS					
Temperature °C	Fe	Fe (σ)	V	V (σ)	O (Stoic.)	Total	Fe	Fe (σ)	V	V (σ)	O (Stoi.)	Total	Fe	Fe (σ)	V	V (σ)	O (Stoi.)	Total
700	2.28	0.33	55.86	0.82	44.76	102.90	29.76	0.37	32.14	0.50	38.03	100.79						
750	4.02	1.36	54.86	1.34	44.81	103.69	29.79	0.32	32.06	0.41	37.98	100.57						
800 (SS)							30.31	0.36	32.59	0.62	37.79	101.68	65.98	0.64	1.31	0.62	29.38	97.93
800	5.85	0.64	52.70	0.59	43.89	102.44	30.30	0.65	32.59	0.40	38.61	102.54						
850	8.06	0.83	51.06	0.62	43.56	102.68	30.43	0.44	32.40	0.43	38.52	102.21						
860	12.14	0.34	48.71	0.61	43.47	104.32							67.54	1.25	1.97	0.29	30.57	100.09
900	13.07	0.40	47.14	0.55	42.63	102.84							65.64	1.21	1.68	0.26	29.53	96.85
950	15.04	0.36	46.31	0.25	42.82	104.17							67.12	0.84	1.90	0.29	30.34	99.36
1000	15.69	0.67	44.74	0.51	41.87	102.30							65.44	0.58	2.24	0.33	29.88	97.56
1050	17.11	1.28	42.17	0.89	40.47	99.76							63.58	1.28	2.26	0.29	29.09	94.92
1100	20.04	0.35	42.28	0.36	41.81	104.14							65.38	0.61	2.70	0.40	30.22	98.31
1150	20.97	1.17	42.42	0.92	42.32	105.71							65.35	1.34	3.06	0.34	30.49	98.90
1200	22.28	0.81	39.70	0.64	40.75	102.72							64.56	1.14	3.54	0.17	30.52	98.63
1250	26.65	1.29	36.66	1.42	40.24	103.55							64.41	0.74	3.96	0.23	30.79	99.16
1300	27.77	1.11	35.14	0.62	39.52	102.43							63.75	0.73	4.15	0.20	30.66	98.56
1350	31.20	2.09	33.19	1.14	38.82	103.21							60.82	1.94	4.35	0.19	29.55	94.73
1400	35.90	1.95	29.04	1.95	39.34	104.29							63.27	1.21	4.34	0.25	30.60	98.21

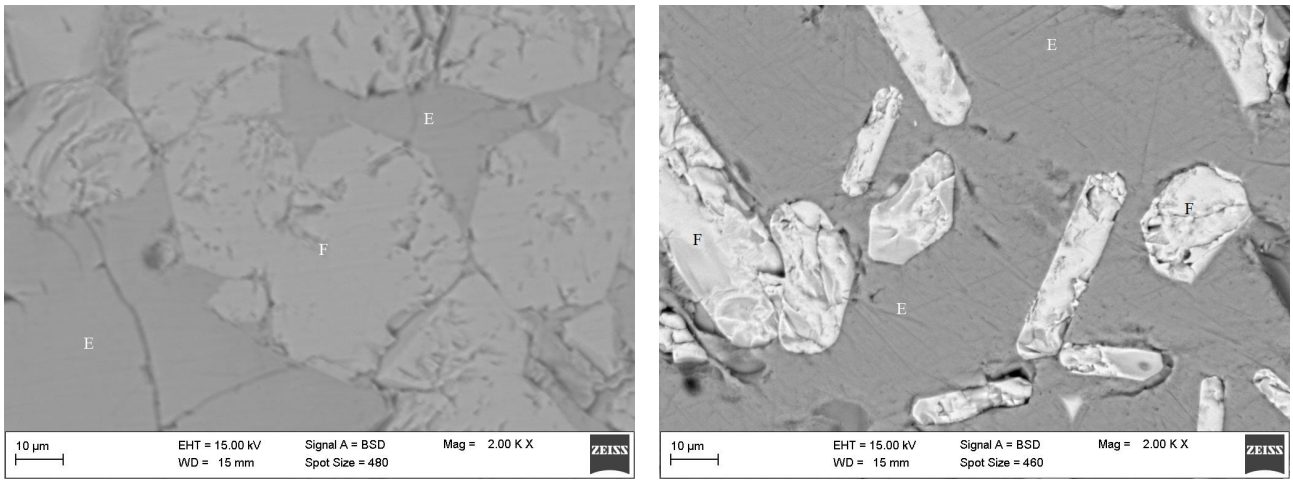

(a) 850 °C (b) 860 °C

Figure 10.3: BSE micrographs of samples quenched at 850 and 860 °C, light crystals in (a) and (b) are $FeVO_4$(F) and Fe_2O_3(F) surrounded by a light non-crystalline slag phase (E).

For the sample quenched at 800 °C, equilibrium was achieved after 16 hours. A slag phase and $FeVO_4$(s) were observed. Experimental results confirmed that $FeVO_4$(s) undergoes a peritectic transition between 850 and 860 °C to form hematite solid solution and molten slag (see Figure 10.3). For the sample quenched at 1000 °C, the hematite solid solution and liquid slag phase were detected. All samples below 800 °C had an equilibration time of 48 hours and sample homogeneity was used to confirm equilibrium. The starting composition for the sample quenched at 700 °C was a mixture of the synthesised compound from Section 10.1 plus a small percentage of V_2O_5(s). However, no traces of the orthovanadate, $Fe_2V_4O_{13}$(s) were detected after equilibration, indicating that the peritectic transition of $Fe_2V_4O_{13}$(s) to form the molten slag phase and $FeVO_4$(s), was below 700 °C.

For the sample quenched at 1200 °C, equilibrium was achieved after 4 hours. An appreciable amount of precipitation was observed in the molten slag phase and was enhanced by an increase in Fe content. This unusual phenomenon indicates that quenching was not fast enough. These light grey precipitate particulates have a significantly higher Fe concentration than the darker glassy phase. The amount of precipitation significantly increases for a sample quenched at 1400 °C. In other words, an increase in Fe solubility in the slag enhanced precipitation. Moreover, reducing the sample size to less than 0.2 g and quenching a sample in brine did not reduce precipitation. The larger grains are Fe_2O_3(s) and have a V concentration of less than 5 wt.% for all samples quenched.

Although some uncertainties exist at temperatures at and above 1400 °C, no liquidus data above 1400 °C could be found in the literature and consequently experimental data had to be accepted and used for the assessment. To date and to the best knowledge of the researcher, no better experimental technique has been developed to investigate element distribution among phase assemblage of oxide systems quantitatively in this temperature range. Other unusual analytical approaches followed for this system include:

- Because of precipitation in the slag phase (light grey particulates embedded in dark glassy phase), the spot size of the electron probe was increased from 5 to 10 μm for samples above 1200 °C. The idea was to analyse a larger area (field analysis) in the slag phase to estimate some average composition between the glassy phase and precipitate. Up to 15 spots in the slag phase were analysed. This technique, although not standard practice, was successful, as the calculated standard deviations for Fe and V were only slightly higher than 1 %, except for the sample quenched at 1450 °C (see Table 10.2). The latter had standard deviations larger than 5 % for both Fe and V, respectively.

- More liquid phase had to be produced to have enough liquid areas larger than 10 μm in diameter

in the sample, to allow for a probe spotsize of 10 μm. However, the slag behaved aggressively at temperatures above 1400 °C and it became increasingly difficult to contain the sample. Furthermore, excessive precipitation from the slag phase made it impossible to estimate Fe and V composition within acceptable error limits. Consequently, liquidus composition could not be estimated at and above 1450 °C.

Although not compelling, the ratio of Fe to O at 1450 °C constitutes that of hematite and not spinel, suggesting that hematite is stabilised by the dissolved V, when compared to pure hematite transition temperature to spinel (see Equation 9.2). However, it is possible that an equilibration time of 4 hours may not have been long enough to allow this transition to occur. Further investigation into these phenomena might be required to confirm the findings from this study.

10.3 Thermodynamic Calculations

Based on all normalised experimental literature data from Chapter 5 and normalised experimental data from this study (see Section 10.2), the thermodynamic properties and optimised model parameters for all phases in the Fe-V-O system in air are presented in Table 10.4 and Table 10.5. Using these parameters, phase equilibria, invariant reactions and thermodynamic properties were calculated and compared with available literature data.

Table 10.4: Optimised parameters of solutions in the Fe-V-O system in air.

Liquid: FeO-Fe_2O_3-V_2O_5
Quasichemical Model (Figure 10.4a) FeO-Fe_2O_3 binary parameters Taken from the study of Degterov et al. (2001) V_2O_5-Fe_2O_3 binary parameters $Z_{Fe^{2+}} = 1.37, Z_{Fe^{3+}} = 2.0661, Z_{V_2O_3^{4+}} = 2.7548$ $g^{10}_{Fe^{3+}-V_2O_3^{4+}} = -58127.5 + 33.8728T^1$ $g^{01}_{Fe^{3+}-V_2O_3^{4+}} = -13515.57$
Associate Species Model (Figure 10.4b) FeO-Fe_2O_3 binary parameters Taken from the study of Kowalski and Spencer (1995) V_2O_5-Fe_2O_3 binary parameters $^0L_{V_2O_5-Fe_2O_3} = -31308.9$ $^1L_{V_2O_5-Fe_2O_3} = 20.2411T$
Hematite Solid Solution For MQM - $G^\circ_{V_2O_5(s)-Hem} = G^\circ_{V_2O_5(s)} - 219004 + 94.629T - 18.651T$ from 298 - 1723 K For ASM - $G^\circ_{V_2O_5(s)-Hem} = G^\circ_{V_2O_5(s)} - 219250 + 93.832T - 18.651T$ from 298 - 1723 K

Table 10.5: Calculated enthalpies and entropies of pure compounds in the Fe-V-O system compared with the experimental data.

Compound	$\Delta H^{\circ}_{f,298}$ J.mol^{-1}	S°_{298} Jmol^{-1}K^{-1}	a	b	c	d	e	C_p range K	Reference
Solids									
Fe_2O_3(s)*	-825787.0	87.7285	137.01				-29.07640	298-2500	(Bale et al. 2016)
V_2O_5(s)	-1550590	130.559	25.970	50.00	5853.80	-76.76761	-7.541627	298- 943	(Bale et al. 2016)
$FeVO_4$(s)	-1186800	128.400	129.51	24.71			-21.60000	298 - 973	(Volkov 1979)
"	-1184723	128.436	"	"			"	298 - 1173	Using MQM
"	-1185083	127.981	"	"			"	298 - 1173	Using ASM
$Fe_2V_4O_{13}$(s)	-3934650	385.700	388.83	73.83			-65.06000	298 - 973	(Volkov 1979)
"	-3937787	382.628	"	"			"	298 - 973	Using MQM
"	-3940147	379.761	"	"			"	298 - 973	Using ASM
Liquid									
V_2O_5(l)	-1491202	191.958	164.31	24.00			-36.28207	298 - 600	(Bale et al. 2016)
			190.79					600 - 3000	(Bale et al. 2016)
FeO(l)	-234643.2	78.4655	-18.024	31.00	1500.90		-25.33300	298 - 1644	(Bale et al. 2016)
			68.199					1644 - 2000	(Bale et al. 2016)
Fe_2O_3(l)	-728657.5	146.050	137.01				-29.07640	298 - 2500	(Kowalski and Spencer 1995)
"	-745158.3	139.467	"				"	298 - 2500	Using MQM
"	-711417.9	159.910	"				"	298 - 2500	Using ASM

$$Cp(J.mol^{-1}K^{-1}) = a + b(10^{-3})T + cT^{-0.5} + d(10^{3})T^{-1} + e(10^{5})T^{-2}$$

*Hematite exhibits magnetic ordering and these values include the magnetic contribution.

10.3.1 Phase Diagrams

Phase diagrams, calculated from optimized parameters, are shown in Figure 10.4. All the experimental data superimposed onto the diagram were considered during optimization. It is observed that the experimental liquidus and solidus data are well reproduced by the calculation. However, the liquidus compositions deviate marginally from the results of this study, since experimental data from Walczak et al. (1985) and Fotiev, Cheshnitskii, and Surat (1983) were also considered with equal weight contribution.

For the MQM, two parameters were required to reproduce the liquidus. Since, $FeVO_4$ and $Fe_2V_4O_{13}$ do not melt congruently, the influence of the $\Delta g^0_{Fe-V_2O_3^{4+}}$ is small compared to $g^{10}_{Fe^{3+}-V_2O_3^{4+}}$ and $g^{01}_{Fe^{3+}-V_2O_3^{4+}}$. No parameters were required for the quasichemical reaction between $V_2O_3^{4+}$ and Fe^{2+}, because Fe^{2+} concentration is very low at oxidizing conditions.

Two parameters were also required when the liquidus was described with the ASM. However, one fewer coefficient was in fact required to reproduce experimental data within similar error limits compared to when the MQM was used to describe the slag phase.

The calculated invariant reactions (see Table 10.6) are in good agreement with the experimental results from this study and the studies of Fotiev, Cheshnitskii, and Surat (1983) and Walczak et al. (1985). For the hematite solid solution, the enthalpy of formation and standard entropy of compound V_2O_5(s) were optimized and then added to $G^\circ_{V_2O_5(s)-Hem}$ to have good agreement with the solidus compositional experimental results from this study.

Table 10.6: Invariant reactions and phase transitions in the Fe−V−O system in air from calculations.

Model for liquid phase	Composition (V_2O_5 mole %)	Temperature °C	Type of invariant	Equilibrium solid phases
MQM	96	656	Eutectic	V_2O_5, $Fe_2V_4O_{13}$
ASM	97	663	Eutectic	V_2O_5, $Fe_2V_4O_{13}$
MQM	94	680	Peritectic	$FeVO_4$, $Fe_2V_4O_{13}$
ASM	95	685	Peritectic	$FeVO_4$, $Fe_2V_4O_{13}$
MQM	80	867	Peritectic	$FeVO_4$, Fe_2O_3
ASM	80	863	Peritectic	$FeVO_4$, Fe_2O_3

Both liquid models successfully described the liquidus composition, which is an indication that both models can be employed to make accurate predictions of the liquid phase. Moreover, the versatility and flexibility of both models are demonstrated and it cannot be said that one model is superior to the other, given that both models only required two parameters to reproduce the liquidus data from this study.

The assessment successfully covered all compounds and solutions up to 1450 °C. Because of the lack of experimental data at and above 1450 °C, it was assumed that the solid state transition of hematite to spinel or magnetite did not take place. Spinel was therefore not included in the final calculation and the melting point of pure hematite shown in both phase diagrams is not entirely correct. The calculated liquidus and solidus compositions above 1400 °C and 1450 °C are from extrapolation of the model equations and in reality, a transition is likely to occur at some temperature above 1450 °C. Moreover, some vanadium is also likely to report to spinel, which in turn can influence the transition temperature of this hematite solid solution to spinel.

10.3.2 Other Thermodynamic Data

The calculated enthalpies of formation and standard entropies of the compounds obtained in this assessment at 298 K (ΔH°_{298}), along with data obtained from the literature are given in Table 10.5.

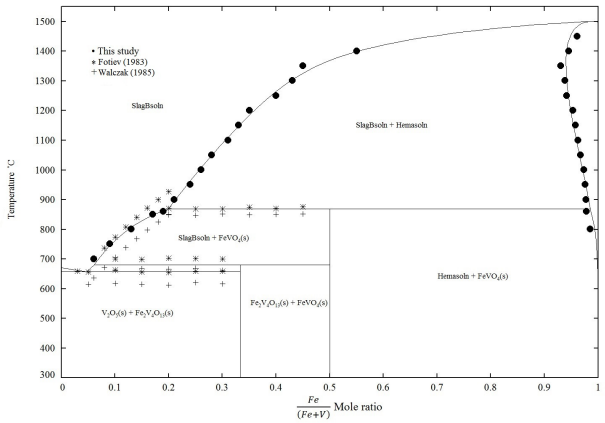

(a) Slag phase calculated with the MQM.

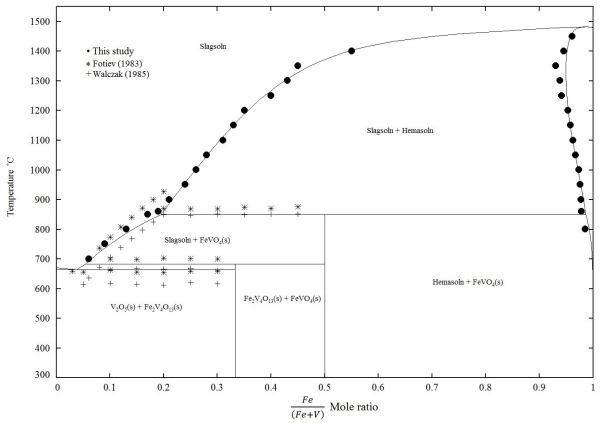

(b) Slag phase calculated with the ASM.

Figure 10.4: Equilibrium phase diagrams of the Fe-V-O system in air compared with the present experimental works and literature data.

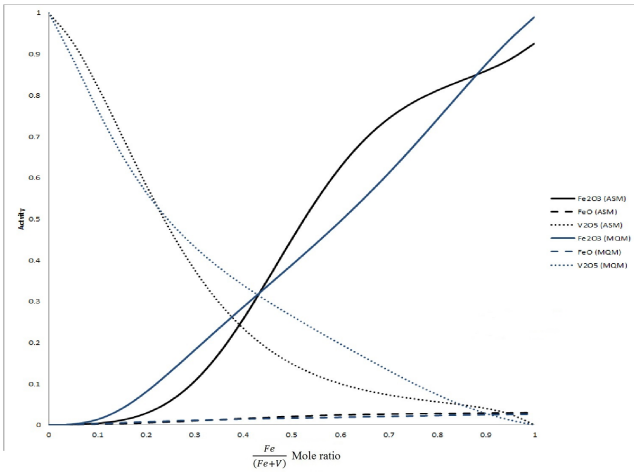

(a) Activities of slag constituents at 1200 °C.

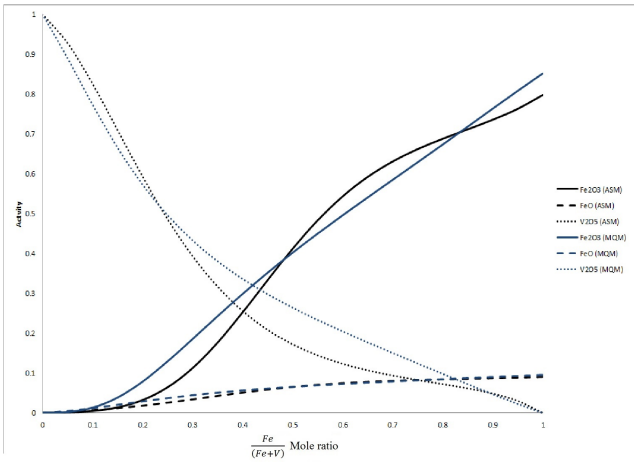

(b) Activities of slag constituents at 1400 °C.

Figure 10.5: Activities of slag constituents calculated with the ASM and MQM and depressed crystalline phases.

Some minor differences exist between calculated and experimental data, and calculated data dependent on the solution model used for describing the slag phase. The heat capacities of compounds, particularly orhto-vanadates, $FeVO_4(s)$ and $Fe_2V_4O_{13}(s)$, were not adjusted in this assessment, granted their negligible effect on an improved fit between calculated and experimental data. Furthermore, it was noted that the solution did not converge when too many parameters were simultaneously optimized with the Bayesian optimization method.

No other thermodynamic experimental data, such as enthalpies of mixing, thermal expansion data, heat contents and activity data of the slag phase, were obtained to support the calculated phase diagrams. However, to demonstrate that other thermodynamic properties can be calculated from phase diagram data, activity data from the calculated model parameters are shown in Figure 10.5a and Figure 10.5b.

The activities of Fe_2O_3, FeO and V_2O_5 were calculated at 1200 and 1400 °C with the MQM and ASM. There were no experimental data in the literature for comparison. The definition of an ideal solution is now defined in order to observe if the slag exhibits positive or negative deviation from ideal behaviour. Since the cationic species in the MQM are Fe^{3+} and $V_2O_3^{4+}$, an ideal solution is defined

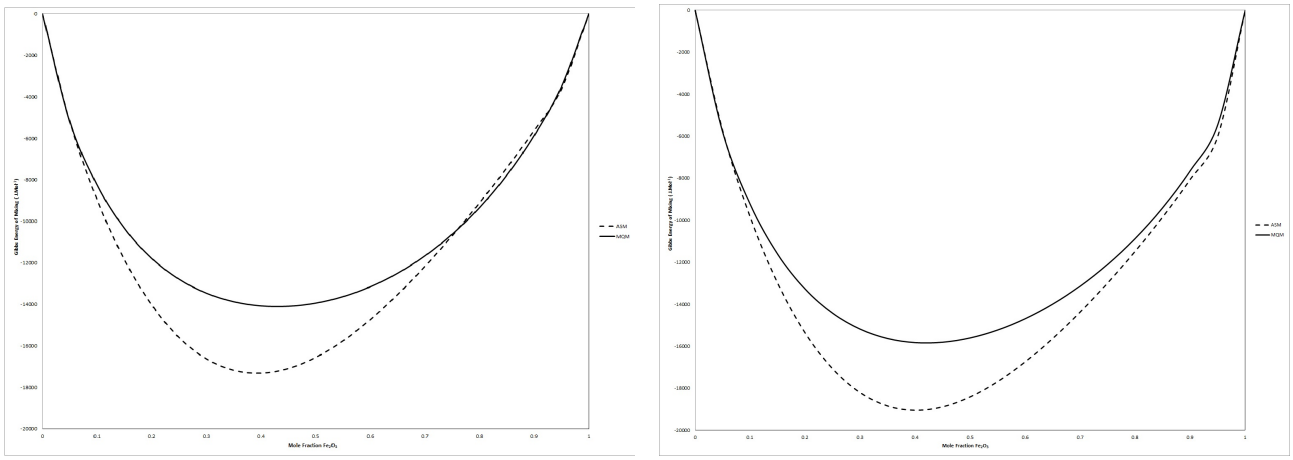

(a) Gibbs free energy of mixing at 1200 °C. (b) Gibbs free energy of mixing at 1400 °C.

Figure 10.6: The calculated Gibbs free energy of mixing of the Fe-V-O liquid using the ASM and MQM. Crystalline phases were depressed.

as a random mixture of these species. That is, approximately: $\mathrm{a_{Fe_2O_3}} = \mathrm{X_{Fe}^2}$ and $\mathrm{a_{V_2O_5}} = \mathrm{X_{V_2O_3}}$ where $\mathrm{X_{Fe}} = (1 - \mathrm{X_{V_2O_3}}) = \mathrm{X_{Fe}}/(\mathrm{X_{Fe}} + 0.5\mathrm{X_V})$. With this definition of ideality, the activity curves in Figure 10.5a and Figure 10.5b are close to ideal.

In the lower mole fraction areas, both models predict some negative deviation from ideal behaviour for slag constituents Fe_2O_3 and V_2O_5 at 1200 and 1400 °C. A negative deviation is characterised by vapour pressures lower than those calculated for a ideal solution. Moreover, the attraction between unlike molecules $(\mathrm{Fe^{3+} - V_2O_3^{4+}})$ is stronger than the mutual attraction of the like molecules $(\mathrm{V_2O_3^{4+} - V_2O_3^{4+}, Fe^{3+} - Fe^{3+}})$, constituting a lower escaping tendency of the molecules in the solution compared to escaping tendencies in the individual liquids. In addition, both models predict a higher FeO activity at 1400 °C, which is consistent with calculations made with the FTOxide database in FactSage involving Fe-O slags.

However, increasing the Fe mole fraction shifts the slag molecular interaction behaviour from negative to positive. This in turn suggests a tendency to de-mixing at higher Fe contents. It is quite possible a stable liquid miscibility gap exists, but was not observed because measurements were not made at the highest temperatures. Moreover, at sub-liquidus temperatures, the likelihood of a metastable liquid miscibility gap is very high.

The Gibbs free energy of mixing at 1200 and 1400 °C of the Fe-V-O liquid was calculated in the present work with Equation 10.1 using the ASM and MQM, is presented in Figure 10.6a and Figure 10.6b.

$$G_{Mix} = RT(y_{Fe_2O_3} ln a_{Fe_2O_3} + y_{V_2O_5} ln a_{V_2O_5}) \tag{10.1}$$

The minimum free energy of mixing for both models is within the compositional range as (35-45) mole % Fe_2O_3 which indicates an area of maximum short-range ordering. Moreover, the calculated Gibbs free energy of mixing is lower at 1400 °C compared to a system at 1200 °C. The shape of the curves, which exhibits one local minima, rather supports the case where unlike interactions are stronger than like interactions, and there is no composition range in which two coexisting liquid phases can occur. However, this does not mean that a metastable liquid miscibility gap can not exist at higher temperatures. More experimental work is required to support this theory.

Chapter 11

Ti-V-O System in Air

The results of the Ti-V-O system in air are summarised in this chapter. Some data are also presented in the appendix section of this dissertation.

11.1 Phase Characterisation and Quantification

The polished and coated samples were analysed with EPMA and SEM-EDS. To confirm sample homogeneity, at least ten points of each phase were analysed to calculate a set of standard deviations for each element. Results from EPMA and SEM-EDS are shown in Table 11.1 and Table 11.1. EDS results did not compare well to EPMA results, because it was noted that X-ray emission peaks of V and Ti overlapped. Oxygen concentration was calculated on the basis of stoichiometry (St.) by assuming V is in the 5+ and Ti in the 4+ oxidation state. The standard deviation (σ) of each element is shown in the table next to its mean concentration.

All samples analysed had two condensed phases in equilibrium with air, rutile solid solution and slag. Micrographs of samples captured from the SEM back-scattered detector are shown in Figure 11.1. For the samples quenched at 800, 1000 and 1200 °C a homogeneous glassy slag phase surrounded by light grey rutile solid solution crystals is observed. Less than 3 wt. % Ti had dissolved in the slag phase, in contrast to a V solubility of more than 15 wt. % in the rutile solid phase at 1400 °C. These findings indicate that the calculated V_2O_5–TiO_2 phase diagram from Yang et al. (2017) (see Figure 5.3) were not entirely accurate owing to the shortage of experimental data on this system. Moreover, the calculated phase diagram from Yang et al. (2017) grossly over-estimated the Ti solubility in the slag and under-estimated the V solubility in the rutile phase.

Some precipitation had formed in the slag phase for the sample quenched at 1500 °C. As reported in Chapter 10, the sample size and quenching medium did not reduce precipitation in the slag phase. Furthermore, the average composition between the precipitate and glassy phase was calculated, utilizing a larger probe spot size and considering at least 15 areas in the slag phase. With this approach, a standard deviation ranging from 1-2 % was calculated for samples quenched at 1500 °C.

11.2 Thermodynamic Calculations

Based on all experimental data from Chapter 8, the optimized model parameters for all phases in the Ti-V-O system in air are presented in Table 11.3 and Table 11.4. Using these parameters, phase equilibria, invariant and thermodynamic properties are calculated and compared with available literature data.

Table 11.1: Summary of raw data from the Ti-V-O system in air analysed using EPMA.

	Molten Phase						Rutile-SS					
Temperature °C	Ti	Ti (σ)	V	V (σ)	O (St.)	Total	Ti	Ti (σ)	V	V (σ)	O (St.)	Total
700	0.93	0.10	58.02	0.68	46.18	105.13	53.13	1.73	5.96	1.01	40.19	99.27
750	1.67	0.69	56.86	0.82	45.77	104.30	53.27	1.35	6.37	1.28	40.62	100.26
800	1.76	0.67	56.78	0.55	45.76	104.29	54.18	1.70	6.45	0.91	41.28	101.91
850	1.99	0.52	56.79	0.51	45.93	104.71	53.80	1.33	6.91	0.70	41.39	102.11
900	2.10	0.22	56.33	0.33	45.64	104.07	54.05	1.40	7.84	0.40	42.29	104.18
950	2.16	0.22	56.01	0.39	45.44	103.60	53.96	0.86	6.56	0.75	41.22	101.74
1000	2.35	0.19	57.11	0.89	46.42	105.88	51.71	0.62	9.23	0.17	41.81	102.75
1050	3.08	0.22	54.59	0.07	44.92	102.59	51.48	0.14	12.44	0.04	41.83	105.75
1100	3.16	0.28	55.35	0.72	45.58	104.09	45.06	0.57	15.14	0.69	42.01	102.20
1150	3.55	0.19	56.11	0.69	46.43	106.08	45.06	0.14	15.14	0.69	42.01	102.20
1200	3.49	0.42	55.25	0.84	45.72	104.46	46.81	0.33	13.44	0.23	41.85	102.09
1250	3.85	0.28	54.40	0.58	45.29	103.54	46.86	0.90	14.03	0.55	42.34	103.23
1300	3.84	0.32	55.25	0.94	45.95	105.04	45.44	1.06	15.43	0.21	42.49	103.37
1350	4.46	0.28	54.28	0.97	45.60	104.33	45.63	0.50	15.79	0.31	42.91	104.33
1400	4.67	0.32	54.53	1.04	45.94	105.15	45.63	0.57	15.57	0.26	42.73	103.93
1450	5.12	0.12	54.54	0.66	46.25	105.90	46.40	0.04	14.72	0.13	42.58	103.70
1500	5.18	0.19	53.88	0.49	45.76	104.82	46.85	0.64	14.49	0.23	42.70	104.05

Table 11.2: Summary of raw data from the Ti-V-O system in air analysed using SEM-EDS.

	Molten Phase						Rutile-SS					
Temperature °C	Ti	Ti (σ)	V	V (σ)	O (St.)	Total	Ti	Ti (σ)	V	V (σ)	O (St.)	Total
700	0.93	0.10	58.02	0.68	46.18	105.13	53.13	1.73	5.96	1.01	40.19	99.27
750	1.67	0.69	56.86	0.82	45.77	104.30	53.27	1.35	6.37	1.28	40.62	100.26
800	1.61	0.63	57.32	0.59	46.09	105.02	54.18	1.70	6.45	0.91	41.28	101.91
850	1.76	0.64	57.38	0.86	46.27	105.40	53.80	1.33	6.91	0.70	41.39	102.11
900	1.80	0.27	58.61	0.57	47.22	107.63	54.05	1.40	7.84	0.40	42.29	104.18
950	1.63	0.27	57.69	0.58	46.39	105.70	53.96	0.86	6.56	0.75	41.22	101.74
1000	2.00	0.85	57.11	0.51	46.18	105.29	51.71	0.62	9.23	0.17	41.81	102.75
1050	2.00	0.85	57.11	0.51	46.18	105.30	51.71	0.62	12.23	0.17	41.81	105.75
1100	2.05	0.54	55.35	0.72	44.83	102.22	45.06	0.57	15.14	0.69	42.01	102.20
1150	2.00	0.85	57.11	1.15	46.18	105.29	45.06	0.62	15.14	0.69	42.01	102.20
1200	3.19	0.45	55.25	0.84	45.52	103.96	46.81	0.33	13.44	0.23	41.85	102.09
1250	3.23	0.46	55.19	0.87	45.50	103.92	46.81	0.33	13.44	0.23	41.85	102.09
1300	1.38	0.34	56.25	1.30	45.10	102.73	45.44	1.06	15.43	0.21	42.49	103.37
1350	2.73	1.81	55.28	1.14	45.20	103.21	45.63	0.50	15.79	0.31	42.91	104.33
1400	1.45	0.44	56.17	0.76	45.07	102.68	45.63	0.57	15.57	0.26	42.73	103.93
1450	1.45	0.44	56.17	0.76	45.07	102.68	45.63	0.57	15.57	0.26	42.73	103.93
1500	1.27	0.37	55.88	0.49	44.72	101.86	46.85	0.64	14.49	0.23	42.70	104.05

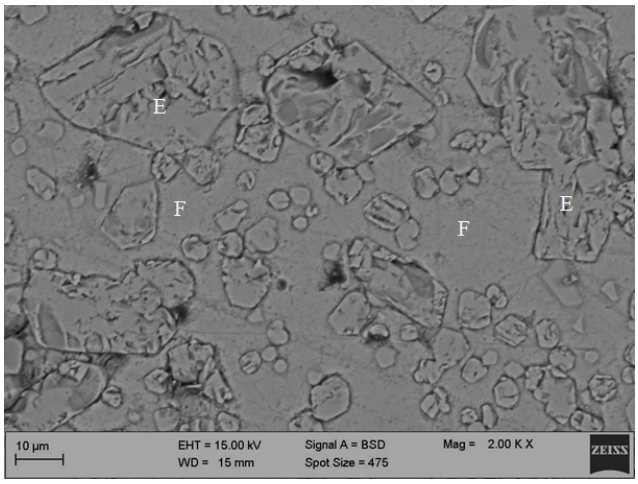

(a) 800 °C

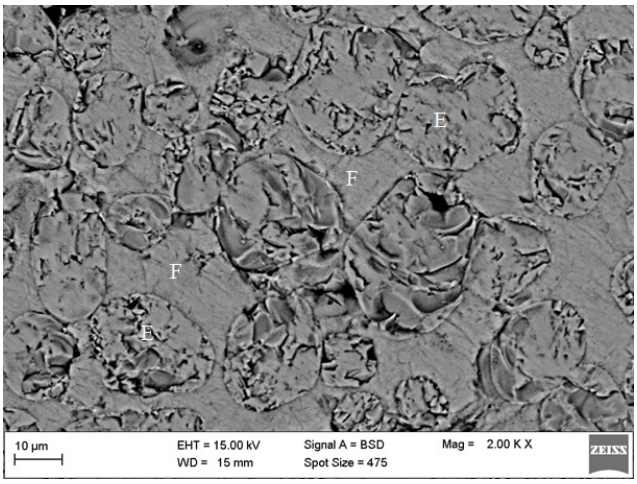

(b) 1000 °C

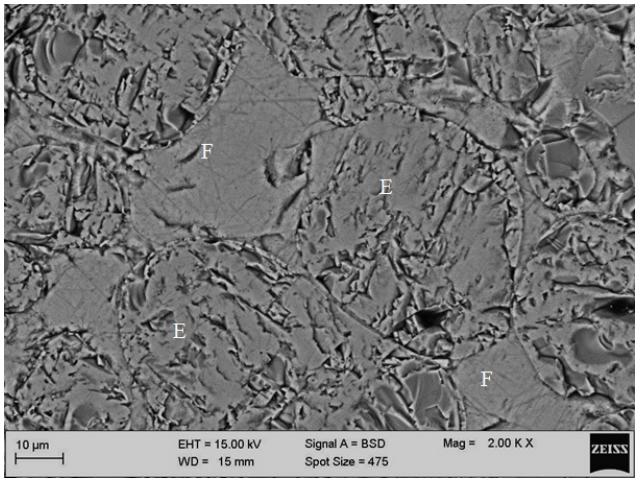

(c) 1200 °C

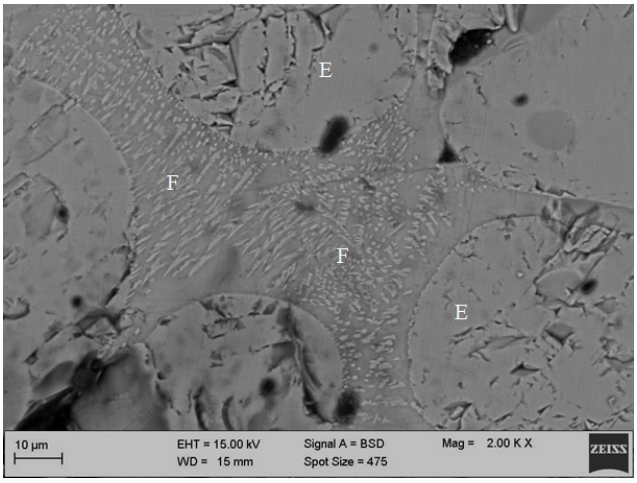

(d) 1500 °C

Figure 11.1: BSE micrographs of quenched samples: light crystals in (a), (b), (c) and (d) are rutile solid solution (E) and the non-crystalline dark glassy phase is molten slag (F). Light crystals embedded in the molten slag are precipitate from quenching.

Table 11.3: The calculated enthalpies and entropies of pure compounds in the Ti-V-O compared with the experimental data.

Compound	$\Delta H^{\circ}_{f,298}$ J.mol^{-1}	S°_{298} Jmol^{-1}K^{-1}	a	b	c	d	e	f	C_p range K	Reference
Solids										
TiO_2(s)	-944750.00	50.460	77.848				- 33.67841	40.2940672	298- 2130	(Bale et al. 2016)
V_2O_5(s)	-1550590	130.559	25.970	50.00	5853.80	-76.76761	-7.541627		298- 943	(Bale et al. 2016)
Liquid										
V_2O_5(l)	-1491202	191.96	164.31	24.00			-36.28207		298 - 600	(Bale et al. 2016)
TiO_2(l)	-898726.0	72.068	77.840				- 33.67841	40.2940672	298- 2130	(Bale et al. 2016) *
Ti_2O_3(l)	-1414375	130.17	169.96		-750.22		16.09649	-15.6552100	298 - 2115	(Bale et al. 2016) *

$$Cp(Jmol^{-1}K^{-1}) = a + b(10^{-3})T + cT^{-0.5} + d(10^{3})T^{-1} + e(10^{5})T^{-2} + f(10^{7})T^{-3}$$

Table 11.4: The optimised parameters of solutions in the Ti-V-O system in air.

Liquid: TiO_2-Ti_2O_3-V_2O_5

Quasichemical Model (Figure 11.2a)
TiO_2-Ti_2O_3 binary parameters
Taken from the study of Kang, Jung, and Lee (2006)
V_2O_5-TiO_2 binary parameters
$Z_{Ti^{4+}}$ $Z_{V2O3^{4+}} = 2.7548$, $Z_{Ti^{3+}} = 2.0661$
$\mathrm{g}^{01}_{\mathrm{Ti}^{4+}-\mathrm{V_2O_3^{4+}}} = -56303.2$
$\mathrm{g}^{0}_{\mathrm{Ti}^{4+}-\mathrm{V_2O_3^{4+}}} = 45402.4$
$\mathrm{g}^{10}_{\mathrm{Ti}^{4+}-\mathrm{V_2O_3^{4+}}} = -33.500T$

Associate Species Model (Figure 11.2b)
TiO_2-Ti_2O_3 binary parameters
Taken from the study of Cancarevic, Zinkevich, and Aldinger (2007)
V_2O_5-TiO_2 binary parameters
${}^0L_{V_2O_5-TiO_2} = -39385.9 + 35.061T$
${}^1L_{V_2O_5-TiO_2} = 6091.448$

Rutile Solid Solution
$G^{\circ}_{V_2O_5(s)-Rut} = G^{\circ}_{V_2O_5(s)} + 195562 - 76.7190T - 20.8017T$ for MQM from 298 K to 1773 K
$G^{\circ}_{V_2O_5(s)-Rut} = G^{\circ}_{V_2O_5(s)} + 213099 - 139.767T - 20.8017T$ for ASM from 298 K to 1773 K

11.2.1 Phase Diagrams

Phase diagrams calculated from optimised parameters, are shown in Figure 11.2. All superimposed experimental data on the diagram were considered during the optimisation sequence. In this case, the eutectic data from Habel et al. (2006) and experimental data from this study were included for the assessment, given that no previous studies had experimentally estimated liquidus and solidus data of the Ti-V-O system in air in the desired temperature range. The low solubility of Ti in the slag was reproduced with the MQM and the ASM.

For the MQM, the parameters $\Delta\mathrm{g}^{0}_{\mathrm{Ti}^{4+}-\mathrm{V_2O_3^{4+}}}$ and $\mathrm{g}^{01}_{\mathrm{Ti}^{4+}-\mathrm{V_2O_3^{4+}}}$ of Equation 9.20 were optimised and each had one temperature-independent coefficient. The $\mathrm{g}^{01}_{\mathrm{Ti}^{4+}-\mathrm{V_2O_3^{4+}}}$ was found to have a negligible influence at low Ti solubility, and may only become plausible and significant at a higher temperatures where Ti solubility is expected to increase. Nevertheless, $\mathrm{g}^{10}_{\mathrm{Ti}^{4+}-\mathrm{V_2O_3^{4+}}}$ had been optimised after all other parameters were optimised to reproduce the melting point of pure rutile. Without this parameter, unrealistic solutions were obtained at some temperatures and compositions between 1500 °C and the melting point of pure rutile. It was found that a temperature-dependent coefficient was more successful for reproducing the melting point of pure rutile. Moreover, the parameter did not significantly compromise the reproduced experimental results.

When the ASM was used to describe the slag phase, parameters, ${}^0\mathrm{L}_{\mathrm{V_2O_5-TiO_2}}$ and ${}^1\mathrm{L}_{\mathrm{V_2O_5-TiO_2}}$ of Equation 9.26 were optimised to reproduce experimental data. Only temperature-independent coefficients were required to reproduce the experimental data from this study. A temperature dependent coefficient was added to the parameter ${}^0\mathrm{L}_{\mathrm{V_2O_5-TiO_2}}$ in an attempt to reproduce a reasonable liquidus and solidus between 1500 °C and the melting point of pure rutile. However, the liquidus was affected marginally by the temperature dependent coefficient, causing it to deviate from the experimental results. Nevertheless, unrealistic solutions between 1500 °C and the melting point of

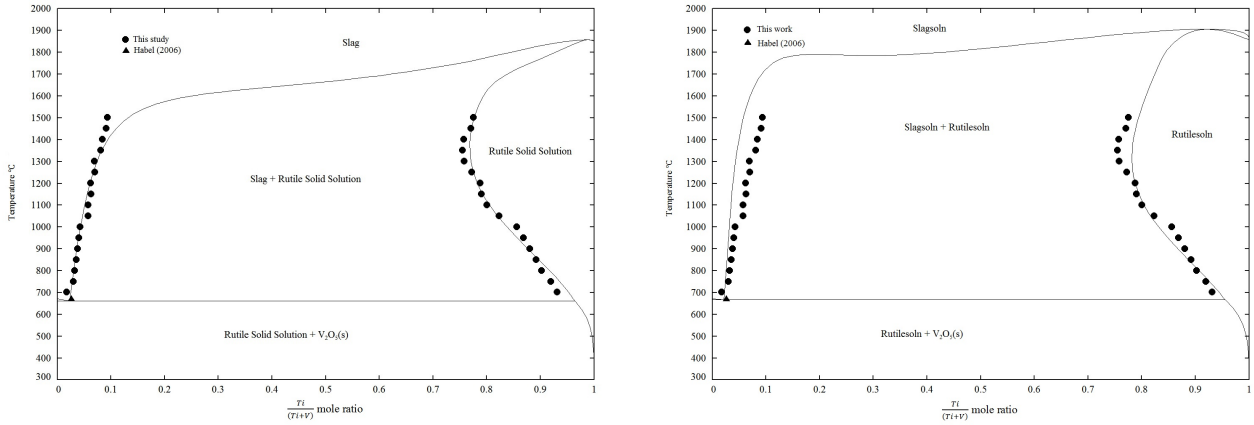

(a) Slag phase calculated with the MQM. (b) Slag phase calculated the ASM.

Figure 11.2: Equilibrium phase diagrams of the Ti-V-O system in air compared with the present experimental works.

pure rutile were obtained when this coefficient was not added to the parameter, ${}^{0}\mathrm{L}_{\mathrm{V_2O_5-TiO_2}}$. The quality of an assessment in most cases does not depend on the model used, but in this case it is the researcher's opinion that better estimations can be made with the MQM, especially in areas near the melting point of pure rutile. Furthermore, it is clear that the optimisation process in OptiSage could lead to incorrectness regarding the liquidus line at higher temperatures (artificial miscibility gap, for instance), but nonetheless, a reasonable liquidus was obtained with the MQM and the ASM.

The rutile solid solution was reproduced successfully by adjustments to the enthalpy of formation and standard entropy of $\mathrm{G}^{\circ}_{\mathrm{V_2O_5(s)}}$. The adjusted value is shown separately to the derived value from the enthalpy of mixing. The eutectic temperature of the molten phase, rutile solid solution and V_2O_5(s) was calculated at 662 °C and had a total V molar composition of 98.1 %. These values compared well with the thermal arrest upon heating, which was estimated by Habel et al. (2006) to be about 670 °C and 97.4 mole % V. Moreover, it is stated in Yang et al. (2017) that it is more appropriate to assign the heating value than the cooling value to the eutectic temperature, given that there is a likelihood of potential supercooling during solidification. Yang et al. (2017) went on to calculate the eutectic temperature at 675 °C and 97.4 mole % V.

11.2.2 Other Thermodynamic Data

No other thermodynamic experimental data, such as enthalpies of mixing, heat contents, thermal expansion data and activity data of the slag phase, were obtained to support the calculated phase diagrams. However, theoretical data from this study can be compared to experimental data of some future study. Activity data of any slag will give an indication of how constituents behave on molecular scale and if, for example, an immiscibility gap at some composition and temperature can occur. In this case only the MQM was used to calculate the activity data of slag constituents because of better agreement obtained between measured and calculated results. The extrapolation ability of the MQM is also superior to the ASM above 1500 °C. The definition of an ideal solution is defined in similar fashion as in Subsection 10.3.2 in order to observe if the slag exhibits positive or negative deviation from ideal behaviour. In this case, the cationic species in the MQM are Ti^{4+} and $V_2O_3^{4+}$. The predicted mole fraction of Ti_2O_3 was negligible at these temperatures under oxidizing conditions. An ideal solution is then defined as a random mixture of these species. That is, approximately: $\mathrm{a_{TiO_2}} = \mathrm{X_{Ti}^2}$ and $\mathrm{a_{V_2O_5}} = \mathrm{X_{V_2O_3}}$ where $\mathrm{X_{Ti}} = (1 - \mathrm{X_{V_2O_3}}) = \mathrm{X_{Ti}}/(\mathrm{X_{Ti}} + 0.5\mathrm{X_V})$ The activity data at 1000, 1200 and 1400 °C from calculated model parameters are shown in Figure 11.3.

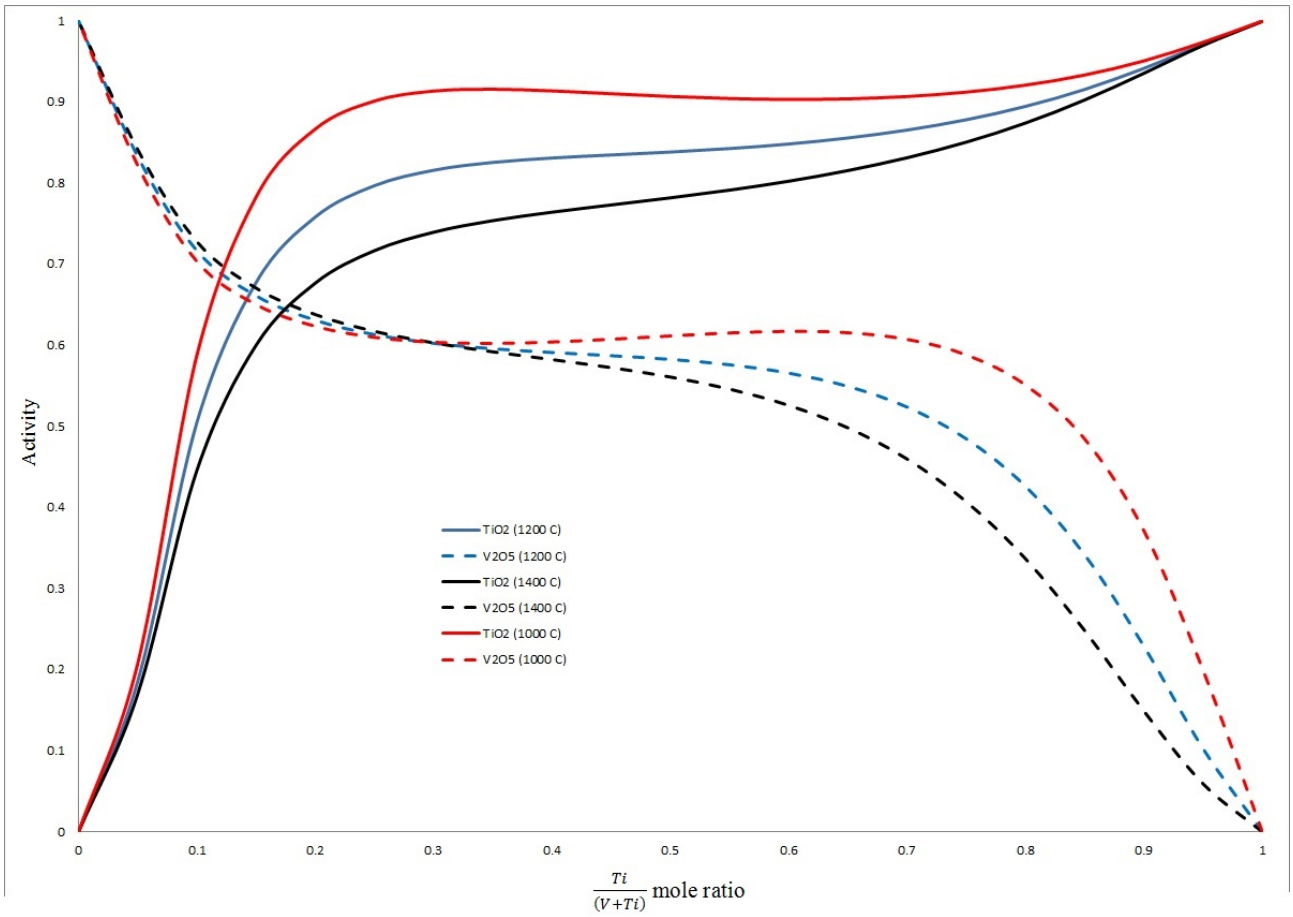

Figure 11.3: Activities of slag constituents calculated with the MQM and depressed crystalline phases.

It has been pointed out in Subsection 10.3.2 that a negative deviation is characterised by stronger unlike molecule attractions. However, in this case, the activities of slag constituents indicate a positive deviation from ideal behaviour, and are observed to be strongest at 1000 °C. The positive deviation is characterised by vapour pressures higher than those calculated for a ideal solution (Lee 1999). In other words, the escaping tendencies of the unlike molecules ($(\mathrm{Ti}^{4+} - \mathrm{V_2O_3^{4+}})$) are higher than the escaping tendencies of the like molecules ($(\mathrm{Ti}^{4+} - \mathrm{Ti}^{4+})$ and $(\mathrm{V_2O_3^{4+}} - \mathrm{V_2O_3^{4+}})$. A positive deviation is often associated with miscibility gaps and has been observed in systems involving silica. This is because silica is a relatively strong acid and exhibits a miscibility gap with oxides of cations with a high field strength (Barry, Dinsdale, and Gisby 1993).

In this case, the low solubility of TiO_2 in the V-O slag has probably contributed to the observation of positive deviation, given that no miscibility gap was observed in slag samples. Nevertheless, the likelihood of a metastable miscibility gap should not be dismissed, given the tendency of Ti de-mixing in the slag at sub-liquidus temperatures. In Figure 11.4 it is observed that a second liquid phase forms in a relatively low temperature area, provided that all crystalline phases have been depressed.

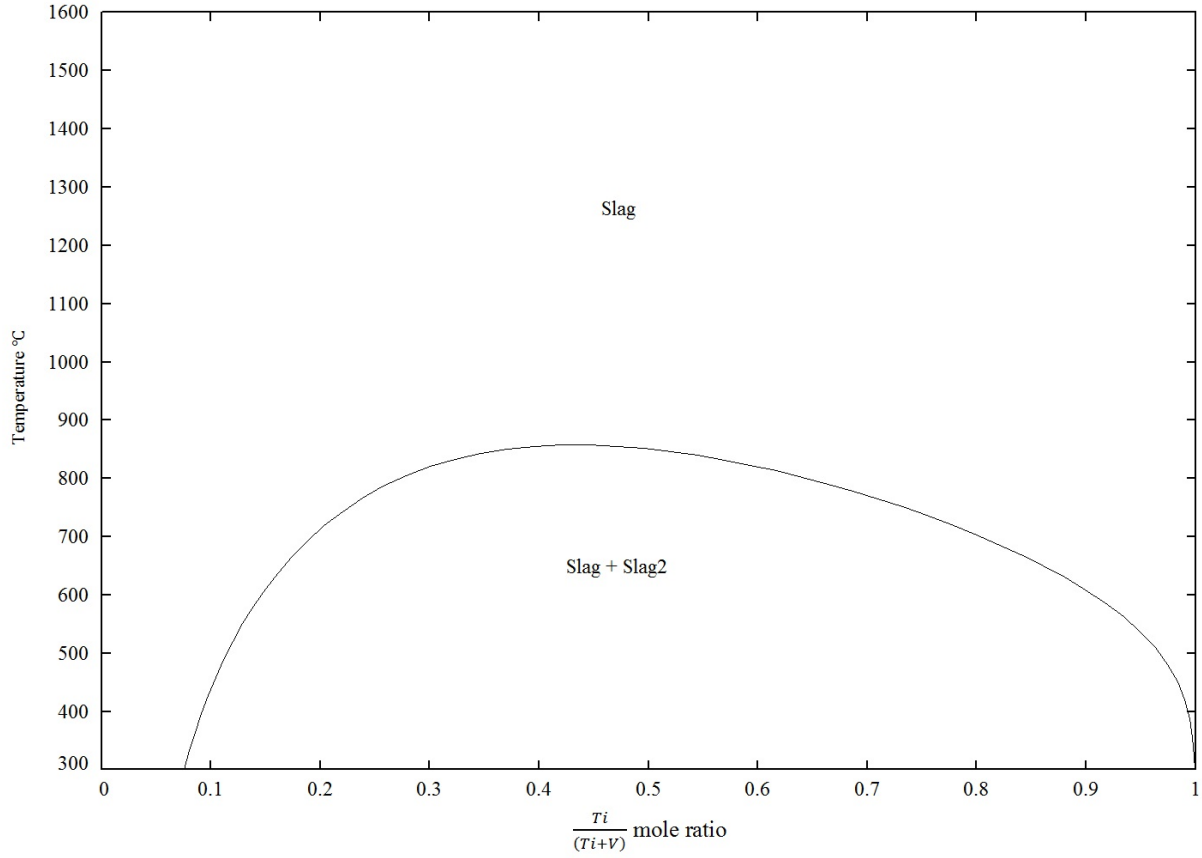

Figure 11.4: Liquid miscibility gap calculated with the MQM and depressed crystalline phases.

Chapter 12

Fe-Ti-V-O System in Air

Before a final set of equations of the Gibbs energies were obtained for the Fe-Ti-V-O system in air, a few prior calculations were required. The order of execution was as follows:

1. A critical assessment and thermodynamic evaluation of the Fe-Ti-O system in air was conducted before any calculations could be done on the Fe-Ti-V-O system in air.
2. The ternary phase diagrams calculated from binary optimised parameters are given along with some newly estimated Gibbs energy parameters.
3. Plausible starting compositions for experiments involving Fe_2O_3(s), TiO_2(s) and V_2O_5(s) were selected from the calculated ternary phase diagrams.
4. The results from the experiments were used to re-evaluate some thermodynamic parameters from the Fe-Ti-O, Fe-V-O and Ti-V-O systems in air and a final set of optimised thermodynamic parameters are given along with phase diagrams with superimposed experimental data.

12.1 Newly Assessed Fe-Ti-O System in Air

A critical evaluation of the literature was performed to gather experimental and theoretical data of the Fe-Ti-O system in air. Afterwards, the guidelines from Section 6.8 were carefully followed to obtain one set of model equations for Gibbs energies for all phases. Phase diagrams (Figure 12.1) were then back-calculated and compared to newly acquired phase diagram data.

The slag phase under reducing conditions was previously described with the MQM (see Subsection 6.3.2) by Eriksson et al. (1996) and no adjustments were made to quasichemical model parameters. Very limited liquidus or other thermodynamic data of a Fe-Ti-O slag phase under oxidizing conditions are available in the literature, therefore an ideal solution between the interaction pair $\mathrm{Fe^{3+} - Ti^{4+}}$ was assumed.

The models for the rutile and hematite solid solution (see Subsection 6.3.3) were developed within the framework of the compound energy formalism and optimised with data from Wittke (1967). The spinel solid solution was modelled assuming that no Ti^{4+} cations had dissolved within its crystal structure, which is obviously not compelling, and in reality some Ti^{4+} cations will deport to the spinel phase. Moreover, spinel solid solution can either be stabilized or destabilized from dissolved Ti^{4+} cations in its tetrahedral or octahedral sub-lattices. However, no experimental evidence in the literature exists to describe the solubility of Ti^{4+} cations in spinel under oxidizing conditions.

Ferropseudobrookite solid solution, $\mathrm{Fe_{2-x}Ti_{x+1}O_5}$ was modelled as a pure compound, Fe_2TiO_5(s). This is a gross simplification and the researcher believes that without any available experimental data to substantiate the assumption, Fe_2O_3(s) and TiO_2(s) are partially soluble at some composition

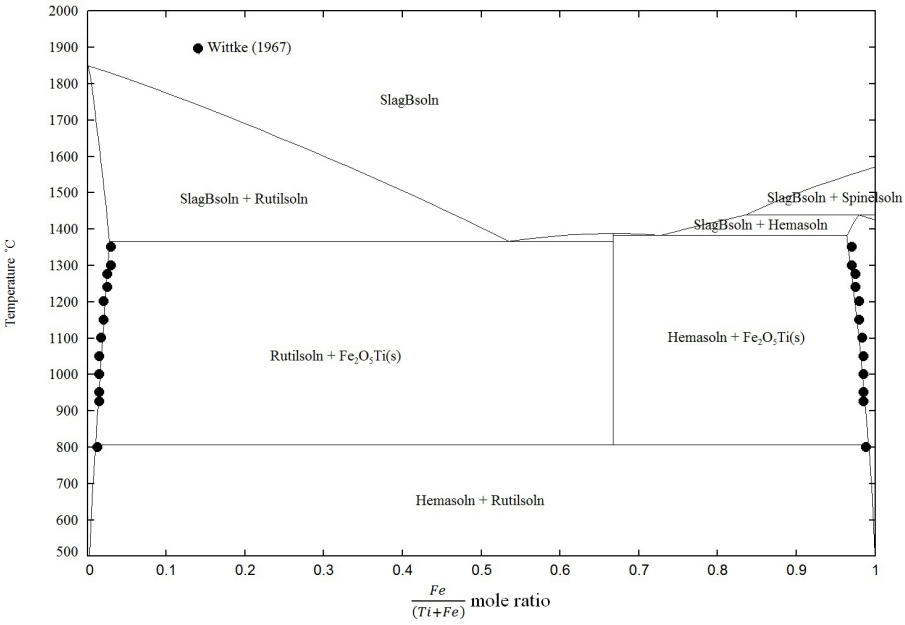

(a) Fe-Ti-O phase diagram in air with spinel solid solution.

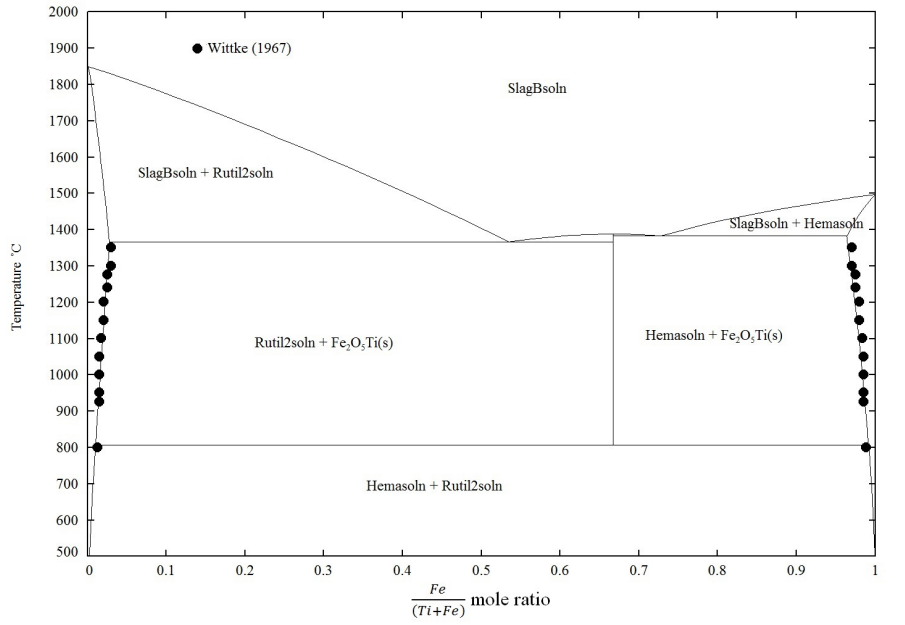

(b) Fe-Ti-O phase diagram in air without spinel solid solution.

Figure 12.1: The improved Fe-Ti-O phase diagrams in air after a critical evaluation of literature and thermodynamic assessment.

Table 12.1: The optimised parameters of solutions in the Fe-Ti-O system in air prior to experiments on the Fe-Ti-V-O system in air.

Liquid: FeO-Fe_2O_3-TiO_2-Ti_2O_3
Quasichemical Model
FeO-Fe_2O_3 binary parameters
Taken from the study of Degterov et al. (2001)
Ti_xO_x-Fe_xO_x binary parameters
Taken from the study of Eriksson et al. (1996)
TiO_2-Ti_2O_3 binary parameters
Taken from the study of Kang, Jung, and Lee (2006)
Hematite Solid Solution
$G^0_{TiO_2(s)-Hem} = G^0_{TiO_2(s)} - 12200.36 - 37.9927T - 12.4673T$ from 298 - 1623 K
Rutile Solid Solution
$G^0_{Fe^{3+}:Va} = -\frac{3}{4}G^0_{O_{2(g)}} + \frac{1}{2}G^0_{Fe_2O_3(s)} + 48393.1 + 8.92733T + 9.35051T$ from 298 - 1623 K
$G^0_{Fe^{3+}:O^{2-}} = \frac{1}{4}G^0_{O_{2(g)}} + \frac{1}{2}G^0_{Fe_2O_3(s)} + 48393.1 + 8.92733T + 9.35051T$ from 298 - 1623 K

and temperature. Therefore, if experimental data were available, ferropseudobrookite solid solution would have had the chemical formula, $(\mathrm{Fe}^{3+}, \mathrm{Ti}^{4+})(\mathrm{Fe}^{3+}, \mathrm{Ti}^{4+})_2\mathrm{O}_5$, and a descriptive model would have been developed within the framework of the CEF, similar to other solid solutions described in Subsection 6.3.3.

Although a more accurate phase diagram has been calculated by a critical assessment and thermodynamic evaluation, it is still incomplete and does not describe all phases comprehensively. Therefore, it is recommended that a thorough literature review be conducted on this system. Nevertheless, the optimised parameters was found to be sufficient for the prediction of starting compositions corresponding to areas with known phase assemblages in the Fe-V-Ti-O system in air (see Section 12.2). The assumptions made have already been discussed, but given the many assumptions, a summary of all are listed:

- **An ideal liquid solution**: This assumption is made on the bases that Fe^{3+} and Ti^{4+} ions are in principle chemically similar and should give reasonably good results. The ionic radii of Fe^{3+} and Ti^{4+} are used to support this paradigm. It was found that Fe^{3+} and Ti^{4+} have ionic radii of 69 pm (pico meter) and 74.5 pm, respectively (Shannon 1976). Consequently, it is recommended that a deviation from ideal behaviour be investigated empirically in order to make more accurate predictions of liquidus compositions.

- **A symmetric hematite solid solution**: A shortage of data on the hematite solid solution has encouraged the decision to accept a symmetric approach, meaning that solubility of Ti^{4+} in the hematite phase is identical to Fe^{3+} solubility in the rutile phase. An ideal solution could also have been considered; however it was observed that such an assumption predicted a Ti^{4+} solubility of more than 10 molar % in some temperature ranges. Therefore, it is the researcher's believe that an ideal solution would have grossly over-estimated Ti^{4+} concentration in the hematite phase.

- **Ferropseudobrookite solid solution modelled as stoichiometric compound**: There is limited experimental evidence to predict whether TiO_2(s) or Fe_2O_3(s) will have partial solubility in the ferropseudobrookite solid solution. Consequently, it is was difficult to develop the solution model for the ferropseudobrookite solid solution under oxidising conditions and

the stoichiometric compound, Fe_2TiO_5(s), is used as a simplification and replacement of the solid solution.

To remain consistent with the modelling methods of the FToxid database, the MQM is the only model used to describe the slag phase in the Fe-Ti-V-O system. An additional reason for this is that no study has used the ASM to describe the liquid phase in the Fe-Ti-O system. In other words, if the pairs, FeO-Fe_2O_3 (Kowalski and Spencer 1995) and TiO_2-Ti_2O_3 (Cancarevic, Zinkevich, and Aldinger 2007), with their respective excess Gibbs energy parameters, were combined into one slag solution with the assumption that the pairs Fe_2O_3-Fe_2TiO_5 and TiO_2-Fe_2TiO_5 exhibited ideal behaviour, an unrealistic solution would be obtained.

This signifies that the pairs Fe_2O_3-Fe_2TiO_5 and TiO_2-Fe_2TiO_5 need to be re-evaluated together with pairs FeO-Fe_2O_3 and TiO_2-Ti_2O_3. Such an investigation needs to be carried out at different temperatures, compositions and oxygen partial pressures, which predominantly falls outside the scope of this study. However, given the high oxygen partial pressure, the number of species in the slag phase could have been reduced to three, which are Fe^{3+}, Ti^{4+} and V^{5+} cations. This is still a simplification, because it is generally believed that Fe^{2+} and Ti^{3+} cations are present under oxidising conditions (see the studies of Hidayat et al. (2015) and Eriksson and Pelton (1993), especially present in significant concentrations in regions close to pure magnetite and TiO_2(s) melting points.

12.2 Calculations from Binary Parameters

The main task to be undertaken in calculating the Fe-Ti-V-O system in air involved modelling the liquid and the extensive series of crystalline solutions from a critical set of experimental data. These solutions were first modelled and included in their respective lower-order systems, which are Fe-V-O, Ti-V-O and Fe-Ti-O in air. Afterwards, ternary interpolation techniques described in Section 6.4 were applied to liquid quasichemical interaction pairs (see Subsection 9.2.1) for identified ternary pairs), from which a set of ternary phase diagrams was calculated. Phase diagrams at constant temperature and fixed $\mathrm{pO_2}$, otherwise known as isothermal planes, were calculated from optimised binary parameters and are shown in Figure 12.2.

Isothermal sections at 1000 °C, 1100 °C, 1200 °C, 1300 °C and 1400 °C are shown in Figure 12.2a, Figure 12.2b, Figure 12.2c, Figure 12.2d, and Figure 12.2e, respectively. Given that there is some uncertainty about the behaviour of the constituents in the higher-order system, only sections marked 1, 2 and 3 in Figure 12.2a, Figure 12.2b, Figure 12.2c, Figure 12.2d, and Figure 12.2e, which correspond to the largest thermodynamic favoured compositions, were experimentally investigated.

12.3 Phase Equilibria Experiments

After the evaluation of calculated phase diagrams from optimized binary parameters, a series of experiments was carried out, which had initial compositions depicted in Table 12.2. These initial compositions were estimated with the assistance of Equation 7.2 to again have a sufficient amount of each phase for SEM-EDS analysis and EPMA.

The importance of the Gibbs phase rule is now evident, given that the number of phases varies between two and four in the respective sub-sections from the calculated isothermal sections in Figure 12.2. The sections marked 1, 2 and 3 were experimentally investigated after the Gibbs phase rule had been applied (see Equation 6.60). For instance, in sub-sections 1 and 2, p = 4 (gas, slag and two solids), c = 5 (Fe, Ti, V, O_2 and N_2) and according to Equation 6.60, f = 3. Therefore, three variables are at the discretion of the researcher and the remaining ones are fixed. Such a system is trivariant. The pressure is fixed at 1 atm (absolute), the temperature is fixed at a furnace set point and the oxygen partial pressure is fixed at 0.21 atm. All three variables are intensive

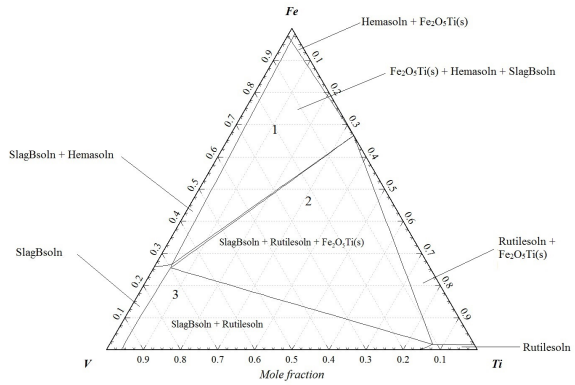

(a) Isothermal section at 1000 °C

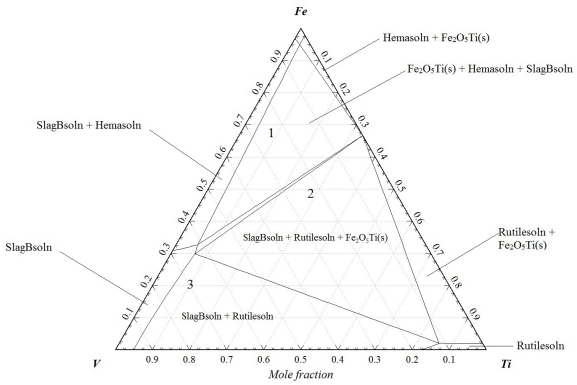

(b) Isothermal section at 1100 °C

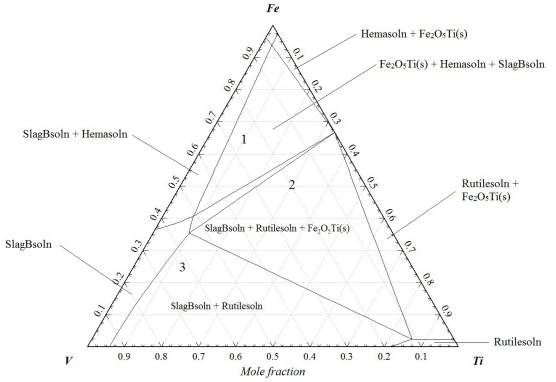

(c) Isothermal section at 1200 °C

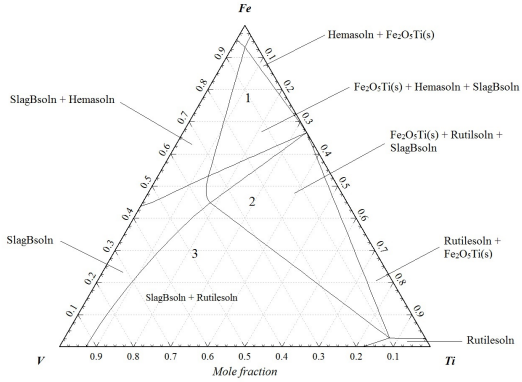

(d) Isothermal section at 1300 °C

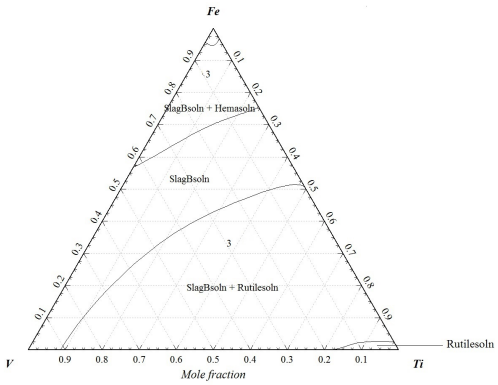

(e) Isothermal section at 1400 °C

Figure 12.2: Isothermal sections of the Fe-Ti-V-O system in air calculated from binary parameters and ternary interpolation.

Table 12.2: Experiments on the system Fe-Ti-V-O in equilibrium with air.

Experiment	Temperature °C	V_2O_5 mass %	Fe_2O_3 mass %	TiO_2 mass %	Equilibration Time (hr)
1	1000	0.600	0.100	0.300	16
2	1000	0.330	0.330	0.340	16
3	1000	0.700	0.150	0.150	16
4	1000	0.200	0.700	0.100	16
5	1100	0.150	0.700	0.150	16
6	1100	0.330	0.330	0.340	16
7	1100	0.600	0.100	0.300	16
8	1100	0.500	0.120	0.380	16
9	1200	0.500	0.200	0.300	16
10	1200	0.600	0.200	0.200	16
11	1200	0.330	0.330	0.340	16
12	1200	0.200	0.700	0.100	16
13	1300	0.400	0.200	0.400	16
14	1300	0.500	0.100	0.400	16
15	1300	0.200	0.300	0.500	16
16	1300	0.200	0.650	0.150	16
17	1400	0.200	0.200	0.600	4
18	1400	0.400	0.200	0.400	4
19	1400	0.150	0.750	0.100	4

properties. Hence, the system is fully defined. However, in sub-section 3, p = 3 (gas, slag and one solid), c = 5 and according to Equation 6.60, f = 4. With four variables at the discretion of the researcher, the composition, another intensive property, of one specie in the slag or solid solution is fixed.

That said, one experiment from sub-sections 1 and 2 is sufficient to determine the composition of the phase assemblage, assuming that the starting composition was within the boundaries of sub-sections 1 and 2. Moreover, any starting composition, as long as it was within the boundaries of sub-sections 1 and 2, will result in an identical equilibrium composition of the phase assemblage. However, because of the disappearance of one phase in sub-section 3, at least two experiments were conducted, which had different initial compositions, but were confined to the boundaries of sub-section 3. Therefore, in this case, the composition of the phase assemblage is indirectly dependent on the initial composition (see Subsection 8.1.7).

12.4 Phase Characterisation and Quantification

Polished and coated samples were analysed with EPMA and SEM-EDS. Results from EPMA and SEM-EDS are shown in Table 12.3 and Table 12.4. To confirm sample homogeneity, at least ten points of each phase were analysed to calculate a set of standard deviations for each element. For samples at and above 1200 °C, at least 15 areas of the slag phase were analysed owing to the occurrence of precipitates. Oxygen concentration was calculated on the basis of stoichiometry (St.) by assuming V is in the 5+, Fe in the 3+ and Ti in the 4+ oxidation state. The standard deviation (σ) of each element is shown in the table next to its mean concentration. The results from EPMA en SEM-EDS compared relatively well, but small differences are observed owing to the overlapping of X-ray emission peaks of V and Ti. Therefore, only EPMA results were normalised and used in the thermodynamic assessment of the Fe-Ti-V-O system in air. Each experiment was repeated at least once.

Table 12.3: Summary of raw data from the Fe-Ti-V-O system in air analysed using EPMA.

Experiment	Initial composition wt.% V2O5	Fe2O3	TiO2	Temperature °C	Phases at equilibrium	Final composition in wt.% Fe	Fe (STD)	V	V (STD)	Ti	Ti (STD)	O (Stoichiometry)	Total
1	60	10	30	1000	Slag	10.28	0.64	47.14	0.94	2.26	0.42	42.94	102.63
					Rutile	4.54	0.10	10.84	0.07	46.39	0.14	41.47	103.23
2	33	33	33	1000	Slag	11.98	0.61	42.88	0.17	2.30	0.13	40.36	97.52
					Rutile	5.25	0.14	11.07	0.12	45.20	0.23	41.17	102.68
					Ferropseudobrookite	45.51	0.26	4.01	0.35	18.13	0.24	34.83	102.47
3	20	70	10	1000	Slag	12.95	1.25	46.70	1.16	0.55	0.14	42.61	102.81
					Hematite	67.07	0.94	1.77	0.14	1.31	0.08	31.09	101.24
					Ferropseudobrookite	45.97	0.79	7.03	0.59	13.04	0.79	33.99	100.02
4	70	15	15	1000	Slag	11.46	0.31	46.40	0.29	2.63	0.11	43.11	103.60
					Rutile	4.89	0.09	11.15	0.18	45.40	0.37	41.21	102.64
5	60	10	30	1100	Slag	14.43	1.46	44.42	0.89	2.70	0.31	42.89	104.43
					Rutile	4.26	0.13	11.06	0.09	45.74	0.10	41.09	102.15
6	50	12	38	1100	Slag	12.54	1.39	45.73	1.42	2.52	0.50	42.98	103.78
					Rutile	4.22	0.06	11.58	0.19	44.85	0.34	40.89	101.54
7	20	70	10	1100	Slag	17.01	0.94	41.89	0.74	0.94	0.16	40.83	100.68
					Hematite	66.78	0.17	1.84	0.04	1.84	0.07	31.37	101.83
					Ferropseudobrookite	46.77	0.29	6.87	0.09	13.69	0.14	34.64	101.97
8	33	33	33	1100	Slag	13.56	0.85	42.40	0.73	3.51	0.26	41.46	100.93
					Rutile	4.49	0.10	10.80	0.12	45.53	0.28	40.85	101.66
					Ferropseudobrookite	44.00	0.43	3.75	0.16	18.72	0.37	34.36	100.83
9	33	33	33	1200	Slag	16.11	0.70	41.31	0.69	3.90	0.56	41.97	103.29
					Rutile	3.87	0.08	10.09	0.06	47.78	0.12	41.53	103.27
					Ferropseudobrookite	43.78	0.19	4.18	0.10	19.64	0.08	35.23	102.84
10	60	20	20	1200	Slag	17.20	1.92	41.17	1.47	3.67	0.38	42.17	104.20
					Rutile	3.51	0.13	10.55	0.10	46.67	0.20	40.99	101.70
11	50	20	30	1200	Slag	18.00	1.46	39.91	0.61	4.22	0.73	41.90	104.03
					Rutile	3.55	0.13	10.35	0.13	47.31	0.08	41.27	102.47
12	20	70	10	1200	Slag	20.17	0.72	40.08	0.91	0.78	0.16	40.66	101.68
					Hematite	62.20	0.97	2.91	0.38	2.70	0.10	30.82	98.63
					Ferropseudobrookite	44.78	1.52	7.33	0.36	13.06	0.92	33.73	98.89
13	40	20	40	1300	Slag	20.63	1.66	37.39	1.89	5.01	1.37	41.58	104.20
					Rutile	3.02	0.11	8.27	0.10	49.74	0.14	41.04	101.70
14	20	65	15	1300	Slag	30.86	1.59	29.82	1.28	2.49	0.47	38.34	101.51
					Hematite	61.99	0.16	2.75	0.09	4.28	0.12	31.66	100.68
					Ferropseudobrookite	44.45	0.28	5.65	0.24	15.81	0.22	34.10	100.00
15	50	10	40	1300	Slag	18.13	1.26	40.59	1.52	2.75	0.78	41.50	102.98
					Rutile	2.57	0.11	9.63	0.27	48.30	0.37	40.95	101.44
16	20	30	50	1300	Slag	20.87	1.62	33.85	1.09	7.34	0.63	40.46	102.52
					Rutile	3.05	0.16	8.27	0.19	49.65	0.09	40.99	101.96
					Ferropseudobrookite	41.26	0.17	3.84	0.07	21.55	0.09	35.16	101.81
17	40	20	40	1400	Slag	22.70	2.44	32.21	2.72	8.56	1.12	40.77	104.24
					Rutile	2.08	0.03	7.61	0.05	50.65	0.09	40.73	101.06
18	20	20	60	1400	Slag	27.92	2.03	22.54	2.57	13.15	1.98	38.49	102.10
					Rutile	2.48	0.14	6.00	0.20	51.81	0.54	40.41	100.70
19	15	75	10	1400	Slag	31.10	0.70	27.27	1.00	5.90	0.71	38.72	102.99
					Hematite	59.48	0.86	2.76	0.18	6.56	0.20	32.12	100.92

Table 12.4: Summary of raw data from the Fe-Ti-V-O system in air analysed using SEM-EDS.

Experiment	Initial composition wt.% V2O5	Fe2O3	TiO2	Temperature	Phases at equilibrium	Final composition in wt.% Fe	Fe (STD)	V	V (STD)	Ti	Ti (STD)	O (Stoichiometry)	Total
1	60	10	30	1000	Slag	9.60	0.43	48.16	0.53	2.11	0.19	43.35	103.21
					Rutile	4.25	0.09	11.57	0.18	44.63	0.46	40.74	101.18
2	33	33	33	1000	Slag	10.76	0.82	46.57	1.89	2.22	0.69	42.67	102.22
					Rutile	5.17	0.31	11.66	0.37	43.81	1.07	40.66	101.29
					Ferropseodobrookite	44.39	0.69	4.18	0.39	18.11	0.46	34.47	101.16
3	20	70	10	1000	Slag	13.06	1.16	46.82	1.24	0.57	0.13	42.76	103.21
					Hematite	67.25	0.88	1.75	0.16	1.31	0.08	31.15	101.47
					Ferropseodobrookite	46.18	0.87	7.04	0.58	12.95	0.80	34.04	100.22
4	70	15	15	1000	Slag	10.83	0.22	46.84	0.33	2.38	0.20	43.03	103.08
					Rutile	4.61	0.21	11.87	0.25	43.51	1.15	40.38	100.36
5	60	10	30	1100	Slag	13.85	0.65	44.31	0.61	1.56	0.27	41.79	101.50
					Rutile	3.95	0.20	11.64	0.16	44.15	0.48	40.35	100.08
6	50	12	38	1100	Slag	12.79	1.53	45.25	1.72	2.17	0.75	42.47	102.68
					Rutile	4.23	0.15	11.55	0.30	44.93	0.48	40.93	101.64
7	20	70	10	1100	Slag	15.41	1.61	44.06	1.78	0.73	0.18	41.71	101.91
					Hematite	64.84	0.60	2.23	0.23	1.85	0.09	30.85	99.77
					Ferropseodobrookite	45.51	0.39	7.44	0.20	13.45	0.23	34.40	100.80
8	33	33	33	1100	Slag	13.13	0.59	44.38	1.26	2.69	0.69	42.29	102.50
					Rutile	4.32	0.13	11.47	0.18	44.85	0.39	40.84	101.48
					Ferropseodobrookite	43.22	0.92	4.31	0.21	18.65	0.39	34.42	100.60
9	33	33	33	1200	Slag	15.37	1.19	41.29	2.19	3.60	1.47	41.43	101.68
					Rutile-SS	3.61	0.11	10.70	0.29	45.54	0.61	45.05	104.89
					Ferropseodobrookite	41.45	0.47	4.60	0.24	19.02	0.31	34.14	99.20
10	60	20	20	1200	Slag	16.20	0.53	41.27	0.89	3.08	0.69	41.43	101.98
					Rutile	3.30	0.09	10.97	0.16	44.85	0.43	40.02	99.15
11	50	20	30	1200	Slag	16.94	0.32	41.04	0.78	3.61	0.81	41.92	103.51
					Rutile	3.35	0.09	10.98	0.14	46.01	0.56	40.82	101.15
12	20	70	10	1200	Slag	18.17	1.87	41.71	1.70	0.67	0.22	41.01	101.57
					Hematite-SS	62.11	0.92	2.95	0.37	2.70	0.11	30.81	98.57
					Ferropseodobrookite	44.35	0.84	7.40	0.28	13.26	0.74	33.74	98.75
13	40	20	40	1300	Slag	20.75	1.61	37.46	0.95	5.16	0.89	41.78	101.98
					Rutile	3.10	0.11	8.55	0.32	49.71	0.17	41.28	99.15
14	20	65	15	1300	Slag	31.10	1.35	29.73	1.16	2.54	0.40	38.40	101.77
					Hematite	62.11	0.23	2.71	0.11	4.28	0.13	31.68	100.78
					Ferropseodobrookite	44.47	0.31	5.61	0.36	15.80	0.21	34.08	99.96
15	50	10	40	1300	Slag	18.22	1.11	40.62	1.17	3.07	0.62	41.78	103.70
					Rutile	2.57	0.20	9.77	0.36	48.08	0.29	40.92	101.34
16	20	30	50	1300	Slag	21.09	1.46	33.98	1.17	7.00	1.18	40.42	102.49
					Rutile	3.06	0.29	8.41	0.34	49.60	0.25	41.08	102.15
					Ferropseodobrookite	41.32	0.18	3.78	0.13	21.55	0.12	35.14	101.79
17	40	20	40	1400	Slag	20.40	0.57	32.91	1.06	8.23	1.21	40.11	101.65
					Rutile	1.98	0.15	8.22	0.20	49.59	0.56	40.46	100.25
18	20	20	60	1400	Slag	26.81	1.81	23.97	2.72	11.76	1.26	38.21	100.75
					Rutile	2.49	0.11	6.07	0.26	52.12	0.72	40.68	101.36
19	15	75	10	1400	Slag	31.93	2.53	25.68	1.82	6.40	0.73	38.16	102.18
					Hematite	59.06	0.79	2.77	0.31	6.52	0.20	31.92	100.28

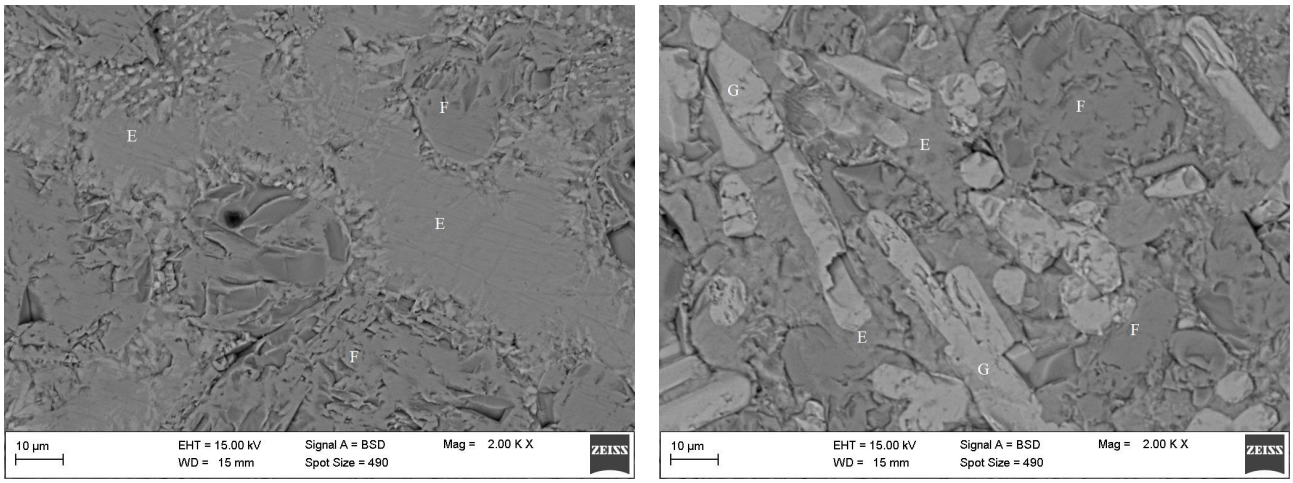

(a) Two phases. (b) Three phases.

Figure 12.3: BSE micrographs of quenched samples at 1000 °C: light crystals in (a) and (b) are rutile solid solution (F) and the non-crystalline dark glassy phase is molten slag (E). The darker crystals in (b) are ferropseudobrookite solid solution (G).

All analysed samples from 1000 °C to 1300 °C have two or three homogeneous condensed phases in equilibrium with air. All analysed samples at 1400 °C have only two phases in equilibrium with air owing to ferropseudobrookite (Fe_2TiO_5(s)) melting congruently at 1388 °C. However, this congruent melting point was estimated with FactSage and has not been determined experimentally. Results from the experiments indicate that the congruent melting point of ferropseudobrookite solid solution is between 1300 °C and 1400 °C. The molar ratio of Fe to Ti in ferropseudobrookite solid solution is higher when in equilibrium with the slag and hematite solid solution compared to a sample where ferropseudobrookite solid solution is in equilbirium with the slag and rutile solid solution. The measured molar ratio of Fe to Ti in the ferropseudobrookite solid solution of the latter constitutes that of the stoichiometric compound, Fe_2TiO_5(s). Furthermore, a small amount of V_2O_5 has dissolved in ferropseudobrookite.

It is also noted that a small amount of TiO_2 and V_2O_5 had dissolved in the hematite phase. Similarly, it is noted that a small amount of Fe_2O_3 and V_2O_5 had dissolved in the rutile phase. The dissolution of V_2O_5 in the hematite and rutile phases was already observed in experimental investigations of the Fe-V-O and Ti-V-O system in air.

Micrographs captured from the SEM back-scattered detector of samples quenched at 1000 °C, 1200 °C and 1400 °C are shown in Figure 12.3, Figure 12.4 and Figure 12.5. For the samples quenched at 1200 °C and 1400 °C, an appreciable amount of precipitation is observed in the molten slag phase and this is enhanced by an increase in Fe content. The samples at and above 1200 °C were analysed by following the analytical procedure outlined in Section 10.2. The calculated standard deviations of samples quenched at 1400 °C were in some cases above 1 wt.%. Nevertheless, given the scarcity of data on this system, experimental data had to be accepted and used for the assessment.

12.5 Thermodynamic Calculations

Based on all experimental data from Section 12.4, the optimized model parameters for all phases in the Fe-Ti-V-O system in air are presented in Table 12.5 and Table 12.6. Using these parameters, phase equilibria, invariant and thermodynamic properties are calculated and can be compared with literature data when these become available.

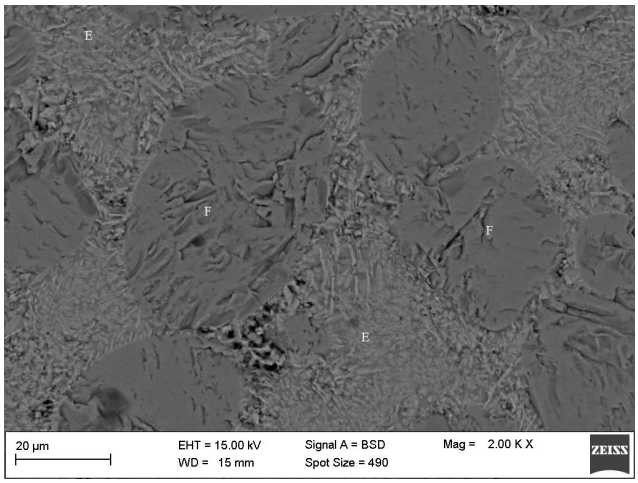

(a) Two phases.

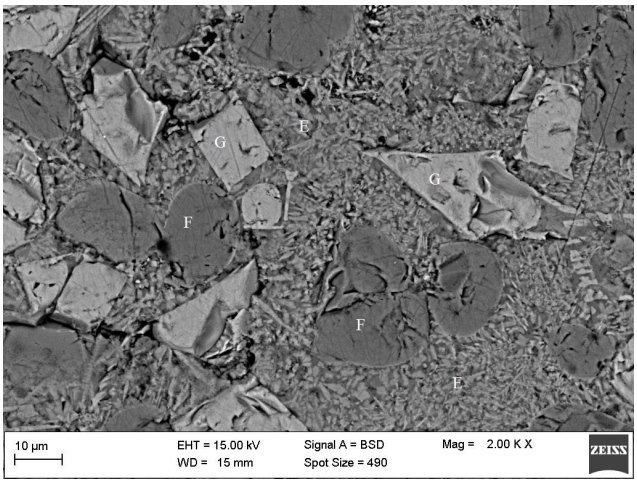

(b) Three phases.

Figure 12.4: BSE micrographs of quenched samples at 1200 °C: light crystals in (a) and (b) are rutile solid solution (F) and the non-crystalline dark glassy phase is molten slag (E). The darker crystals in (b) are ferropseudobrookite solid solution (G).

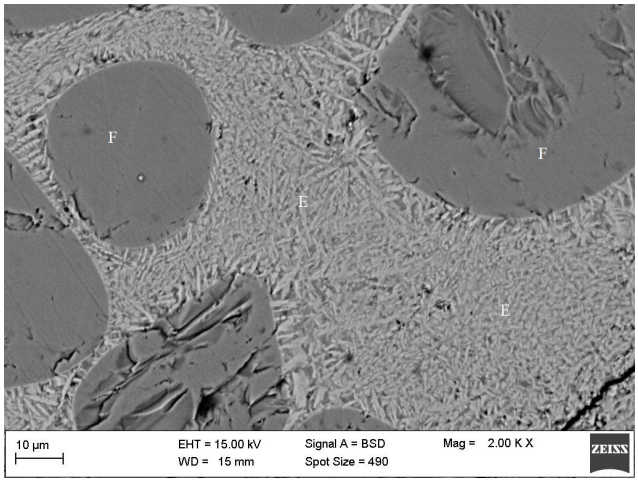

(a) Slag and rutile solid solution.

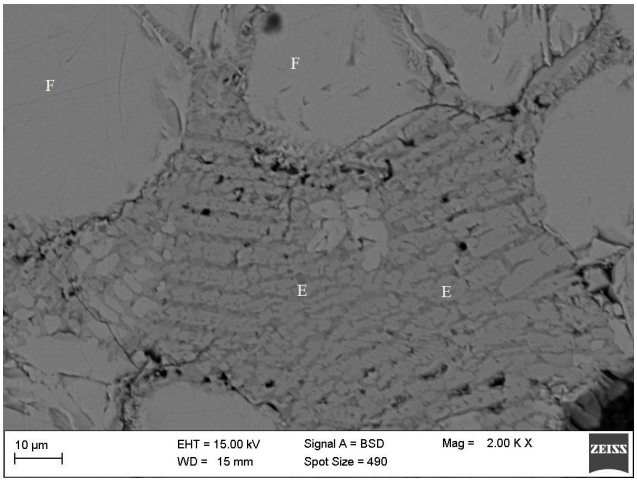

(b) Slag and hematite solid solution.

Figure 12.5: BSE micrographs of quenched samples at 1400 °C: light crystals in (a) are rutile solid solution (F) and darker crystals in (b) are hematite solid solution. The non-crystalline dark glassy phase in (a) and (b) is molten slag (E).

Table 12.5: The optimised parameters of solutions in the Fe-Ti-V-O system in air.

Liquid: FeO-Fe_2O_3-TiO_2-Ti_2O_3-V_2O_5

Quasichemical Model
FeO-Fe_2O_3 binary parameters
Taken from the study of Degterov et al. (2001)
TiO_2-Ti_2O_3 binary parameters
Taken from the study of Kang, Jung, and Lee (2006)
Ti_xO_x-FeO binary parameters
Taken from the study of Eriksson et al. (1996)
TiO_2-Fe_2O_3 binary parameters
$\Delta g^{\circ}_{Fe^{3+}-Ti^{4+}} = 225211 - 134.46T$
V_2O_5-Fe_2O_3 binary parameters
Taken from Chapter 10
V_2O_5-TiO_2 binary parameters
Taken from Chapter 11

Hematite solid solution: $Fe_2O_3{-}TiO_2{-}V_2O_5$
$G^{\circ}_{TiO_2(s)-Hem} = G^{\circ}_{TiO_2(s)} - 12200.36 - 37.9927T - 12.4673T$ from 298 - 1673 K
$G^{\circ}_{V_2O_5(s)-Hem}$ - Taken from Chapter 10
Rutile solid solution: $TiO_2{-}Fe_2O_3{-}V_2O_5$
$G^{\circ}_{Fe^{3+}:Va} = -\frac{3}{4}G^{\circ}_{O_{2(g)}} + \frac{1}{2}G^{\circ}_{Fe_2O_3(s)} + 71146.2 + 36.1442T + 9.35051T$ from 298 - 1673 K
$G^{\circ}_{Fe^{3+}:O^{2-}} = \frac{1}{4}G^{\circ}_{O_{2(g)}} + \frac{1}{2}G^{\circ}_{Fe_2O_3(s)} + 71146.2 + 36.1442T + 9.35051T$ from 298 - 1673 K
$G^{\circ}_{V_2O_5(s)-Rut} = G^{\circ}_{V_2O_5(s)} + 171607 - 32.96704T$
$G^{\circ}_{V^{5+}:Va_2} = \frac{1}{2}G^{\circ}_{V_2O_5(s)-Rut} - G^{\circ}_{O_2(g)} - 10.4009T$
$G^{\circ}_{Va:Va_2} = -G^{\circ}_{O_2(g)}$
Ferricpseudobrooktie solid solution: $Fe_2TiO_5{-}V_2O_5$
$L^{10}_{V_2O_5-Fe_2TiO_5} = 64754.8 - 57.652T$

Table 12.6: The calculated enthalpies and entropies of pure compounds in the Fe-Ti-V-O.

Compound	$\Delta H^{\circ}_{f,298}$	S°_{298}	a	b	c	d	e	f	C_p range	Reference
Solids										
Fe_2O_3(s)*	-825787.0	87.7285	137.01				-29.07640		298-2500	(Bale et al. 2016)
$FeVO_4$(s)	-1184723	128.436	129.51	24.71			-21.60000		298 - 973	Chapter 10
$Fe_2V_4O_{13}$(s)	-3937787	382.628	388.83	73.83			-65.06000		298 - 973	Chapter 10
Fe_2TiO_5(s)	-1738786.72	192.59	22.008				-31.00344		298-2000	(Bale et al. 2016)
TiO_2(s)	-944750.00	50.460	77.848				- 33.67841	40.2940672	298- 2130	(Bale et al. 2016)
V_2O_5(s)	-1550590	130.559	25.970	50.00	5853.80	-76.76761	-7.541627		298- 943	(Bale et al. 2016)
Liquid										
Fe_2O_3(l)	-745158.3	139.467	137.01				-29.07640		298 - 2500	Chapter 10
FeO(l)	-234643.2	78.4655	-18.024	31.00	1500.90		-25.33300		298 - 1644	(Bale et al. 2016)
			68.199						1644 - 2000	(Bale et al. 2016)
TiO_2(l)	-898726.0	72.068	77.840				- 33.67841	40.2940672	298- 2130	(Bale et al. 2016)
Ti_2O_3(l)	-1414375	130.17	169.96		-750.22		16.09649	-15.6552100	298 - 2115	(Bale et al. 2016)
V_2O_5(l)	-1491202	191.958	164.31	24.00			-36.28207		298 - 600	(Bale et al. 2016)
			190.79						600 - 3000	(Bale et al. 2016)
Gasses										
O_2(g)	0	205.04	26.924	16.97868	-79.16166		2.29329		298-1000	(Bale et al. 2016)
	”	”	89.681	-1.44745	-4126.537	95.80396	-186.82686		298-1000	(Bale et al. 2016)

$$Cp(Jmol^{-1}K^{-1}) = a + b(10^{-3})T + cT^{-0.5} + d(10^{3})T^{-1} + e(10^{5})T^{-2} + f(10^{7})T^{-3}$$

12.5.1 Phase Diagrams

Isothermal sections at 1000 °C, 1100 °C, 1200 °C, 1300 °C and 1400 °C, calculated from optimised parameters, are shown in Figure 12.6, Figure 12.7, Figure 12.8, Figure 12.9, and Figure 12.10. All superimposed experimental data on the isothermal sections were considered during optimisation. The calculated liquidus projection along with primary fields and phases of the Fe-Ti-V-O system are shown in Figure 12.11. The calculated invariant reactions are shown in Table 12.7. No other phase diagram data were found in the literature, consequently only experimental data from this study were used for the assessment.

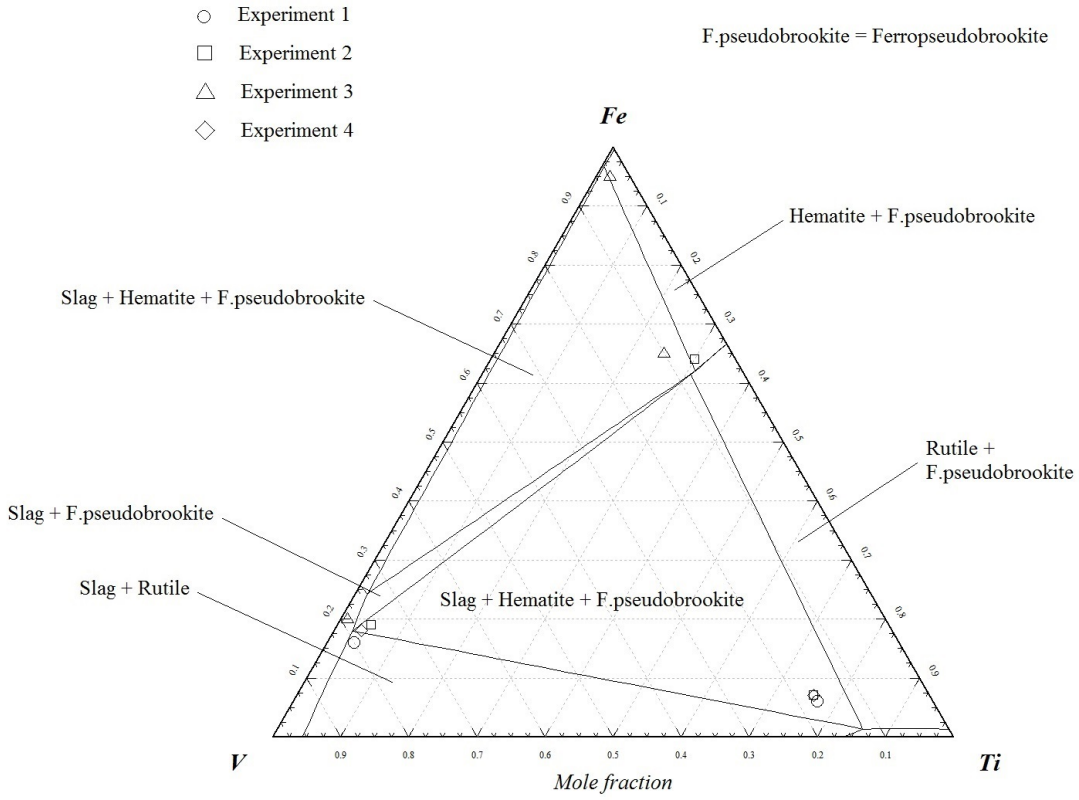

Figure 12.6: Isothermal section at 1000 °C compared with present experimental works.

Table 12.7: Calculated invariant reactions and phase transitions in the Fe−Ti−V−O system in air from optimized parameters.

V mole %	Fe mole %	Temperature °C	Type of invariant	Equilibrium solid phases
94	4	649	Eutectic	V_2O_5, $Fe_2V_4O_{13}$, rutile-SS
92	6	674	Peritectic	$FeVO_4$, $Fe_2V_4O_{13}$, rutile-SS
81	17	849	Eutectic	$FeVO_4$, Ferropseudobrookite-SS, rutile-SS
80	18	860	Peritectic	$FeVO_4$, Ferropseudobrookite-SS, hematite-SS

Given that no previous study had thermodynamically evaluated the Fe-Ti-O system under oxidising conditions, it was undertaken to optimise quasichemical parameters only related to the Fe-Ti-O system. In this case, only one parameter was required to reproduce the liquidus accurately. $\Delta g^{\circ}_{Fe^{3+}-Ti^{4+}}$ has a major influence at compositions of maximum short-range ordering and in this case, maximum short-range ordering occurs at the congruent melting point of the ferropseudobrookite solid solution. Furthermore, no ternary parameters were required for the liquid phase.

Parameters of the rutile and hematite solid solutions were optimised to reproduce Fe_2O_3(s) and TiO_2(s) solubility, thereby re-evaluating parameters previously optimised in Section 12.1. Moreover,

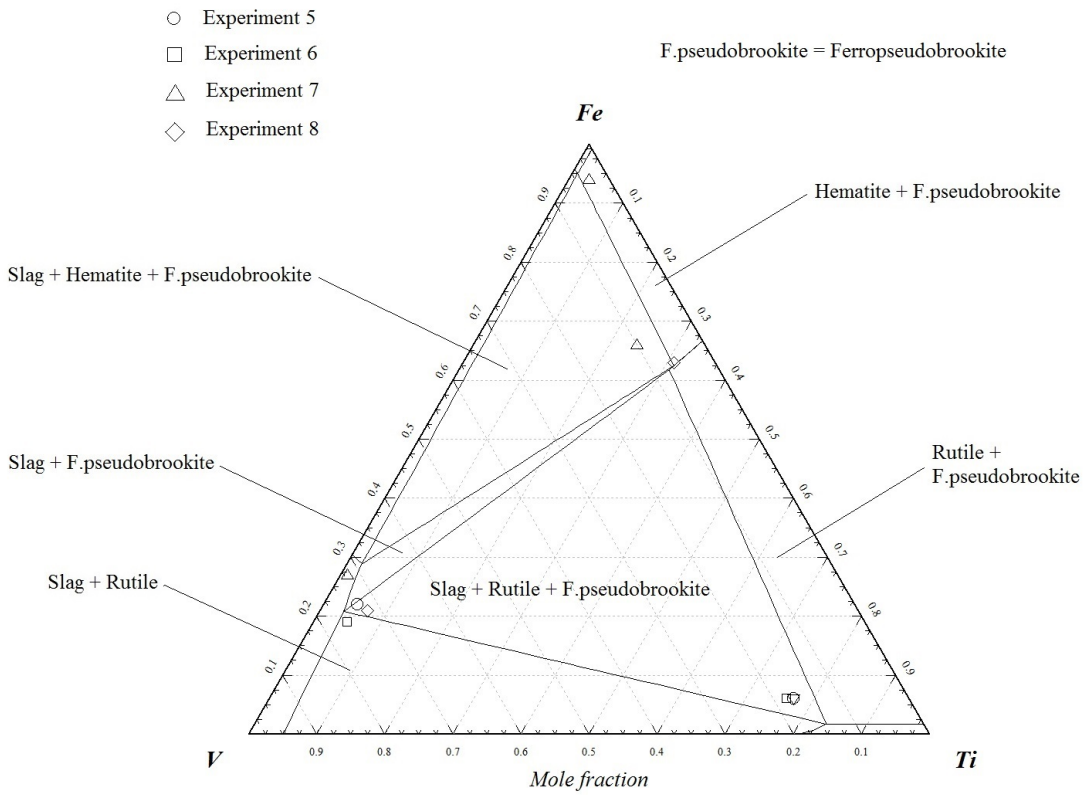

Figure 12.7: Isothermal section at 1100 °C compared with present experimental works.

a small adjustment was made to $G^{\circ}_{V_2O_5(s)-Rut}$ to reproduce solidus data from the Ti-V-O system in air, given that two additional end-members, ($G^{\circ}_{V^{5+}:Va_2}$ and $G^{\circ}_{Va:Va_2}$) were derived and optimised for the expanded model of rutile solid solution.

The composition of the ferropseudobrookite solid solution was accurately described when in equilibrium with the slag and rutile solid solution. However, when the ferropseudobrookite solid solution was in equilibrium with the slag and hematite solid solution, the simple polynomial model failed to reproduce the ratio of Fe to Ti accurately. This can be corrected by including Fe_2O_3(s) and TiO_2(s) in the model of ferropseudobrookite solid solution, and developing the model within the framework of the CEF. However, more solubility and occupancy data of the ferropseudobrookite solid solution in the lower order Fe-T-O system under oxidising conditions are firstly required.

The optimised parameters related to the Fe-Ti-O system were finally cross-checked by back-calculating the lower order Fe-Ti-O phase diagram under oxidizing conditions and comparing to the available Fe-Ti-O phase diagram ($pO_2 = 0.21$ atm) in FactSage.

In the phase diagram estimated with FactSage (Figure 12.12a) there are three solid compounds, Fe_2TiO_5(s), rutile and hematite, and one slag phase. It is stated in the documentation of the FtOxid database that the slag phase of the Fe-Ti-O system has not been evaluated under oxidising conditions (see Section 5.3). There is also an area where a transition of hematite to pure spinel/magnetite takes place. Supported by the experimental results from this study, it is our finding that the phase diagram estimated with FactSage is incomplete and does not show all solution phases in detail.

Conversely, the phases shown in Figure 12.12b have been evaluated in this study from the assessment of the Fe-Ti-V-O system in air. Clearly, better estimations on TiO_2(s) and Fe_2O_3(s) solubility, and slag mixing properties can be made from the assessed parameters of this study. Furthermore, the decomposition temperature of Fe_2TiO_5(s) into Fe_2O_3(s) and TiO_2(s) in Figure 12.12b corresponds significantly better with the reported temperature of 565±15 °C. Although the calculated phase diagram shown in Figure 12.12b describes the slag, hematite and rutile solid solutions better, it is

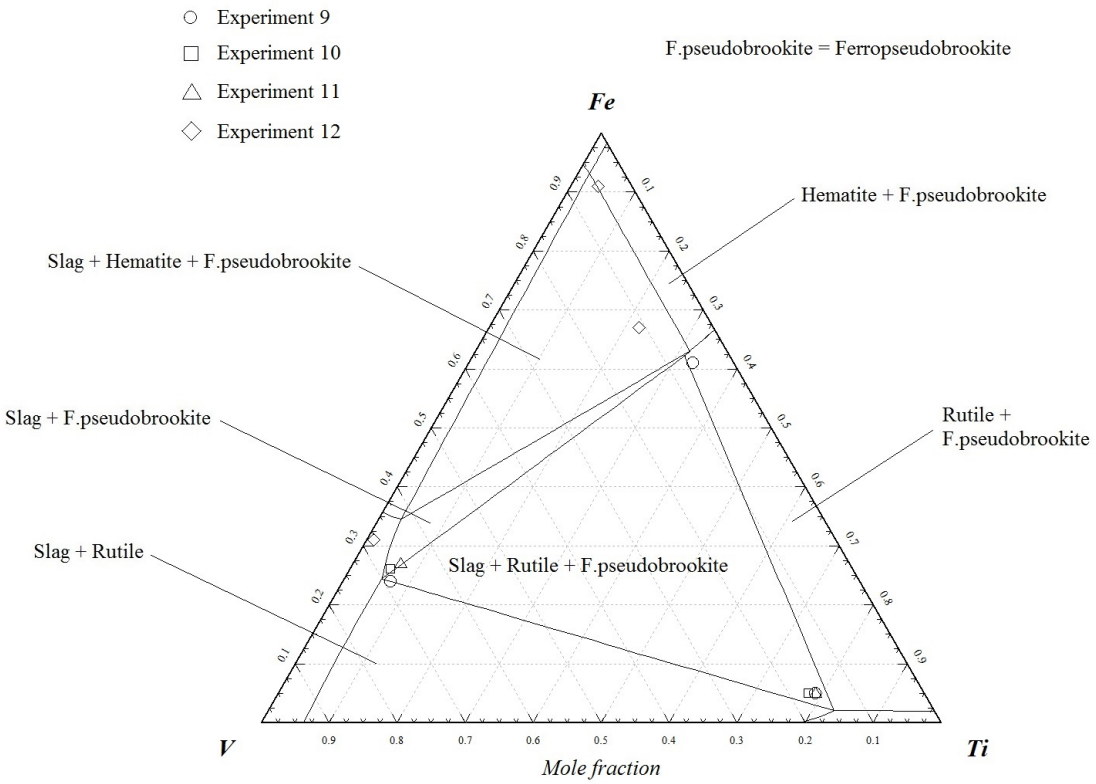

Figure 12.8: Isothermal section at 1200 °C compared with present experimental works.

still incomplete due to the shortage of occupancy data on the ferropseudobrookite and spinel solid solution.

For instance, in these calculations it was assumed that the solid state transition of hematite to spinel or magnetite does not take place. In other words, spinel was not included in the final calculation and the melting point of pure hematite shown in Figure 12.12b may not be entirely correct. The calculated liquidus and solidus compositions above 1400 °C are from extrapolation of the model equations and in reality, a transition is likely to occur at some temperature above 1400 °C. Moreover, some titanium is also likely to report to spinel, which in turn can influence the transition temperature of this hematite solid solution to spinel. More experimental data are required to substantiate such an assumption.

If the spinel phase described in Subsection 6.3.3 was included, a phase diagram shown in Figure 12.12c is calculated. In this case the real melting point of magnetite is estimated accurately, but the model for spinel does not account for the partial dissolution of TiO_2, Therefore, it is unlikely that such a instantaneous transition between hematite and spinel seen in Figure 12.12c can occur, but having said that, it is also difficult to estimate the solubility of TiO_2 and the effect it has on the transition temperature without reliable experimental data. Nevertheless, is important that reasonable calculations be made in these areas where there are a shortage in experimental data, up to the known melting point of magnetite.

12.5.2 Other Thermodynamic Data

No other thermodynamic experimental data were found in the literature pertaining to the Fe-Ti-V-O system under oxidizing conditions. Nevertheless, thermodynamic data such as enthalpies of mixing, heat contents, thermal expansion data and activity data of the slag phase can be calculated from the optimised parameters. This will again demonstrate that phase diagram data alone are sufficient for

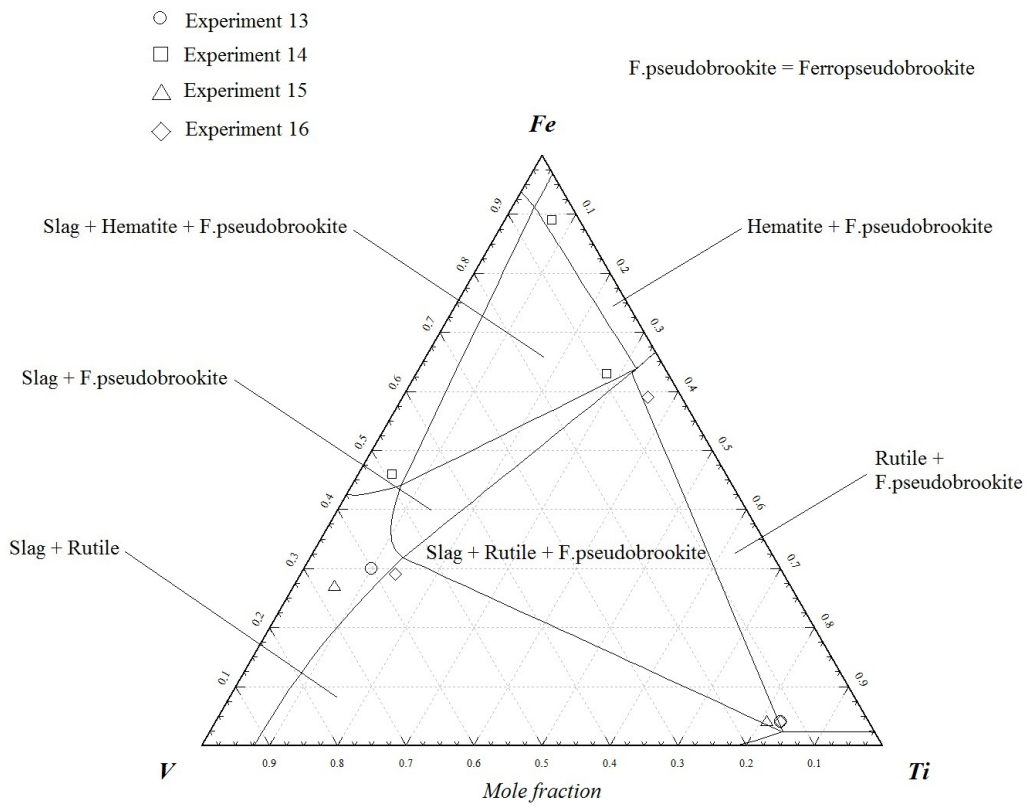

Figure 12.9: Isothermal section at 1300 °C compared with present experimental works.

estimating a set of equations capable of making equilibrium calculations. In this case, the activities of constituents at 1200 and 1400 °C were calculated and shown in Figure 12.13. It is known that the activity of a constituent gives an indication of the extent of deviation from ideal behaviour and is of prime importance in chemical thermodynamics (see also Subsection 10.3.2 and Subsection 11.2.2). The variation of activity with temperature and composition is generally determined experimentally, but can also be estimated from Gibbs energy equations of phases, as in this case.

In most regions at 1400 °C, where equal molar amounts of Fe, Ti and V are present in the system, the activity curves are close to ideal, or exhibit moderate negative deviation from ideality. This implies that the components in the system have a tendency to react with one another to form compounds such as Fe_2TiO_5(s). Strong positive deviation from ideal behaviour is observed for TiO_2 at 1200 °C and low Fe concentration. This behaviour is diminished by the addition of Fe to the system, as seen in the activity curves of TiO_2 in Figure 12.13c and Figure 12.13d. Hence, there is a likelihood of a metastable liquid miscibility gap at sub-liquidus temperatures and high $\mathrm{Ti}/(\mathrm{V}+\mathrm{Ti})$ ratios. This finding is consistent with the observations made in Subsection 11.2.2.

Furthermore, the activity of FeO becomes more significant at 1400 °C, indicating that a small amount of Fe molecules had reduced to Fe^{2+} in order to preserve a state of equilibrium. The activity of Ti_2O_3 was negligible at 1200 and 1400 °C, and was therefore not included in any of the figures. However, it can be expected that a small number of Ti molecules will reduce to Ti^{3+} near the melting point of pure TiO_2 according to the following chemical reaction (Cancarevic, Zinkevich, and Aldinger 2007; Hampl and Schmid-Fetzer 2015):

$$2\mathrm{TiO_2(l)} = \mathrm{Ti_2O_3(l)} + 0.5\mathrm{O_2(g)} \tag{12.1}$$

The temperature range, in which Equation 12.1 becomes favourable is not known, because it is possible that Fe and V ions can increase or decrease the temperature at which the reaction becomes favourable. The same can be said for the possible presence of V^{4+} ions (see Equation 12.2), albeit

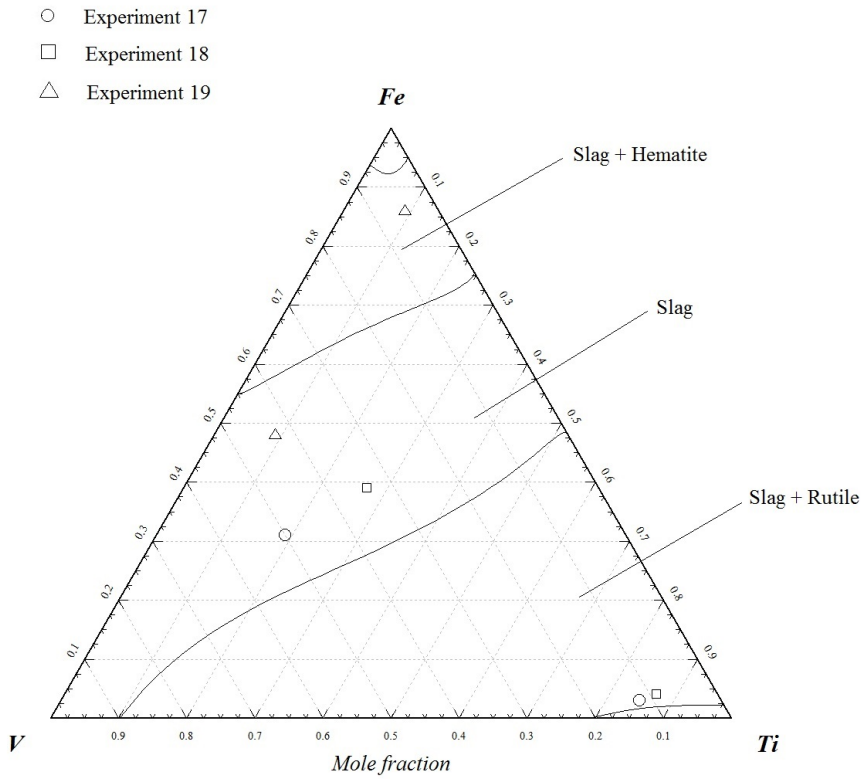

Figure 12.10: Isothermal section at 1400 °C compared with present experimental works.

it was assumed that the liquid phase in the Fe-Ti-V-O system in air comprises V^{5+}, Fe^{3+}, Fe^{2+}, Ti^{4+} and Ti^{3+} ions. In this case, the chemical reaction shown in Equation 12.2 (Suito and Gaskell 1971) can either be stabilized or destabilized with respect to temperature by Fe and Ti ions.

$$V_2O_5(l) = 2VO_2(l) + 0.5O_2(g) \tag{12.2}$$

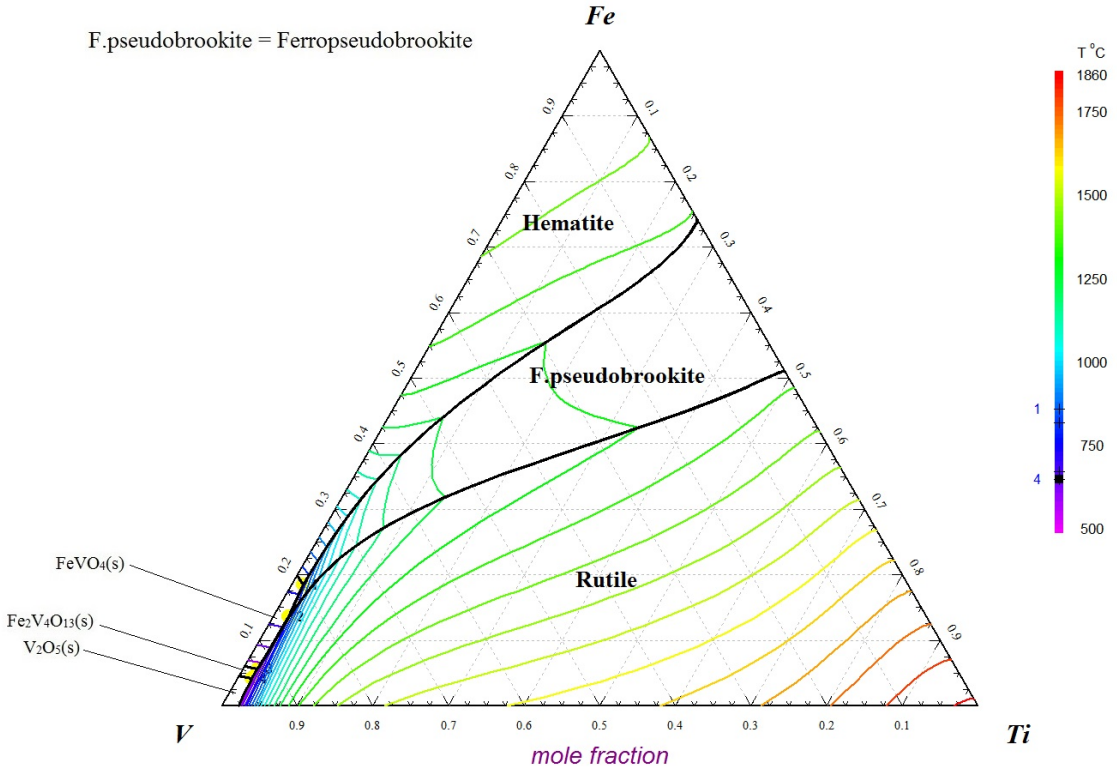

Figure 12.11: Calculated liquidus projection of the Fe-Ti-V-O system in air from optimised parameters.

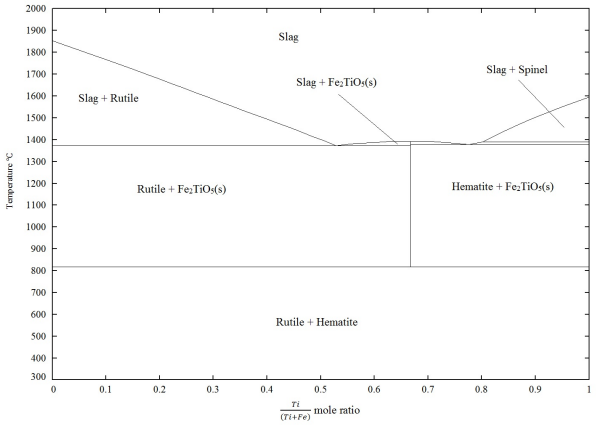

(a) The Fe-Ti-O phase diagram in air estimated with FactSage Bale et al. 2016.

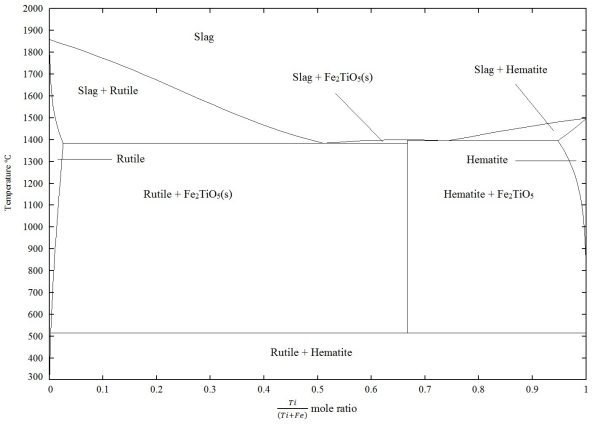

(b) The calculated Fe-Ti-O phase diagrams in air using optimised parameters of this study.

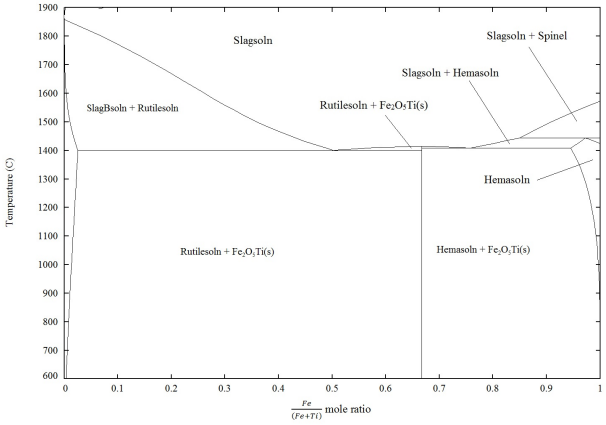

(c) The calculated Fe-Ti-O phase diagrams in air using optimised parameters of this study and the inclusion of spinel solid solution.

Figure 12.12: Comparing the calculated Fe-Ti-O phase diagram in air ($pO_2 = 0.21$ atm) from this study to the phase diagram available in FactSage.

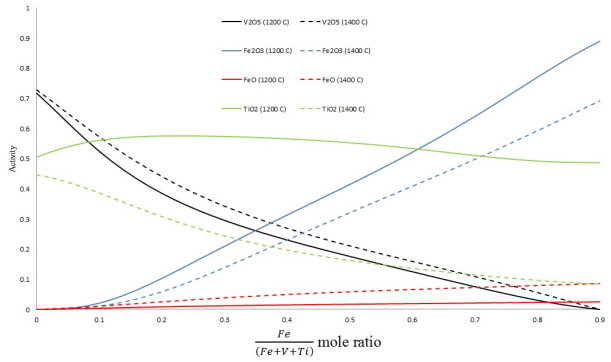

(a) Activities of slag constituents at a fixed Ti composition of 10 mole %.

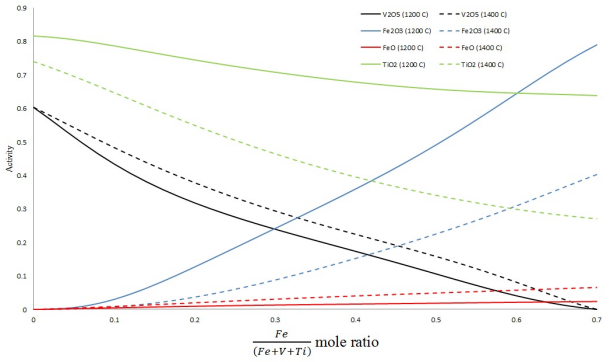

(b) Activities of slag constituents at a fixed Ti composition of 30 mole %.

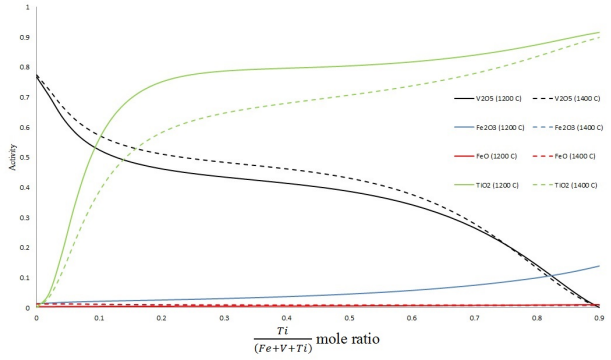

(c) Activities of slag constituents at a fixed Fe composition of 10 mole %.

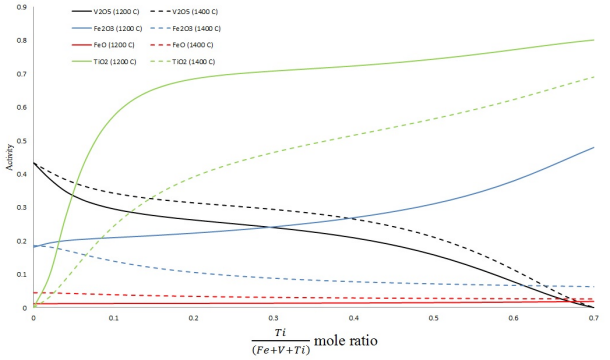

(d) Activities of slag constituents at a fixed Fe composition of 30 mole %.

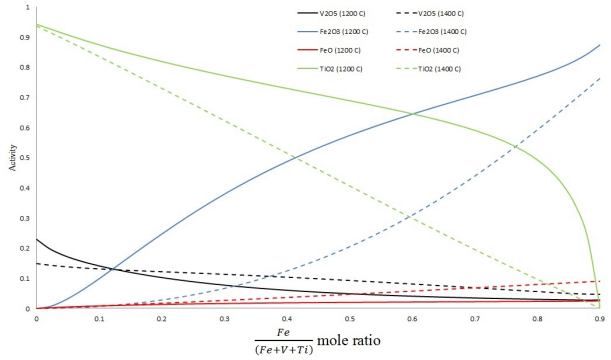

(e) Activities of slag constituents at a fixed V composition of 10 mole %.

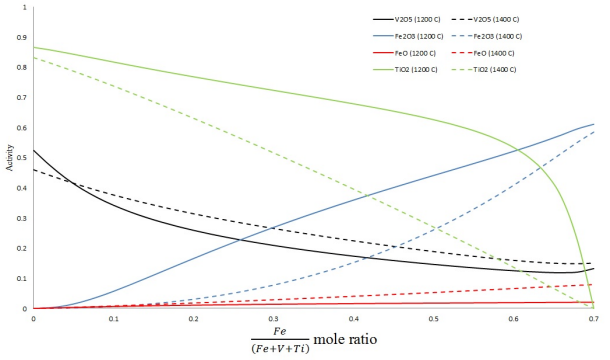

(f) Activities of slag constituents at a fixed V composition of 30 mole %.

Figure 12.13: Activities of slag constituents in the Fe-Ti-V-O system calculated at 1200 and 1400 °C.

Part V

Closure

Overview

Purpose

The main purpose of the closure is to present a concise summary of experimental and modelling results of the Fe-Ti-V-O system in air, and to indicate research areas for future work.

Organization

The closure is divided into two chapters:

- Chapter 13 presents experimental and thermodynamic modelling conclusions of the Fe-V-O, Ti-V-O and Fe-Ti-V-O systems in air.
- Chapter 14 presents recommendations for future work of the Fe-V-O, Ti-V-O and Fe-Ti-V-O systems in air.

Chapter 13

Conclusions

In this study, the thermochemical behaviour of the Fe-V-Ti-O system in air was investigated. The purpose of the study was to develop a customised thermodynamic database from a set of critically assessed experimental data to back-calculate phase diagrams and other thermodynamic properties. This critical set of experimental data is reproduced with thermodynamic modelling techniques, otherwise known as CALPHAD. The CALPHAD technique has been implemented digitally and has been demonstrated to estimate phase equilibria in multi-component systems successfully. FactSage thermochemical software, uses a SOLGASMIX type solver (Gibbs minimisation algorithm) and has several modules for predicting and estimating chemical equilibrium of multi-component systems. However, largely owing to a shortage of experimental data, databases from FactSage modelling software do not have the capability to make equilibrium calculations for systems containing vanadium oxides.

Therefore, in this study the phase assemblage of the Fe-Ti-V-O system in equilibrium with air up to 1400 °C was experimentally characterised by means of an equilibration-quench analysis static technique. Afterwards, phase equilibria data from experiments were used to optimise excess Gibbs and other thermodynamic parameters with the assistance of a Bayesian optimization method coupled with a SOLGASMIX type solver in the FactSage OPTISAGE module. On the basis of the experimental and modelling results, the main conclusions of this study are listed in this section. The chapter is divided into three sections, given that Fe-V-O and Ti-V-O systems in equilibrium with air were experimentally investigated and thermodynamically assessed separately. This chapter also reaches conclusions on the objectives set in Section 2.3 of the thesis.

13.1 Fe-V-O System in Air

13.1.1 Experimental

The solutions and compounds in the Fe-V-O system were successfully characterised by means of equilibration-quench analysis. The orthovanadate, $Fe_2V_4O_{13}$(s), was synthesised and identified with SEM-EDS. The slow formation of $Fe_2V_4O_{13}$(s) explained why some authors did not detect it. The liquidus and solidus composition in the Fe-rich section was experimentally determined and analysed with EPMA. The coexistence of a homogeneous liquid phase and orthovanadate, $FeVO_4$(s) at and below 850 °C, was observed. Above 860 °C, $FeVO_4$(s) decomposed into Fe_2O_3(s) and liquid. Very little precipitation was observed in the liquid phase at 1000 °C, continuing to increase from 1200 °C to 1400 °C, whereas a significant amount of precipitation was observed in the liquid phase at 1400 °C. Precipitation was not subdued by a smaller sample size or a brine quenching medium. Consequently, the calculated standard deviation of measured Fe and V content increased with more precipitation. Nevertheless, the standard deviation of the liquid phase composition was still below or just marginally above 2 % for most samples quenched below 1400 °C.

13.1.2 Thermodynamic Modelling

A thermodynamic assessment was conducted on the basis of phase equilibria results from this and other studies. The MQM and ASM were used to describe the properties of the liquid. The solubility of vanadium in the hematite phase was developed within the framework of the CEF. Two sets of consistent thermodynamic parameters were obtained. Moreover, both liquid models required two parameters to reproduce liquidus data and calculated phase diagrams showed good agreement with experimental data. However, more experimental data are required to determine the transition temperature and vanadium solubility in spinel. All calculated liquidus data above 1400 °C were extrapolated based on the assumption that no vanadium had dissolved in spinel.

13.2 Ti-V-O System in Air

13.2.1 Experimental

The liquidus and solidus composition in the Ti-rich section was experimentally determined and analysed with EPMA and SEM-EDS. The results from SEM-EDS were compromised by the overlapping of the X-ray emission peaks of V and Ti. As a result, results from SEM-EDS and EPMA did not compare very well. The liquid phase had a Ti concentration lower than 5 wt.% in the entire investigated temperature range and coexisted with a rutile solid solution. Very little precipitation was observed in the liquid phase. The rutile solid solution had dissolved a maximum of 15 wt.% V at 1400 °C. This phenomenon has not been reported in any previous investigation.

13.2.2 Thermodynamic Modelling

The MQM and ASM were used to describe the properties of the liquid. The solubility of vanadium in the rutile phase was developed within the framework of the CEF. Two sets of consistent thermodynamic parameters were obtained. A set of self-consistent thermodynamic parameters was achieved on the basis of the optimisation considering data from present experiments. Calculated phase diagrams were provided, and both liquid models were successful to reproduce thermodynamic and experimental data. However, better estimations were made with the MQM between 1500 °C and the melting point of pure rutile.

13.3 Fe-Ti-V-O System in Air

In the last part of the investigation, phase equilibria were experimentally investigated in the Fe-Ti-V-O system coupled with thermodynamic evaluation. However, before experiments were carried out, a thermodynamic evaluation was conducted on the Fe-Ti-O system under oxidising conditions, because calculations of this system in FactSage are limited to reducing conditions. A critical assessment of the literature found that data were scarce for the Fe-Ti-O system under oxidising conditions. Therefore, a number of assumptions were required to produce an improved phase diagram.

13.3.1 Experimental

A set of isothermal sections were calculated at 1000 °C, 1100 °C, 1200 °C, 1300 °C and 1400 °C, using ternary interpolation techniques. The Gibbs phase rule was carefully applied, from which a set of plausible starting compositions for experiments on the Fe-Ti-V-O system in air was determined. Polished and coated samples were analysed with EPMA and SEM-EDS. However, the results from SEM-EDS were compromised by the overlapping of the X-ray emission peaks of V and Ti. The results showed that Ti concentration in the V-O slag phase increased when more Fe dissolved in

the slag. This was significant, given that very little TiO_2 dissolved in the slag phase of the Ti-V-O system in air at similar temperatures. Furthermore, it was observed that a small amount of Fe_2O_3(s) and V_2O_5 dissolved in the ferropseudobrookite phase.

13.3.2 Thermodynamic Modelling

Only the MQM was used to describe the properties of the liquid. The liquidus was successfully reproduced by optimizing only parameters applicable to the Fe-Ti-O system. The optimized parameters indicated strong short-range ordering near the congruent melting point of ferropseudobrookite. It should be pointed out that the domination of the ferropseudobrookite associate in the present work is calculated based on the mathematical expression of the Gibbs energy functions, instead of being experimentally confirmed. This also means that the congruent melting point of the ferropseudobrookite solid solution was not experimentally determined, but that the best agreement between experimental and calculated results was achieved when such an assumption was made.

The dissolution of TiO_2 and V_2O_5 in the hematite phase and V_2O_5 and Fe_2O_3 in the rutile phase was developed within the framework of the CEF. Both models were derived and expanded from the Fe-V-O, Ti-V-O and Fe-Ti-O systems. The dissolution of V_2O_5 in the ferropseudobrookite phase was described with a simple polynomial model. A set of self-consistent thermodynamic parameters was achieved on the basis of the optimisation considering data from present experiments. A final set of calculated isothermal sections with superimposed experimental data and liquidus projection was provided, together with calculated temperatures and compositions of invariant reactions.

Chapter 14

Recommendations for Future Work

The results from this study should be extended to multicomponent systems in the future to facilitate the establishment of the complete thermodynamic database containing vanadium oxide. This chapter identifies other areas of future work on the Fe-V-O, Ti-V-O and Fe-Ti-V-O systems in air.

14.1 Fe-V-O System in Air

It is recommended that an experimental technique, which overcomes difficulties from excess precipitation associated with this system, be developed to obtain liquidus and solidus data above 1400 °C. At the same time, the transition temperature of hematite solid solution to spinel solid solution and the solubility of V_2O_5 in spinel can be experimentally investigated.

14.2 Ti-V-O System in Air

Future work can focus on acquiring liquidus and solidus data above 1500 °C; however other thermodynamic data such as enthalpy of mixing for liquid and activities of constituents of the liquid will be more valuable for an accurate description of the liquid phase in a similar temperature range as in this study. The researcher recommends that better understanding be gained of the defect models proposed and subsequently used to model the rutile solid solution. Moreover, the model can be expanded to include non-stoichiometry from oxygen deficiency with V dissolving interstitially.

14.3 Fe-Ti-V-O System in Air

Future work can focus on an experimental investigation of the Fe-Ti-O system under oxidizing conditions to acquire data on the bonding between constituents of the ferropseudobrookite solid solution. This will improve researchers' understanding and knowledge to such an extent that they will be able to make use of the CEF, and have a more accurate representation with regard to bonding between constituents of solubility regions. Because of the poor availability of liquidus data on the Fe-Ti-O system under conditions, the equilibration-quenching analysis technique can be used to acquire data to re-evaluate MQM parameters related to this system. In such a study it will also be possible to confirm experimentally if the ferropseudobrookite solid solution melts congruently, and if so, to estimate a small temperature range in which melting occurs. Such a study can also be expanded to include vanadium oxide to observe if the small solubility of V_2O_5 has an effect on the melting behaviour of ferropseudobrookite solid solution.

It is also recommended that the ASM be used to describe the properties of the liquid phase in the Fe-Ti-V-O system, given that the extrapolation towards higher orders is done with relative

ease and with high accuracy and reliability, in contrast to the MQM, in which extrapolation towards higher orders becomes extremely complicated. Additional shortcomings of the recent modifications of the quasichemical solution model were investigated by Saulov (2007). In this study shortcomings of these modifications are pointed out, and alternative approaches to overcome the concerns are recommended.

Detailed information about phase equilibria (e.g. liquidus temperatures) of the V-Al-Ca-Fe-Na-Ti-Si-O system, especially in the shaking ladle process where reactions take place fast and under reducing conditions, is essential to understand how vanadium distributes among phases. Therefore, for the system to become applicable to this process and other processes used to treat vanadium-containing metallurgical slag, more work needs to be done under reducing conditions. The results from this study can then be combined with results from such studies to expand databases such as the FToxid database in order to estimate the thermochemical behaviour of vanadium-containing oxide systems in FactSage.

Part VI

Appendices

Appendix A

Experimental Data

A.1 Normalised Data from Literature

A.1.1 Fe-V-O System in Air

In the assessment of the Fe-V-O system in air, phase diagram data from Fotiev, Cheshnitskii, and Surat (1983) and Walczak et al. (1985) were included in the critical set of data. The normalised phase diagram data in Table A.1, Table A.2 and Table A.3 are presented in the form, $\frac{x}{x+y}$ mole fraction, which was also the format of data entered in OPTISAGE (see Appendix C) experimental groups.

Table A.1: Normalised liquidus data used for the thermodynamic assessment of the Fe-V-O system in air.

This study (From EPMA)			Fotiev, Cheshnitskii, and Surat (1983)			Walczak et al. (1985)		
Temperature °C	Mole Fraction V/(V+Fe)	Mole Fraction Fe/(Fe+V)	Temperature °C	Mole Fraction V/(V+Fe)	Mole Fraction Fe/(Fe+V)	Temperature °C	Mole Fraction V/(V+Fe)	Mole Fraction Fe/(Fe+V)
700	0.96	0.04	699	0.94	0.06	636	0.94	0.06
750	0.94	0.06	737	0.92	0.08	672	0.92	0.08
800 (SS)	0.91	0.09	773	0.9	0.1	706	0.9	0.1
800	0.87	0.13	808	0.88	0.12	738	0.88	0.12
850	0.87	0.13	840	0.86	0.14	768	0.86	0.14
860	0.83	0.17	871	0.84	0.16	797	0.84	0.16
900	0.81	0.19	899	0.82	0.18	824	0.82	0.18
950	0.80	0.20	926	0.8	0.2	849	0.8	0.2
1000	0.79	0.21						
1050	0.76	0.24						
1100	0.74	0.26						
1150	0.72	0.28						
1200	0.69	0.31						
1250	0.67	0.33						
1300	0.65	0.35						
1350	0.60	0.40						
1400	0.57	0.43						

Table A.2: Normalised solidus data used for the thermodynamic assessment of the Fe-V-O system in air.

This study (From EPMA)			Fotiev, Cheshnitskii, and Surat (1983)			Walczak et al. (1985)		
Temperature °C	Mole Fraction V/(V+Fe)	Mole Fraction Fe/(Fe+V)	Temperature °C	Mole Fraction V/(V+Fe)	Mole Fraction Fe/(Fe+V)	Temperature °C	Mole Fraction V/(V+Fe)	Mole Fraction Fe/(Fe+V)
800	0.015	0.985						
860	0.022034	0.978						
875	0.024346	0.976						
900	0.023301	0.977						
950	0.024481	0.976						
1000	0.026709	0.973						
1050	0.032739	0.967						
1100	0.037891	0.962	No data available			No data available		
1150	0.041715	0.958						
1200	0.056733	0.943						
1250	0.058758	0.941						
1300	0.061985	0.938						
1350	0.072709	0.927						
1400	0.069965	0.930						

Table A.3: Additional data of invariant reactions used for the thermodynamic assessment of the Fe-V-O system in air.

Type of invariant reaction	This study			Fotiev, Cheshnitskii, and Surat (1983)			Walczak et al. (1985)		
	Temperature °C	Mole Fraction V/(V+Fe)	Mole Fraction Fe/(Fe+V)	Temperature °C	Mole Fraction V/(V+Fe)	Mole Fraction Fe/(Fe+V)	Temperature °C	Mole Fraction V/(V+Fe)	Mole Fraction Fe/(Fe+V)
Eutectic: $V_2O_5(s) + Fe_2V_4O_{13}(s) = Liquid$	No data available			658	0.97	0.03	615	0.95	0.05
				656	0.95	0.05	618	0.9	0.1
				663	0.9	0.1	614	0.85	0.15
				656	0.85	0.15	612	0.8	0.2
				655	0.8	0.2	620	0.75	0.25
				659	0.75	0.25	616	0.7	0.3
Peritectic: $Fe_2V_4O_{13}(s) = FeVO_4(s) + Liquid$	No data available			700	0.9	0.1	662	0.9	0.1
				698	0.85	0.15	667	0.85	0.15
				702	0.8	0.2	665	0.8	0.2
				701	0.75	0.25	669	0.75	0.25
				700	0.7	0.3	662	0.7	0.3
Peritectic: $FeVO_4(s) = Fe_2O_3(s) + Liquid$	850	0.83	0.17	870	0.8	0.2	850	0.8	0.2
	860	0.81	0.19	869	0.75	0.25	847	0.75	0.25
				868	0.7	0.3	852	0.7	0.3
				874	0.65	0.35	848	0.65	0.35
				870	0.6	0.4	850	0.6	0.4
				875	0.55	0.45	851	0.55	0.45

A.1.2 Ti-V-O System in Air

Normalised liquidus and solidus data used in the thermodynamic assessment of the Ti-V-O system in air are given in Table A.4 and are in the same format as in Subsection A.1.1. No other data for this system were found in the literature.

Table A.4: Additional liquidus and solidus data used for the thermodynamic assessment of the Ti-V-O system in air.

Liquidus data			Solidus data		
Temperature °C	Mole Fraction V/(V+Ti)	Mole Fraction Ti/(Ti+V)	Temperature °C	Mole Fraction V/(V+Ti)	Mole Fraction Ti/(Ti+V)
700	0.971	0.029	700	0.069	0.931
750	0.970	0.030	750	0.081	0.919
800	0.966	0.034	800	0.098	0.902
850	0.960	0.040	850	0.108	0.892
900	0.958	0.042	900	0.120	0.880
950	0.958	0.042	950	0.132	0.868
1000	0.949	0.051	1000	0.144	0.856
1050	0.943	0.057	1050	0.177	0.823
1100	0.942	0.058	1100	0.200	0.800
1150	0.939	0.061	1150	0.210	0.790
1200	0.936	0.064	1200	0.212	0.788
1250	0.933	0.067	1250	0.228	0.772
1300	0.926	0.074	1300	0.242	0.758
1350	0.914	0.086	1350	0.245	0.755
1400	0.913	0.087	1400	0.243	0.757
1450	0.910	0.090	1450	0.230	0.770
1500	0.905	0.095	1500	0.225	0.775

A.1.3 Fe-Ti-V-O System in Air

Normalised liquidus and solidus data used in the thermodynamic assessment of the Fe-Ti-V-O system in air are given in Table A.5 in the same format as in Subsection A.1.1. No other data for this system were found in the literature.

Table A.5: Additional liquidus and solidus data used for the thermodynamic assessment of the Fe-Ti-V-O system in air.

	Liquidus			Solidus 1 (Rutile-SS or hematite-SS)					
	Mole Fraction			Mole Fraction			Mole Fraction		
Temperature °C	Ti/(Ti+V+Fe)	Fe/(Ti+V+Fe)	V/(Ti+V+Fe)	Ti/(Ti+V+Fe)	Fe/(Ti+V+Fe)	V/(Ti+V+Fe)	Ti/(Ti+V+Fe)	Fe/(Ti+V+Fe)	V/(Ti+V+Fe)
1000	0.04	0.16	0.80	0.77	0.06	0.17			
1000	0.04	0.19	0.76	0.75	0.07	0.17	0.30	0.64	0.06
1000	0.01	0.20	0.79	0.02	0.95	0.03	0.22	0.67	0.11
1000	0.05	0.18	0.78	0.76	0.07	0.17			
1100	0.05	0.22	0.73	0.77	0.06	0.17			
1100	0.04	0.19	0.76	0.76	0.06	0.18			
1100	0.02	0.27	0.72	0.03	0.94	0.03	0.23	0.67	0.11
1100	0.06	0.21	0.72	0.76	0.06	0.17	0.31	0.63	0.06
1200	0.07	0.24	0.69	0.79	0.05	0.16	0.32	0.61	0.06
1200	0.06	0.26	0.68	0.78	0.05	0.17			
1200	0.07	0.27	0.66	0.79	0.05	0.16			
1200	0.01	0.31	0.68	0.05	0.91	0.05	0.22	0.66	0.12
1300	0.09	0.31	0.61	0.83	0.04	0.13			
1300	0.04	0.46	0.49	0.07	0.89	0.04	0.27	0.64	0.09
1300	0.05	0.28	0.68	0.81	0.04	0.15			
1300	0.13	0.31	0.56	0.83	0.04	0.13	0.36	0.58	0.06
1400	0.15	0.33	0.52	0.85	0.03	0.12			
1400	0.23	0.41	0.36	0.87	0.04	0.09			
1400	0.10	0.46	0.44	0.11	0.85	0.04			

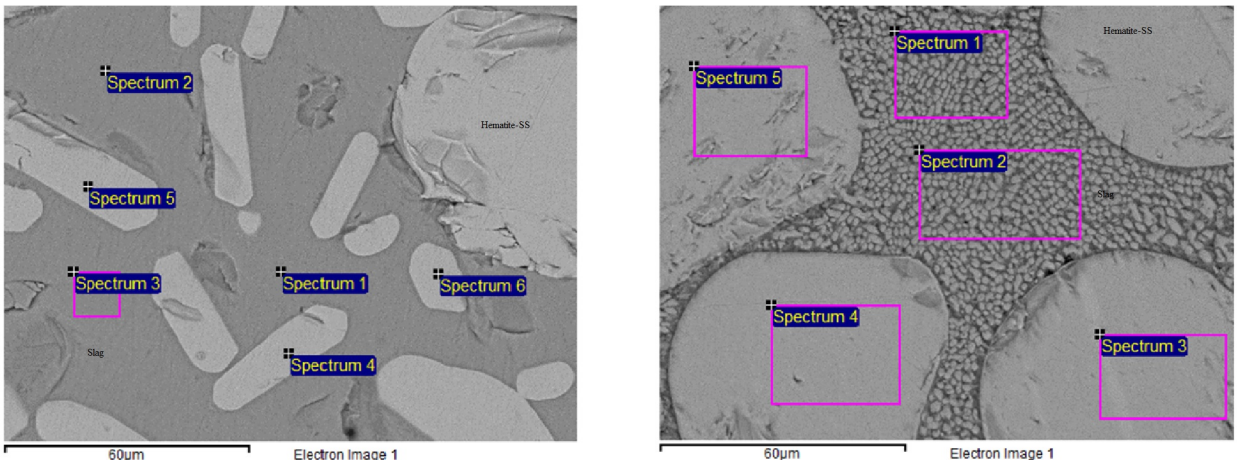

(a) Sample at 900 °C. (b) Sample at 1400 °C.

Figure A.1: Samples from the Fe-V-O system in air analysed with SEM-EDS.

A.2 Examples of Samples Analysed with SEM-EDS

All samples from equilibration-quench analysis experiments were analysed with SEM-EDS and EPMA. Both techniques were quantitative and the results compared well. However, SEM-EDS has better image capturing capabilities, therefore it will be easier to demonstrate the procedure followed to analyse polished sections from samples.

A.2.1 Fe-V-O System in Air

The samples analysed at 900 and 1400 °C are used to visually illustrate the procedure followed to analyse samples with and without precipitation.

The BSD visuals shown in Figure A.1 were analysed at a magnification of 2000 "X" and an accelerating voltage of 15 KV. These were the settings at which the SEM-EDS was calibrated for full quantitative analysis. To analyse a sample quenched at 900 °C quantitatively, at least 10 spots or small rectangles were analysed throughout well-polished sections. Typically, three to five sections were randomly chosen and analysed. Calculated standard deviations of slag phases with no or little precipitation were smaller than 1. Typical raw data of sections analysed in Figure A.1 from SEM-EDS are given in the format shown in Table A.6.

For a sample quenched at 1400 °C, at least 15 large rectangles were analysed. Samples quenched at 1250 °C and higher have notable precipitation and calculated standard deviations are larger than 1. In this case, four to six sections were randomly chosen and analysed. Data from all sections and samples are evaluated and processed and given as one final set of values in Table 10.2.

Table A.6: Raw data of sections analysed for samples quenched at 900 °C and 1400 °C.

	Section of Sample at 900 C					Section of Sample at 1400 C			
Spectrum	O	K	V	Fe	Total	O	V	Fe	Total
1	21.2	0.26	46.81	13.84	82.11	24.35	27.06	37.44	88.85
2	22.76	0.23	46.86	13.96	83.8	24.7	27.27	37.34	89.31
3	23.97	0.25	46.99	14.22	85.42	24.22	4.36	63.3	91.88
4	30.93		2.17	67.23	100.34	24.72	4.4	64.29	93.41
5	30.48		2.08	67.95	100.51	24.65	4.58	64.17	93.4
6	31.09		2.39	67.57	101.05				

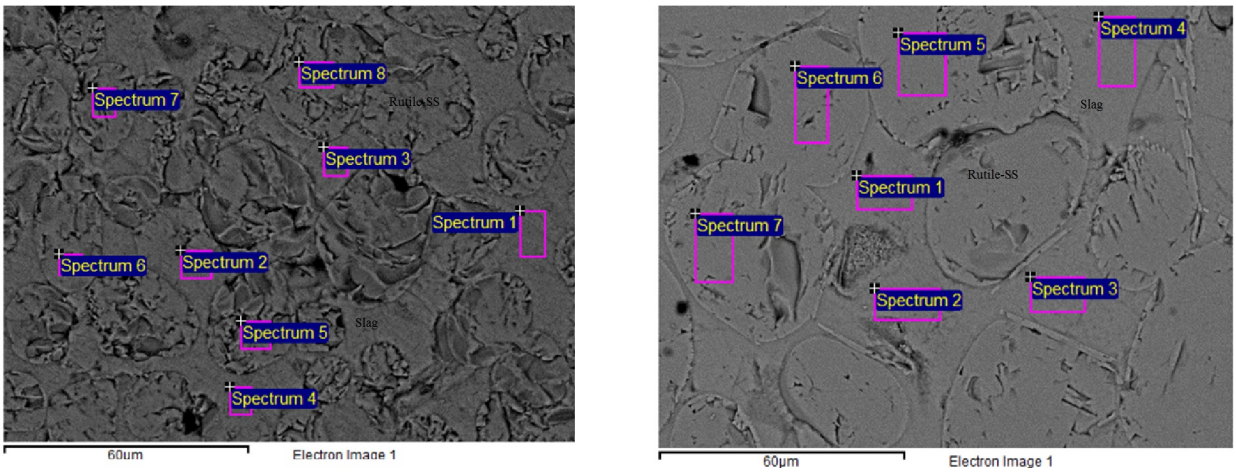

(a) Sample at 1000 °C. (b) Sample at 1400 °C.

Figure A.2: Samples from the Ti-V-O system in air analysed with SEM-EDS.

A.2.2 Ti-V-O System in Air

Two sections from samples quenched at 1000 and 1400 °C for the Ti-V-O system in air that were analysed with SEM-EDS are shown in Figure A.2. The raw compositional data of the slag and rutile solid solution are given in Table A.7. Little or no precipitation was observed for a sample quenched at 1400 °C. All other settings and procedures followed were identical to that of Subsection A.2.1.

Table A.7: Raw data of sections analysed for samples quenched at 1000 °C and 1400 °C.

	Section of Sample at 1000 C				Section of Sample at 1400 C			
Spectrum	O	Ti	V	Total	O	Ti	V	Total
1	21.34	2.62	55.66	79.63	23.42	4.11	55.01	82.54
2	22.31	2.19	54.84	79.33	25.24	3.53	55.69	84.45
3	21.6	2.94	55.95	80.48	23.77	3.95	56.19	83.92
4	22.39	22.32	37.84	82.55	23.75	4.24	54.85	82.84
5	28.81	51.54	9.53	89.88	24.57	45.72	15.57	85.86
6	27.84	52.65	9.34	89.83	25.29	45.72	15.81	86.82
7	31.16	52.42	9.46	93.04	25.71	46.27	15.84	87.82
8	28.25	51.46	9.13	88.84				

A.2.3 Fe-Ti-V-O System in Air

For experiments of the Fe-Ti-V-O system in air, two or three condensed phases were produced. In this case, a sample quenched at 1200 °C with two condensed phases in equilibrium air and a sample quenched at 1200 °C with three condensed phases in equilibrium air, are given in Figure A.3. No significant precipitation is observed. The raw compositional data of the slag, rutile and solid solution and Fe_2TiO_5 (only present in Figure A.3b) are given in Table Table A.8.

A.3 Repeatability of Experiments

Each experiment in the Fe-V-O, Ti-V-O and Fe-Ti-V-O systems was repeated at least once to ensure confidence in the experimental set-up and procedure. Experiments were repeated after the first set of experiments had been conducted for each system.

During the time in which experiments were carried out, the thermocouple was replaced after the first set of experiments had been carried out on the Fe-V-O system in air. The broken S-type thermocouple was probably caused by exposure to the high temperature and corrosive environment.

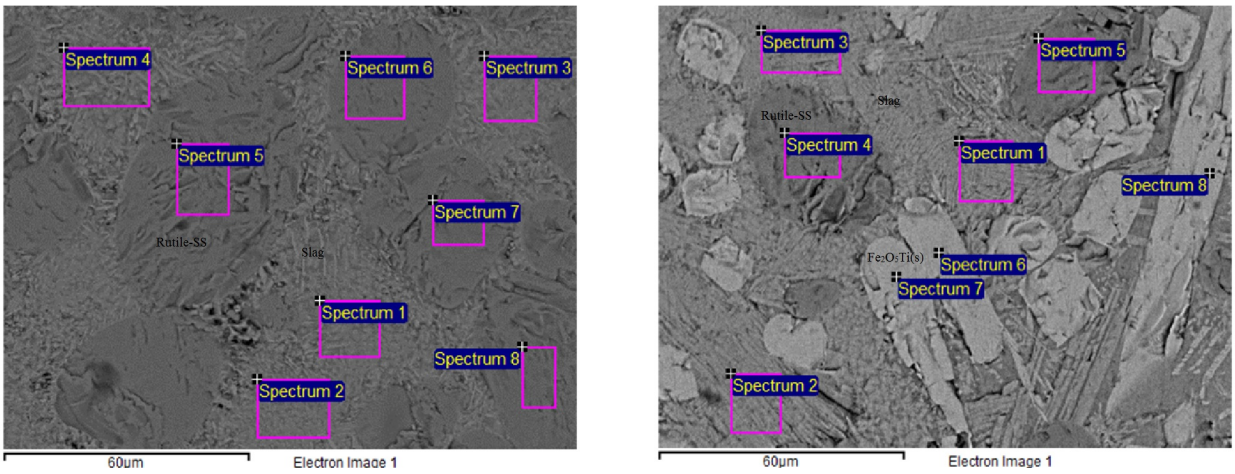

(a) Sample with two condensed phases.

(b) Sample with three condensed phases.

Figure A.3: Samples from the Fe-Ti-V-O system in air at 1200 °C analysed with SEM-EDS.

Table A.8: Raw data of sections analysed for samples quenched at 1200 °C.

	Sample with 2 condensed phases					Sample with 3 condensed phases				
Spectrum	O	Ti	V	Fe	Total	O	Ti	V	Fe	Total
1	20.13	3.86	40.87	16.97	81.83	17.94	4.94	38.47	16.44	77.78
2	20.37	3.75	41.71	16.52	82.35	19.07	5.44	38.89	17.09	80.49
3	19.07	3.65	40.47	16.67	79.85	19.18	5.28	38.82	16.48	79.76
4	21.03	3.38	41.51	16.94	82.86	30.43	46.00	10.79	3.75	90.97
5	28.43	46.23	10.93	3.44	89.04	27.72	44.92	10.36	3.46	86.47
6	27.35	45.98	11.12	3.31	87.77	28.64	18.85	5.05	41.8	94.34
7	26.29	45.84	10.92	3.30	86.35	31.48	19.29	4.6	42.41	97.79
8	24.20	45.13	10.87	3.30	83.51	29.09	18.45	4.91	41.09	93.55

As a result, the replaced thermocouple had to be calibrated and the hot zone in the furnace had to be determined again. This was required each time the thermocouple was replaced. This is just one reason why it is important to repeat experiments, particularly when a thermocouple has been replaced. No other major experimental malfunctions were experienced during the time in which experiments were carried out.

The liquidus composition of the Fe-V-O system in air is used as an example in which the first set and second set of experiments are compared. The second set of experiments were carried out after the thermocouple had been replaced.

In Figure A.4 a trend line is observed, which was calculated as the average composition between a sample before and after thermocouple replacement. The compositions of Fe and V before and after thermocouple replacement are scattered around the trend lines in Figure A.4a and Figure A.4b, respectively. It is obvious that there was no significant effect on the liquidus composition as a result of the replacement of the thermocouple. In other words, there was a good agreement between the liquidus results before and after thermocouple replacement. Moreover, this result indicates that the replaced thermocouple was correctly calibrated.

However, this result would have been more decisive if a statistical approach had been followed, but given the constraints on experimental consumables and research time, multiple experiments under the same conditions were not possible. For instance, a few experiments could have been conducted at the same temperature, and again at a later stage, provided that a thermocouple or any other auxiliary equipment was replaced. In addition, it is recommended that experiments be repeated even if no experimental equipment is replaced, because of human error. The sample was weighed, introduced into the furnace and prepared for analysis by hand, hence minor and major mistakes were possible. For this reason, experiments were repeated once to determine if any major mistake had been made before and after equilibration.

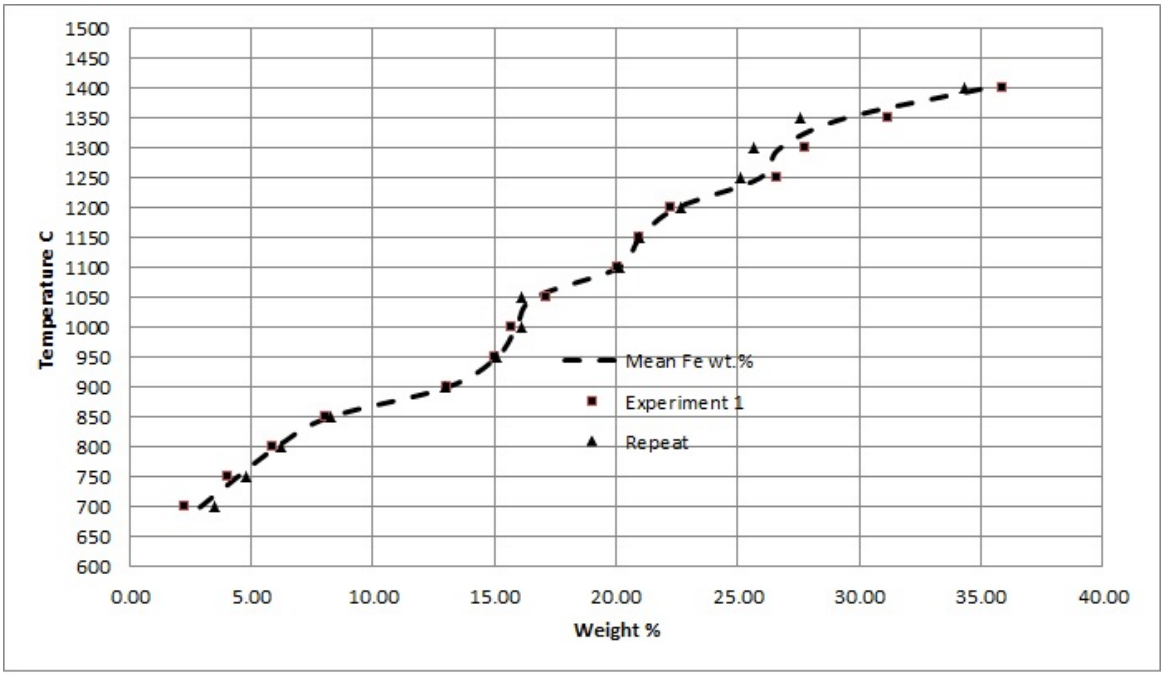

(a) Comparing Fe wt.%.

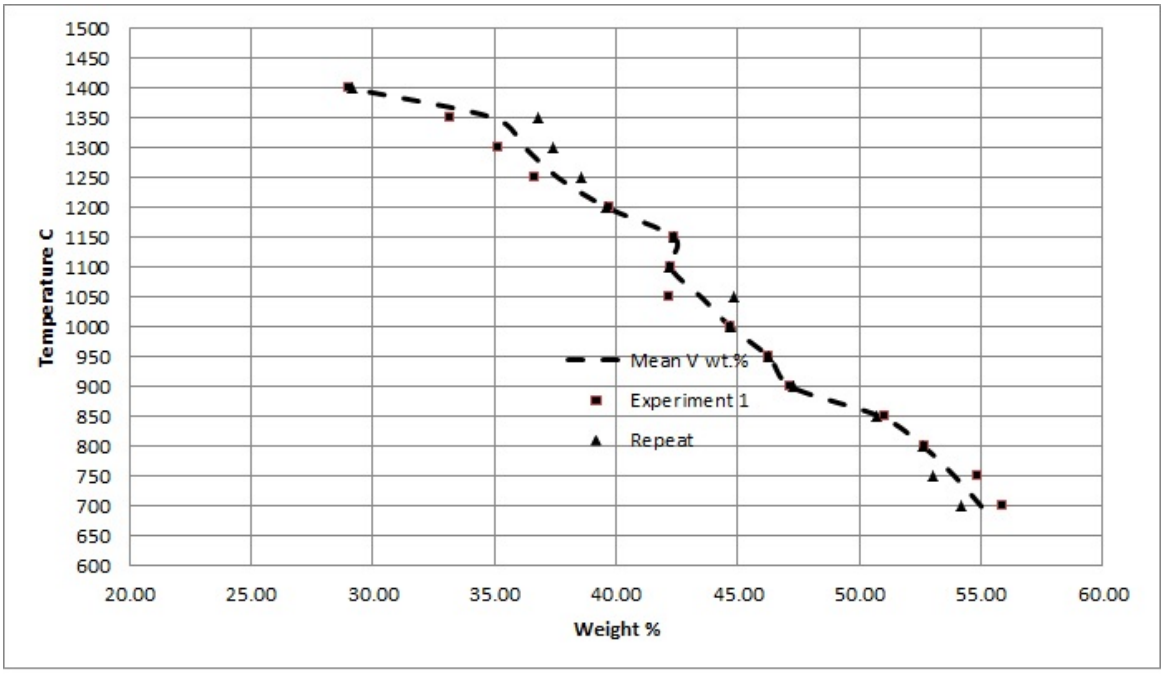

(b) Comparing V wt.%.

Figure A.4: Comparing the first set of liquidus results on the Fe-V-O system in air to a second set of experiments after thermocouple replacement.

A common approach to ascertain if a replaced thermocouple or any other auxiliary equipment had an influence on repeatability would be to analyse the average composition of multiple experiments under identical conditions. This technique, which compares the samples on the basis of their means, is called analysis of variance (ANOVA). ANOVA is a statistical technique that is used to check if the means of two or more groups are significantly different from each other. ANOVA checks the impact of one or more experimental variables (temperature and thermocouple replacement) by comparing the means of different samples (Box, Hunter, and Hunter 2005).

Nevertheless, the repeatability of experiments was adequate, because no significant difference was observed between the first and second set of experiments on all the investigated systems, irrespective of thermocouple replacement.

A.4 Additional Statistical Formulae and Calculations

The following statistical equations were used for processing raw SEM and EPMA data.

Average

The average, or arithmetic mean is given by the following expression (Box, Hunter, and Hunter 2005):

$$(\chi) = \sum x/n \tag{A.1}$$

where x = individual measured values, and n = the number of times an element has been measured. Equation A.1 was used to calculate the arithmetic means of measured elemental compositions presented in Table 10.2, Table 10.2, Table 11.1, Table 11.1, Table 12.3 and Table 12.4.

Standard Deviation

The standard diaviation, or root mean square deviation is given by the following expression (Box, Hunter, and Hunter 2005):

$$(\sigma_x) = (\sum (x - (\chi))^2/n)^{1/2}. \tag{A.2}$$

Equation A.2 was used to calculate the standard deviations of measured elemental compositions presented in Table 10.2, Table 10.2, Table 11.1, Table 11.1, Table 12.3 and Table 12.4.

Appendix B

Additional Molecular and Thermodynamic Data

The molecular masses of some compounds used in the calculations are given in Table B.1.

Table B.1: Molecular masses of some pure compounds used in this study.

Compound	Molecular Mass ($\frac{gram}{mole}$)	Reference
Fe_2O_3	159.69	Bale et al. (2016)
TiO_2	79.866	Bale et al. (2016)
V_2O_5	181.88	Bale et al. (2016)
Ti_2O_3	143.73	Bale et al. (2016)
FeO	71.844	Bale et al. (2016)
Fe_3O_4	231.53	Bale et al. (2016)
$FeVO_4$	170.78	Bale et al. (2016)
$Fe_2V_4O_{13}$	523.45	Bale et al. (2016)
Fe_2TiO_5	239.55	Bale et al. (2016)

The thermodynamic data presented in Table B are the enthalpy of formations, standard entropies and heat capacities of all compounds of the Fe-Ti-V-O system in air before any adjustments were made.

Table B.2: Enthalpies and entropies of pure compounds in the Fe-Ti-V-O system in air before the thermodynamic assessment.

Substance	$\Delta H^0_{f,298}$	S^0_{298}	C_p	C_p range	Reference
Fe_2O_3(s)	-825786.99*	87.73*	$137.00893 - 2907640T^{-2}$	298- 2500 K	Bale et al. (2016)
V_2O_5(s)	-155059000	.13 0.55	$25.97 + 0.05T + 5853.80T^{-0.5} - 76767.61T^{-1} - 754162.65T^{-2}$	298- 943 K	Bale et al. (2016)
$FeVO_4$(s)	-1186800.00	128.04	$129.51 + 0.02471T - 2160000T^{-2}$	298 - 973 K	Kesler et al. (1985) and Cheshnitski, Kozhevnikov, and Fotiev (1985)
$Fe_2V_4O_{13}$(s)	-3600500.00	385.7	$388.83 + 0.07383T - 6506000T^{-2}$	298 - 973 K	Volkov (1979), Kesler et al. (1985), and Cheshnitski, Kozhevnikov, and Fotiev (1985)
TiO_2(s)	-944750.00	50.46	$77.84 - 3367841.01T^{-2} - 402940672.29T^{-3}$	298- 2130 K	Bale et al. (2016)
Fe_2TiO_5(s)	-1738786.72	171.96	$192.59 - 0.02200784T - -3100344T^{-2}$	298- 2130 K	Bale et al. (2016)
V_2O_5(l)	-1491201.97	191.96	$164.31 + 0.024T - 3628206.49T^{-2}$	298 - 600 K	Bale et al. (2016)
			190.79	600 - 3000 K	Bale et al. (2016)
FeO(l)	-234643.15	78.47	$-18.02 + 0.031T + 1500.90T^{-0.5} - 2533299.99T^{-2}$	298 - 1644 K	Bale et al. (2016)
			68.2	1644 - 2000 K	Bale et al. (2016)
Fe_2O_3(l)	-731157.57	145.95	$137.01 - 2907640.00T^{-2}$	298 - 2500 K	Kowalski and Spencer (1995)
TiO_2(l)	-898726.00	72.07	$77.84 - 3367841.01T^{-2} + 402940672.29T^{-3}$	298 - 2130 K	Bale et al. (2016)
			100.416	2130 - 3000 K	Bale et al. (2016)
Ti_2O_3(l)	-898726.00	72.07	$169.96 - 750.22T^{-0.5}1609648.94072T^{-2} - 1565521004T^{-3}$	298 - 2115	Bale et al. (2016)
			100.416	2115 - 2500 K	Bale et al. (2016)

*Hematite exhibits magnetic ordering and these values include the magnetic contribution.

Appendix C

FactSage Example

In Subsection 6.8.1 the principle of data fitting and parameter optimisation along with a set of guidelines for selection of experimental data, reliability of experimental data, determining the effect of adjustable model parameters and verifying the results of an optimisation were discussed. FactSage 7.0 with its ChemSage solver is able to optimise a set of thermodynamic parameters simultaneously by means of its SOLUTION and OPTISAGE module. The SOLUTION module gives one the ability to create, display and edit private non-ideal solution databases using a wide variety of solution models. The OPTISAGE module uses a Bayesian optimisation technique coupled with a ChemSage solver to calculate parameter coefficients. Therefore, it is in the interest of new FactSage users to have a practical demonstration of another example where these modules were used aside from the given example from FactSage documentation (see slideshow of OPTIGAGE module in FactSage 7.0). In the present example SOLUTION and OPTISAGE modules are used to treat the various phase diagram and other thermodynamic data of the Fe-V-O system in air.

C.1 Using the COMPOUND module

C.1.1 Step 1.1: Adding New Compounds

Before the SOLUTION and OPTISAGE modules were used, two new compounds were added to a customised compound database. A new compound database was added by selecting the "file" option, followed by selecting the "new database" option.

C.1.2 Step 1.2: Entering Data for New Compounds

The two orthovanadates, $FeVO_4$(s) and $Fe_2V_4O_{13}$(s), coupled with assigning values to ΔH°_{298}, S°_{298} and C_P, were added to the WIL-customised database. Figure C.1 and Figure C.2 show the steps that were followed to add $FeVO_4$(s) and $Fe_2V_4O_{13}$(s) to a new customised database. The values of ΔH°_{298}, S°_{298} and C_P were acquired from Volkov (1979) and Cheshnitski, Kozhevnikov, and Fotiev (1985) and were first entered. However, values shown in Figure C.1 and Figure C.2 are the optimized ones.

C.2 Using the SOLUTION module

C.2.1 Step 2.1: Creating a New Solution File

The SOLUTION module is launched after the new compounds have been added in Section C.1. In the first step, a new solution file is created by selecting the "new" option from the "file" tab. The solution is named and stored as "Qausisoln" (see Figure C.3).

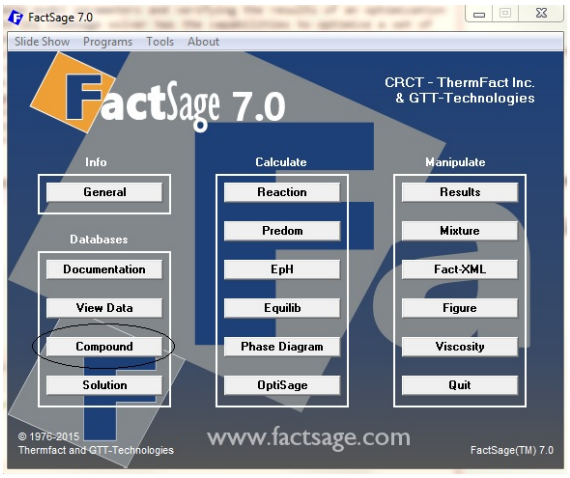

(a) Launching the COMPOUND module.

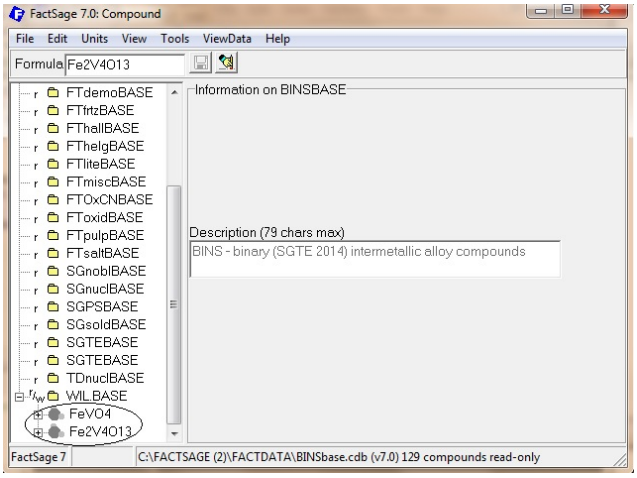

(b) Entering $FeVO_4$(s) and $Fe_2V_4O_{13}$(s) as new compounds using the "add compound" function from the "edit" tab.

Figure C.1: Thermodynamic evaluation example in FactSage: Step 1.1.

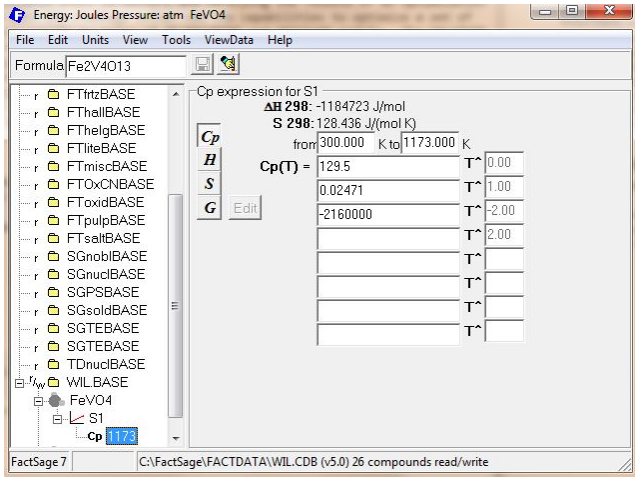

(a) Entering values forΔH_{298}, S_{298} and C_P of compound $FeVO_4$(s).

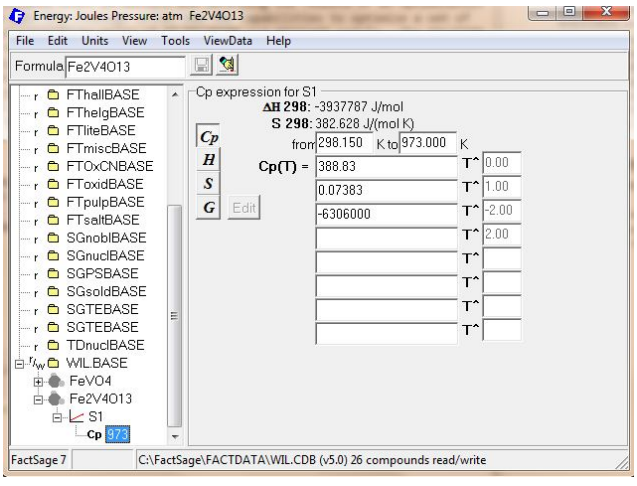

(b) Entering values for ΔH_{298}, S_{298} and C_P of compound $Fe_2V_4O_{13}$(s).

Figure C.2: Thermodynamic evaluation example in FactSage: Step 1.2.

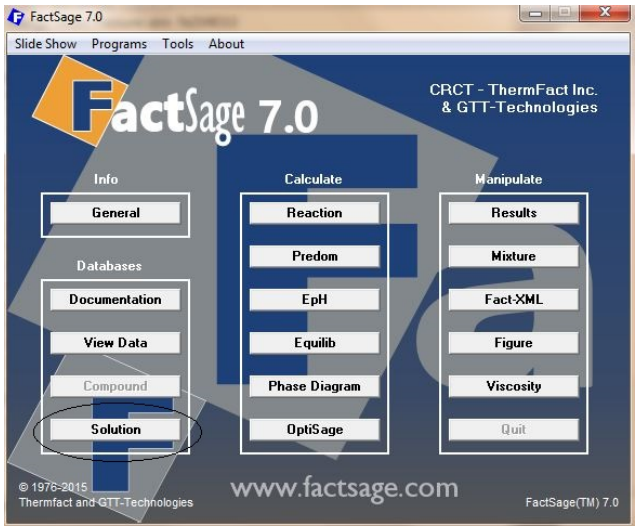

(a) Launching the SOLUTION module.

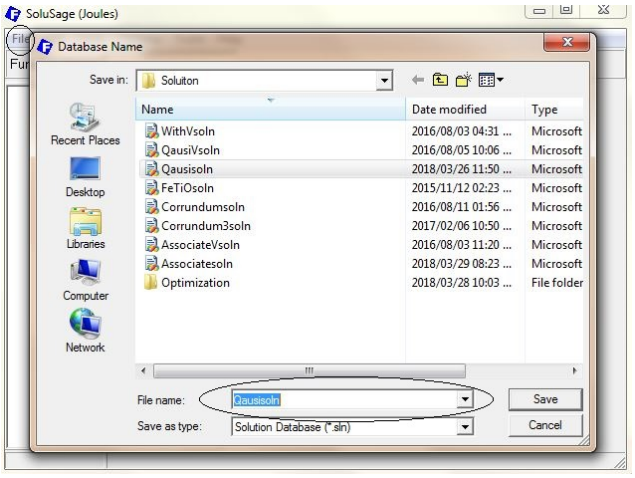

(b) Creating a new solution file, "Qausisoln".

Figure C.3: Thermodynamic evaluation example in FactSage: Step 2.1.

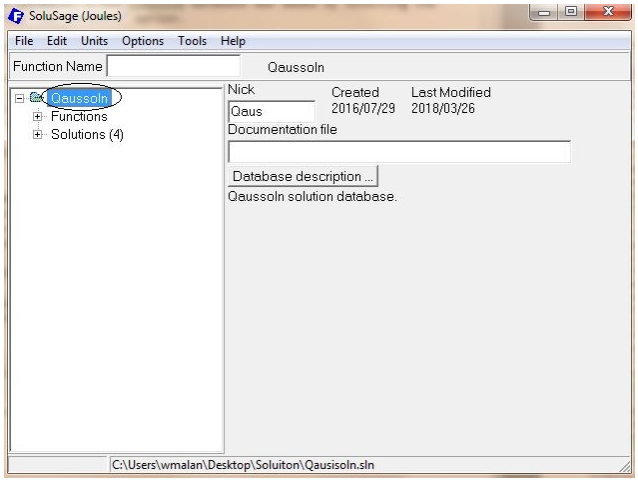

(a) Adding a solution to the "Qaussoln" file.

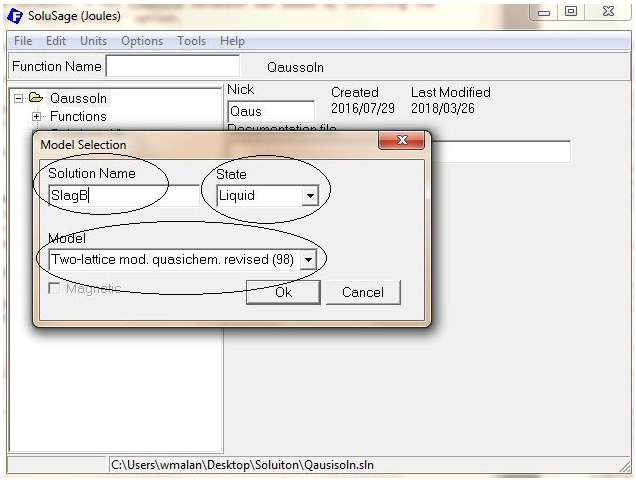

(b) Selecting the state and model for the "SlagB" solution.

Figure C.4: Thermodynamic evaluation example in FactSage: Step 2.2.

C.2.2 Step 2.2 : Creating a Liquid Solution

A new solution is created by selecting the "new solution" option by right-clicking with the mouse cursor on the "Qaussoln" file. The slag phase from the Fe-V-O system in air is used as an illustrative example. From the "model selection" window, the solution is named, "SlagB", the state is "liquid" and the model that is used is the "Two-lattice mod. quasichem. revised" (see Figure C.4).

C.2.3 Step 2.3: Adding Species to the Liquid Solution

Next, all the cation species are added to sub-lattice "A" and oxygen, the only anion specie, is added to the second sub-lattice, "B". Each specie is given a name coupled with assigning a valence and formula. Fe has two valances (3+ and 2+) and V in a slag solution is entered as V_2O_3 with a positive valence of 4 (See Figure C.5a). Furthermore, if a formula is entered, then the formula for the end-member is generated automatically. Va is acceptable notation for a vacancy when vacancies are present on a lattice. The chemical group is kept at 1 because all species are chemically similar.

An end-member is created by selecting one specie from the cation sub-lattice and one specie

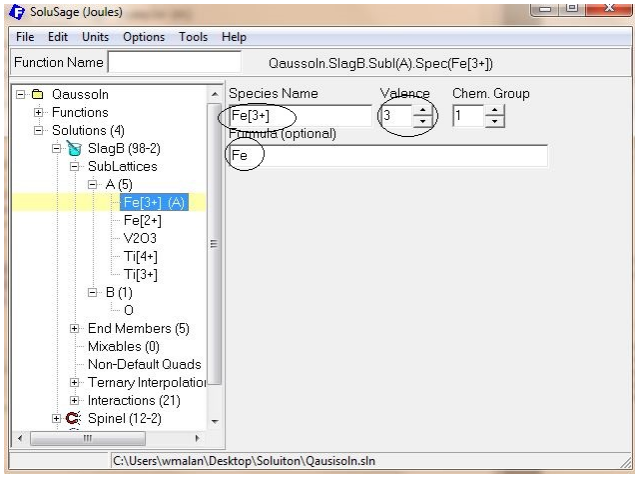

(a) Adding Fe^{2+}, Fe^{3+} and $V_2O_3^{4+}$ to sub-lattice "A" and O to sub-lattice "B".

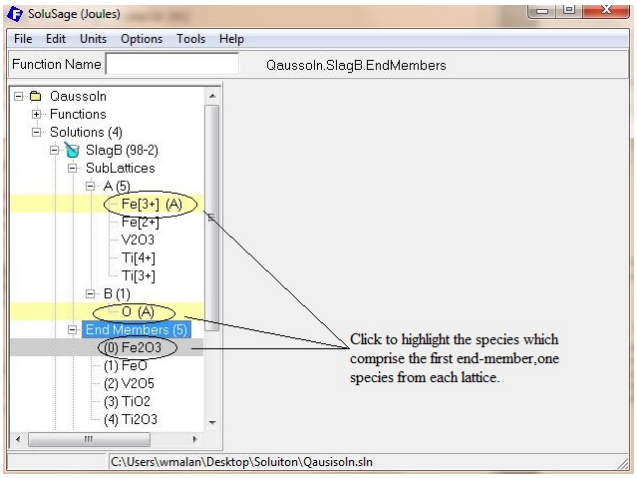

(b) Creation of end-member species from species in sub-lattice "A" and "B".

Figure C.5: Thermodynamic evaluation example in FactSage: Step 2.3.

from the anion specie simultaneously followed by selecting "add end member" from the generated tab. This was done for all species (see Figure C.5b).

C.2.4 Step 2.4: Assigning Gibbs Energy Functions to End-member Species

Each end-member is given a name, preferably the specie's chemical formula and if not neutral, the charge in parentheses next to the chemical formula. However, in this case all end-member species are neutral and a net charge of zero is not written next to the formula. The formula is automatically generated if entered in Subsection C.2.3. The coordination numbers are entered according to Equation 6.21. ζ is set at 2.4, which is also the default value.

The "Gibbs energy function" of all end-member species requires "FUNCTIONS" from the Quassln.fdb file. A function is created by "dragging" the compound from the COMPOUND module onto the functions tab, as shown in Figure C.6a. Thereafter, it is possible to assign a function to the "Gibbs energy function" in the end-member species window, as shown in Figure C.6b. The formula is entered first, followed by the "phase name". The phase names in this case for all end-members are "liquid". The function name must always be consistent with the assigned phase name in the "functions" tab.

C.2.5 Step 2.5: Adding Interactions between Species

In this step, interactions between species are identified and defined as demonstrated in Figure C.7. Quasichemical terms in the expansion for $\Delta g_{Fe^{2+}-V_2O_3^{4+}}$ and $\Delta g_{Fe^{3+}-V_2O_3^{4+}}$ as described in Subsubsection 9.1.5 are added for the pairs $\mathrm{Fe^{2+} - V_2O_3^{4+}}$ and $\mathrm{Fe^{3+} - V_2O_3^{4+}}$ as a function of the pair fractions $\mathrm{X_{Fe^{2+}-Fe^{2+}}}$ and $\mathrm{X_{V_2O_3^{4+}-V_2O_3^{4+}}}$, $\mathrm{X_{Fe^{3+}-Fe^{3+}}}$ and $\mathrm{X_{V_2O_3^{4+}-V_2O_3^{4+}}}$, respectively. The coefficients of the quasichemical terms, $\mathrm{\Delta g^{\circ}_{Fe-V_2O_3^{4+}}}$, $\mathrm{g^{01}_{Fe-V_2O_3}}$ and $\mathrm{g^{10}_{Fe-V_2O_3^{4+}}}$ will be optimised. Where Fe represents Fe^{3+} and Fe^{3+} Moreover, a quasichemical term in the expansion for $\Delta g_{Fe^{2+}-Fe^{3+}}$ will also be added for the pair $\mathrm{Fe^{2+} - Fe^{3+}}$ as a function of the equivalent fractions $\mathrm{Y_{Fe^{2+}}}$ and $\mathrm{Y_{Fe^{3+}}}$. The values of these coefficients were acquired from Degterov et al. (2001).

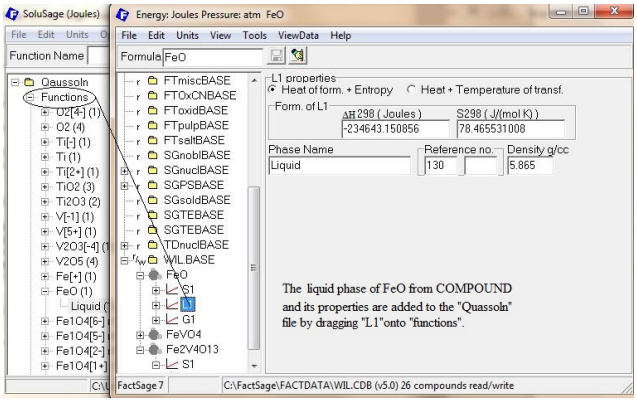

(a) Adding a compound form COMPOUND module to the functions tab in SOLUTION module.

(b) Entering data for end-members.

Figure C.6: Thermodynamic evaluation example in FactSage: Step 2.4.

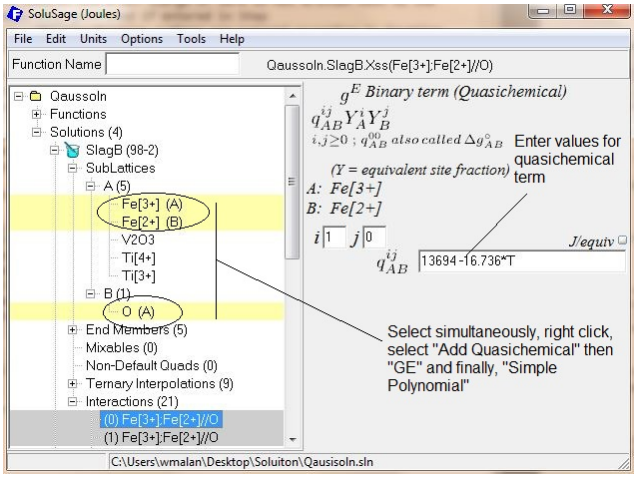

(a) Adding interaction parameters for the pair $Fe^{2+} - Fe^{3+}$.

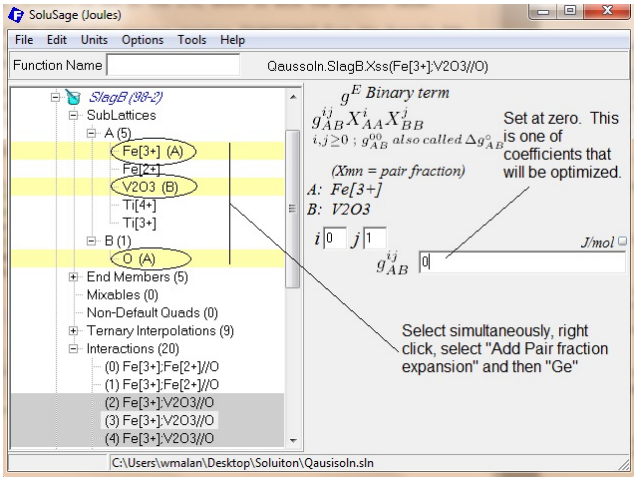

(b) Adding interaction parameters for the pairs $Fe^{2+} - V_2O_3$ and $Fe^{3+} - V_2O_3$.

Figure C.7: Thermodynamic evaluation example in FactSage: Step 2.5.

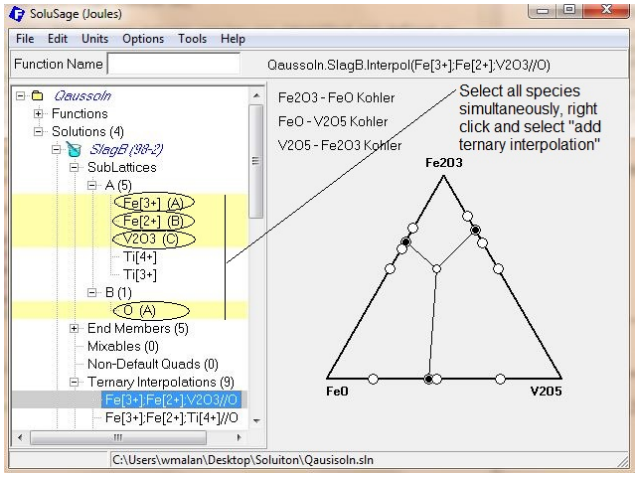

(a) Selecting the ternary interpolation configuration for the Fe^{3+}, Fe^{2+} and $V_2O_3^{4+}$ sub-system.

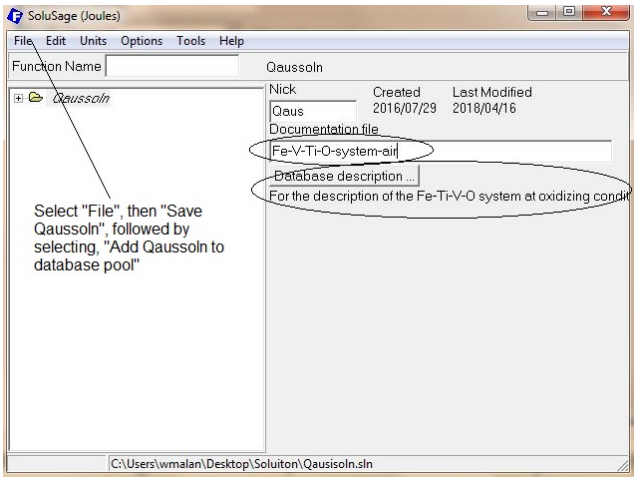

(b) Saving and adding the "Qaussoln" as a customised database to the solution database of FactSage.

Figure C.8: Thermodynamic evaluation example in FactSage: Step 2.6.

C.2.6 Step 2.6: Ternary Interpolation

There are three species on the cation sub-lattice, namely, Fe^{3+}, Fe^{3+} and $V_2O_3^{4+}$. Hence, binary interaction terms need to be interpolated into a ternary solution phase and knowing that Fe^{3+}, Fe^{3+} and $V_2O_3^{4+}$ are all members of the same chemical group, an all "Kohler" configuration was used as ternary interpolation technique (see Figure C.8a). The ternary interpolation techniques were discussed in Section 6.4.

This step-by-step guide can be followed meticulously to set up and create a solution file for the Fe-Ti-O, Ti-V-O and Fe-Ti-V-O systems in air. Moreover, solutions are stored as one solution file (and given a description), ultimately to have the capability to make calculations for the Fe-Ti-V-O system in air (see Figure C.8b).

C.3 Using the OPTISAGE module

C.3.1 Step 3.1: Creating and Storing a ChemSage File

Step 3.1.1

Before optimisation of quasichemical terms and other thermodynamic properties, a "ChemSageFile" needs to be generated in the EQUILIB module. The EQUILIB module is launched and three reactants, Fe, V and O_2, are entered. The elements are preferred to the oxides Fe_2O_3 and V_2O_5 because the oxidation states of Fe and V are dependent on pO_2.

Step 3.1.2

Next, from the reactants window, the "Data Search" tab is selected and from the "Private databases", "Qaus" and "Wil." are activated after both have been added from the directories in which they were stored. These are the customised solution and compound databases created and stored in Steps 1 and 2 (Section C.1 and Section C.2). All other databases are deactivated except for the elemental database (see Figure C.10a).

In the main menu of EQUILIB module (see Figure C.10b), under "Products", the ideal gas phase and pure solids are activated. Moreover, right-clicking on "pure solids" opens a window, displaying

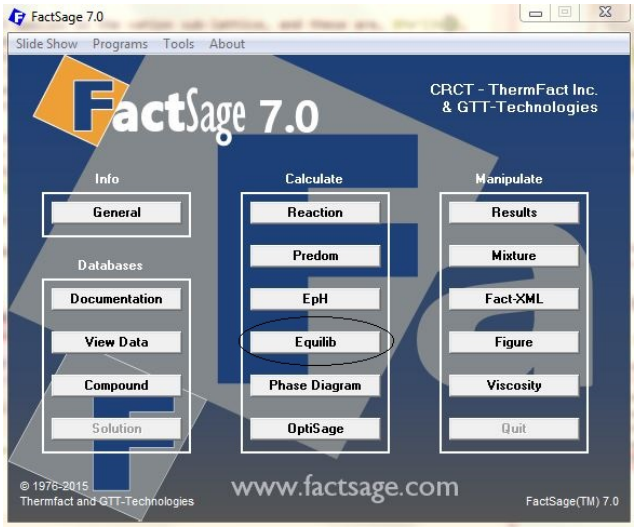

(a) Launching the EQUILIB module.

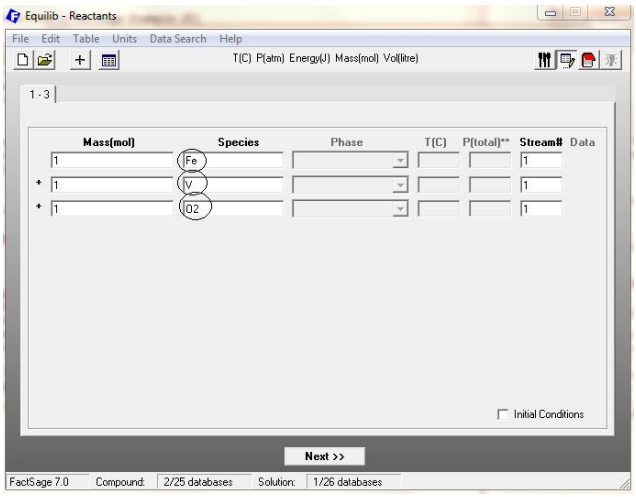

(b) Fe, V and O_2 are added as reactants.

Figure C.9: Thermodynamic evaluation example in FactSage: Step 3.1.1.

all possible solid compounds from the "Wil."compound database. The assessment is conducted under oxidizing conditions and therefore, only V_2O_5(s), Fe_2O_3(s), $FeVO_4$(s) and $Fe_2V_4O_{13}$(s) were shown experimentally to exist at equilibrium. The "Qaus-Slag" (Slag solution), "Qaus-Spin"(Spinel) and "Qaus-Hema"(Hematite solid solution) are activated from the list of solutions. Finally, the "file" is stored as a ChemSage file in a "DAT" format.

C.3.2 Step 3.2: Loading the ChemSage File in OPTISAGE

When the ChemSage "DAT"file has been created and experimental data from a critical assessment of the literature and from this study have been organised into groups, the OPTISAGE module can be launched and the ChemSage file loaded (see Figure C.11).

C.3.3 Step 3.3: Creating OPTISAGE Input for the Experimental Data

All the experimental data gathered from the literature are used in this step of the assessment. In this case, only liquidus data of the Fe-V-O system in air were obtained from the literature. The liquidus data from Fotiev, Cheshnitskii, and Surat (1983) and Walczak et al. (1985) were scrutinised and it was found that these results were realistic, feasible and complied with standards set in Subsection 6.8.5. Moreover, liquidus and solidus data from equilibration-quench analysis experiments in this study will be used for optimisation purposes. All the data were reorganised into spreadsheets and were entered into OPTISAGE as mole fractions. For example, all data are entered as mole fractions of the total mole of elements because the slag can contain low concentrations of Fe^{3+} and V^{4+}.

For all experimental input, a distinction is made between the experimental conditions and the measured variables. In the present case, liquidus composition had been measured as a function of temperature. Therefore, temperature is an experimental condition and the measured composition (from EPMA), as well as total pressure and oxygen partial pressure, are experimental conditions and the measured liquidus and solidus compositions are the measured variables. However, in this case, and given that OPTISAGE does not allow for liquidus compositions to be entered as measured variable, the liquidus temperature was instead entered as measured variable. This was done by selecting the "Precipitation target" option with "SlagB" being the "Target phase". The temperature at which the first solid is formed (Fe_2O_3(s), $FeVO_4$(s) or $Fe_2V_4O_{13}$(s)), or the liquidus temperature

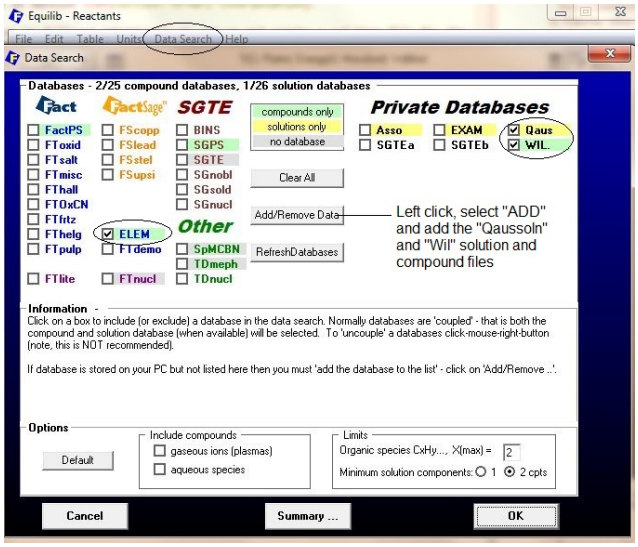

(a) Adding and selecting customised compound and solution databases.

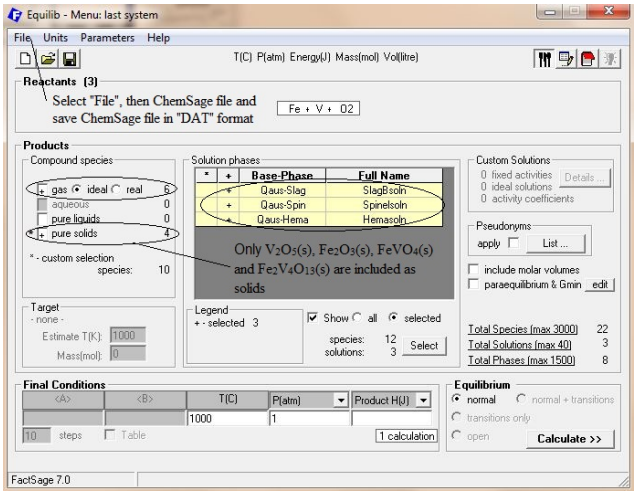

(b) Selecting compound species and solutions from main-menu in EQUILIB module and storing as ChemSage "DAT" file.

Figure C.10: Thermodynamic evaluation example in FactSage: Step 3.1.2.

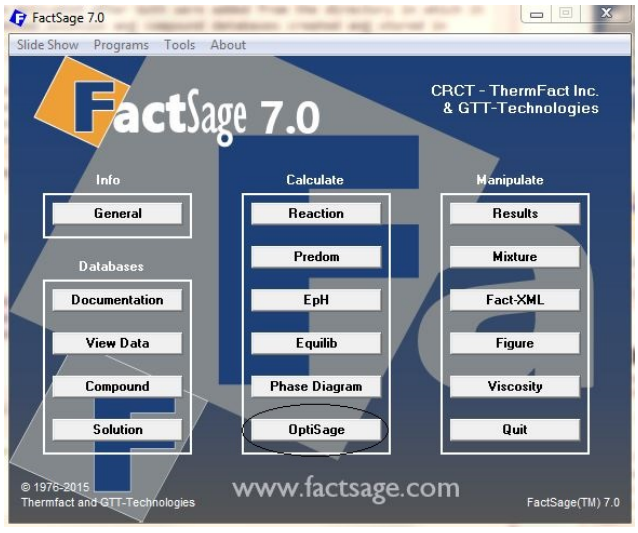

(a) Launching OPTISAGE module.

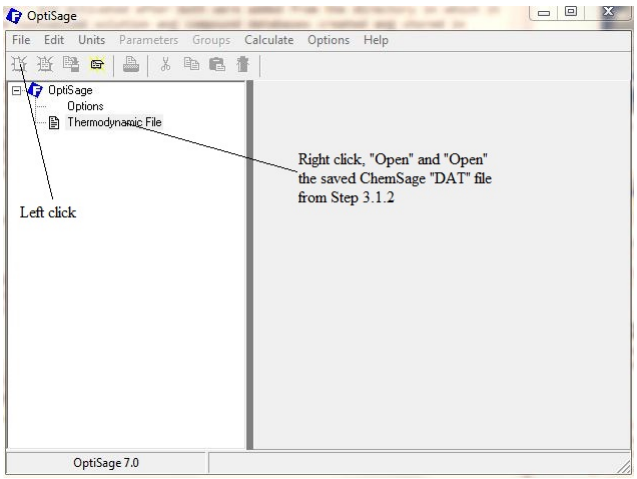

(b) Opening the saved ChemSage "DAT" file from Step 3.1.

Figure C.11: Thermodynamic evaluation example in FactSage: Step 3.2.

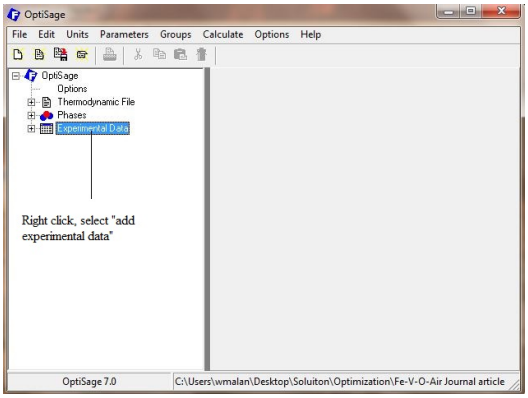

(a) Adding experimental data to OPTISAGE.

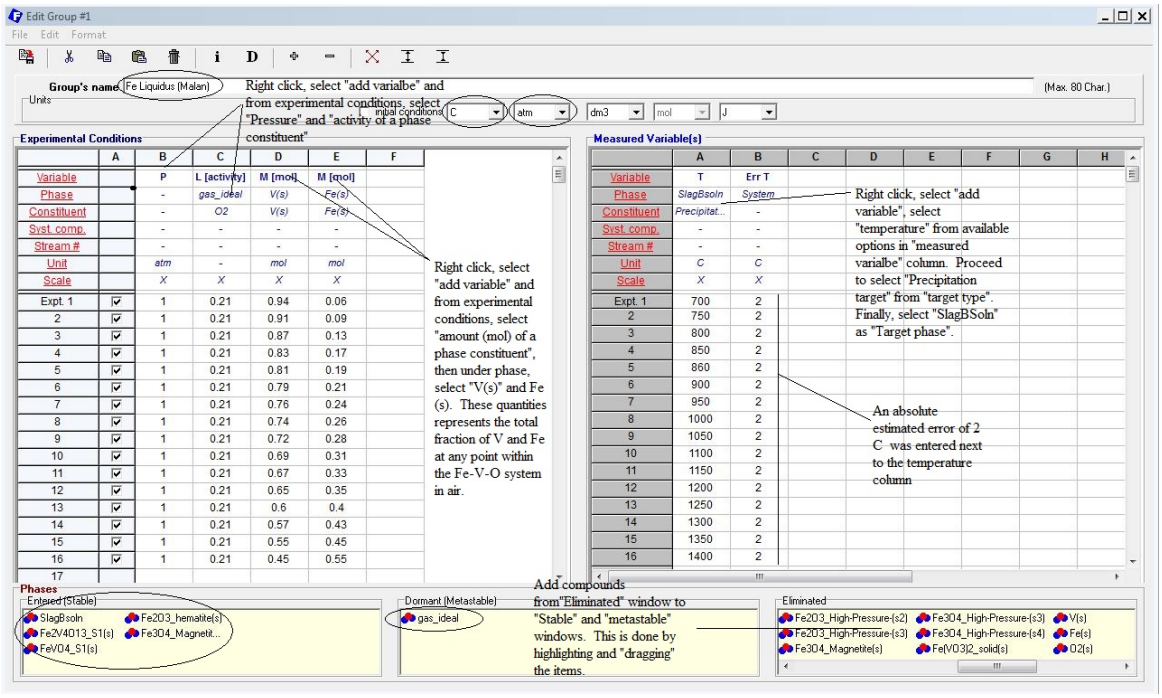

(b) Entering liquidus data into OPTISAGE. These are the data from the Fe-V-O system in air of this study.

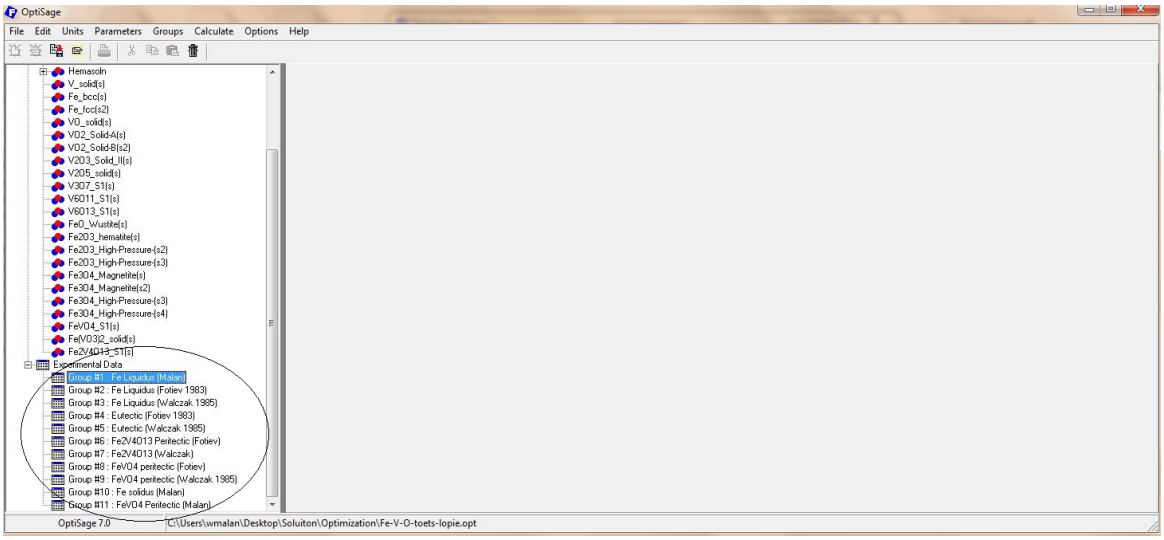

(c) All experimental data entered into OPTISAGE.

Figure C.12: Thermodynamic evaluation example in FactSage: Step 3.3.

corresponding to the measured liquidus composition is entered. Fe_2O_3(s) and Fe_3O_4 are exchanged for "Hemasoln"(hematite solid solution) and "Spinelsoln" (spinel solid solution), respectively, after the quasichemical coefficients have been optimised. This is done for liquidus data from this study and Fotiev, Cheshnitskii, and Surat (1983) and Walczak et al. (1985). Entering liquidus data into OPTISAGE from this study is used as illustrative example and is shown in Figure C.12b. Similarly, other phase diagram data were entered in OPTISAGE and are shown in Figure C.12c under experimental data.

C.3.4 Step 3.4: Optimizing Quasichemical Coefficients with Bayesian Technique

Step 3.4.1: Selecting and Initializing Adjustable Model Parameters

It is recommended that determining the effect of adjustable model parameters (quasichemical pair terms), $\Delta g_{Fe^{2+}-V_2O_3^{4+}}$ and $\Delta g_{Fe^{3+}-V_2O_3^{4+}}$ be investigated before optimisation is carried out. Following instructions from Subsection 6.8.6 it is important to guess a set of parameters that can be used to calculate a phase diagram with reasonable agreement with the critical set of data. In this case, a trial and error method revealed that $\Delta g_{Fe^{2+}-V_2O_3^{4+}}$ can be set at zero, by assuming that there is a very low concentration of Fe^{3+} under oxidising conditions. The correction value (difference between the new value of the optimised parameter and its value obtained in the previous iteration) from Bayesian optimisation is also an indication to determine the effect of the adjustable model parameter. A large correction value for a small increase or decrease of order of magnitude for any coefficient is an indication that a parameter has a significant effect on the shape of a phase diagram and other thermodynamic properties.

Furthermore, $\Delta g^0_{Fe^{3+}-V_2O_3^{4+}}$ are known to have a less significant effect on this critical set of data (liquidus composition). $g^{01}_{Fe^{3+}-V_2O_3^{4+}}$ and $g^{10}_{Fe^{3+}-V_2O_3^{4+}}$ are therefore optimised in the form, $A + BT$, where A and B are the coefficients to optimise. However, determining the effect of adjustable model parameters will differ from system to system and usually the term $\Delta g^0_{Fe^{3+}-V_2O_3^{4+}}$ contributes to the shape of a phase diagram. In any system, the number of coefficients should be minimised and the effect of any coefficient must be well defined. For the Fe-V-O system in air, parameter $g^{01}_{Fe^{3+}-V_2O_3^{4+}}$ and its coefficients are known to have a significant effect on liquidus temperatures at high V concentration in the slag, as well as on the eutectic and two peritectic reactions, which were experimentally investigated and shown to exist in areas highly concentrated in V_2O_5. The parameter, $g^{10}_{Fe^{3+}-V_2O_3^{4+}}$ has a smaller effect on eutectic and peritectic reactions, but has a significant effect on liquidus temperatures in regions with high Fe concentration concentration. In Figure C.13, the selection and initialisation of parameter $g^{10}_{Fe^{3+}-V_2O_3^{4+}}$ in OPTISAGE is illustrated.

Step 3.4.2: Initiating an Optimization

The conditions for Bayesian optimisation are set in this step. In this case, the maximum number of iterations are ten; however this value can be increased to 25 iterations (see Figure C.14a). The results and errors from the optimisation can also be saved in an external "txt"file. The optimisation is then started by selecting "Calculate", followed by selecting "Optimise with Bayesian".

Although the initial quasichemical coefficients were set at zero, an approximation could have been made with Non-linear Optimiser with Mesh Adaptive Direct search, known as NOMAD. NOMAD has been integrated in OPTISAGE to give the user the option of estimating the selected optimised parameters from scratch. It permits the minimisation of an objective function (such as the sum of squared errors in OPTISAGE) without involving any derivatives (black-box optimisation) and several hundreds of iterations can be performed (Bale et al. 2009). This approximation is particularly useful

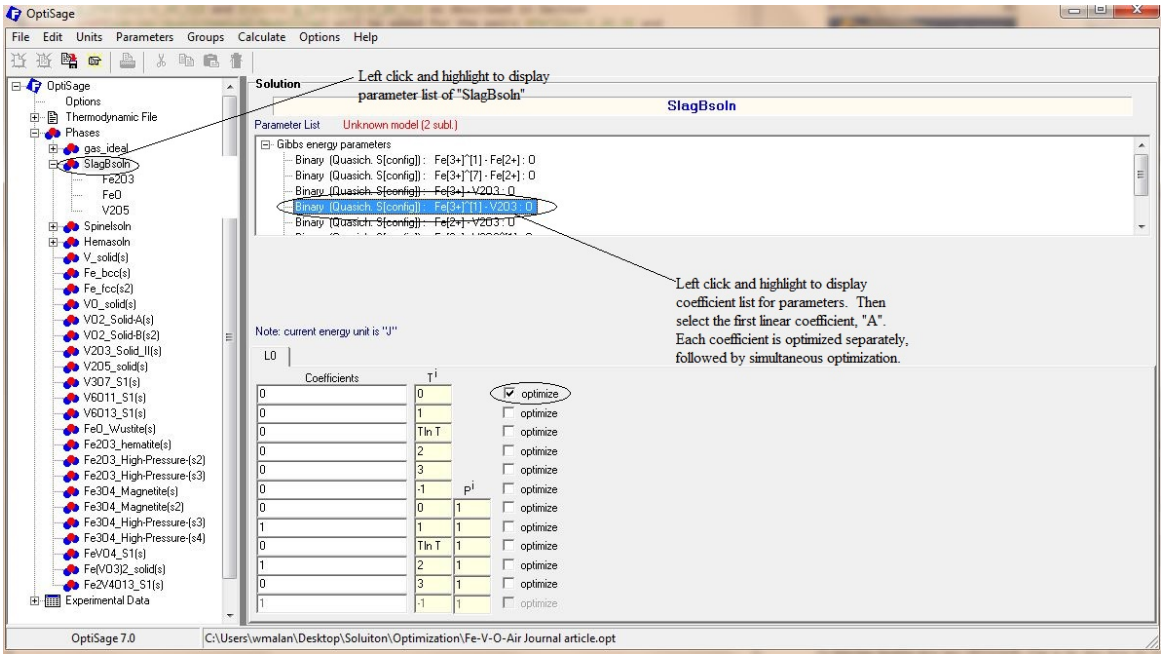

(a) Selection of phase and parameters to be optimised.

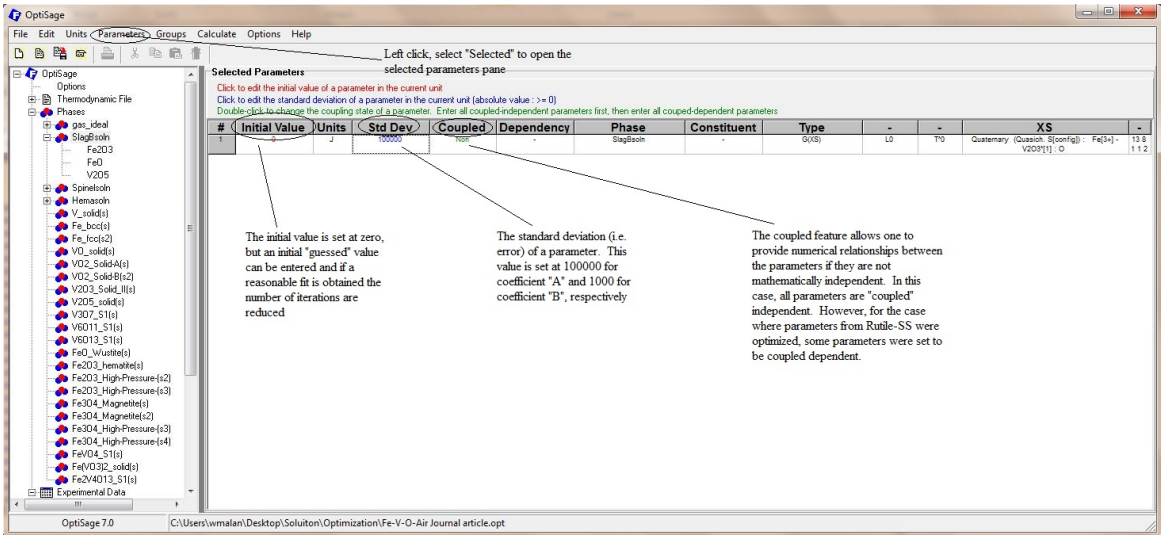

(b) Parameters menu and edition of selected parameters.

Figure C.13: Thermodynamic evaluation example in FactSage: Step 3.4.1.

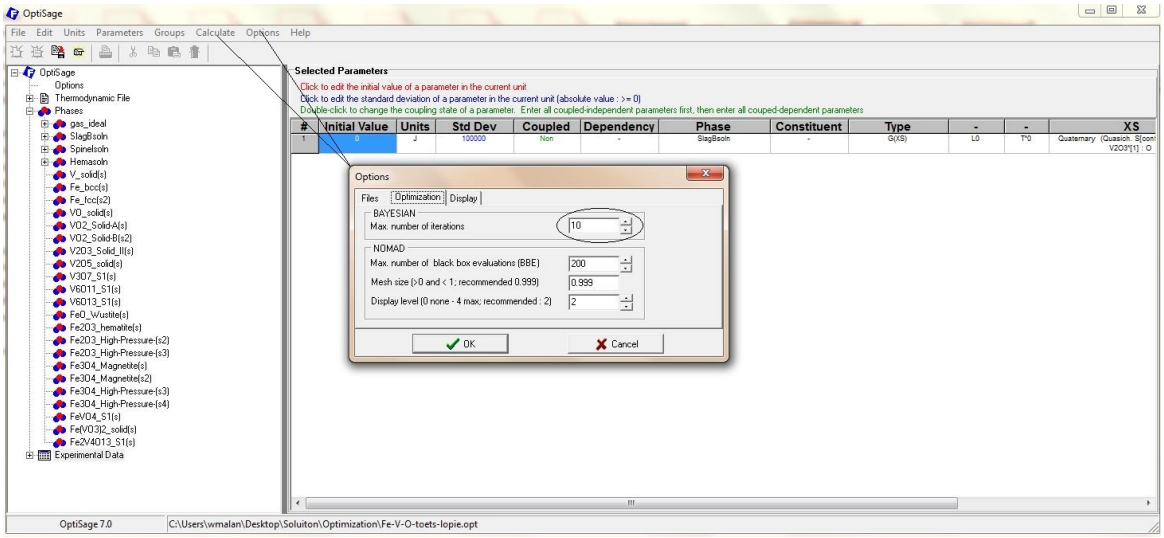

(a) Setting the number of iterations to 10.

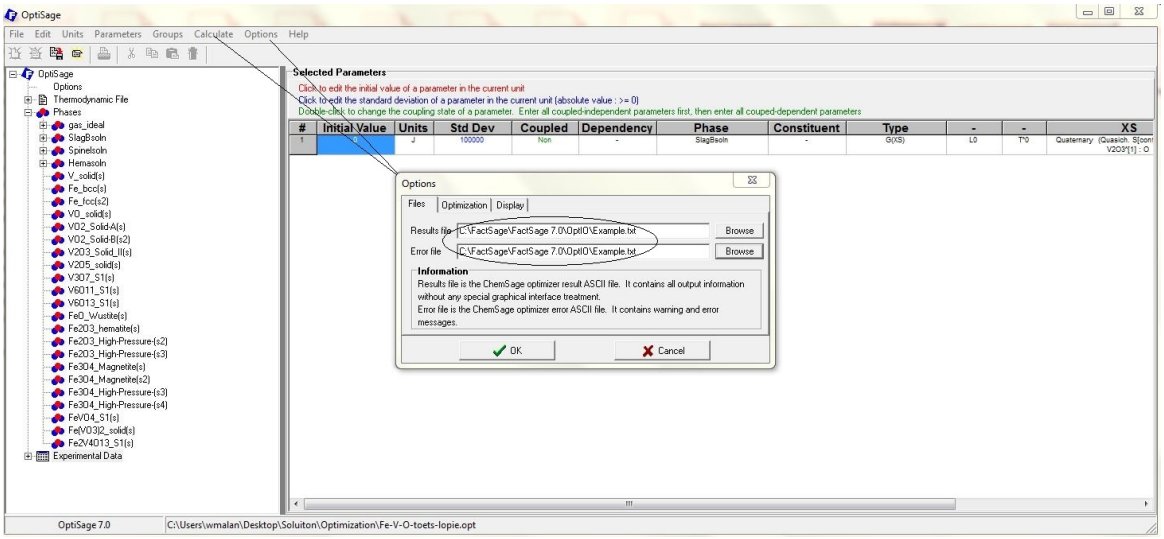

(b) Changing the directories for the results and errors files.

Figure C.14: Thermodynamic evaluation example in FactSage: Step 3.4.2.

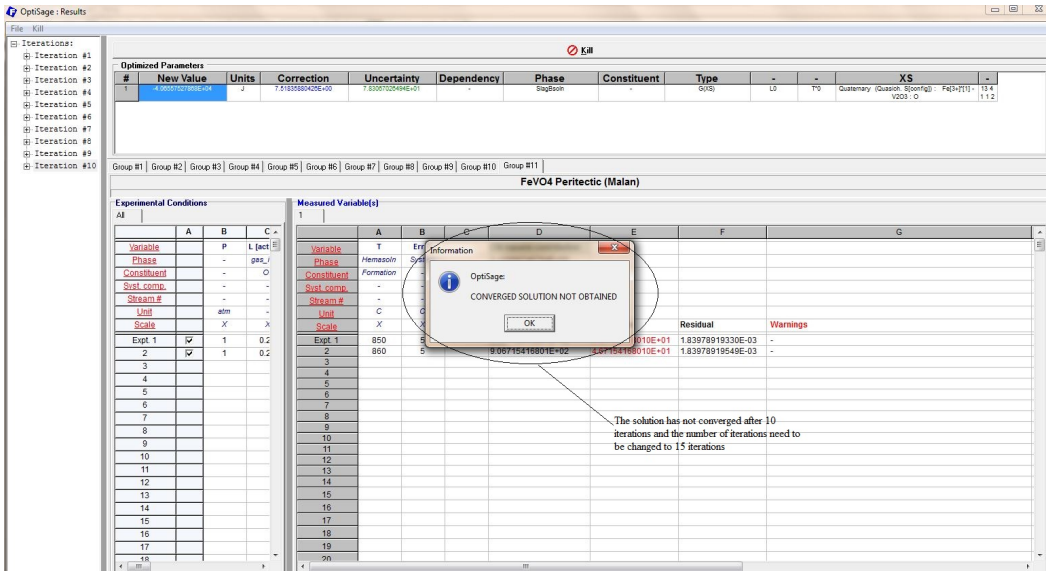

(a) Optimization results after 10 iterations.

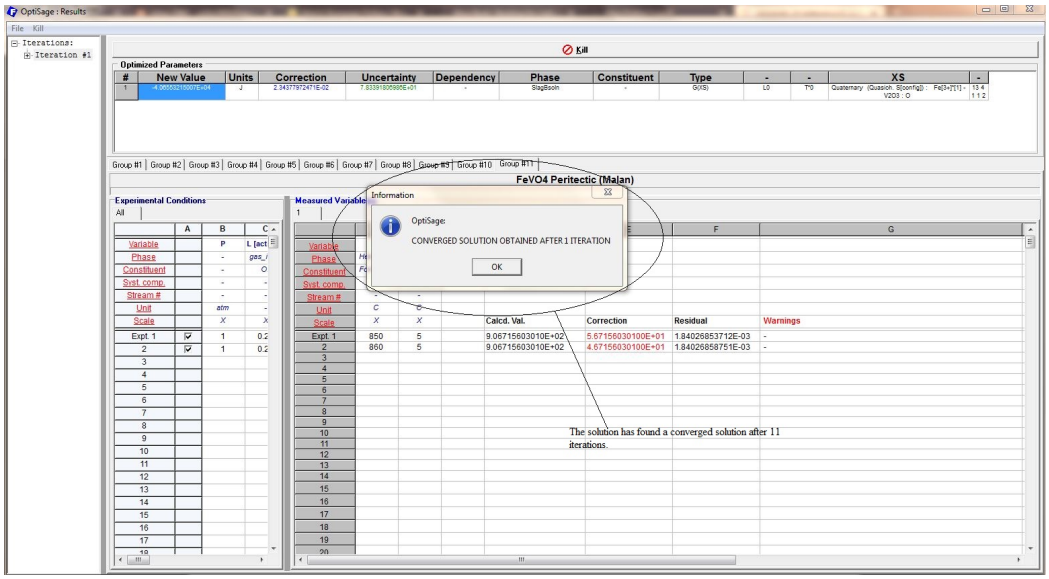

(b) Converged solution after 11 iterations.

Figure C.15: Thermodynamic evaluation example in FactSage: Step 3.5.1.

for systems with many coefficients, where many iterations are required to obtain a converge solution if per se coefficients were initially set at zero.

C.3.5 Step 3.5: Evaluating Results from Optimisation

Optimising One Quasichemical Coefficient

The results from Bayesian optimization are presented in this section. In the present example, only the results from coefficient A from parameter $g^{10}_{Fe^{3+}-V_2O_3^{4+}}$ are shown in Figure C.15. This process is repeated until all parameters from all solutions and compounds have been simultaneously optimised.

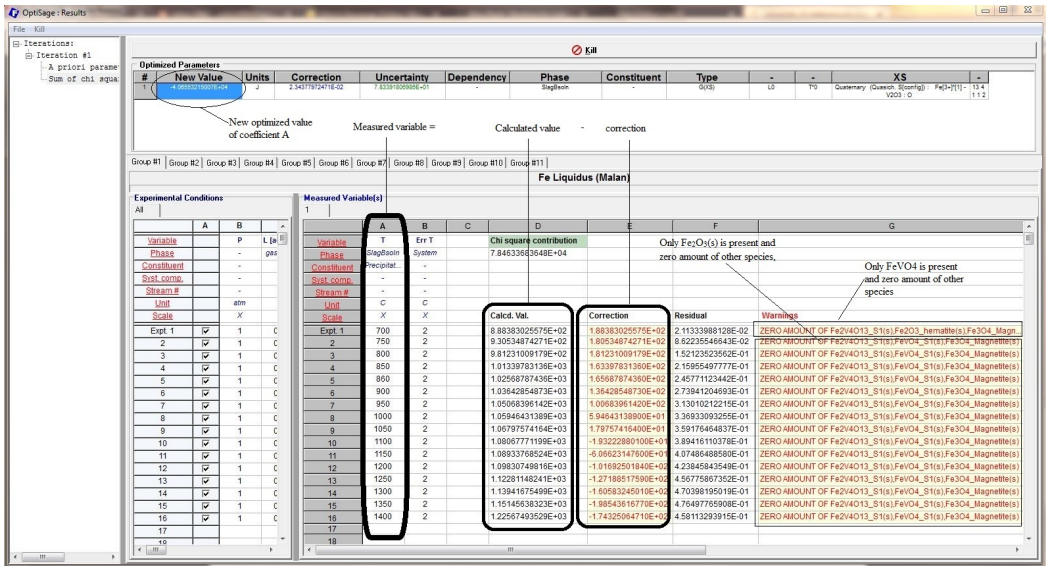

(a) Calculated values of the measured variables with the optimised parameters.

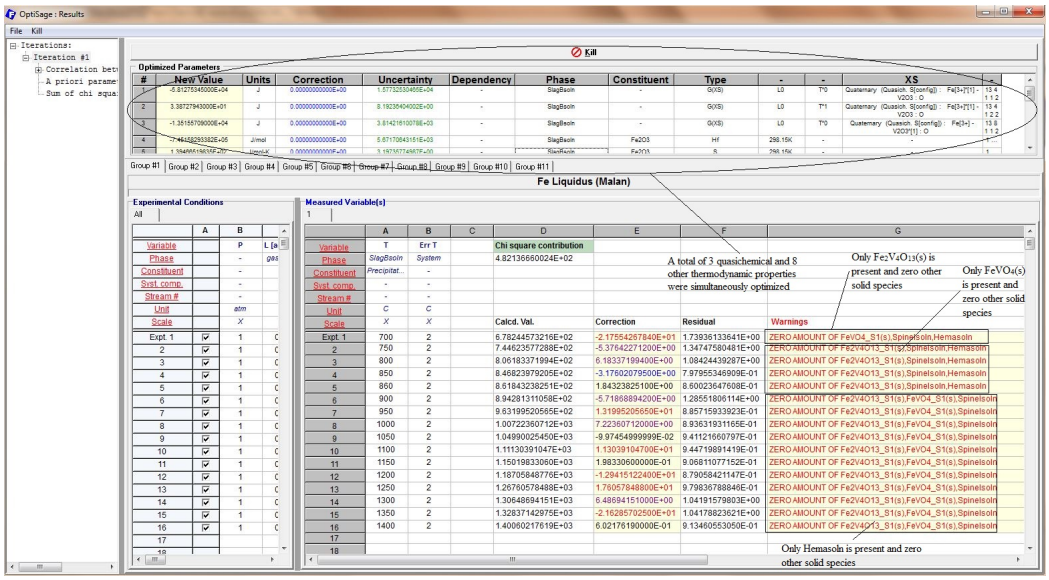

(b) Final optimised quasichemical pair coefficients and other thermodynamic properties of the Fe-V-O system in air.

Figure C.16: Thermodynamic evaluation example in FactSage: Step 3.5.2.

Optimising All Quasichemical Coefficients and Other Thermodynamic Properties Simultaneously

It was found that parameters $g^{10}_{Fe^{3+}-V_2O_3^{4+}}$ and $g^{01}_{Fe^{3+}-V_2O_3^{4+}}$ required $A + BT$ and A coefficients, respectively for successful optimisation. The B coefficient of parameter $g^{01}_{Fe^{3+}-V_2O_3^{4+}}$ did not significantly contribute to reduce the "Correction value". Moreover, the final solution of the optimisation did not converge at all times when this coefficient was included along with other parameters from compounds and solid solutions. The final set of coefficients and other thermodynamic properties that were optimised is shown in Figure C.16. These values correspond to the final values shown in Table 10.4 and Table 10.5.

C.3.6 Step 3.6: Verifying Results from Optimisation

In Subsection 6.8.7 a set of guidelines were given to verify that results from an optimisation are plausible. In this section, an attempt is made to comply with most of these guidelines.

- Calculated phase diagrams compared well to experimental observations (see Subsection 10.3.1)
- The correction value on Figure C.16 is similar to the sum of squares of errors, indicating that the majority of calculated liquidus and solidus temperatures were within ±20 °C of experimentally determined liquidus and solidus temperatures.
- Negative values for thermodynamic properties such as $\mathrm{a_0}$ of the $\mathrm{C_p}$ term and standard entropy are not physically possible. $\mathrm{a_0}$ of the $\mathrm{c_p}$ term was not optimised for any compound; however optimised entropies of pure compounds Fe_2O_3(l), $FeVO_4$(s) and $Fe_2V_4O_{13}$(s)), and hematite solid solution were all positive and therefore plausible.
- The number of significant numbers was set at five for all optimized excess Gibbs energy and other thermodynamic properties. This number of significant numbers was accepted from an inspection of a number of other thermodynamic evaluation studies.
- Limits of $\mathrm{S^\circ_{298}}$ and $\mathrm{C_p}$ terms of new compounds and solutions were all within the investigated temperature range from 700 °C to 1450 °C. However, $\mathrm{C_p}$ terms of $FeVO_4$(s) and $Fe_2V_4O_{13}$(s) were experimentally investigated by other authors from 298 to 900K and had to be accepted to be plausible up to their respective pertitectic transition points. The acceptable limits of $\mathrm{S^\circ_{298}}$ and $\mathrm{C_p}$ for all other pure compounds were all within and beyond the investigated temperature range.

The OPTISAGE module has no own calculational capabilities for thermodynamic properties or phase diagrams. The values of coefficients and parameters are re-entered into the "Qaussoln" file and "WIL"compound database. Equilib and phase diagram modules can extract the data for appropriate calculations and graphical comparison between calculated and experimental data, which was demonstrated in Section 10.3. Alternatively, all data from OPTISAGE can directly be saved to a database.

Part VII

Bibliography

Bibliography

Alcock, C.B. and C. Ji (1990). "Vanadium-oxygen system. A Review". In: *High Temperature - High Pressures* 22.2, pp. 139 –147.

Anderson, J.O et al. (2002). "Thermo-calc & DICTRA, computational tools for materials science". In: *CALPHAD: Computer Coupling of Phase Diagrams and Thermochemistry* 26, pp. 273–312. URL: doi:10.1016/S0364-5916(02)00037-8.

Bale, C.W. et al. (2002). "FactSage thermochemical software and databases". In: *CALPHAD: Computer Coupling of Phase Diagrams and Thermochemistry* 26.2, pp. 189–228. URL: http://dx.doi.org/10.1016/S0364-5916(02)00035-4.

Bale, C.W. et al. (2009). "FactSage thermochemical sofware and databases - recent developments". In: *CALPHAD: Computer Coupling of Phase Diagrams and Thermochemistry* 33.2, pp. 295–311. URL: https://doi.org/10.1016/j.calphad.2008.09.009.

— (2016). "FactSage thermochemical software and databases, 2010-2016". In: *CALPHAD: Computer Coupling of Phase Diagrams and Thermochemistry* 54.2, pp. 35–53. URL: https://doi.org/10.1016/j.calphad.2016.05.002.

Barry, T. I., A. T. Dinsdale, and J.A. Gisby (1993). "Predictive thermochemistry and phase equilibria of slags". In: *Review of Extraction & Processing* April, pp. 32–38. URL: https://doi.org/10.1007/BF03223284.

Barry, T.I. et al. (1992). "The compound energy model for ionic solutions with applications to solid solutions". In: *Journal of Phase Equilibria* 13.5, pp. 459–475. URL: http://dx.doi.org/10.1007/BF02665760.

Batalin, G.I. and T.N. Zinewich (1988). "Thermodynamic study of Fe-V-O melts". In: *Russ. J. Phys. Chem.* 62.2, pp. 127–129.

Besman, T.M., N.S. Kulkarni, and K.E. Spear (2006). "Thermochemical analysis and modeling of the Al_2O_3-Cr_2O_3, Cr_2O_3-SiO_2, and Al_2O_3-Cr_2O_3-SiO_2 systems relevant to refractories". In: *J. Am. Ceram. Soc.* 89.2, pp. 638–644. URL: http://dx.doi.org/10.1111/j.1551-2916.2005.00719.x.

Besman, T.M. and K.E. Spear (2002). "Thermochemical modeling of oxide glasses". In: *J. Am. Ceram. Soc.* 85.12, pp. 2887–2994. URL: http://dx.doi.org/10.1111/j.1151-2916.2002.tb00552.x.

Besman, T.M., K.E. Spear, and E.C. Beahm (2002). *Thermochemical models for nuclear waste glass subsystems - MgO-CaO and MgO-Al_2O_3*. Tech. rep. P.O. box 2008, Oak Ridge, TN 37831-6063: Oak Ridge National Laboratory and Pennsylvania State University. URL: http://dx.doi.org/10.1557/PROC-556-383.

Bjorkman, B. (1985). "An assessment of the system Fe-O-SiO_2 using a structure based model for the liquid silicate". In: *CALPHAD: Computer Coupling of Phase Diagrams and Thermochemistry* 9.3, pp. 271 –282. URL: http://dx.doi.org/10.1016/0364-5916(85)90012-4.

Bond, G.C., A. J. Sarkany, and G.D. Parfitt (1979). "The vanadium pentoxide-titanium dioxide system: Structural investigation and actvity for the oxidation of Butadiene". In: *Journal of Catalysis* 57.4, pp. 476–493. URL: http://dx.doi.org/10.1016/0021-9517(79)90013-7.

Bonnell, D. W. and J. W. Hastie (1989). "A predictive thermodynamic model for complex high-temperature solution phases". In: *High Temp. Sci.* 26.313.

Borukhovich, A.S. et al. (1975). "Heat capacity of iron, chromium, and nickel orthovanadates". In: *Russian Journal of Inorganic chemistry* 11.5, pp. 830–831.

Box, G.E.P., W.G. Hunter, and J.S. Hunter (2005). *Statistics for experimenters*. Vol. 2. New York, USA: John Wiley.

Brauer, G. and W. Litttke (1960). "The melting point and the thermal dissociation of titanium oxide". In: *Journal of Inorganic and Nuclear Chemistry* 16.1, pp. 67–76. URL: http://dx.doi.org/10.1016/0022-1902(60)80089-9.

Brochu, E., V.M. Cora, and N. de Freitas (2010). *A tutorial on Bayesian Optimization of expernsive cost functions, with application to active user modeling and hierarchical reinforcement learning*. Cornell University. URL: http://arxiv.org/pdf/1012.2599.pdf.

Burdese, A. (1957). "The system Fe_2O_3-V_2O_5". In: *Ann. Chim. (Rome)* 47.7-8, pp. 797–805.

Burzo., E. and L. Stanescu (1976). "Crystallographic investigation of the V_2O_5 - Fe_2O_3 solid solution using Mössbauer Effect". In: *Solid State Commun.* 20.7l, pp. 653–655.

— (1978). "On the charge Compensation of iron ions in V_2O_5 Lattice". In: *Phys. Status Solidi A.* 46.2l, K163–K166.

Burzo, E. et al. (1978). "Some physical properties of $V_2O_5-Fe_2O_3$ and $V_2O_5-Fe_2O_3-Li_2O$ systems". In: *J. Mater. Sci.* 13.9, pp. 1855 –1867.

Callister, W.D. (2007). *Materials Science and Engineering: An introduction*. Vol. 7. New York, USA: John Wiley and Sons, Inc.

Cancarevic, M., M. Zinkevich, and F. Aldinger (2007). "Thermodynamic description of the Ti-O system using the associate model for the liquid phase". In: *CALPHAD: Computer Coupling of Phase Diagrams and Thermochemistry* 31, pp. 330–342. URL: http://dx.doi.org/10.1016/j.calphad.2007.01.009.

Cao, Z. et al. (2017). "Critical evaluation and thermodynamic assessment of the $MgO-V_2O_5$ and $CaO-V_2O_5$ systems in air". In: *CALPHAD: Computer Coupling of Phase Diagrams and Thermochemistry* 56, pp. 72–79. URL: http://dx.doi.org/10.1016/j.calphad.2016.12.001.

Chartrand, P. and A.D. Pelton (2001a). "Thermodynamic evaluation and optimization of the LiCl-NaCl-KCl-RbCl-CsCl-$MgCl_2-CaCl_2$". In: *Metall Mater Trans A* 32.A, pp. 1361–1383. URL: https://doi.org/10.1007/s11661-001-0227-2.

— (2001b). "Thermodynamic evaluation and optimization of the LiF-NaF-KF-MgF2-CaF2 system using the modified quasichemical model". In: *Metall Mater Trans A* 32.A, pp. 1385–1396. URL: https://doi.org/10.1007/s11661-001-0228-1.

Chase, M.W. et al. (1975). "JANAF thermochemical tables supplement". In: *Journal of Physical Chemistry Data* 4. URL: http://dx.doi.org/10.1007/BF02873201.

Chen, S.L. et al. (2003). "Calculating phase diagrams using PANDATA and panengine." In: *The Journal of Minerals, Metals and Materials Society* 55.12, pp. 48–51. URL: https://doi.org/10.1007/s11837-003-0010-5.

Cheshnitski, S.M., V.L. Kozhevnikov, and A.A. Fotiev (1985). "Heat capacity of ferrous orthovanadate in the range from 5 to 300 K". In: *Inorg. Mater.* 21.4, pp. 594–595.

Coetsee, T. and C. Pretorius (2000). "Preliminary observations on phase relations in the V_2O_3-FeO and $V_2O_3-TiO_2$ systems from 1400 C to 1600 C in reducing atmospheres". In: *J. Am. Ceram. Soc* 83.6, pp. 1485–1488. URL: https://DOI:10.1111/j.1151-2916.2000.tb01414.x.

Davies, R.H. et al. (2002). "MTDATA - thermodynamic and phase equilibrium software from the national physical laboratory". In: *CALPHAD: Computer Coupling of Phase Diagrams and Thermochemistry* 26, pp. 229–271. URL: doi:10.1016/S0364-5916(02)00036-6.

Degterov, S. A. et al. (2001). "Experimental study of phase equilibria and thermodynamic optimization of the Fe-Zn-O system". In: *Metallurgical and Materials Transactions B* 32.B, pp. 643–657. URL: http://dx.doi.org/10.1007/s11663-001-0119-2.

Enomoto, M. (1996). "The O-Ti-V system (oxygen-titanium-vanadium)". In: *J. Phase Equilib.* 17.6, pp. 539–545. URL: https://doi.org/10.1007/BF02666001.

Eriksson, G. (1971). "Thermodynamic studies of high temperature equilibria: SOLGAS, a computer program for calculating the composition and heat condition of an equilibrium mixture". In: *Acta Chemica Scandinavica* 25, pp. 2651–2658. URL: https://doi.org/10.3891/acta.chem.scand.25-2651.

Eriksson, G. and E.Rosen (1973). "Thermodynamic studies of high temperature equilibria." In: *Chemica Scripta* 4, pp. 193–194.

Eriksson, G. and K. Hack (1990). "ChemSage - a computer program for the calculation of complex chemical equilibria". In: *Metallurgical Transactions B* 21.6, pp. 1013–1023. URL: https://doi.org/10.1007/BF02670272.

Eriksson, G. and A.D. Pelton (1993). "Critical evaluation and optimization of the thermodynamic properties and phase diagrams of the $MnO-TiO_2$, $MgO-TiO_2$, $FeO-TiO_2$, $Ti_2O_3-TiO_2$, Na_2O-TiO_2 and K_2O-TiO_2 systems". In: *Metallurgical Transactions B* 24.B, pp. 795–805. URL: http://dx.doi.org/10.1007/BF02663140.

Eriksson, G. and E. Rosen (1984). "Calculation of phase equilibria in multicomponent alloy systems using a specially adapted version of the program "SOLGASMIX"". In: *CALPHAD: Computer Coupling of Phase Diagrams and Thermochemistry* 8.1, pp. 1–15. URL: https://doi.org/10.1016/0364-5916(84)90025-7.

Eriksson, G. et al. (1996). "Measurement and thermodynamic evaluation of phase equilibria in the Fe-Ti-O system". In: *Berichte Der Bunsengesellshaft* 100.11, pp. 1839–1849. URL: http://dx.doi.org/10.1002/bbpc.19961001114.

Eriksson, G. et al. (2000). "The modified quasichemical model I-binary solutions". In: *Metallurgical and Materials Transactions B* 31.B, pp. 651–659. URL: http://dx.doi.org/10.1007/s11663-000-0103-2.

Flynn, J.H. (1988). "Phase equilibria determination in complex slag systems". In: *Thermal analysis kinetics-problems, pitfalls and how to deal with them* 34.1, pp. 367–381. URL: http://dx.org.doi./10.1007/BF01913405.

Fogler, H.S. (2006). *Elements of chemical reaction engineering*. Vol. 4. New Jersey, USA: Pearson Education, Inc.

Fotiev, A. A., S. M. Cheshnitskii, and L. L. Surat (1983). "The thermal properties of iron orthovanadate". In: *Russ. J. Inorg.* 28.4, pp. 560–562.

Fotiev, A. A., L. L. Surat, and A. I. Tret'yakov (1981). "Compatibility relations in the $FeO_3-TiO_2-V_2O_5$ system". In: *Russian Journal of Inorganic Chemistry* 26.5, pp. 1377–1382.

Fotiev, A.A., L.L. Surat, and A.I. Tretyakov (1980). "Formation conditions and nature of solid solutions in the $Fe_2O_3-V_2O_3$ system". In: *Russ. J. Inorg. Chem.*. 25.12, pp. 1840–1843.

Gibbs, J.W. (1875-1876). In: *Transactions of the Connecticut Academy of Arts and Sciences-Part 1* 3, pp. 108–248.

— (1877-1878). In: *Transactions of the Connecticut Academy of Sciences - Part 2* 3, pp. 348–524.

Gisby, J. A. et al. (2002). "Predicting phase equilibria in oxide and sulphide systems". In: *The Minerals, Metals & Materials Society*, pp. 533–545. URL: https://www.researchgate.net/profile/Pekka_Taskinen/publication/289125733_PREDICTING_PHASE_EQUILIBRIA_IN_OXIDE_AND_SULPHIDE_SYSTEMS/links/56894e2208aebccc4e170771/PREDICTING-PHASE-EQUILIBRIA-IN-OXIDE-AND-SULPHIDE-SYSTEMS.pdf.

Goel, R.P., H.H. Kellogg, and J.L Rrain (1980). "Mathematical desription of the thermodynamic properties of the systems Fe-O and Fe-O-SiO_2". In: *Matallurgical Transactions B* 11.1, pp. 107–117. URL: http://dx.doi.org/10.1007/BF02657179.

Goldstein, J.I. et al. (1981). *Scanning electron microscopy and X-ray microanalysis*. New York: Plumum.

Golovkin, B. G., V. L. Volkov, and V. D. Skobeleva (1989). "Subsolidus regions in the $CaO-TiO_2-V_2O_5$ system". In: *Russian Journal of Inorganic Chemistry* 34.9, pp. 1337–1339.

Guo, W.Q. et al. (1999). "Crystal structure and cation distributions in the $FeTi_2O_5$-Fe_2TiO_5 solid solution series". In: *Journal of Physics: Condensed Matter* 11.4, pp. 413–419. URL: https://doi.org/10.1016/j.pnsc.2013.06.012.

Habashi, F. (1997). *Handbook of extractive metallurgy*. Vol. 2. Heidelberg, Germany: Wiley-VCH.

Habel, D. et al. (2006). "Phase development in the catalytic system $V_2O_{5/}TiO_2$ under oxidiising conditions". In: *Journal of European Ceramic Society* 26, pp. 3287–3294. URL: http://dx.doi.org/10.1016/j.jeurceramsoc.2005.09.108.

Habel, D. et al. (2008). "Phase relations in the system TiO_2-V_2Ox under oxidizing and reducing conditions". In: *Journal of Phase Equilibria and Diffusion* 29.6, pp. 482–487. URL: http://dx.doi.org/110.1007/s11669-008-9391-z.

Haggerty, S.E. and D.H. Lindsley (1970). "Stability of the pseudobrookite (Fe_2TiO_6) ferropseudobrookite (Fe_2TiO_5) series". In: *Carnegie Inst. Wash. Year Book* 68, pp. 247–249.

Hampl, M. and R. Schmid-Fetzer (2015). "Thermodynamic description of the Ti-O system". In: *Journal of Alloys and Compounds* 106.5, pp. 439–453. URL: https://doi.org/10.3139/146.111210.

Hamuyuni, J. (2016). "Solubility of high melting temperature oxides (CaO, Al_2O_3, Cr_2O_3 in copper oxide liquid". Ph.D. thesis. Aalto University, Helsinki, Finland.

Hanaor, D.A.H. and C.C. Sorrel (2009). "Review of the anatase to rutile phase transformation". In: *J. Mater. Sci.* 46, pp. 855–874. URL: https://doi.org/10.1007/s10853-010-5113-0.

Hastie, J. W. (1984). "New techniques and opportunities in high-temperature mass spectrometry". In: *Pure Appl. Chem.* 56.11.

Hastie, J. W. and D. W. Bonnell (1985). "A predictive phase-equilibrium model for multicomponent oxide mixtures. 2. oxides of Na-K-Ca-Mg-Al-Si". In: *High Temp. Sci.* 19.3.

Hastie, J. W., E. R. Plante, and D. W. Bonnell (1983). "Vaporization of simulated nuclear waste glass". In: *NBSIR 83-2731* NIST.

Hawakawa, S. and T. Yoko (1995). "IR and NMR structural studies on lead vanadate glasses". In: *Journal of Non-crystalline Solids* 183, pp. 73–84.

Hidayat, T. et al. (2015). "Thermodynamic reevaluation of the Fe-O system". In: *CALPHAD: Computer Coupling of Phase Diagrams and Thermochemistry* 48, pp. 131 –144. URL: http://dx.doi.org/10.1016/j.calphad.2014.12.005.

Hillert, M. (2001). "The compound energy formalism". In: *Journal of Alloys and Compounds* 320.2, pp. 161–176. URL: https://doi.org/10.1016/S0925-8388(00)01481-X.

Hillert, M. and L.I. Staffansson (1970). "The regular solution model for stoichiometric phases and ionic melts." In: *Acta Chem. Scand.* 24, pp. 3618–3626. URL: http://dx.doi.org/10.3891/acta.chem.scand.24-3618.

Hiroi, Z. et al. (2013). "Spinodal Decomposition in the TiO_2-VO_2 System". In: *Journal of Alloys and Compounds* 25.11, pp. 2202–2210. URL: https://DOI:10.1021/cm400236p.

Hotta, Y. et al. (1984). "Pressure-products diagram of $Fe_xV_{1-x}O_2$ system ($0 < x \leq 0.5$)". In: *J.Solid State Chem.* 55.3, pp. 314 –319. URL: http://dx.doi.org/10.1016/0022-4596(84)90283-4.

Hudon, P. and I.H. Jung (2014). "Critical evaluation and thermodynamic optimization of the $CaO-P_2O_5$ system". In: *Metallurgical and Materials Transactions B* 46.B, pp. 494–522. URL: https://doi.org/10.1007/s11663-014-0193-x.

Inden, G. (1976). "Computer calculation of the free energy contributions due to chemical and/or magnetic ordering". In: *In Proc. CALPHAD V*, pp. 1–13.

Jak, E. and P.C. Hayes (2008). "Phase equilibria determination in complex slag systems". In: *Mineral Processing and Extractive Metalllurgy: Transactions of the Institutions of Mining and Metallurgy* 117.1, pp. 1–17. URL: http://dx.doi.org/10.1179/174328508X272344.

Janssens, K.G.F. et al. (2007). *Computational materials engineering*. Vol. 1. Oxford, UK: Elsevier Science Ltd.

Jung, I., S.A. Deceterov, and A.D. Pelton (2004). "Critical thermodynamic optimization of the Fe-Mg-O system". In: *Journal of Physics and Chemistry of Solids* 65.1, pp. 1683–1695. URL: http://dx.doi.org/10.1016/j.jpcs.2004.04.005.

Kang, Y.B. (2012). "Critical evaluation and thermodynamic optimization of the VO - $VO_{2.5}$". In: *Journal of the European Ceramic Society* 32, pp. 3187 –3198. URL: http://dx.doi.org/10.1016/j.jeurceramsoc.2012.04.45.

Kang, Y.B., I.H. Jung, and H.G. Lee (2006). "Critical evaluation and optimization of the MnO-TiO_2–Ti_2O_3 system". In: *CALPHAD: Computer Coupling of Phase Diagrams and Thermochemistry* 30, pp. 235–247. URL: http://dx.doi.org/10.1016/j.calphad.2006.05.001.

Kang, Y.B. et al. (2007). "Critical evaluation and thermodyanamic optimizaiton of the binary systems in the Mg-Ce-Mn-Y system". In: *J. Phase Equilib. Diff.* 28, pp. 342–354. URL: https://doi.org/10.1007/s11669-007-9095-9.

Kang, Y.B. et al. (2008). "Critical evaluation and thermodyanamic optimizaiton of the Al-Ce, Al-Y, Al-Sc and Mg-Sc binary systems". In: *CALPHAD: Computer Coupling of Phase Diagrams and Thermochemistry* 32, pp. 413–422. URL: https://doi.org/10.1016/j.calphad.2008.03.002.

Kang, Y.B. et al. (2009). "Thermodynamic and volumetric databases and software for magnesium alloys". In: *JOM* 61, pp. 75–82. URL: https://doi.org/10.1007/s11837-009-0076-9.

Kawakita, Y. et al. (1999). "Local structures of liquid and vitreous V_2O_5 and P_2O_5". In: *Journal of Physics and Chemistry of Solids* 60, pp. 1483 –1486. URL: http://dx.doi.org/S0022-3697(99)00148-1.

Kerby, R. C. and J. R. Wilson (1973). "Solid-siquid phase equilibria for the ternary systems, V205 - Na20 - Fe203, V205 - Na20 - Cr2O3 and V205 - Na20 - MgO". In: *Can. J. Chem.* 51.7, pp. 1032–1040. URL: http://dx.doi.org/10.1139/v73-153.

Kesler, Ya.A. et al. (1985). "Enthalpy of formation of vanadates of iron, chromium and aluminium". In: *Inorg. Mater.* 21.4, pp. 649–651.

Kohler, H. (1960). "Predicting ternary activities using Binary Data". In: *Monatsh. Chemie* 91, p. 738.

Königsberger, E. and H. Gämsjager (1990). "Analysis of phase diagrams employing Bayesian excess parameter estimation". In: *Monatsh Chem* 121.2-3, pp. 119–127. URL: https://doi.org/10.1007/BF00809524.

Koretsky, M.D. (2004). *Engineering and chemical thermodynamics*. Vol. 1. 111 River Street, Hoboken, NJ 07030: John Wiley and Sons, Inc.

Kowalski, M. and P.J. Spencer (1995). "Thermodynamic reevaluation of the Cr-O, Fe-O and Ni-O systems: Remodelling of the liquid, BCC and FCC phases". In: *CALPHAD: Computer Coupling of Phase Diagrams and Thermochemistry* 19.3, pp. 229 –243. URL: http://dx.doi.org/10.1016/0364-5916(95)00024-9.

Kumar, B.V. and K.T. Jacob (1987). "Alloy oxide equilibria in the Fe-V-O and Fe-Nb-O systems". In: *Steel Research* 58.2, pp. 71–76.

Lebrun, N. and P. Perrot (2010). *Refroctory metal systems: phase diagrams, crystollographic and thermodynamic data*. Vol. 11E3. Berlin, Heidelberg: Springer. URL: http://dx.doi.org/10.1007/978-3-642-00771-2_25.

Lee, H.G. (1999). *Chemical thermodynamics for metal and materials*. Vol. 1. 57 Shelton Street, Convent Garden, London: Imperial College Press.

Leitner, J. et al. (2002). "Estimation of heat capacities of solid mixed oxides". In: *Thermochimica Acta* 395.1, pp. 27–46. URL: https://doi.org/10.1016/S0040-6031(02)00177-6.

Lu, X.G., M. Selleby, and B. Sundman (2005). "Implementation of a new model for pressure dependence of condensed phases in Thermo-Calc." In: *CALPHAD: Computer Coupling of Phase Diagrams and Thermochemistry* 29, pp. 49–55. URL: http://dx.doi.org/10.1016/j.calphad.2005.04.001.

Lukas, H.L., S.G. Fries, and B. Sundman (2007). *Computational thermodynamics, the Calphad method*. Cambridge, UK: Cambridge University press.

Merlet, C. (1994). "An accurate computer correction program for quantitative electron probe microanalysis". In: *Mikrochim. Acta* 114/115, pp. 363–376.

Millet, J.M., R.S. Roth, and H.S. Parker (1986). "Phase relations between the polytitanates of barium and the barium borates, vanadates and Molybdatas". In: *Journal of the Americal Ceramic Society* 69.11, pp. 811–814. URL: http://dx.doi.org/10.1111/j.1151-2916.1986.tb07365.x.

Moskalyk, R.R. and A.M. Alfantazi (2003). "Processing of vanadium: a review". In: *Minerals Engineering* 16, pp. 793–805.

Muggianu, Y.M., M. Gambino, and J.P. Bros (1975). "Enthalpies of formation of liquid alloys bismuth-gallium-tin at 723 K. Choice of an analytical representation of integral and partial thermodynamic functions of mixing for this ternary-system". In: *Chim. Phys.* 72.1, pp. 83–88.

Muller, J. and J.C. Joubert (1975). "Synthesis of a high pressure high temperature form of dense $FeVO_4$ and evidence for an allotropic form of the $CrVO_4$ type". In: *J. Solid State Chem* 14, pp. 8 –13. URL: http://dx.doi.org/10.1016/0022-4596(75)90355-2.

Murnaghan, F.D. (1944). "The compressibility of media under exteme pressure". In: *Proc. Nat. Acad. Sci. (USA)* 30, pp. 244–247.

Murray, J.L. and H.A. Wriedt (1987). "The O-Ti (oxygen-titanium) system". In: *Bulletin of Alloy Phase Diagrams* 8.2, pp. 148–165. URL: http://dx.doi.org/10.1007/BF02873201.

Navrotsky, A. (1975). "Thermodynamics of formation of some compounds with the pseudobrookite structure and of the $FeTi_2O_5$–Ti_3O_5 solid solution series". In: *American Mineralogist* 320.3-4, pp. 249–256.

Newbury, D.E. and N.W.M. Ritchie (2015). "Performing elemental microanalysis with high accuracy and high precision by scanning electron microscopy/silicon dirft detector energy-dispersive X-ray spectrometry". In: *Journal of Material Science* 50, pp. 493–518. URL: http://dx.doi.org/10.1007/s10853-014-8685-2.

Otsubu, Y. and K. Utsumi (1971). "Thermochemical properties of $Fe_2O_3 \cdot 2\,V_2O_5$ in the iron oxide-vanadium pentoxide system". In: *Nippon Kagaku Zasshi* 92.8, p. 737.

Palanna, O.G.M., A.L.S. Mohanand, and A.B. Biswas (1978). "Electrical properties of Fe_2O_3-V_2O_5 system". In: *Proc. Indian Acad. Sci. A* 87.8l, pp. 259–265.

Pelton, A.D. (2001). "A general "geometric" thermodynamic model for multicomponent solutions". In: *CALPHAD: Computer Coupling of Phase Diagrams and Thermochemistry* 25.2, pp. 319–328. URL: https://doi.org/10.1016/S0364-5916(01)00052-9.

Pelton, A.D. and M. Blander (1986). "Thermodynamic analysis of ordered liquid Solutions by a modified quasichemical Approach - application to silicate slags". In: *Met. Trans. B* 17B (4), pp. 805–815. URL: https://doi.org/10.1007/BF02657144.

— (1987). "Thermodynamic analysis of binary-liquid silicates and prediction of ternary solution properties by modified quasi-chemical equations". In: *Geochim. Cosmochim. Acta* 51 (1), pp. 85–95. URL: https://doi.org/10.1016/0016-7037(87)90009-3.

Permer, L. and Y. Laligant (1997). "Crystal structure of the Tetrapolyvanadate $Fe_2V_4O_{13}$". In: *Eur. J. Solid State Inorg. Chem.* 34, pp. 41 –52.

Perron, L. (2001). "Vanadium, natural resources Canada". In: *Minerals and Resource Section, Canada Minerals Yearbook*, pp. 59.1 –59.7.

Petric, A. and K.T. Jacob (1982). "Thermodynamic Properties of Fe_3O_4–FeV_2O_4 and Fe_3O_4–$FeCr_2O_4$ Spinel Solid Solutions". In: *J. Am. Ceram. Soc.* 65.2, pp. 117–123. URL: https://doi.org/10.1111/j.1151-2916.1982.tb10368.x.

Pletnev, R.N., A.A. Fotiev, and V.N. Lisson (1975). "Phase composition of the Fe_2O_3–V_2O_5 system". In: *Russ. J. Inorg. Chem.* 20.3, pp. 1356 –1357.

Prostakova, V. et al. (2015). "Experimental investigation and thermodynamic modeling of the NiO–CaO–SiO_2, NiO-CaO-SiO2 and NiO–CaO–MgO–SiO_2 systems". In: *Journal of Chemical*

Thermodyanamics 86, pp. 130–142. URL: http://dx.doi.org/10.1016/j.jct.2015.01.017.

Protstakova, V. et al. (2015). "Experimental investigation and thermodynamic modelling of the ($NiO + CaO + SiO_2$) and ($NiO + CaO + MgO + SiO_2$)". In: *J. Chem. Thermodynamics* 86.B, pp. 130–142. URL: http://dx.doi.org/10.1016/j.jct.2015.01.017.

Qiu, L. and M.A. White (2001). "The constituent addivity method to estimate heat capacities of complex inorganic solids". In: *Journal of Chemical Education* 78.1, pp. 1076–1079. URL: https://doi.org/10.1021/ed078p1076.

Raghavan, V. (1989). "The Fe-O-V (iron-oxygen-vanadium) system". In: *Phase Diagrams of Ternary Iron Alloys, Indian Institute of Metals, Calcutta* 5, pp. 336–348.

Rahman, M., P. Hudon, and I.H. Jung (2013). "A coupled experimental study and thermodynamic modelling of the SiO_2–P_2O_5 system". In: *Metallurgical and Materials Transactions B* 44.B, pp. 837–852. URL: https://doi.org/10.1007/s11663-013-9847-3.

Reese, R.G. Jr. (2001). *Vanadium*. URL: https://minerals.usgs.gov/minerals/pubs/commodity/vanadium/700400.pdf (visited on 2001).

Rhohrmann, B. (1985). "Vanadium in South Africa". In: *Journal of the South African institute of mining and metallurgy* 85, pp. 141–150.

Robert, R.C. (1981). *CRC handbook of chemistry and physics*. Vol. 62. Cambridge, UK: Boca Raton, FL: CRC Press. URL: ISBN0-8493-0462-8.

Saulov, D. (2007). "Shortcomings of the recent modifications of the quasichemical solution model". In: *CALPHAD: Computer Coupling of Phase Diagrams and Thermochemistry* 31, pp. 390–395. URL: https://doi:10.1016/j.calphad.2007.01.006.

Saunders, N. and A.P. Miodownik (1998). *CALPHAD (Calculation of phase diagrams) A comprehensive guide*. Vol. 1. Oxford, UK: Elsevier Science Ltd.

Shannon, R.D. (1976). "Revised effective ionic radii and systematic studies of interatomic distances in halides and chalcogenides". In: *Acta Crystallogr A.* 32, pp. 751–767. URL: https://doi:10.1107/S0567739476001551.

Si, Y. et al. (2012). "A novel amorphous $Fe_2V_4O_{13}$ as cathode material for lithium secondary batteries". In: *Materials Letters* 27, pp. 145–147. URL: http://dx.doi.org/10.1016/j.matlet.2011.12.104.

Slobodin, B.V., A.A. Fotiev, and I.I. Miller (1976). "The thermal Properties of iron orthovanadate". In: *Russ. J. Inorg. Chem.* 21.2, pp. 175–178.

Smyth, J.R. (1997). *Mineral structure data*. URL: http://ruby.colorado.edu/~smyth/min/minerals.html (visited on 04/11/2018).

Society, The American Ceramic (2003). URL: http://www.ceramic.org/phase (visited on 2018).

Solacolu, S., R. Dinescu, and M. Zaharescu (1970). "The thermal phase equilibria in the system BaO–TiO_2–V_2O_5". In: *Romanian Journal of Chemistry* 15, pp. 401–408.

Solacolu, S. and M. Zaharescu (1972). In: *Rev. Roum. Chim.* 17, pp. 1715–1724.

Steinberg, W.S. and W. Geyser (2011). "The history and development of the pyrometallurgical processes at Evraz Highveld Steel & Vanadium". In: *Southern African Institute of Mining and Metallurgy*. Ed. by R.T Jones and P.den Hoed, pp. 1034–1045.

Suito, H. and D.R. Gaskell (1971). "The thermodynamics of melts in the system VO_2–V_2O_5". In: *Metallurgical and Materials Transactions B* 2.12, pp. 3299–3303. URL: https://doi.org/10.1007/BF02811610.

Sundman, B. (1991). "An assessment of the Fe-O system". In: *Journal of Phase Equilibria* 12.2, pp. 127–140. URL: http://dx.doi.org/10.1007/BF02645709.

Sundman, B. and J. Agren (1981). "A regular solution model for phases with several components and sublattices, suitable for computer applications." In: *Journal of Physics and Chemistry of Solids* 42.4, pp. 297–301. URL: http://dx.doi.org/10.1016/0022-3697(81)90144-X.

Taylor, P.R. et al. (2005). "Extractive metallurgy of vanadium containing titaniaferous magnetite ores: A review". In: pp. 1–9.

Toop, G.W. (1965). "Predicting ternary activities using binary data". In: *Trans. Met. Soc. AIME* 233.4, p. 850.

Vejux, A. and P. Courtine (1978). "Interfacial reactions between V_2O_5 and TiO_2 (Anatase): Role of the structural properties". In: *Journal of Solid State chemistry* 23.1, pp. 93–103. URL: http://dx.doi.org/10.1016/0022-4596(78)90055-5.

Volkov, V.L. (1979). "Equilibrium diagram and thermodynamic charateristics of vanadates of the $V_2O_5-Fe_2O_3-VO_2$ system". In: *Russ. J. Inorg. Chem.* 24.4, pp. 1062–1066.

— (1980). "The p-T diagram and thermodynamics of compounds of the $Fe_2O_3-V_2O_5-VO_2$System". In: *Inorg. Mater* 16.2, pp. 212–215.

Walczak, J. et al. (1985). "Solid-liquid phase equilibria for the ternary systems, V_2O_5-Na_2O-Fe_2O_3, V_2O_5-Na_2O-Cr_2O_3 and V_2O_5-Na_2O-MgO". In: *Pol. J. Chem.* 59.3, pp. 255–262.

Waldner, P. and A.D. Pelton (2004a). "Critical thermodynamic assessment and modelling of the Fe-Ni-S system". In: *Metall Mater Trans B* 35.B, pp. 897–907. URL: https://doi.org/10.1007/s11663-004-0084-7.

— (2004b). "Thermodynamic modelling of the Ni-S system". In: *Z Metallkd* 95.8, pp. 672–681. URL: https://doi.org/10.3139/146.018005.

— (2005). "Thermodynamic modelling of the Fe-S system". In: *J Phase Equilib Diff* 26, pp. 23–38. URL: https://doi.org/10.1007/s11669-005-0055-y.

Wang, X. et al. (1998). "Structure comparison of iron tetrapolyvanadate $Fe_2V_4O_{13}$ and iron polyvanadomolybate $Fe_2V_3 \cdot 16\,Mo_0 \cdot 84\,O_{13} \cdot 42$: A new substitution mechanism of molybdenum vi for vanadium v". In: *Inorg. Chem.* 37.26, pp. 6921–6927.

Weddle, L.G. and M. Preece (1955). "The liquidus of metal-oxide V_2O_5 systems". In: *J. Iron Steel Inst.* 179, pp. 342 –347.

Wittke, J.P. (1967). "Solubility of iron in TiO_2 (Rutile)". In: *Journal of the American Ceramic Society* 50.11, pp. 586–588. URL: https://doi.org/10.1111/j.1151-2916.1967.tb15004.x.

Wriedt, H.A. (1989). "The O-V Oxygen - Vanadium system". In: *Bulletin of Alloy Phase Diagrams* 10.3, pp. 271 –277. URL: http://dx.doi.org/10.1007/BF02877512.

— (1991). "The Fe-O system". In: *Journal of Phase Equilibria* 13.2, pp. 170–200. URL: http://dx.doi.org/10.1007/BF02645713.

Wu, P., G. Eriksson, and A.D. Pelton (1993). "Critical evaluation and optimization of the thermodynamic properties and phase diagrams of the CaO-FeO,CaO-MgO,CaO-MnO, FeO-MgO, FeO-MnO, and MgO-MnO Systems". In: *J. Am. Ceram. Soc.* 76.7, pp. 2065–2075. URL: http://dx.doi.org/10.1111/j.1151-2916.1993.tb08334.x.

Wu, P. et al. (1993). "Prediction of the thermodynamic properties and phase diagrams of silicate systems - evaluations of the FeO-MgO-SiO_2 systems". In: *ISIJ International* 33.1, pp. 26 –35. URL: http://dx.doi.org/10.2355/isijinternational.33.26.

Xie, W. et al. (2016). "Thermodynamic assessment of the PbO - V_2O_5 system". In: *CALPHAD: Computer Coupling of Phase Diagrams and Thermochemistry*. URL: http://dx.doi.org/10.1016/j.calphad.2016.04.005.

Yang, Y., H. Mao, and M. Selleby (2015). "Thermodynamic assessment of the V-O system". In: *CALPHAD: Computer Coupling of Phase Diagrams and Thermochemistry* 51, pp. 144–160. URL: http://dx.doi.org/10.1016/j.calphad.2015.08.003.

Yang, Y. et al. (2017). "An assessment of the Ti-V-O system". In: *Journal of Alloys and Compounds* 722, pp. 365–374. URL: https://doi.org/10.1016/j.jallcom.2017.05.326.

Zhang, R. (2016). "Experimental investigation and thermodynamic description of the BaO- containg oxide systems". Ph.D. thesis. Aalto University, Helsinki, Finland.

Zhang, W. and M. Chen (2013). "Thermodynamic modelling of the Co-Fe-O system". In: *CALPHAD: Computer Coupling of Phase Diagrams and Thermochemistry* 41.1, pp. 76–88. URL: http://dx.doi.org/10.1016/j.calphad.2013.02.002.

Zieniert, T. and O. Fabrischnaya (2015). "Thermodynamic assessment and experiments in the system $MgO-Al_2O_3$". In: *CALPHAD: Computer Coupling of Phase Diagrams and Thermochemistry* 40, pp. 1–9. URL: http://dx.doi.org/10.1016/j.calphad.2012.10.001.

Glossary

Abbreviations

ANOVA	Analysis of variance
BSE	Backscattered electrons
CALPHAD	CALculation of PHase Diagrams
CEF	Compound Energy formalism
ChemSage	Integrated Thermodynamic Databank System
DAT	OPTISAGE data file
DSC	Differential Scanning Calorimetry
DTA	Differential Thermal Analysis
EDS	Energy Dispersive Spectrometry
ELEM	Standard state data of all pure elements
EMF	Electromotive Fore
EPMA	Electron Probe Micron-Analyser
EXL	Experimental data file from Excel
F*A*C*T	Facility for the Analysis of Chemical Thermodynamics
FactSage	Thermochemical software from Thermfact and GTT technologies
FACTPS	Pure substance database in FactSage
FTOXID	Pure oxide and oxide solid solution database
LRO	Long Range Ordering
MTDATA	Thermochemical software from National Physical Laboratory
OF	Objective Function
OPTISAGE	Optimisation algorithm
PANDAT	Thermochemical software
PARROT	Optimisation algorithm

SEM	Scanning electron microscope
SER	Standard Element Reference
SGTE	Scientific Group Thermodata Europe
SOLGASMIX	Gibbs minimisation computer algorithm
SRO	Short-Range Ordering
SS	Solid solution
TGA	Thermogravimetric Analysis
Thermo-calc	Thermochemistrysoftware
XRD	X-Ray Powder Diffraction
XPS	X-Ray Photoelectron spectroscopy

Symbols

A_m	Molar Helmholz energy
$a_0, a_1, a_2...$	Gibbs energy coefficients of a compound in solution
a, b, c	Gibbs energy coefficients of a pure compound
c	Number of components in the Gibbs phase rule
a_i	Activity of component, i
β_{ij}	Formula coefficient matrix
β_m	Magnetic moment
C_p	Heat capacity
f_i	Fugacity of component, i
G_m	Molar Gibbs energy
G_m°	Standard molar Gibbs energy
$\Delta G_{f,298K}^\circ$	Standard molar Gibbs energy of formation of a component at 298K
G_m^{phys}	Physical contribution to the Gibbs energy
G_e	Excess Gibbs energy
$\Delta H_{f,298K}^\circ$	Enthalpy of formation of a component at 298K
H_m	Molar enthalpy
λ_j	Langrangian multiplier
L_i	Interaction parameter of component, i

μ_i	Chemical potential of component, i
m	Stoichiometric constant
n	Stoichiometric constant
n_i	Mole of constituent, i
o	Stoichiometric constant
P	Total pressure
P_i	Partial pressure of gaseous component, i
p	Phase
R	Universal gas constant
S°_{298K}	Standard entropy of a component at 298K
ΔS^{config}_{m}	Configurational entropy in terms of pair fractions
S^{config}_{m}	Configurational entropy of a phase
S_m	Molar entropy of a component
T	Temperature
T_c	Curie temperature
U_m	Molar internal energy
v_i	specific volume of constituent, i
x_i	Molar fraction of a constituent, i
X_i	Molar pair fraction of constituent, i
X_{ii}	Molar pair fraction of constituent, i
y_i	Molar fraction of component, i
Y_i	Coordination equivalent site fraction of constituent, i
Z	MQM coordination number

Superscripts and Subscripts

$_{A,B}$	element
$_{a,b,c}$	stoichiometric coefficient
$_{A,B}$	cation species from qausichemical formulation
$_{config}$	configurational
$_{e}$	excess

f	formation
i,j,k	element or component
m	molar
q,p,r	order of the polynomial
$\circ$	standard state
$phys$	physical
SER	standard element reference state at 298 K and 1 bar
θ	a phase

DECLARATION ON PLAGIARISM
UNIVERSITY OF PRETORIA
Faculty of Engineering, the Built Environment and Information Technology
Department of Materials Science and Metallurgical Engineering

The University places great emphasis upon integrity and ethical conduct in the preparation of all written work submitted for academic evaluation. While academic staff teach you about systems of referring and how to avoid plagiarism, you too have a responsibility in this regard. If you are at any stage uncertain as to what is required, you should speak to your lecturer before any written work is submitted.

You are guilty of plagiarism if you copy something from a book, article or website without acknowledging the source and pass it off as your own. In effect you are stealing something that belongs to someone else. This is not only the case when you copy work word-by-word (verbatim), but also when you submit someone else's work in a slightly altered form (paraphrase) or use a line of argument without acknowledging it. You are not allowed to use another student's past written work. You are also not allowed to let anybody copy your work with the intention of passing it off as his/her work.

Students who commit plagiarism will lose all credits obtained in the plagiarised work. The matter may also be referred to the Disciplinary Committee (Students) for a ruling. Plagiarism is regarded as a serious contravention of the University's rules and can lead to expulsion from the University.

The declaration which follows must be appended to all written work submitted within the department. No written work will be accepted unless the declaration has been completed and attached.

I (full names) _____

Student number _____

Topic of work _____

Declaration
1. I understand what plagiarism is and am aware of the University's policy in this regard.
2. I declare that this report is my own original work. Where other people's work has been used (from a printed source, internet or any other source), this has been properly acknowledged and referenced in accordance with departmental requirements.
3. I have not used another student's past written work to hand in as my own.
4. I have not allowed, and will not allow, anyone to copy my work with the intention of passing it off as his or her own work.

Signature _____